ELECTROTRANSPORT IN METALS

ELECTROLUMINESCENCE IN ZINC TELLURIDE

by

D. I. KENNEDY

Thesis submitted
for the degree of
Doctor of Philosophy
University of Edinburgh

October 1967

ACKNOWLEDGMENTS

I wish to thank Professor N. Feather, F.R.S. for the provision of the facilities of the Natural Philosophy Department. I am grateful to Professor A. F. Brown for supervision and encouragement throughout the course of this project. I also wish to express my appreciation to Dr. M. J. Russ, Director of Research and Development, Bowmar Canada Limited, for permission to incorporate in this thesis the results of a research project conducted at Bowmar Canada Limited and for numerous helpful discussions.

SUMMARY

(i) ELECTROTRANSPORT IN METALS

The effects of an applied electric field on diffusion in metals is discussed. Frequently, under high current densities, and for temperatures in the diffusion range, a directed displacement of the diffusion species results. This mass transport is described by the term electrotransport. The major theoretical considerations relevant to the development of this topic are described, with particular emphasis on derivations which have been applied to the interpretation of experimental results. Previous experimental investigations of electrotransport in metals are reviewed.

The results of experiments on electrotransport of indium, using a radioactive isotope technique, are presented. The investigations are concerned with the electrotransport of the isotope In^{114m} in solid gold, thin gold films and thin indium films. Electrotransport phenomena in thin films have not previously been investigated in any detail. The results are amenable to interpretation in terms of the interaction of electrons with an activated complex associated with the diffusing species.

(ii) ELECTROLUMINESCENCE IN ZINC TELLURIDE

This section reports on the electroluminescent properties of the II-VI semiconducting compound zinc telluride. Previous investigations into the preparation of zinc telluride crystals and the optical, electrical and electroluminescent properties of the material are reviewed. The results of an experimental programme concerned

with the preparation of zinc telluride crystals and the electroluminescent properties of devices fabricated from several forms of the material are presented. Relatively simple contacting and processing techniques are utilised and the electroluminescence is primarily associated with metal:semiconductor junctions and contact barrier regions. Particular emphasis is placed on the observation of room-temperature electroluminescence in zinc telluride as this has not been the subject of previous detailed investigation. The incorporation of oxygen in the crystals results in radiative recombinations in which temperature quenching of the emission is not pronounced. This results in considerable improvement in room-temperature emission efficiencies; the associated emission is located in the red region of the visible spectrum. Other forms of zinc telluride investigated include nominally undoped and semi-insulating single crystals and also polycrystalline material. The potential of electroluminescent devices based on these various forms of zinc telluride as room-temperature visible emitters is evaluated. Possible mechanisms of electroluminescence are discussed.

CONTENTS

Page No.

ACKNOWLEDGMENTS i

SUMMARY ii

(i) ELECTROTRANSPORT IN METALS

1. INTRODUCTION 1

2. THEORETICAL CONSIDERATIONS 6

2.1 Previous Theories 11

2.1.1 Diffusion Under an Externally Applied Field 15

2.1.2 The Theory of Fiks 19

2.1.2.1 Relation to Experimental Results 26

2.1.3 The Theory of Huntington 30

2.1.4 The Hole Wind Paradox 37

3. PREVIOUS EXPERIMENTAL WORK 42

3.1 Experimental Techniques and Results 43

3.1.1 The Work of Wever 46

3.1.2 The Work of Huntington and Associates 49

3.1.3 The Work of Kuz'menko and Khar'kov 65

3.1.4 Electrotransport of Interstitial Solutes and Solid Solution Components 71

3.1.5 Electrotransport in Thin Metal Films 77

4. EXPERIMENTAL PROGRAMME 81

4.1 Apparatus and Experimental Techniques 85

4.2 Electrotransport of In^{114m} in Solid Gold 91

4.3 Electrotransport of In^{114m} in Thin Gold Films 101

4.4 Electrotransport of In^{114m} in Thin Indium Films 113

5. CONCLUSIONS 121

REFERENCES 128

Page No.

(ii) ELECTROLUMINESCENCE IN ZINC TELLURIDE

1. INTRODUCTION 1

2. PREVIOUS WORK 6
   - 2.1 Structure and Crystal Growth 9
     - 2.1.1 Crystallography 9
     - 2.1.2 Crystal Growth 13
       - 2.1.2.1 Vapour Growth 17
       - 2.1.2.2 Melt Growth 21
       - 2.1.2.3 Solution Growth 24
     - 2.1.3 Purification 25
   - 2.2 Material Properties 29
     - 2.2.1 Absorption Properties 32
     - 2.2.2 Electrical Transport Properties 42
     - 2.2.3 Electroluminescence 58
       - 2.2.3.1 Mechanisms of Electroluminescence 61
         - 2.2.3.1.1 Minority Carrier Injection 61
         - 2.2.3.1.2 Carrier Acceleration and Impact Ionisation 79
       - 2.2.3.2 Electroluminescence in ZnTe 82

3. CRYSTAL GROWTH 105
   - 3.1 Bridgman Growth 111
   - 3.2 Vapour Growth 115
   - 3.3 Solution Regrowth 119
   - 3.4 Crystal Purification 121
   - 3.5 Conclusions 122

4. MATERIAL PROPERTIES 126
   - 4.1 Material Evaluation 126
     - 4.1.1 Optical 126
     - 4.1.2 X-Ray 127
     - 4.1.3 Chemical 130
   - 4.2 Absorption 131
   - 4.3 Electrical Transport 143

5. DEVICES 153
   - 5.1 Device Fabrication 154
   - 5.2 Electro-optical Characteristics 160

Page No.

		Page No.
5.2.1	Semi-Insulating ZnTe	162
5.2.2	Nominally Undoped ZnTe	188
5.2.3	ZnTe Incorporating Oxygen Centres	207
5.2.4	Polycrystalline ZnTe	224
5.2.5	Special Devices	236

6. DISCUSSIONS AND CONCLUSIONS 241

APPENDIX 1 THEORETICAL CONSIDERATIONS OF BAND STRUCTURE 269

APPENDIX 2 THEORETICAL CONSIDERATIONS OF OPTICAL PROPERTIES 280

REFERENCES 289

PUBLICATIONS 295

(i)

ELECTROTRANSPORT IN METALS

1. INTRODUCTION

When a driving force is imposed on the random motion of atoms in a metal in thermal equilibrium it is possible for mass transport to result. If the form of the driving force is an applied direct electric field the mass transport of metals ions is referred to as electrotransport. The synonymous terms electromigration and electrodiffusion are sometimes encountered. As the preferential migration of ions in a solid is relatively small in comparison to the transport of electrons, it is normally necessary for observation of the effect to conduct experiments at temperatures close to the melting point of the material.

If by the passage of direct current or by other means a non-uniform temperature gradient is set up in the conductor, then this form of driving force can result in a form of mass transport known as thermal migration or the Sôret effect. In many cases electrotransport and thermal migration occur together and it is necessary to separate these effects to permit quantitative analysis of experimental results.

The study of electrotransport has been pursued in solid as well as liquid systems. As would be expected electrotransport in solid metals takes place at a much reduced rate compared with liquid metals. The earliest observation of electrotransport in metals is attributed to Gerardin (1961) who noticed that

after electrolysis in the molten state a lead-tin alloy became soft at one end and brittle at the other, and that a sodium-mercury alloy would decompose water only at one end. In the period since 1930 numerous investigations have been conducted to determine the possible electrolytic effects of high current densities in metals and alloy systems. The early experiments were carried out by German investigators, mainly on alloy systems. In the past decade this work has been extended to pure metals and important contributions have been made by workers in the U.S.A. and U.S.S.R.. General reviews of electrotransport in solid and liquid metals have been published by Schwarz (1940), Jost (1952), Seith (1955) and Verhoeven (1963). This report will mainly be confined to the more recent experimental work on electrotransport in solid metals and the theoretical background which has been used in the interpretation of these results.

In terms of practical applications the phenomenon of electrotransport may prove valuable in the purification of metals and alloys and the separation of alloys and isotopes. To date, however, the practical manifestations of electrotransport have related to its deleterious affects on the lifetime of conductors operating under high levels of direct current and/or high temperatures. The failure of tungsten filaments which developed "hot spots" in the region of one electrode when run on direct current was reported in 1924 by Skaupy. In a more modern

context, the failure of transistors and integrated circuit components after prolonged operation or testing at high current levels has been interpreted in terms of electrotransport effects in metal and alloy contacts and thin film metal resistive elements (Berry et al., 1966; Ghate, 1967, Mutter, 1967).

The main importance of the phenomenon of electrotransport is that it provides an alternative insight into the physics of diffusion processes and the electrical resistivity of metals and alloys. It is unique in that it readily provides a method of investigating the interaction of electrons with lattice defects and determining the specific resistivity of the activated complex taking part in the diffusion process. In the past there has been a tendency for investigations of diffusion and electrical conductivity to proceed independently, since the mechanisms of the two phenomena are essentially different. Diffusion is determined by the interaction of atoms with their neighbours in the lattice whereas electrical conductivity is determined by the interaction of electrons with ions of the lattice. The two phenomena are linked by the mobility of ions in metals and the fact that electrotransport is also a thermally activated process. The effective mobility of ions undergoing transport, on the one hand, is determined by the coefficient of diffusion or self-diffusion (a measure of the true mobility of the ions), and on the other, it depends on the interaction of electrons with ions, i.e. on the electrical properties of the metal. The measurement of material transport in a homogeneous metal is

a method of direct measurement of the effective mobility and thus investigations of ionic migration may be effective in clarifying both mechanisms, diffusion and electrical conduction, and their interconnection. Electrotransport also provides an alternative method for the determination of the activation energy for diffusion. This may be particularly useful in metals having no radioisotope suitable for diffusion studies. The interpretation of the results of electrotransport experiments in terms of the various theoretical models permits the evaluation of a defect resistivity associated with an activated complex participating in the diffusion process. Although this cannot rigourously be interpreted as the defect resistivity, as it is in most theories a measure of the resistivity due to electron scattering from ions in a position intermediate between two neighbouring equilibrium positions, it has, however, in a number of cases been identified with the vacancy resistivity. Electrotransport studies yield quantitative information on the strength of the interaction of electrons and lattice defects; however, theoretical progress has still to be made on the rather complex scattering problems if the results are to be related with confidence to the specific resistivity of lattice defects as they are ordinarily considered. In any event this technique does provide a measurement of "a" defect resistivity which, if measured by other methods such as quenching, radiation damage, and work hardening, is subject to uncertainty due to the difficulty in determining the number of defects involved. Finally investigations of mass transport may provide an insight into the mechanisms

of vacancy creation and annihilation and may result in a deeper understanding of vacancy kinetics.

2. THEORETICAL CONSIDERATIONS

The major theories which have been applied to the analysis of the results of experiments on electrotransport in metals conducted over the past decade have adopted the same basic phenomenological approach to the problem of the interaction of conduction electrons with metal ions.

In a current-carrying metal the conducting electrons possess a considerable momentum which they continually transfer to the metal ions. As a consequence of this, in addition to the electrostatic force exerted on the metals ions by the applied electric field there is a second force resulting from the interaction of electrons and ions during collision. The forces resulting from this momentum exchange have been referred to as "electron friction" forces. It therefore results that the force acting on atoms undergoing diffusion is the resultant of these forces. If all the atoms in a metal are considered to be positively charged owing to the loss of electrons to the "electron gas", the resultant force produced by an electric field on a metal alloy may be expressed as

$$F = \sum_i n_i e Z_i E - n_e eE \qquad (2.1)$$

where n_i is the number of ions or atoms of component i per unit volume, n_e is the number of electrons per unit volume, Z_i is the valence of component i, E is the electric field intensity and e the charge on the electron. The electron valence is taken as -1. Since there is no net charge within the metal this force

must necessarily be zero.

if the frictional force of the electrons upon component i is designated F_{ei} and assumed proportional to the electric field, then,

$$F_{ei} = g_{ei}E \tag{2.2}$$

where g_{ei} is a "friction" coefficient. Since the conducting electrons move through the lattice with a steady state velocity:

$$n_e eE = \sum_i n_i g_{ei} E \tag{2.3}$$

Combining equation (2.3) with equation (2.1) gives

$$\sum_i n_i eE(Z_i - g_{ei}/e) = 0 \tag{2.4}$$

The net force on component i of charge Z_i must be

$$F_i = eE(Z_i - g_{ei}/e) \tag{2.5}$$

It should be stated that the transport of matter is not in contradiction of the fact that the sum of the forces acting on a metal is zero, since a force which is equal in magnitude but opposite in sign to the force acting on all of the migrating ions. However, this latter force is compensated by reactions where the conductor is supported.

When an external force is applied to an ion within a conductor of uniform composition the ion will move with a terminal velocity. The magnitude of this velocity for a given force is determined by the frictional drag force of the lattice. The motion of the ion

is characterised by its mobility, i.e. by the coefficient of proportionality between the velocity of the ion and the force acting on it. This mobility can be considered as the absolute mobility and is supposedly independent of the nature of the external force. This mobility of the component i can be related to the diffusion coefficient, D_i, of the moving ion by the modified Einstein relation

$$B_i = D_i/fkT \qquad (2.6)$$

where k is Boltzmann's constant, T the absolute temperature and f is a correlation coefficient introduced to account for the non-random nature of the diffusion jumps in a crystalline solid (Bardeen and Herring, 1951). The correlation coefficients for various types of crystal lattice structure have been evaluated by Le Claire and Lidiard (1956). From Frenkel's theory of activated diffusion processes (Frenkel, 1955) it can be shown that there is an upper limit to the external force under which the Einstein relation is valid. (In a solid for electric fields less than 10^6 V/cm.)

Using equation (2.5) and the absolute mobility the velocity of an ion undergoing electrotransport may be expressed as

$$v_i = B_i F_i = B_i eE\,(Z_i - g_{ei}/e) \qquad (2.7)$$

A mobility, u_i, is defined as the velocity per unit electric field, v_i/E, where u_i is related to B by

$$u_i = B_i e\,(Z_i - g_{ei}/e) \qquad (2.8)$$

To avoid confusion between this parameter and the absolute mobility it can be described as the effective mobility. Using equation (2.6) gives

$$u_i = \frac{D_i}{fkT} e(Z_i - g_{ei}/e) \qquad (2.9)$$

A related composite parameter which is frequently encountered is the velocity per unit current density. From equations (2.6) and (2.7)

$$v_i/j = \frac{D_i}{fkT} e\rho(Z_i - g_{ei}/e) \qquad (2.10)$$

where j is the density of the current flowing through the conductor and ρ is the specific resistivity.

Equation (2.10) illustrates one of the main complications affecting the interpretation of electrotransport data. Since v_i (or u_i) and D_i are the only quantities which may be obtained from transport experiments, it is not possible to determine the individual terms within the brackets. Consequently, the true charge on a component, Z_i, can only be obtained if the frictional coefficient, g_{ei}, can be determined independently, or vice versa. Thus experimental results yield the bracketed terms generally referred to as the effective valence, Z_i^o giving

$$u_i = \frac{D_i}{fkT} eZ_i^o \qquad (2.11)$$

where Z_i^o has the form

$$Z_i^o = (Z_i - g_{ei}/e) \qquad (2.12)$$

Hence, equation (2.5) can be written in the simplified form

$$F_i = eEZ_i^o \qquad (2.13)$$

The sign of Z_i^o will predict the direction of transport of component i in an electrotransport experiment in solid metals and dilute metallic alloys. A negative sign indicates that the electron-friction force, often referred to as the "electron wind" force will predominate over the electrostatic field force and transport takes place towards the anodic terminal of the conductor. (The anodic terminal is defined conventionally as that at which electrons leave the conductor.) A positive effective charge infers the opposite, or else that a "hole wind" force dominates the transport process. The term "hole-wind" refers to the transfer of momentum from positive charge carriers to the migration ion, resulting in cathode-directed mass transport. There has been considerable dispute over the theoretical validity of this concept and this will be discussed in a later section. The aim of various theoretical treatments is to develop an expression for g_{ei}, which would then permit the determination of Z_i from experimental measurements.

In addition to the effective mobility and velocity per unit current density investigators in Germany and Russia have presented electrotransport data in terms of a transport number. This is usually expressed as moles of component i transported per Faraday of charge. The relationship between transport number and effect-

ive mobility is

$$TN = u_i N_i F \qquad (2.14)$$

where N_i is the number of moles of component i per unit volume and F is the Faraday constant. Alternatively,

$$TN = \frac{v_i}{j} N_i F \qquad (2.15)$$

2.1. Previous Theories

The above discussion indicates that a theoretical understanding of the nature of the frictional electron force is necessary for the detailed interpretation of the results of electrotransport experiments. In general theoretical treatments have met with limited success in explaining experimental data. This is attributable to the complexity of the electron: ion interaction and the difficulty in ascribing a specific charge to a metal atom in a lattice.

The importance of the concept of electron:ion interaction has not always been recognised. Although two early investigators, Skaupy (1914) and Lewis et al. (1915), proposed qualitative theories which were complete in the sense that they considered both a field force and an electron-friction force, subsequent theories neglected to take account of the frictional electron force, perhaps due to its complexity. Wagner (1933) considered that the ions did not interact with the electrons and moved as particles whose mobility was connected with the coefficient of diffusion

or self-diffusion by the Einstein relation. Schwarz (1933) introduced a fictitious "electrohydrostatic" force acting on an ion in addition to the force of the electric field. Much of the Russian work on transport, carried out prior to the resurrection by Fiks (1959) of the electron friction force concept, implicitly assumed the electron:ion interaction to be negligible. (Yavoisky and Chernega, 1956; Frantsevich et al., 1957, 1958, 1959; Babikova and Gruzin, 1957.)

In the past ten years there have been a number of new attempts to evolve a theory describing quantitatively electrotransport in metals. Two broad categories can be distinguished. In the first a macroscopic approach involving the methods of irreversible thermodynamics is employed. In the second the problem is considered on the atomic scale, and the momentum exchange of the electron:atom interaction is discussed.

One of the more authoriative treatments in the first category was presented by Klemm (1953, 1954). This author evaluated the total force on a component i by considerations of the irreversible thermodynamics of the electrotransport process. In this novel approach the usual technique of evaluating the transport fluxes as linear functions of the forces was abandoned and instead Klemm evaluated the forces in terms of linear functions of the fluxes. It has been pointed out (Laity, 1959) that Klemm's result can be derived from the Onsager relation (Onsager, 1945); indeed, the electron:ion interaction in electrotransport is an

example of non-vanishing of the Onsager cross-coefficients leading to departure from the simple Einstein relation. In a metal the components are electrons and ions. Other theoretical treatments utilising similar concepts have been advanced by Baranowski (1955) and Belashenko and Zhukovitsky (1961). Drakin (1953) treated the electrotransport phenomenon by the application of classical thermodynamics. The highly irreversible nature of the electrotransport process casts doubt on the theoretical justification for this latter approach (Baranowski, 1955).

The other approach in terms of evaluation of the electron:ion interaction has been considered by several authors. Manglesdorf, 1960, and de Gennes, 1956, considered the problem of momentum exchange in liquid metals and alloys and Bresler and Pikus (1958) determined the electron friction force in a solid by a relatively simple theoretical approach which involved a number of broad assumptions. Bosvieux and Friedel (1962) considered the net force produced by the electric field on not one, but three types of defect - interstitials, vacancies and substitutional defects. The treatment was quantum mechanical in nature and was based on perturbation of the electron wave function in the region of a lattice position by the flow of charge carriers. The concept of "electron-friction" was considered as arising from the polarisation of the screening charge of an atom in a metal induced by displacement of the Fermi level. The force on the charge was considered to be entirely electrostatic in nature; however, the effective part of the electrostatic force resulting in mass trans-

port was considered to arise from the perturbation effect. That is, from the altered charge distribution in the vicinity of the defect. This charge was calculated from the electron scattering by the Born approximation. The theoretical treatments which are most commonly applied to the interpretation of the results of electrotransport experiments in solid metals are those of Fiks (1959) and Huntington (1961, 1963). The theoretical treatment developed by Fiks has been used by all the recent Soviet investigators. It is based on the electron theory of metals and the force exerted by the electrons upon a metal ion is evaluated in terms of ion scattering cross sections and mean free paths of charge carriers. The electrons, assumed free, are considered to lose to the activated ion all the extra momentum acquired from each collision. Huntington's treatment has been widely used by investigators in the U.S.A., and is based on momentum conservation considerations when charge carriers interact with lattice defects. The total momentum exchange between the charge carriers and the moving atoms is related to the effective contribution to the resistivity associated with atoms in the activated configuration for diffusion. There is a distinct similarity between the two approaches.

The theoretical treatments of the various authors have been summarised, in greater or less detail, by Verhoeven (1963). This author has shown that, despite the diversity of approaches to the problem of electrotransport adopted by the various authors, the expressions obtained for the electron:ion interaction force

by Klemm, Mangelsdorf, Bressler and Pikus, Bosvieuz and Friedel, Fiks, and Huntington are remarkably similar.

As this report is primarily concerned with electrotransport phenomena in pure solid metals, the theoretical treatments which in the past have found widest application to the interpretation of data from electrotransport experiments on such materials, namely those of Fiks and Huntington, will now be presented in some greater detail.

2.1.1 Diffusion Under An Externally Applied Force

At this juncture it is relevant to consider the "classical" approach to diffusion under an externally applied force field. This is particularly relevant as it substantiates the validity of the Nerst-Einstein relationship as applied to the field influenced transport of matter in solids. From the theoretical concepts discussed briefly in the preceeding section, and the theories of previous authors which will be presented in the succeeding sections, it will be apparent that this relationship is of central importance in the establishment of theoretical models for the electrotransport process.

Jost (1952) has derived expressions for the mobility of an ion migrating under an electric field. By means of the Nernst - Einstein relationship the mobility of charged particles in a solid under an electric field can be equated to the diffusion

coefficient by, (Mott and Gurney, 1948)

$$\frac{u}{D} = \frac{1}{kT} \qquad (2.16)$$

For ionic crystals it is possible to calculate the self-diffusion coefficient from the electrolytic conductivity and transference numbers, since the electronic conductivity, is given by,

$$\sigma = \sum \sigma_i = \sum n_i Z_i^2 e^2 u_i \qquad (2.17)$$

where n_i, $Z_i e$ and u_i are the concentration, electronic charge and mobility of the component i respectively. From this equation the mobility u_i may and hence the diffusion coefficient may be calculated if the transference numbers, $t_i = \sigma_i/\sigma$, are known.

It is possible to derive the Nernst-Einstein relationship by considerations of the migration of ions both with and without an applied electric field. Figure 2.1 schematically depicts the potential energy of a migrating ion in the two cases. In this one dimensional case of a particle moving in a periodic field of force, the height of the potential barriers is indicated by the energy E_M. Taking d as the distance between equivalent equilibrium positions and v is the mean thermal velocity of the particles, the matter flux flowing in the direction of positive x is

$$J_+ = n' \exp(-E_M/RT)v \qquad (2.18)$$

where n' is the concentration of diffusing particles. For the opposite direction

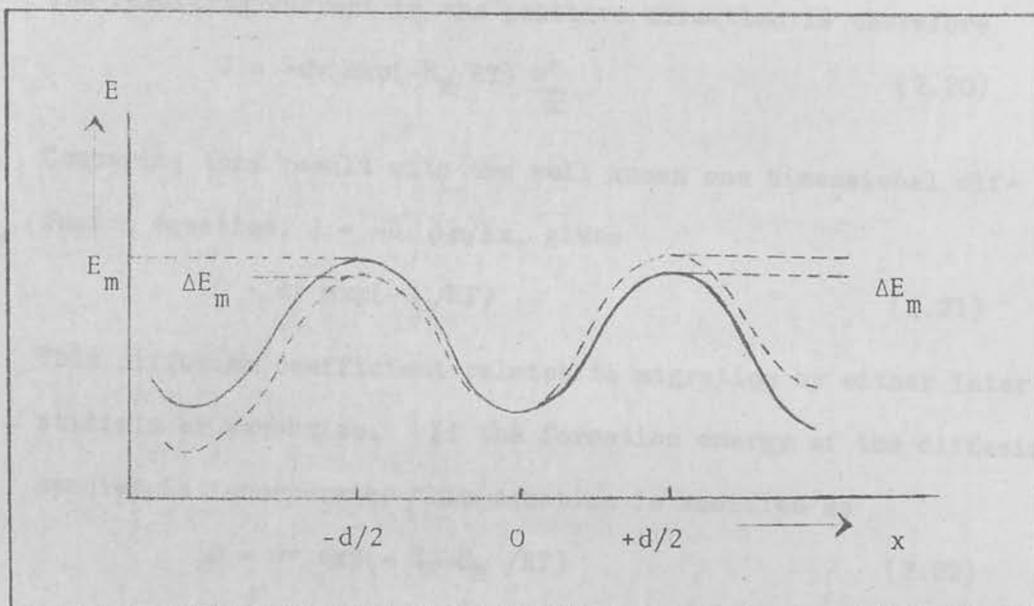

FIGURE 2.1 Potential energy of a migrating ion with electric field (dashed curve) and without electric field (solid curve); d distance between equivalent sites.

$$J_- = (n' + d \frac{n'}{x}) \exp(-E_M/RT)v \qquad (2.19)$$

The resulting current in the positive direction is therefore

$$J = -dv \exp(-E_M/RT) \frac{n'}{x} \qquad (2.20)$$

Comparing this result with the well known one dimensional diffusion equation, $J = -D\ \partial n/\partial x$, gives

$$D = dv \exp(-E_M/RT) \qquad (2.21)$$

This diffusion coefficient relates to migration by either interstitials or vacancies. If the formation energy of the diffusing species is incorporated this equation is modified as

$$D = dv \exp(-\ E_F + E_M\ /RT) \qquad (2.22)$$

The same process can be repeated in the presence of an externally applied field and in the absence of a concentration gradient. Due to the presence, of say, an electric field, $F = d\varphi/dx$, the original potential distribution is distorted as shown in the figure as a result of the additional term in the potential energy $-\ Ze$, where Ze is the charge of the mobile particles. The expressions for the matter flux with and against the direction of the field now are

$$J_+ = n'v \exp(-\ E_M - NZe \frac{d\varphi}{dx} \frac{d}{2}\ /RT) \qquad (2.23)$$

$$J_- = n'v \exp(-\ E_M + NZe \frac{d\varphi}{dx} \frac{d}{2}\ /RT) \qquad (2.24)$$

Here the energy barrier to be surmounted by a particle moving from one equilibrium position to the next in the same direction

as the field is given by the interior bracket in eq. (2.23). Similarly the barrier for a particle moving in the opposite direction is given by the interior bracket of eq. (2.24). Hence the resultant flow of matter is given by

$$J = n'v \exp(-E_M/RT) \left[\exp\left(Ze\frac{d\varphi}{dx}\frac{d}{2}/kT\right) - \exp\left(-Ze\frac{d}{dx}\frac{d}{2}/kT\right) \right] \qquad (2.25)$$

This reduces to

$$J \approx n'v \exp(-E_M/RT)\ \frac{Zed}{kT}\frac{d\varphi}{dx} \qquad (2.26)$$

assuming $\left(\frac{Zed}{2}\right)\left(\frac{d\varphi}{dx}\right)$ is small compared with kT. If one neglects the possible effects of electron-ion interactions and considers only the electrostatic force then this condition is readily met for the field strength applied in the normal run of electrotransport experiments. At very high fields Ohm's law may not be obeyed and Jost has pointed out that an exponential increase in current with increasing voltage is to be expected.

If equation (2.26) is multiplied by the charge Ze, the current is obtained as

$$JeZ = \frac{n'dv}{kT} Z^2e^2 \frac{d\varphi}{dx} \exp(-E_M/RT) \qquad (2.27)$$

This equation can be compared with Ohm's law

$$J_{el} = \frac{d\varphi}{dx}$$

It therefore results that the conductivity can be taken as

$$\sigma = n' \frac{dv}{kT} Z^2 e^2 \exp(-E_M/RT) \qquad (2.28)$$

and mobility as

$$u = dv/kT \exp(E_M/RT) \qquad (2.29)$$

Comparison with eq. (2.21) shows that the Nernst-Einstein relation is fulfilled.

This type of analysis was applied by Wagner (1938) to results obtained from electrolytic transport experiments.

As remarked previously, in any quantitative analysis of electrotransport in solids it is necessary to take into account the affects of momentum exchange between charge carriers and the moving atoms. Two modern theories which advocate this interaction model will now be discussed in detail.

2.1.2 The Theory of Fiks

The concept of the electron friction force was revived by Fiks and applied to the determination of the resultant force on the ions of a material during the passage of an electric current. As stated in the introduction, the results of this theoretical treatment have subsequently been applied by several groups of

Soviet investigators to the analysis of electrotransport experiments.

This theory utilised the concept of effective mobility which was described earlier in this section. The formulation of an expression for the force resulting from the interaction of electrons with ions was examined in terms of the electron theory of metals. Although the assumptions implicit in this derivation would appear to limit its validity to cases where the solvents are alkali metals, this has not deterred experimental investigators from interpreting results obtained with other materials in terms of this theory. The expression for this force was derived as a function of the ion scattering cross-section for electrons.

It was assumed that in each collision the electrons only lose that part of their mementum which they had acquired since the previous collision. Therefore, the momentum increment ΔP transferred to the ion is

$$\Delta P = eEl/v \qquad (2.30)$$

Since $eEl/v \ll \overline{P}$, where $\overline{P}$ is the average momentum of an electron in a metal, the collisions of the electrons with the ions are still regarded as elastic. The carrier acceleration produced by the electric field causes some directional asymmetry of the electron velocity distribution. Since subsequent

to the collision this asymmetry is removed, the number of electrons whose momentum lies between P and P + dP equals

$$2/h^3 \, fdP \qquad (2.31)$$

where f is the distribution function of electrons with regard to meomentum, and dP is the volume element in momentum space. The number of collisions per unit time of such electrons, in which the additional momentum ΔP is lost, is

$$2/h^3 \, A_i vfdP \qquad (2.32)$$

where A_i is the scattering cross-section for electrons. The total momentum transferred to an ion in unit time is equated to the interaction force, F_{ei}, of the electrons on the ions;

$$F_{ei} = 2/h^3 \int eElA_i fdP = -eEn\overline{lA}_i \qquad (2.33)$$

Here n is the concentration of the electrons and $\overline{lA}_i$ is the mean value of lA_i. Fiks also derived this expression from more rigourous quantum-mechanical considerations.

Since the field exerts the force eE on the ion, the resultant force F, taking into account collisions of electrons with ions, is

$$F_i = eE(1-nlA_i) \qquad (2.34)$$

Fiks pointed out that the resultant force acting on a natural ion of the metal is zero since $A_i = 1/nl$. Therefore, in order

to have a resultant force different from zero, it is necessary to postulate the presence of an activated complex undergoing diffusion. The scattering of cross-section electrons at this activated complex is considered to differ from A_i.

Fiks next proceeded to relate the scattering cross-section to the residual resistance of a metal connected with scattering at impurity ions. Use of the derivation of Mott and Jones (1936) for the ratio of this resistance to the specific resistance of a pure metal, allowed the expression for F_{ei} to be written as

$$F_{ei} = eE\,\frac{1}{c}\,\frac{\Delta\rho_i}{\rho_o} \qquad (2.35)$$

where ρ_o is the specific resistance of the pure metal and $\Delta\rho_i$ the residual resistance. The relative concentration of impurities is given by c_i. The resultant force on the ion is now given by

$$F_i = eE(1-\frac{1}{c_i}\,\frac{\Delta\rho_i)}{\rho_o} \qquad (2.36)$$

Considerations of the activated complex for diffusion and the use of the Frenkel approach presented earlier allows evaluation of the resultant force determining the motion of the ion as

$$F_i = eE(1-nlA_i^*) \qquad (2.37)$$

where A_i^* is the scattering cross-section for the activated ion. Since in solids and liquids a diffusing ion is to a large degree free, and the electronic interaction between this ion and its neighbours differs from the normal ion, $A_i^* \neq A_i$.

By application of the Nernst-Einstein relation the effective mobility is obtained from eq. (2.37) as

$$u_i = v_i/eE = D_i/kT(1-neA_i^*) \qquad (2.38)$$

The effective mobility may differ in magnitude and sign from the true mobility $u_o = D_o/kT$. If it is assumed that $A_i^* = A_i$ the expression for the effective mobility becomes, from eq. (2.36)

$$u_i = u_o \left(1 - \frac{1}{c_i}\frac{\Delta\rho_i}{\rho_o}\right) \qquad (2.39)$$

Under this assumption it is possible to correlate the scattering cross section with experimentally determinable parameters.

The above considerations have tacitly assumed that the concentration of free electrons equals that of the atoms in the material. If the number of free electrons is smaller than the number of atoms then it is necessary to attribute an effective charge $\overline{Z}$ to a normal ion. It is also necessary to recognise that the effective charge of activated ions Z_i^* may, in general, differ from $\overline{Z}$. It will be seen, however, that in most applications of the theory Z_i^* is equated to $\overline{Z}$.

From considerations of charge neutrality in the metal, and assuming that the scattering cross-sections are additive quantities, the expression obtained for the total force on the activated ion is

$$F_i = eE(Z_i^* - \bar{Z}\, A_i^*/\bar{A}) \tag{2.40}$$

Assuming that $Z_i^* = \bar{Z}$ the expression obtained for the effective mobility is

$$u_i = \frac{D_i}{kT}\,\frac{n}{N}\,(1 - A_i^*/\bar{A}) \tag{2.41}$$

where N is the concentration of atoms in the material. The ratio n/N is a measure of the "degree of dissociation" of atoms into ions. Since the net force on the average, unactivated ion is zero, eq. (2.37) combines with eq. (2.40) to give

$$\bar{Z} = n\bar{l}\bar{A} \tag{2.42}$$

In the general case the sign of the effective mobility is determined by the relation

$$Z_i^*\,\bar{A} \lessgtr \bar{Z}A^* \tag{2.43}$$

and for the special case of eq. (2.42)

$$A^* \lessgtr \bar{A} = \frac{1}{nl} \tag{2.44}$$

where $\bar{l}$ is the mean free path of a normal ion.

For the case of natural ions of the lattice where, as stated previously, $A^* > A_i$, and therefore $A^* > 1/nl$, then the positive ions should move to the anode under the action of the resultand force. This statement applies only to electron:ion interactions and neglects the possible effects of positive charge

carriers. Neutral atoms in a metal will move against the field as if they had a negative effective charge.

For the case if impurity ions in a metal having an effective mobility given by eq. (2.43) then if $A^* > A_i$ Fiks considered that the situation might not be identical to the natural ion case, since it is possible to have $A_i < \overline{A}$ but $A^* > \overline{A}$; in this case the sign of the effective mobility would be positive.

Fiks showed that the criterion for the sign of the effective mobility expressed in eq. (2.42) was exactly analagous to that obtained by Klemm (1954) in his treatment of the problem by an approach based on irreversible thermodynamics. He also demonstrated that the theoretical treatment was applicable to non-homogeneous as well as homogeneous metals.

In an extension of Fik's theory, Glinchuk (1959) suggested that, since positive Hall coefficients have been obtained for some metals, there would be momentum transfer from positive charge carriers in the opposite direction to that resulting from electron scattering. This is the concept of the "hole wind". With this modification eq. (2.33) becomes

$$F_{ei} = eE(l_p pA_p - l_n nA_n) \qquad (2.45)$$

where p and n refer to positive and negative charge carriers

respectively. In considerations of this composite effect it is relevant that the experiments of Brown and Barnett (1952) indicated that the electrons in a metal which has a positive Hall coefficient show a negative e/m ratio when accelerated with respect to the lattice. This has resulted in controversy over the validity of the "hole wind" concept. It is indisputable, however, that electrotransport in certain metals has been directed towards the cathode with associated effective charges in excess of the value which can be attributed to the effect of the electrostatic field. This situation will be discussed in a later section.

2.1.2.1 Relation to Experimental Results

It is relevant to consider at this point the methods used by Soviet investigators to develop the Fiks theory so that it can be applied to the analysis of results obtained from electrotransport experiments.

Kuz'menko (1960, 1962) considered the determination of the effective charge on an activated ion. In this treatment the electrical resistivity is taken as $\rho = m/ne^2\tau$ (n is the electron concentration). The mean free time, τ , is equated to $1/v_e$, and the equation solved for the product nl. The result is

$$nl = \frac{(2mE_F)^{1/2}}{\rho e^2} \qquad (2.46)$$

From Fik's eq. (2.41) the product equals $\overline{Z}/\overline{A}$. From his experimental results, Kuz'menko considered that the field force could be neglected in comparison with the electron-friction, permitting Fik's expression for the effective valence to be rearranged as

$$A^* = Z^o\overline{A}/\overline{Z} = Z^o e^2 \rho \; /(2mE_F)^{1/2} \qquad (2.47)$$

where Z^o is the effective valence. From the experimental results of electrotransport measurements on silver and assuming a value for the Fermi energy, A^* was determined. This parameter was found, as required by the theory, to be temperature insensitive.

Kuz'menko also applied an expression for the activated scattering cross-section

$$A^* = \frac{\pi}{2}\,\frac{Z^{*2}e^6}{E_F^2}\left[\ln(1+\frac{1}{y}) - \frac{1}{1+y}\right] \qquad (2.48)$$

Here y is a constant having the value $5.14 \times 10^{-8} n^{1/3}$. Equations (2.47) and (2.48) were used to estimate the true value of the valence of the activated ion.

Frantsevich and his co-workers have conducted a large number of experiments on the electrotransport of impurity ions in metals. Since, in many cases, the resulting mass transport was cathode-directed, these

authors advocated the existence of a "hole wind" force and in the analysis of their results an expression for the effective charge based on eq. (2.45) is used (Frantsevich and Kovensky, 1961a; 1961b). This has the form

$$Z_i^o = Z_i - l_n n A_n + l_p n_p A_p \qquad (2.49)$$

Here Z_i^o is the effective valence of the component i. An expression for the electrical resistivity identical to eq. (2.46) is used, and the free-electron approximation, $E_F = (h^2/2m)(3n/8\pi)^{2/3}$, is substituted in this equation giving the electrical conductivity as

$$\sigma = \left(\frac{8\pi}{3}\right)^{1/3} \frac{e^2}{h} \, l_n n^{2/3} = K_n l_n n^{2/3} \qquad (2.50)$$

where K_n is a constant. Assuming that this equation applies to both positive and negative charge carriers substitution in eq. (2.49) gives the effective valence

$$Z_i^o = Z_i - \frac{\sigma_n A_n n^{1/3}}{K_n} + \frac{\sigma_p A_p p^{1/3}}{K_n} \qquad (2.51)$$

Several assumptions are involved in the next steps in the calculation. Firstly, the conductivity is expressed as $\sigma = \sigma_n + \sigma_p$, and the total resistivity ρ, and ρ_n are expressed as linear functions of temperature, $\rho = \rho_o + \alpha T$ and $\rho_n = \rho_{on} + \alpha_n T$, and substituted in eq. (2.51) to give a complex algebraic expression for Z_i. Secondly, the scattering cross-

sections A_n, A_p and carrier concentrations n_n, n_p are considered temperature independent, which reduces the algebraic expression to the form

$$AX^2 + BZ_i^oX - CX - Z_i^o + Z_i = 0 \qquad (2.52)$$

where $X = (T + \rho_o/\alpha)^{-1}$ and A, B, C, are constants. Thus, determination of the effective valence Z_i^o at various temperatures permits calculation of the true valence Z_i. If the resistivity is a linear function of concentration, the same approach gives an expression similar to eq. (2.52) so that the true valence may be determined from the concentration dependence of the effective valence. Frantsevich pointed out that if the ratio ρ_n/ρ_p is a constant over the temperature range under investigation eq. (2.52) reduces from a hyperbolic to a linear form:

$$Z_i^o = Z_i - a/\rho \qquad (2.53)$$

where a is a constant.

In their experimental work the authors used radiactive tracers such as C^{14} in metals such as iron and titanium. The electrical mobility was calculated from the results and the effective valence obtained from eq. (2.11). This was then fitted into eq. (2.52) by the method of least squares.

2.1.3 The Theory of Huntington

Huntington and his associates have conducted a considerable number of investigations into electrotransport in pure metals. Although the details of the theoretical approach used by Huntington to evaluate the magnitude of the electron:ion interaction differ from those of Fiks, there is a distinct similarity between the fundamental concepts of the two authors relating to the exchange of momentum between the charge carriers and the diffusing species.

In Huntington's treatment (Huntington and Grone, 1961; Huntington and Ho, 1963) the momentum transferred per unit time to a point defect in a current-conducting metal was calculated. The basic simplifying assumptions of the approach were that the electrons are considered to be scattered by the defect alone and that the defect was decoupled from the lattice. These assumptions were stated to result in scattering without the creation or annihilation of phonons. Under these assumptions, the momentum transfer to the electrons it can be taken as m_o times the group velocity of the Bloch wave (m_o is the electron mass). The x component of the momentum transferred per unit time is derived from this quantum-mechanical approach by application of functions giving the transition probability per unit time an electron in a state with wave number k will jump to a state k' by virtue of its interaction with the class of defects under consideration. The assumption of a unique

mean free time independent of wave number gives for the rate of momentum transfer

$$\frac{dM_x}{dt} = \frac{m_o}{\tau_d \hbar} \int \frac{\partial E}{\partial k_x} f(k)\,dk/4\pi^3 \qquad (2.54)$$

Since the current density can be written as

$$j_x = \frac{-e}{4\pi^3} \int f(k) \frac{\partial E(k)}{\hbar \partial k_x} dk \qquad (2.55)$$

it follows that

$$\frac{dM_x}{dt} = \frac{-j_x m_o}{e\tau_d} \qquad (2.56)$$

Huntington then considered that the effect of the rate momentum transfer was to produce a continuous force on each defect. It was shown that roughly 10 electrons could undergo scattering during the time of an atomic jump (Fiks, in his treatment, estimated that 10 to 100 electrons would undergo scattering). This was considered sufficient to justify the assumption that on the average the effect could be approximated by a continuous force. Hence, eq. (2.56) becomes

$$F_x = -(j_x m_o)/(e\tau_d n_d) \qquad (2.57)$$

where n_d is the defect density. If the contribution of the defects to the resistivity is $\Delta\rho_d = |m^*|/ne^2\tau_d$, where m^* is the effective mass of the conduction electrons, then

$$F_x = \frac{m_o j}{N_d} \frac{\Delta\rho_d(\bar{Z}N)e}{|m^*|} = -eE_x\bar{Z} \frac{(\Delta\rho_d N)}{\rho_o N_d} \frac{m_o}{|m^*|} \qquad (2.58)$$

where the density of the conduction electrons has been replaced by $\overline{Z}$ times the density of metallic ions N. This formulation indicates that the friction force is proportional to the ratio of the resistivity of a defect site to that of a lattice site. It is also proportional to the ratio of the electron mass to the absolute value of the effective mass. The above expression imposes the condition that, even when the charge carriers have a negative mass, the overall momentum transfer will still be in the direction of the anode. This is in agreement with the work of Barnett. However, in a later re-evaluation of his theory Huntington suggested (Huntington and Ho, 1963) that the change in momentum should have been averaged with respect to $\hbar k$, i.e. the pseudo-momentum, rather than $m_o v_g$. This was considered to be more correct, since the interactions between electrons and defects are predominantly electrostatic in nature, and the magnitude of the force on the moving ion can be calculated directly from the time rate of change of the average of $\hbar k$. The force on the defect under these considerations is

$$F_x = -eE_x\overline{Z} \left(\frac{\Delta\rho_d}{\rho_o} \frac{N}{N_d}\right) \frac{m^*}{|m^*|} \qquad (2.59)$$

Hence, the electron friction force is dependent on the sign of the effective electron mass m^*. This revised theory therefore allows for the occurrence of cathode-directed momentum transfer.

Huntington next considered the modification of the Nernst-Einstein

equation appropriate to a particle whose charge was a function of its position. That is, on the assumption that the charge on an activated ion differs from that of an unactivated ion. Taking the moving vacancy as an example of the defect responsible for atom movement, it was argued that, for an ion at the saddle point halfway between and equilibrium lattice site and a vacancy, the interaction with the charge carriers would be strong, whereas, at the lattice sites, the same interaction would be a minimum. This means that F_x and $\Delta\rho_d$ would be position dependent and possess the periodicity of the lattice. The evaluation of the net flow of atoms proceeded under the assumption that this periodicity was sinusoidal in form. When applied to the net flow of atoms resulting from electron friction. This treatment results in a form of the Nernst-Einstein equation differing by a factor of 1/2 from the usual expression. The component of this equation associated with the electron-friction force therefore has the form

$$B_{ei_x} = \frac{D_i}{2kT} F_x \qquad (2.60)$$

where B_{ei} is the mobility component resulting from the electron-defect interaction. Under these conditions the final form for the mobility due to self-transport becomes

$$u_i = \frac{D_i \alpha}{fkT} e E \overline{Z} \left[1 - \tfrac{1}{2} \left(\frac{\Delta\rho_d N}{\rho_o N_d} \right) \frac{m^*}{|m^*|} \right] \qquad (2.61)$$

The factor α in this equation is introduced to account for the fact that, in experimental electrotransport experiments using inert markers to follow the change in position of the

lattice planes, the velocity of the markers v_m, cannot be exactly equated to the velocity of the ions, v_i, due to the possible effects of void formation and changes in specimen shape. If this is not taken into account the value obtained for the effective mobility will be larger than the true value. It therefore results that $\alpha \leq 1$. The limiting value $\alpha = 1$ will occur only (1) if no voids are formed and (2) if the creation and elimination of vacancies causes no changes in the lateral dimensions. If (1) is neglected and the dimensional change is assumed to be isotropic has the value 1/3. This value was frequently used by members of Huntington's group in the evaluation of their experimental results. This situation does not arise if the transport velocity of the ions is measured directly, for example by radioactive isotopes.

Comparison of the expression for u_i given above with the relationship between u_i and F_i as exemplified by eqs.(2.11) and (2.13) gives the expression for the resultant force on an ion in the lattice as

$$F_i = eE\overline{Z}\alpha\left(1 - \tfrac{1}{2}\left(\frac{\Delta\rho_d . N}{\rho_o . N_d}\right)\frac{m^*}{|m^*|}\right) \qquad (2.62)$$

This can be compared with the expression for F_i obtained from the Fiks theory as given by eq.(2.40).

Verhoeven has compared the theoretical expressions for the

net force per ion as obtained from various theories. It was shown that the Fiks theory and that of Huntington gave essentially the same expression for the case of self-transport. That is, where mass transfer results from directed diffusion of natural ions of the material and the defect responsible for this motion is the moving vacancy. Only minor variations existed between the two expressions. These were the experimental factor α, the Nernst-Einstein modifiying factor of 1/2 and the ratio of the algebraic to absolute value of the effective mass used by Huntington. Treatment of the defect in Huntington's theory as an interstitial rather than a marker indentation results in the following equation for the net force per interstitial

$$F_i = eE\alpha \left(Z_i - \tfrac{1}{2}\bar{Z} \left(\frac{\Delta\rho_d.}{\rho_o} \frac{N_o}{N_d} \right) \frac{m^*}{|m^*|} \right) \qquad (2.63)$$

which was also shown by Verhoeven to be equivalent to Fik's eq.(2.40), which was derived for mass transport associated with impurity ions. Here the subscript o refers to either the matrix or solvent atoms.

Although the two theoretical treatments outlined above are considered to be of particular importance in the development of the subject of electrotransport due to their wide application to the evaluation of experimental results, there have been a number of other analyses which are referred to in the introduction to this section.

One theory, which is of interest due to the novel and sophisticated approach adopted, is that of Bosvieux and Friedel (1962). As remarked previously, these authors used the Born approximation to calculate the perturbation of the electron wave function in the neighbourhood of a moving ion and then evaluated the electrostatic force from the corresponding change in the charge density. For the case of interstitials the net force on the defect resulting from this quantum-mechanical treatment is

$$F_d = -eE\overline{Z}\,\frac{\Delta\rho_d}{\rho_o}\cdot\frac{N_o}{N_d} \qquad (2.64)$$

This is essentially the same as the result derived by Huntington for the electron-defect friction force. In agreement with the revised theory of Huntington eq.(2.64) indicates that the direction of the net force is dependent on the sign of the charge carriers. One significant feature of this derivation is that the interstitial defect is not subjected to a direct force from the electric field. This was attributed to the screening effect from the charge carriers. The authors advanced a qualitative explanation for this deviation from previous theories and pointed out that their theory could be tested by interstitial electrotransport experiments conducted on the noble metals; the theory was not considered applicable to transition metals due to mixed conductivity between 4s electrons and 3d holes.

The derivation of an expression for the resultant force on an ion for the case of self-transport in metals involved the formulation of an expression for the force exerted on an ion at

the saddle point. It was assumed that, at this position, the ion behaved as an interstitial experiencing a force given by eq.(2.64) and resulted in a complex expression incorporating Bessel functions. A similar expression was derived for the case of a substitutional defect.

2.1.4 The Hole Wind Paradox

At several places in this section it has been indicated that the various theoretical predictions on the dependence of the direction of mass transport on the sign of the charge carriers are not in complete agreement with the experimental results. The following are the salient features of this controversial situation.

(1) For metals with a negative Hall coefficient it has been found that the direction of transport is in agreement with the sign of the charge carriers. The force of interaction between electrons and ions is referred to as the "electron wind" and is directed towards the anode.

(2) For metals with a positive Hall coefficient the transport is found for some cases to be cathode-directed and for other cases to be anode-directed.

(3) The majority of the theoretical derivations indicate that the transport direction should be dependent on the sign of the charge carriers. These derivations therefore postulate the existence of a "hole wind"

in addition to the "electron wind".

(4) From the work of Brown and Barnett (1952) and Klemm's (1954) discussion of the pertinence of their conclusions as applied to the electrotransport problem, it appears that electrons in a metal which has a positive Hall coefficient show a negative e/m ratio when accelerated with respect to the lattice. Therefore, the overall electron-momentum transfer must be anode-directed in hole-conductors.

In discussing the possible explanation of this apparently paradoxical situation it is necessary to consider the results on positive Hall coefficient metals in some greater detail. Firstly, if it is postulated that in some metals the momentum transfer between the current carriers and the activated ions may be cathode-directed, then, either the electron-ion friction force is directed towards the anode and the field force exceeds the friction force, or both forces are directed towards the cathode. This means that in order to ascertain the presence of cathode-directed momentum transfer it is necessary to ensure that the effective charge evaluated from the experimental results exceeds the valence charge on the natural ion of the lattice. This has been found to be the case for metals such as iron (Wever, 1959) and cobalt (Ho, 1966). It should be stated in this connection that if the Bosvieux and Friedel theory is

correct, then any cathode-directed transport must result from the "hole wind".

Secondly, as discussed by Ho (1966), care is required in correlating the direction of mass transport with the sign of the Hall coefficient, especially in the case of metals with complicated electronic structures. Ho illustrated his argument by consideration of a two-band which was advanced as an approximation to the electronic structure of the conductors which had a positive Hall coefficient, yet exhibited mass motion in the direction of the anode. The Hall coefficient was accordingly written as:

$$R_H = \frac{-1}{|e|c} \cdot \frac{nu_n^2 - pu_p^2}{(nu_n^2 + pu_p^2)^2} \qquad (2.65)$$

where u_n is the mobility of electrons with density n and p referring to holes. A positive R_H would result if $pu_p^2 > nu_n^2$.

For electrotransport, the electron friction force, based on the two-band model, was generalised for comparison purposes in the form:

$$F_i = \frac{1}{2}e^2 EZ\frac{N}{N_d}\,(nu_n\rho_{de} - pu_p\rho_{dh}) \qquad (2.66)$$

Written in this form, the equation illustrates the dependence of the interaction force on the mobilities and also on defect resistivities which characterise respectively the interactions

of ions with electrons and holes. The values of these two resistivities could be quite different. Comparison of eqs. (2.65) and (2.66) shows that the contribution to F_i from the charge carriers varies as the product of the mobility and carrier density, whereas, for the Hall coefficient the square of the mobility is involved. Since, in general, the electron mobility is believed to exceed the hole mobility due to the larger effective mass of holes and, if ρ_{de} and ρ_{dh} were equal, it would result that a positive R_H would imply a negative F_i. In this case, therefore, the overall momentum exchange would be cathode-directed in agreement with the theoretical predictions. Variations in ρ_{de} and ρ_{dh} may, of course, alter this interdependence of R_H and F_i.

For the case of metals with a positive Hall coefficient and anode directed mass transport, it is necessary to consider the discrepancy which exists between this experimental result and the restrictions imposed by the Brown and Barnett experiments. A possible explanation was advanced by Wever and Seith (1955). These authors postulated that the defect electrons interact preferentially with the activated ions. Such preferential interaction would therefore allow a net transport toward the cathode while maintaining the overall electron-ion momentum transfer in the anode direction. This would be in agreement with the theretical treatments, since the majority

of authors have considered the interaction force on the activated ion or complex and have derived expressions in which the direction of this force is dependent on whether the current carriers were electrons or positive holes.

If this interpretation is correct then this concept should also be valid for metals which have a positive Hall coefficient and yet exhibit anode-directed transport. That is, these materials cannot justifiably be considered special cases to which the Brown and Barnett restriction is applicable. The explanation expounded by Ho, which would appear to be compatible with that of Wever and Seith, (1966) was that, in addition to the possible complexity of the resultant Hall coefficient and the interaction force, the activated ions acquire considerably greater momentum transfer from scattering the electrons than the holes, whereas the reverse holds for metals exhibiting cathode-directed transport.

For materials in which the transport is associated with the diffusion of foreign ions or interstitials, the situation is even more complicated due to the dependence of the sign of the interaction force on the relative magnitudes of the scattering cross-sections of the activated ions, natural ions, and average scattering cross-sections for charge carriers. This was previously discussed in section 2.1.2.

3. PREVIOUS EXPERIMENTAL WORK

Experimental investigations into electrotransport can be divided into several classes. These are:

1. Self-electrotransport in solid metals.
2. Electrotransport of interstitial solutes in solid metals.
3. Electrotransport of solid-solution components in metals.
4. Self-electrotransport in liquid metals.
5. Electrotransport of liquid-solution components in metals.
6. Electrotransport of metal impurities in semiconductors.

This report is primarily concerned with electrotransport in solid metals. No differentiation is between metals in bulk and thin film form. Although, at the time this project was commenced, a volume of literature existed on electrotransport in bulk metals, there were no published reports of similar studies on thin films; subsequently a small number of purely qualitative reports have appeared.

The last three groups on the above list, although outwith the present terms of reference, are of considerable practical importance. Many of the early investigations of electrotransport were concerned with liquid metals and alloys and in more recent years interest in this topic has been stimulated by the work of Haeffner (1953), illustrating the effectiveness of electrotransport as a means of separating isotopes. The

early work in this field was reviewed by Schwarz (1940) and the more recent work by Lodding (1961) and Verhoeven (1963).

The experimental investigations of electrotransport in semiconductors are of recent vintage, and have been reviewed by Verhoeven (1963). It appears that this work has been primarily concerned with the transport of metal impurities in elemental semiconductors. The more recent investigations have been conducted by Russian workers, and an extension of the Fiks theory (Fiks 1959(b)) used to analyse the results. Although this topic has received less attention than investigations of the phenomenon in other materials, the practical significance of electrotransport, in terms of its effect on the performance and reliability of semiconducting devices, should not be overlooked.

In the remainder of this section details will be presented of the previous experimental investigations into electrotransport in solid metals, precedence being given to the results relating to self-transport.

3.1 Experimental Techniques and Results

The two favoured techniques for following the motion of a migrating component in a solid involve the use of either inert markers, such as surface scratches or microhardness indentations,

or radioactive tracers. The former method has been widely used by investigators in Germany and the United States, whereas the latter method has been the main technique used by Soviet investigators. Radioisotope techniques have the advantage that the velocity of the migrating component can be measured directly.

In marker displacement studies, allowance must be made for possible changes in specimen dimensions which might influence the overall displacement of the markers. Also, the physical movement of the markers is in the opposite direction to the mass transport. If it is envisaged that a temperature gradient exists in the sample, then from a phenomenological viewpoint, the transport of mobile atoms across the hottest region causes a build-up of lattice planes in cool regions where they come to rest and a destruction of lattice planes in the cool region where they originated. As a result the markers fixed to the lattice travel in the direction opposite to the flow of charge carriers. In the majority of marker experiments the specimens used were in the form of bars, rods or tubes, normally held with clamps and supported so as to introduce the minimum of strain. The current passed through the specimens from regulated high-current, power supplies was associated with current densities of the order of 10^4 A/cm^2 and concomitant temperatures in the region of the melting points of the materials. The clamped ends of the specimens were frequently water-cooled. A number

of novel techniques were adopted to measure or estimate the temperature of the specimens without the measurement affecting the equilibrium conditions of the transport process.

In the experiments using radiotracers similar specimens and experimental set-ups were utilised. In some cases the tracer was applied to an area of the surface of the specimen and in others two ends of a specimen were coated with a radiotracer and subsequently butted together during the passage of current. In experiments in which the tracer was applied to the surface of the specimen, the transport was measured by comparing the initial and final position of the active zone. The activity distribution along the length of the specimen was measured by a counting system. In the second method, the initial position of the active zone was known accurately, and the final distribution determined by sectioning the specimen and measuring the activity distribution in the various sections. This latter method has some obvious disadvantages, but has one positive advantage in that the transport associated with volume diffusion effects is measured, whereas,when a surface tracer is used, allowance must be made for possible differences between the volume and surface diffusion coefficients. (This consideration also applies to marker motion studies). Another technique, similar in principle to the last technique described above, consisted of weighing the "anode" and "cathode" halves

of a rod which were butted together during the experiment. Thus, the mass transferred was measured directly.

In the remainder of this section, the work of particular authors, or groups of investigators, on self-electrotransport in solid metals is reviewed, together with less detailed consideration of previous work on interstitial and alloy transport in metal systems.

3.1.1 The Work of Wever

In 1955 Wever and Seith conducted an experiment on marker motion in the Al-Cu system, which showed that mass transport of both constituents took place towards the anode in the β-phase (which is an electron conductor), but that the direction of transport was reversed in the γ-phase, where the current is carried by holes. This experiment strongly supports the concept of momentum transfer from the charge carriers to the diffusing ions, and could be regarded as the starting point of the controversy concerning the dependence of the inertial properties of the electrons on the sign of the effective mass.

In subsequent experiments Wever (1956, 1959) investigated electrotransport in copper, nickel and iron by measuring

the separation of microhardness indentations in rods carrying current densities of $2 \times 10^4 A/cm^2$. In reporting his data he used an expression for the transport number

$$TN = \frac{D^*}{fkT} FN \rho e(Z + z) \qquad (3.1)$$

From eqs. (2.11) and (2.14) this can be written

$$TN = \frac{D^*}{fkT} FN \rho eZ^o \qquad (3.2)$$

Thus, the quantity $(Z + z)$ is equal to the effective valence Z^o as defined by eq. (2.13)

$$Z^o = F_i/eE \qquad (3.3)$$

Consequently, the effective valence is the ratio of the actual force exerted on an ion to the field force on an ion having a true valence of +1. Movement in the direction of the anode would be associated with a negative effective valence. Hence, although Wever had not developed a theory which interpreted the effective valence force in terms of an electron:ion momentum exchange, the determination of the effective valence itself, which is the initial step in all such calculations, is consistent with the approach of other authors.

The results of Wever's experiments at particular temperatures are included in Table 3.1. This table is an updated version of that presented by Lodding (1965) and in it the defect resistivity etc. are evaluated from Wever's

TABLE 3.1 SELF-TRANSPORT PARAMETERS IN METALS ACCORDING TO RESULTS IN DIFFERENT LABORATORIES*

Metal	Reference	$-TN \times 10^9$ (mole/F)		$D \times 10^9$ (cm^2/sec)	
		0.90	0.95	0.90	0.95
Gold	Huntington and Grone (1961)	16.4	32.8	2.0	6.2
	Kuz'menko and Grom (1961)	90.0			
Silver	Ho and Huntington (1966)	33	42	0.43	2.9
	Kuz'menko and Khar'kov (1958)	34	91		
Copper	Wever (1956)	+2.5	-3	0.83	2.4
	Grone (1961)	4.5	~0		
	Khar'kov and Kuz'menko (1960)	18	56		
	Sullivan (1967b)	4.4	9.5		
Platinum	Huntington and Ho (1963)	-1.4	-4.9	0.20	0.78
Nickel	Wever (1959)	8.4	20	0.56	1.72
Iron	Wever (1959)	-69	-94	0.5	1.1
Indium	Lodding (1965)	2.76	8.90	0.078	0.282
Aluminium	Penney (1964)	39	72	2.1	6.8
	Kuz'menko and Khar'kov (1959a)	43			
Zinc	Kuz'menko and Khar'kov (1959a)	26.6		2.2	
Cadmium	Kuz'menko and Khar'kov (1959a)	14.4		1.2	
Tin	Lodding (1965)	3.4	5.6	0.005	0.021
	Kuz'menko and Kharkov (1959a)	3.2			
Lead	Khar'kov and Kuz'menko (1960)	9.2	32	0.04	0.13
Cobalt	Ho (1966)	-1.2	-3.8		
Sodium	Sullivan (1967a)	1100	3000		

* The transport number TN denotes the fractional molar number of ions flowing towards the cathode for every Faraday of charge through the specimen. The "defect resistivity" $\Delta\rho_d N/N_d$ is computed using $\alpha=1/3$, and $m^*/|m^*|=+1$, except for Fe and Co, where the negative value is taken.

TABLE 3.1

$\rho \times 10^6$ Ω		Z (assumed)	$-Z°$		$\Delta\rho_d N/N_d \times 10^6$ (Ω-cm/%def.)	
0.90	0.95		0.90	0.95	0.90	0.95 T/Tm
9.9	10.4	1	6.6	5.5	1.5	1.3
			32		6.5	
7.0	7.4	1	25.5	24.0	3.3	3.4
			27	16.5	3.9	2.6
8.1	8.5	1	+2.5	-1.5	0.5	-0.1
			4.5	~0	0.9	0.2
			18	22	2.9	3.7
			4.7	7.5	1.0	1.4
61.3	64.7	0.55	-0.28	-0.32	0.60	0.55
58	60	0.6	1.9	1.6	4.8	4.4
126	133	0.2	-9.5	-6	117	77
13.6	15.1	3	10.2	9.2	1.20	1.22
9.6	10.3	3	11.2	6.3	0.91	0.64
			12.4		0.98	
13.5		2	4		0.8	
13.8		2	5.5		1.0	
20	21	4	160	72	16.3	8.0
			151		15.5	
40.1	40.3	4	46	45	10.1	9.9
		0.6	-1.4	-2.6	2.2	4.5
		1	1.95	3.19	0.38	0.54

results on the basis of Huntington's theory.

Wever found that in copper the direction of migration reversed from anode to cathode at a temperature between 900 and 1000°C. Although this unusual result could be attributed to a relative decrease in the electron/ion friction force with increasing temperature, it does not justify detailed consideration since the recent experiments of Sullivan (1967b) on high-purity copper have shown that, under carefully controlled conditions, the transport is undirectional throughout this temperature range. For nickel, which is predominantly n-conducting, the transport was anode directed with the friction force slightly larger than the field force. In the case of iron a large cathode directed force was obtained. Even allowing for the absence of screening effects, and thus taking the valence of the metal ions as the true valence of iron (+4), the net force is ten times larger than the field force. Iron is predominantly p-conducting and it would therefore appear that the considerable cathode-directed force received by the iron atoms is associated with preferential momentum transfer from the defect electrons to the activated complex.

3.1.2. The Work of Huntington and Associates

Electrotransport experiments on a large number of metals have been conducted by a group under the direction of H.B. Huntington at the Rensselaer Polytechnic Institute, New York. Without exception, the experiments on solid metals have involved the measurement of marker movements, usually scratches, on the surface of the metal. In these investigations, experimental and theoretical techniques have been evolved to account for other factors which may introduce changes in specimen dimensions other than those resulting from transport. For example, the effects of thermal transport at temperature gradients (Sôret effect) creep under surface tension, gravitational sag and void formation are all accounted for in the more sophisticated experiments. In addition special experimental techniques were developed in which the stresses imposed on the specimen undergoing transport by its physical environment were reduced to a minimum. Novel methods of temperature monitoring and measurement were used in which it was not necessary to attach thermocouples directly to the specimen in order to perform the measurement. The experiments were normally performed in containers which allowed the control of the atmosphere around the specimen and thus prevented oxidation and surface evaporation which could have adversely affect the distinctness of the marker scratches.

In the following paragraphs details are given of typical experiments on electrotransport reported by this group of investigators.

The first reported experiment (Huntington and Grone, 1961) was concerned with electrotransport in gold wires. Water-cooled clamps were used to support the wire and act as current connections. One clamp floated on mercury to prevent the development of longitudinal stress. The experiment was conducted inside a container under a positive pressure of argon gas. The wire undergoing transport was viewed through a glass plate in the lid of the container and the position of the micro-scratches on the surface followed by use of a comparator microscope accurate to within one micron. The markers at the cold ends of the specimen were not subjected to transport and provided the frame of reference for the measurements.

Similar apparatus was used for the experiments on other metals. However, the degree of complexity of the experiments, in relation to the preparation of the specimen and its environment was, of necessity, dependent on the metal investigated. For example, on measurements on gold and indium (Lodding, 1965) the gaseous environment had no significant influence on the transport process, whereas for copper (Sullivan, 1967b) a highly purified argon

atmosphere was used to prevent oxidation of the specimen. For the case of sodium (Sullivan, 1967a), the experiments were more complex, since, in order to avoid oxidation effects, special specimen handling techniques were required; for this metal the transport experiments were conducted under vacuum.

One major problem in this type of experiment is the provision of a high-current, regulated, power supply. For measurements on solid specimens such as were typically used by previous authors, currents of the order of 1500A were required in order to achieve current densities in excess of 10^4A/cm^2. Huntington, in his initial experiments, used cascade configurations of Sola transformers in conjunction with a bridge-rectifier system. The temperature stability obtainable with this supply was ±15°C. In later experiments a feed-back regulation system using photosensitive resistors was added, which reduced the temperature fluctuations to ±5°C.

In the measurements on gold, the temperature was measured directly by an optical pyrometer calibrated for the surface of gold wire by previous observation of a similar specimen to which a thermocouple was attached. Extension of the calibration to the melting point of gold provided a means of determining possible errors in the calibration. The temperature accuracy in these first experiments was ±10°C. By attaching a thermocouple to a second gold

wire, identical to the first, and connected in series with it, a continuous record of the temperature was obtained. In later measurements on other metals, a photosensitive resistor was incorporated in the eyepiece of the microscope allowing the accurate determination of the temperature over selected small areas of the specimen.

In some experiments completely different methods were used to evaluate the temperature. For example, Sullivan (1967b) for copper electrotransport, determined the temperature by measuring the thermal expansion of a number of adjoining sections of the specimen and fitting the data by computer to a parabolic temperature distribution. Using a more direct approach Lodding (1965), in his experiments on indium, measured the temperature directly by inserting a thermocouple into the bulk of the specimen and, at the completion of the experiment, calibrated the thermocouple by heating the specimen to the melting point. In experiments conducted on tubular silver (Ho and Huntington, 1966) and aluminium (Penney, 1964) samples, the temperature was monitored by a thermocouple positioned inside the tube.

The duration of the experiments depended on the type of material being investigated and varied from one day to one week.

The Effects of the Temperature Distribution in Solid Specimens

As remarked previously, the passage of current through a solid metal specimen of sufficient magnitude to raise the temperature of the centre section to within a few percent of the melting point can result in the occurrence of several other effects in addition to electrotransport.

Principal among these is the Sôret effect, which is the thermal transport of material taking place in those regions of the specimen where a temperature gradient exists. In the transport of ions resulting from the Soret effect diffusion can occur either "up" or "down" the thermal gradient depending on the particular material investigated. Thus, under a.c. conditions, if the displacements of the surface markers from their original position were plotted along the length of the specimen, then their distribution about the centre line would be asymmetrical with maxima in the region of maximum temperature gradient and

zero displacement in regions of uniform temperature. On the other hand, for a specimen undergoing electrotransport in the absence of the Sôret effect, the distribution of markers would be symmetrical about the centre line of the specimen. It is therefore possible to separate these two effects by conducting two experiments, one under d.c. conditions, and the other under a.c. From the latter, the distribution attributable to the Sôret effect alone could be determined and subtracted from the composite d.c. result to give the distribution resulting from electrotransport.

Unfortunately, there are several other effects which can contribute to the overall marker distribution. These are (a) creep, (b) sagging or twisting, (c) specimen elongation or contraction, (d) Thomson effect.

(a) Wires of most metals, when held at high temperatures, are found to contract under the influence of surface tension. For a specimen with one end unconstrained this also produces an antisymmetrical marker distribution, with the greatest slope in the middle.

(b) As the specimen sags under its own weight, the horizontal coordinates, viz. the distances between markers, change, usually showing an apparent contraction. Due to faulty clamp alignment, this effect can combine with twisting in both the horizontal and vertical plane, and can result in

a more irregular "creep profile.

(c) Under constant temperature, and in the absence of the above effects, the reason for any observed contraction must be evaluated in terms of structural changes, such as annealing or disappearance of voids or absorption of impurities. Another possible cause might be the collapse or building-up of a macrodefect at a particular position in the specimen.

(d) In a material with a high Thomson coefficient it is possible for the position of the temperature maximum to become displaced from the centre line of the specimen.

The above considerations serve to indicate that the interpretation of marker displacements in a solid material can involve a number of factors which may significantly influence the overall shape of the distribution. Attempts to extract the displacement associated with electrotransport from such a resultant distribution can prove to be a complex procedure.

As discussed above, the effects of thermal transfer can be accounted for by conducting an experiment under identical temperature conditions using a.c. current.

The effects of creep under surface tension are normally determined empirically from the known temperature distribution and activation energy for creep (often taken as the value for self-diffusion), normalised to give the correct observed relative displacement between the cold ends of

sample, and applied to the individual marker displacements over the remainder of the sample length. If creep occurs, the correction would, of course, be necessary under both d.c. and a.c. conditions.

The correction for specimen sag can normally be readily estimated from the vertical change in the focus position of the microscope.

Contraction of the specimen may also be attributable to annealing of voids as stated in (d) above. This may be difficult to separate from the other effects producing specimen contraction. Conversely, elongation is frequently associated with the formation of voids, perhaps due to the agglomeration of migrating vacancies, or possible interstitial transport of ambient gas atoms absorbed by the material. In any event, the correction factor applicable here is difficult to assess.

The Thomson shift can be calculated for the particular material from the known temperature gradient and the Thomson coefficient, if known.

By good experimental design the number of correction factors which require consideration can be reduced and in some fortuitous cases no correction factors at all need be applied. For the case of gold wires, it was found that a satisfactory estimate of the electrotransport velocity could be obtained from the experimental data without the necessity of incorporating any correction factors, and for transport in indium

Lėdding (1965) found that it was only necessary to take specimen elongation into account. In contrast, the processing of data from experiments on platinum required the application of correction factors for thermal transport, creep and Thomson heating.

It should be stated that the experiments of Huntington and his associates are the first in which quantitative correction has been made for these effects. It is, of course, correct that, in an experimental technique which requires the incorporation of several such correction factors, the accuracy of the transport velocity measurement is reduced.

Strain Effects

In a previous section it was indicated that the transport velocity estimated from the linear movement of inert markers, v_m, is not a direct measurement of the ion velocity, v_i, due to possible changes in specimen dimensions resulting from mass transport. Penney (1964) presented a detailed evaluation of the motion of scratches on the surface of a material in terms of the dilatation resulting from mass flow. He showed that the ratio of longitudinal strain to lateral strain, m, could be related to the "drift" velocity of the atom flux by the expression

$$v_m = -\frac{m}{m+2} v_i \qquad (3.4)$$

In Huntington's (1960) notation,

$$\alpha = \frac{m}{m+2}$$

Thus, if transport caused isotropic changes in specimen dimensions then a value of $\alpha = 1/3$ is obtained.

Penney also showed that the value of "m" would depend on the specimen shape and would be expected to exceed unity if the shape of the specimen constrained the lateral movement, and would be less than unity if the surface were important as a source or sink of defects responsible for the mass transport. He considered the conditions under which plastic flow might be expected to be induced by the strains resulting from mass transport.

Subsequent authors have widely applied these considerations in their selection of specimen dimensions in order to permit analysis of the results in terms of isotropic dimension changes.

Huntington has pointed out that the value of "m" should also depend on whether voids are formed. These theoretical discussions were subsequently developed by Ho and Huntington (1966) in the analysis of mass transport and void formation in silver. It was shown, from measurements on silver tubes, that the dimension changes were indeed isotropic and that void formation resulted directly from the electromigration process.

Analysis of Experimental Results

In the analysis of experimental results Huntington et al. normally presented their data as a plot of $\ln v_m/j$ as a function of

inverse temperature. Equation (2.11) can be rewritten in the form

$$\frac{v_m}{j} = -\alpha \frac{D_i}{fk} \frac{\rho}{T} eZ^o \qquad (3.5)$$

taking into account the sign and proportionality dependence of the marker velocity, v_m, on the true ion velocity, v_i. Here again, j is the current density. Frequently this plot resulted in a straight line, the slope of which was interpreted as the activation energy for mass transport. The value obtained was normally of the same order as the activation energy for self diffusion in the metal.

Since the resistivity of a metal is generally a linear function of temperature, the factor ρ/T in eq.(3.5) should be temperature independent; and since Z^o decreases slowly with temperature, due to the occurrence of the lattice resistivity in the expression for the electron-friction force, one would expect the temperature variation of v_m/j to be slightly less than the temperature variation of the self-diffusion coefficient. In agreement with this prediction, the transport activation energies were slightly less than those associated with self-diffusion for gold, silver, aluminium and sodium. The values for cobalt, indium and platinum were found to be up to 12% higher than those determined from self-diffusion. In this connection it should be pointed out that the Huntington theory was derived for a monovalent metal.

The next step in the analysis consisted of the evaluation of the effective charge of the migrating ions. It is not possible from marker measurement experiments to determine the self-diffusion coefficients of the metal. (In comparison, another advantage of radiotracer measurements is that, in addition to the determination of the transport velocity from the overall shift of the active region, the self-diffusion coefficient can readily be determined from the spread of the activity distribution). Using eq. (3.5) the effective charge or effective valence $Z^{o}e$, was evaluated using available values for the self-diffusion coefficient at particular temperatures. The values of the effective charge obtained at two temperatures are shown in Table 3.1. The majority of metals investigated were electron conductors and the effective charge is shown to be many times greater than the true valence of the ion. As expected for these metals, the direction of transport was in agreement with the concept of momentum exchange between the electrons and the activated scattering complex. There were two exceptions to this; both are discussed in some detail below.

Considering the dependence of the effective charge on temperature, for the metals gold, silver, and aluminium the effective charge decreased slowly with increasing temperature, in agreement with the theory discussed in the preceding paragraph,

whereas, for cobalt and platinum, the opposite dependence was obtained. For the case of copper, sodium and indium the results were inconclusive.

From Huntingtons theory, if values can be given to $\bar{Z}$ and $m^*/|m^*|$, then it is possible to solve eq. (2.59) for $\Delta\rho_d \, N/N_d$. Theoretically, this quantity, described as the "specific resistivity" or "defect resistivity" should be insensitive to temperature. It is therefore possible to obtain some estimation of the validity of the theory as applied to a particular metal in terms of this criterion. In the early experiments on copper and gold $\bar{Z}$ was taken as unity, and in later experiments on other metals the values were based on the work of other investigators, eg. X-ray studies. It was found that the specific-resistivity of the activated complex in gold, silver, aluminium, indium, cobalt and sodium was virtually temperature independent, whereas a slight monotonic decrease was obtained for copper and platinum.

As stated above, the results of Huntington's investigations on a number of metals (Au, Ag, Cu, In, Al) which are accepted to be electron conductors, have shown that the effective charge of the migrating ion is larger, generally by at least an order of magnitude, than that of the electronic charge. This indicates that the electron wind force in these metals is greater than the electrostatic force. In other words, the scattering of the

conduction electrons with the defect associated with diffusion, is mainly responsible for electrotransport.

The results on copper, platinum, cobalt and sodium show some interesting and unique features and merit further discussion.

Grone's (1961) experiments on copper appeared to confirm the presence of an anamolous reversal in the transport direction at temperatures between 900 and 1000°C, as first reported by Wever. There was, however, considerable scatter in the data derived from the Grone's experiments. This author also stated that photomicrographic analysis revealed the presence of pore formation in the specimens; this was not sufficient, however, to result in detectable specimen elongation. Sullivan (1967b) recently conducted a more elaborate and better controlled experiment on copper which failed to reveal the presence of a reversal in the electrotransport. Kuz'menko (1962) using a radiotracer method also failed to observe this reversal. The results obtained by these two latter authors for copper were commensurate, in terms of relative values and temperature dependence of the various parameters, to those reported for the other noble metals. Sullivan concluded there was no intrinsic reversal, or even reduction in the rate of increase of marker velocity, as the temperature was raised. Although the reversal observed by the previous authors has not yet

been satisfactorily explained, Sullivan advanced two tentative explanations. Firstly, the presence of impurities in the metal could be reflected in a complex dependence of the transport direction on temperature. Secondly, if considerable void formation did occur on the cathode side of the hot centre, and if this was balanced by contraction due to surface tension, the markers near the centre could appear to be moving away from the cathode, while all the others might still move toward it.

Huntington and Ho (1963), in experiments on platinum, found the mass transport was in the direction of the anode. The algebraic sign of the effective mass, m^*, was taken as positive on the basis of the negative Hall coefficient. This gave a negative sign to the effective charge, Z^o, which was found to be of the same order as the valence charge, assumed to be 0.55 (Mott and Jones, 1958). This implied that the electrostatic field force out-balanced the effect of the electron wind and the hole wind was negligible. Therefore, for this metal, the straightforward electrostatic force is dominant.

For cobalt, a hole conductor, Ho (1960) also found transport in the direction of the anode. In this case, however, the effective charge was calculated to exceed the valence charge. It was , therefore, concluded that the hole wind force,

resulting from the interaction of holes with the migrating ions, was at least 1.5 times greater than the electrostatic force and was in the direction of hole flow. Ho postulated, under the assumption of mixed electronic conduction in cobalt, the presence of a compensating electron wind force acting in the opposite direction. Thus, the true hole wind force may have been much larger than the value derived from the results, as the analysis only permits the evaluation of the resultant interaction force.

In the most recent paper on work conducted at the Rensslaer Institute, Sullivan (1967a) performed measurements on sodium. In these experiments considerable effort was devoted to the preservation of sample purity. In agreement with theory, the activation energy for mass transport was comparable with the value obtained from self-diffusion experiments and the variation of the defect resistivity with temperature was negligible. However, when the values of the defect resistivity were compared with values of an analagous parameter derived from measurements of melting-point vacancy concentrations, a discrepancy of a factor of ten was found in the results. Since the quantity measured in electrotransport experiments was not the true vacancy resistivity, but the resistivity due to scattering from the ions in the saddle point, it appeared that this quantity should have been larger than the resistivity of a simple vacant lattice site, since

the scattering at activated centres is more analagous to an interstititial process. Sullivan therefore considered the experimental results to demonstrate a weakness in the Huntington theory.

The factor 1/2 in the electron wind term is derived for the case where the momentum exchange between the ion and the electron wind depends on position in a sinusoidal manner, with a maximum at the saddle-point and zero at the lattice site. This would appear to be a satisfactory model for an f.c.c. metal where the saddle-point is relatively simple, having a single potential-energy maximum. However, as Sullivan remarked, in b.c.c. metals, the jumping ion must pass through two close-neighbour configurations which consist of six atoms in the formation of a pair of equilateral triangles, and this might require the consideration of the effects of a potential "minimum" at the actual midpoint. The hypothesis was advanced that this could in some manner result in the momentum transferred from the electrons to the ions having a reduced contribution to the net mass transport. This problem may be resolved by detailed calculation of b.c.c. saddle-point energies.

3.1.3 The Work of Kuz'menko and Khar'kov

Kuz'menko and his co-workers have studied self-transport

in a number of metals.

Electrotransport was studied in silver and zinc using either a radioactive tracer or a weighing technique (Kuz'menko and Khar'kov, 1958, 1959a; Khar'kov and Kuz'menko, 1960) and in cadmium, (Kuz'menko and Khar'kov, 1959a) aluminium, (Kuz'menko and Khar'kov, 1956) copper, lead, tin (Khar'kov and Kuz'menko, 1960) and gold (Kuz'menko and Grom, 1961) using a weighing technique.

In the radiotracer experiments an isotope of the metal was electroplated on the end faces of two rods, which were subsequently butted together during the passage of current. After completion of the experiment the rod was broken at the original joint and the activity distribution on either side of this line measured by a sectioning and counting technique similar to that employed in conventional tracer-diffusion experiments. In the weighing technique the mass transported was evaluated directly by weighing the cathode and anode halves of the rod before and after the experiment.

In this form of experiment, the reference point relative to which the mass-transport is measured is provided by the line joining the two sections of the specimen.

Comparison of Transport Velocities Obtained from Inert Marker and Radioactive Isotope Studies

An important distinction must be made between the evaluation of results obtained from inert marker and radiotracer experiments. In the latter the velocity of the transported ions is measured directly. It is envisaged that, as in the marker experiments, the passage of current elevates the temperature in the centre zone of the specimen while the ends remain at a considerably reduced temperature at which no appreciable electro-transport can take place. In marker experiments the reference points are provided by indentations in these cold regions. However, for tracer experiments conducted under the same conditions, it is necessary to have a "lattice" marker located in the hot zone. This requirement arises from considerations of the displacement of the region of the lattice in the high temperature zone. As discussed previously, the lattice comprising the hot zone is effectively displaced in the opposite direction to the ion migration - it is this oppositely-directed transport which is measured by inert markers positioned in the hot zone. Since the radioactive isotope ions participate in the migration process, and therefore move in the direction of transport, it results that, if the displacement of the active zone is measured with respect to either the cold ends of the specimen or

markers positioned in these regions, the associated transport velocity, v_t, will be the difference between the ion and "lattice" velocities. (In this context, the "lattice velocity" is defined as the velocity of an inert marker positioned in a uniform high-temperature zone and measured with respect to the cold ends of the specimens). In the absence of changes in specimen dimensions, the limiting case results where the resultant transport velocity would be zero. For isotropic dimensional changes where, as discussed previously, the marker velocity can be taken as one-third of the ion velocity, the resultant transport velocity be 33% smaller than the correct value.

This problem can be overcome, and the true ion velocity measured, by the simple expedient of measuring the displacement of the active region with respect to an inert marker positioned in the hot zone, e.g. in Kuz'menko's experiments the join between the two sections of the specimen.

For the case of experiments on interstitial transport, the error introduced by measuring the active-ion velocity with respect to the cold ends of the specimen may be significantly reduced if the transport velocity of the interstitial is considerably

greater than the self-transport velocity of the lattice ions. Similarly, this would apply to transport in alloy systems if the transport velocity of the solute greatly exceeded that of the solvent. (This reference system was used by Kalinovich (1956) in his investigations of interstitial and alloy electrotransport).

Kuz'menko reduced data obtained from his experiments to give the velocity of transport and, in common with the majority of investigators, used the correlated Einstein equation (eq. 2.11) to determine the effective valence. Typical results are contained in Table 3.1. It can be seen from the sign of the effective valence that all the metals investigated, migrated toward the anode. As discussed above, no reversal was found in the direction of migration of copper at 1000°C. Also, the transport parameters derived for a number of metals are not in good agreement with those reported by other authors. These discrepancies are not understood, although they may be attributable to differences in method.

With relevance to the previous discussion of the validity of the hole wind concept, it is interesting to note that the metals zinc, cadmium, and tin, which have been reported to have a positive Hall coefficient, were transported to the anode.

Kuz'menko made a particular study of the effect of current density on the velocity of migration. For cadmium and zinc the current density was varied by a factor of 10-15 and for silver, tin and lead by a factor of 5-8. In all cases the ion velocity varied linearly with current density within the limits of experimental error. Hence, it appears that the effective valence is not a function of field strength.

In determinations of the activation energy for electrotransport, as evaluated from the temperature dependence of the transport velocity, the values obtained by Kuz'menko were also less than the self-diffusion activation energies. The temperature dependence of the effective charge for the various metals was qualitatively similar to that found by previous authors.

As discussed in section 2.1.2.1 Kuz'menko developed a method of evaluating the activated scattering cross-section A^*, and the true valence Z, of the activated ion. For silver the average value of A^* in the temperature range 675 to 900°C was calculated as 3.6×10^{-16} cm^2 and the true valence as 0.86. (As shown in Table 3.1, the

effective charge Z^o on the silver ion was of the order of -25). For the other metals investigated the true values ranged from 0.62 for zinc to 4.1 for tin.

3.1.4 Electrotransport of Interstitial Solutes and Solid Solution Components

To complete this section the experimental results on electrotransport of interstitials and alloy components are briefly discussed.

Interstitial Transport

In interstitial electrotransport it is commonly found that the migration velocity of the interstitial is many times greater than the velocity of the host lattice ions. Thus, no restrictions are placed on the choice of reference system and also measurable result is obtained from experiments of relatively short duration. There have been several reviews of the experimental work on interstitial transport. (Seith, 1955; Heumann, 1959; Frantsevich et al, 1959; Kalinovich, 1961, Verhoeven, 1963). Some of the representative results are presented below.

In investigations of the transport of nitrogen in γ-iron (Seith and Daur, 1938) and oxygen in β-titanium (Claisse and Koenig, 1956) and zirconium (deBoer and Fast, 1940), the interstitial element was transported to the anode.

Doubt exists as to whether the electrostatic field force or the electron friction force predominated in these cases. If the electron friction force was assumed to be cathode-directed because of the defect-electron conduction in these metals, then the interstitial ions would require to be present as negative ions.

From early experiments on transport of hydrogen in palladium, (Coehn and Specht, 1930; Wagner and Heller, 1940) it was shown that hydrogen migrated to the anode. The presence of hydrogen as a positive ion would be associated with a cathode directed field-force. Since palladium is predominantly n-conducting the electron friction force would be anode-directed and it would therefore seem reasonable to conclude that the electrostatic field force was predominant. More recent data published on oxygen transport in yttrium (Williams and Huffine, 1961), an electron conductor, showed transport in the anode direction.

The electrotransport of interstitial carbon in iron has been extensively studied in recent years by radiotracer techniques. For the diffusion of carbon in Fe-Cr, Fe-Ni, Fe-Mn, Fe-Si, Ni and Ni-Cr (Babikova and Gruzin, 1957, Gruzin et al., 1957) and in γ-iron (Frantsevich, 1957; Frantsevich et al, 1958, 1959) the transport was cathode-directed. Although the majority of these results were

analysed without consideration of the electron friction force, much of the data was subsequently reanalysed by Kalinovich (1961) in terms of the effective valence model. In γ-iron the temperature dependence of the effective charge was commensurate with the results of self-transport experiments. The effective charge varied from +13.4 at 950°C to +8.1 at 1150°C. A charge of this magnitude is indicative of a cathode-directed force in addition to the field force, since it is improbable that the carbon atom is ionised $>$ +4. This could be considered as resulting from momentum transfer of the defect electrons in p-conducting iron. Frantsevich and Kovensky (1958, 1961b) also conducted in experiments on carbon transport in iron, nickel, cobalt, titanium, tantalum, and tungsten. In addition to the measurement of transport velocities the experimental technique used by these authors allowed the evaluation of the diffusion coefficient of C^{14} in these metals from the spread of an active zone deposited on the iron wire. The data was analysed in terms of the Fiks theory and, as previously discussed, the true valence of the carbon ion was determined by analysing the concentration-dependence of the resistivity and effective charge in terms of expressions derived from this theory.

Electrotransport of Alloy Components

During electrotransport in solid-solution metallic phases a relative transport of both components occurs. Consequently,

in general, transport numbers or effective mobilities determined with respect to a fixed reference system are a measure of relative movement. Such parameters are related to a differential mobility or transport number. Exceptions to this are alloys in which the transport velocity of one component is significantly different from the other, or experiments in which a localised alloy region is created by the deposition of a radioactive layer of the solute, and where it is assumed that the transport of the solvent can be measured by inert markers positioned in the hot zone. Some of the more interesting results are discussed below.

Seith and Wever (1953), in investigations of the copper-aluminium system found that in going from the beta to the gamma phase, the conduction mechanism changed from n-to p-type, and concomitantly the direction of aluminium transport changed from anode to cathode. In the copper-tin and silver-zinc systems the same correlation was found across a phase change. This evidence supports Wever's hypothesis of cathode-directed momentum transfer between defect electrons and activated ions.

A considerable amount of investigation into electrotransport in alloy systems has been conducted by Soviet workers. These experiments utilised radiotracer techniques and , in

addition to electrotransport velocities, the diffusion coefficients of the active component were normally evaluated from these measurements (Kuz'menko, 1962).

Frantsevich and co-workers used the technique of following the movement of a radioactive zone deposited onto a wire of the alloy under study. A variety of alloys including Ni-Cr, Mo-Cr, Ni-W, Fe-W, Cr-Fe, Mo-Fe and Co-W were studied. These authors found the temperature-dependence of the effective valence to be consistent with the results of interstitial and self-transport experiments. Both anode- and cathode-directed transport was found. In the work on nickel-chromium (Kalinovich et al., 1960) surface electrotransport was investigated. The authors conducted experiments in which successive surface layers were removed from wire specimens following transport. They claimed that the surface transport was greater than the volume transport by a factor of four. This could be associated with a higher surface diffusion coefficient.

Frantsevich et al. used theoretical treatment discussed previously to evaluate the true valence of the migrating component for the molybdenum-tungsten and nickel-chromium systems by measuring the concentration-dependence of the effective charge, Z_i^o, and the resistivity. For low concentrations of migrating molybdenum or chromium and high

concentrations of migrating tungsten or nickel a large negative valence was associated with the migrating ion. The concept of the "electron gas" requires that the average metal ion be positively charged, therefore suggesting that this negative charge can only apply to the ion in its activated position. The "true" valence of activated molybdenum was found to change from -4.7 to +2.4 in going from 75 to 25 at.% molybdenum in tungsten.

The experimental technique used by Kuz'menko's group for the study of electrotransport in alloys was identical to that described for investigations of self-transport. The systems investigated included Fe-Al (Khar'kov and Kuz'menko, 1959), Al-Zn (Kuz'menko and Ostrovsky, 1961) and Cu-Sn (Kuz'menko et al., 1962). The authors again used a revised form of eq.(2.11) to calculate the effective valence, and the true valence was derived by the method described previously (section 2.1.2.1). This true charge was interpreted as being the charge experienced by a conduction electron in the vicinity of an activated ion. From the Fiks theory and data on residual resistance the true charge on the non-activated ion was calculated (Kuz'menko, 1961). This charge was found to be greater than that of the activated ions. This was attributed to possible screening of these ions. The experimentally determined values of the effective charge Z_i^o varied from -0.6 for a Zn-50 at%

Ag alloy to -51 for a Cu-0.1 at % Sn alloy. The estimated true valence charges, Z, ranged from 1.1 to 1.4. The transport was found to be anode-directed for all alloys with the exception of aluminium migration in Fe—23-40 at% Al alloys. In measurements over the temperature range 1000-1300°C this component was transported to the cathode. No conclusions were drawn from this result at the experimental results were not considered sufficiently reliable to justify calculation of the effective charge.

3.1.5 Electrotransport in Thin Metal Films

As the experimental work to be described in this report was principally concerned with electrotransport in thin films, it is in order to review this aspect of electrotransport in metals.

As remarked in the introduction to this section, this topic has been almost completely neglected by workers in the field, and to date the only reports of electrotransport in thin films have originated from investigations into the failure of microelectronic components. In such applications thin metals films are widely used as resistive and capacitive components and also as connectors. Due to the physical nature of thin film conductors the applied current densities can be considerably greater than in the corresponding bulk material; concomitantly the effects of electrotransport

may be more pronounced and may become manifest over shorter periods of operation.

The three recently published papers on this topic adopt a phenomenological approach and the results are discussed in a qualitative manner.

Berry et al. (1966) observed electrotransport effects when passing currents of unstated magnitude through tantalum nitride thin film resistors undergoing accelerated life tests. These resistors had complex terminations of 60-40% Sn-Pb and 50-50% Sn-In over nichrome plus copper plus palladium. In the majority of cases tin whiskers were formed at the anode and occasionally lead whiskers grew at the cathode. The growth took from seconds to hours to appear. The authors considered the effects to be due to the separation of the tin-lead eutectic with the formation of crystals and filaments resulting from preferential nucleation and growth at a pore in the constraining oxide film protecting the resistor.

Mutter (1967) and Ghate (1967) conducted electrotransport experiments on thin-film aluminium resistors. The current densities used ranged from 5×10^5 to 2×10^6 A/cm^2 (between 25 and 100 times greater than have been able to be applied to bulk metals). The resistors attained temperatures of

between 170 and 200°C. It was observed that mass was transported in the anode direction and the resistors developed physical breaks toward the cathode end. This transport direction is in agreement with Penney's (1964) results on bulk aluminium. Ghate extrapolated Penney's data to the level of current density used in his experiments and estimated a vacancy flux of 2.5×10^{11} vacancies/cm^2-sec. toward the cathode. The smaller diameter of the grains in a metal film as compared with the bulk was advanced as an argument in favour of a higher vacancy source concentration in a thin film, and therefore it was concluded that the rate of electromigration per unit current density would be greater. The explanation of the physical breakdown of the film was also considered in terms of the large number of grain boundaries, in this case providing nucleation centres for voids. The time to achieve breakdown was between three and ten hours. Mutter correlated his results with self-diffusion effects at low temperatures and electrotransport effects at higher temperatures. Neither author reported the effects on transport of temperature gradients along the length of the resistor.

It therefore appears that investigations of electrotransport in thin metal films are still at a rudimentary stage. However, it is considered that this preliminary work indicates that fruitful results may be obtained from investi-

gations on such systems and may be particularly valuable in permitting a deeper understanding of vacancy kinetics. Electrotransport effects have been demonstrated to deleteriously affect the reliability of thin film components. Experiments to further elucidate these effects in thin film materials may be of practical importance in influencing the design and operation of integrated circuits and thin film components.

4. EXPERIMENTAL PROGRAMME

In the experimental investigations into electrotransport it was decided to study the migration of diffusing ions by a radioactive tracer technique. As discussed previously, this technique possesses advantages over marker motion experiments, since the electrotransport of the migrating ions can be measured directly, and, if required, information on diffusion coefficients can also be extracted from the activity distribution. (Although it is theoretically feasible to relate the movement of inert markers to the diffusion coefficient, in electrotransport studies, the data obtained from such measurements has not been used for this purpose.)

The factors which influenced the design of the apparatus, and to some extent the materials to be investigated, are discussed below.

Firstly, it was decided to deposit the tracers to be studied in thin film form using conventional vacuum evaporation techniques. Secondly, in order to eliminate possible reproducibility and correlation errors resulting from the preparation of multiple specimens, it was anticipated that electrotransport of a single specimen would be measured over a range of temperatures by progressive comparison of the activity distributions. This immediately eliminates destructive methods of determining the activity

distribution at each temperature - for example, the sectioning method of Kuz'menko. This consideration was one of the major influences on the design of the apparatus. To non-destructively measure the activity distribution along the length of the specimen, required the use of a counting system in which the activity was counted over successive segments, thereby necessitating the construction of a specimen or detector traversing system. As the resolution of the measurement was dependent on the exposed area of the sample surface and also on the thickness of shield required to reduce to a low level the contribution from other areas, these factors placed restrictions on the activity characteristics, and hence on the choice of isotope.

The second factor affecting the design of the apparatus and one which also further restricted the choice of isotope concerned the desirability of performing the transport experiment with the minimum of disturbance to the counting system. In order to conduct the experiment in the open laboratory using shielding, which although adequate, would still allow easy manipulation of the specimen and associated equipment, eliminated isotopes having specific activities and radiative disintegrations which required heavy shielding. The isotope selected was also required to have a half-life of sufficient duration to permit several transport experiments to be conducted within this period.

Another important factor was the selection of an experimental material in which diffusion range temperatures (temperatures approaching the melting point) were compatible with the output of the available power supplies and did not require the construction of counting/transport apparatus capable of withstanding high temperatures.

The design of the apparatus based on these considerations will be discussed in the succeeding section.

Despite the restrictions placed on the choice of a suitable transport material, several metals remained which were considered to have suitable isotopes. Of these, indium (isotope In^{114m}) was selected since, at that time, it had not been the subject of electrotransport investigations.

Although both the physical characteristics of indium and the activity characteristics of the isotope In^{114m} suited the requirements of the experiment, the metal has one disadvantage from the viewpoint of its suitability for the observation of electrotransport. Due to the small self-diffusion coefficient of indium (Dickey, 1959) it was anticipated that, in comparison with a number of other metals, a slow rate of electrotransport would be observed; concomitantly for this low melting point metal, the range of diffusion temperatures over which an observable electrotransport effect might be obtained would probably be

restricted. This disadvantage was, however, considered to be outweighed by compatibility of indium with the requirements of the experiment, and it was felt that a slow rate of transport could be offset by experiments of sufficient duration.

As a test of the experimental method it was considered desirable to conduct a preliminary experiment using In^{114m} as the transport species in a system where electrotransport might be detectable in an experiment of limited duration. The solvent metal chosen was gold. It was hoped that more pronounced transport would be observed in this alloy system. Unfortunately the Au-In system consists of a number of phases, and although it was intended to restrict the investigations to constituent ratios and temperatures at which transport was predominantly associated with a single phase, the multiplicity of phases prohibited transport investigations at elevated temperatures. However, some useful rudimentary results were obtained from results of experiments at lower temperatures.

The experimental programme can be divided into three phases
(1) electrotransport of the component In^{114m} in solid gold;
(2) electrotransport of the component In^{114m} in thin gold films;
(3) self-electrotransport of In^{114m} in thin indium films.

These experiments are described in the following sections and the results obtained presented.

4.1 Apparatus and Experimental Techniques

Analysis of Activity Distribution

The apparatus used for the measurement of the activity distribution is shown in Fig. 4.1. It consisted basically of a carriage which supported the specimen and could be traversed horizontally beneath a scintillator crystal/end-window photomultiplier assembly. A bridge supporting the shielding material was interposed between the scintillator and the specimen. The shielding material was in the form of two rectangular blocks separated by a gap at right angles to the direction of motion of the specimen.

In the early experiments on the electrotransport of In^{114m} in solid gold, a tube of the metal was clamped in insulated supports attached to each end of the carriage. These blocks served to introduce the current into the specimen and, for a number of experiments, were water-cooled; hence the actual transport experiment could be conducted in situ.

To prevent contamination of the shielding material if the specimen became distorted, the bridge and photomultiplier assemblies were removed during the experiment. These were accurately replaced by positioning the bridge on pins protruding from its supports and reinstalling the photomultiplier in an accurately machined hole recessed in the upper surface of the bridge.

Although the figure shows the system as used with the solid metal,

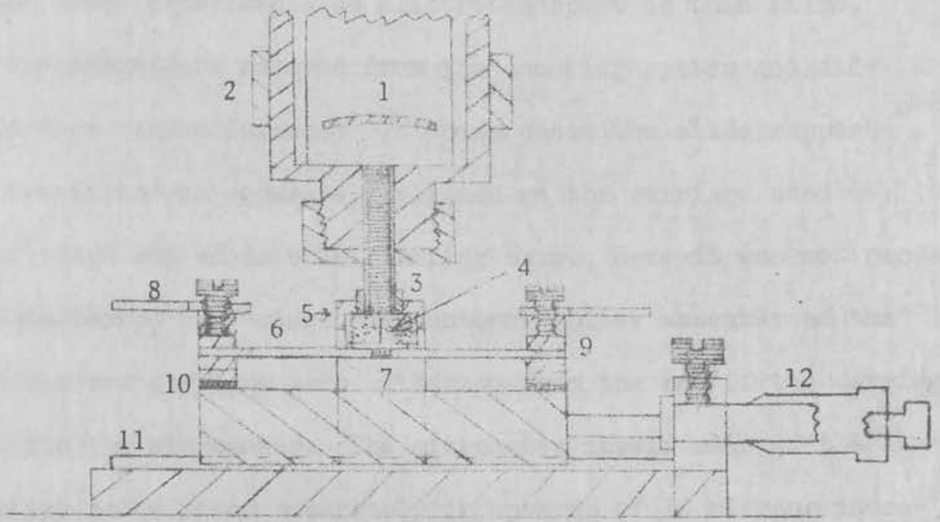

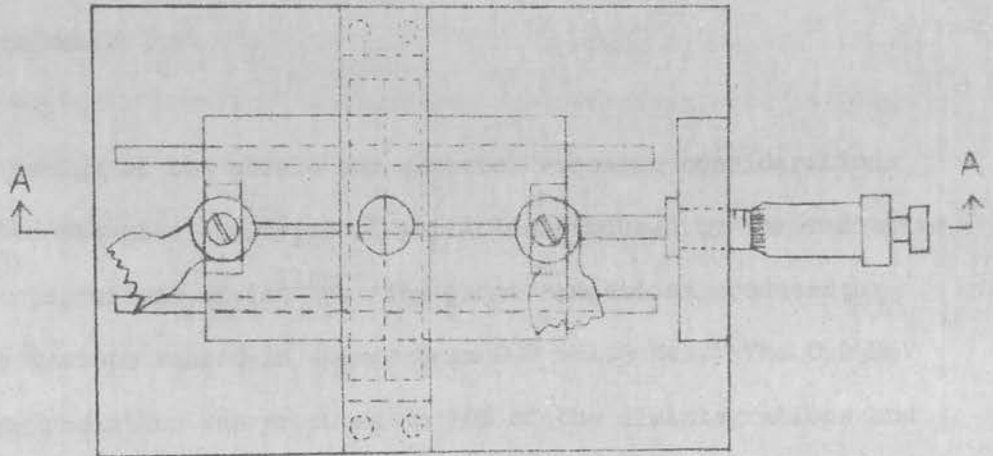

(Photomultiplier assembly removed)

1. Photomultiplier
2. Photomultiplier clamp
3. Scintillating crystal
4. Lead shield
5. Bridge
6. Gold tube
7. Active region
8. Current connectors
9. Gold tube clamps
10. Insulator
11. Guide rails
12. Micrometer

FIGURE 4.1 Experimental apparatus

in the later experiments on electrotransport in thin films, the specimens were removed from the counting system and diffused in a vacuum furnace. In these cases the slide supporting the films was accurately aligned on the carriage used fixed stops and adjustable clamping bars. Here it was not necessary to remove the bridge and photomultiplier assembly as the specimen and carriage were withdrawn from the end of the carriage opposite the micrometer. The micrometer itself allowed the carriage to be moved accurately in upwards of 10 microns increments, and the total available traverse length was 2.5cm. The carriage moved on two cylindrical steel rails attached to a brass base.

The design of the shield and detector required considerations of the energies and types of particles produced by the radiative disintegrations of In^{114m}. The gamma radiations produced by this isotope ranged in energy from 0.2 - 1.3 MeV. The 0.2 MeV gamma radiation was produced in 20% of the disintegrations and estimates of the thickness of shielding and dectector size were based on these figures. It was calculated that, in order to reduce the background to 1%, 0.41 cm of lead were required. Using a slit of width between 50 and 100 microns and length 0.6 cm, the solid angle subtended by the specimen at the face of the detector was 2×10^{-3} steradians. A NaI crystal of diameter 0.25" and length 1.0", supplied by Nuclear Enterprises (G.B.) Ltd., was used as the gamma detector.

A beta particle of energy 2 MeV is also produced in the In^{114m} disintegration. The maximum range of this particle in aluminium is 0.4 cm and in plastic scintillator 1 cm. A bridge system using this thickness of aluminium and the same slit size as the lead shield was thought to provide good resolution of source to background counting rates for this radiation. For the plastic scintillator (type NE102A) a thickness of 4mm was selected to reduce the absorption of the lower energy gamma radiations. A light pipe and 25 micron aluminium window were used in conjunction with this detector; the overall dimensions matched those of the NaI scintillator.

The specific activity of the isotope required to produce an acceptable counting rate and source to background discrimination ratio was calculated from the selected values of detector absorption, shield thickness, and aperture width. This was estimated as 28mC/gm. The indium used in the experiments was high purity material (99.999%) supplied by the Johnson Matthey Company. Before sending the indium to the Harwell Atomic Energy Research Centre for irradiation, the material, in the form of 1 mm diam wire, was cut into small segments of suitable volume for evaporation purposes; these weighed 40mg. Normally four to six pieces were irradiated at one time. One week's irradiation at Pile Factor 12 induced an activity level of 32.5 mC/gm. (The associated dosage rate at one foot was 0.2 mR/hr).

The photomultiplier used in conjunction with the two detectors was an EMI 9524B, one inch diameter tube. The associated electronic equipment typified that commonly used in activity analysis experiments, consisting of a highly-regulated H.T. power supply, pulse amplifier, discriminator, and scaler with coupled preset-count timer.

<u>Current Supplies and Specimen Heating</u>

As remarked above, the initial experiments utilised tubular gold specimens of outside diameter 1 mm and wall thickness 250 microns. This tube was resistively heated in the counting apparatus by attaching current leads to the supports. The power supply used consisted of a constant voltage supply and variable transformer coupled to the primary of a step-down transformer. The maximum rated output of this latter transformer was 36A. (The maximum current density obtained in the gold tube using this power supply was $10^4 A/cm^2$.) Two 100 ohm rheostats were used as ballast resistors. For d.c. measurements a bridge rectifier of silicon diodes mounted on a heat sink was incorporated. The diodes, of 70A rating, were forced-convection cooled. The current through the sample was monitored by recording the voltage developed across one ballast rheostat. Fluctuations in current level were correlated with temperature variations measured using a thermocouple positioned in the centre of the tube. For current densities resulting in temperatures of less than $200^{\circ}C$, the temperature fluctuations were

$\pm$ 5°C, whereas for temperatures above this value, and using water cooling of the clamps holding the tube, long-term variations of up to $\pm$ 15°C were recorded.

For these experiments a vacuum system was constructed and the counting system mounted on the base plate. This allowed the annealing procedures to be carried out in an inert atmosphere or, if required, under varying degrees of vacuum. The water and electrical supplies were brought into the system using vacuum-tight couplings and electrodes. It was found that, for a given current level, the reduction in convective cooling associated with evacuation resulted in the attainment of a wide range of temperatures for a given current level. However, the temperature stability of sample was found to be a sensitive residual pressure and this increased the inaccuracy of the temperature measurement. In addition, precautions were required in order to prevent depletion of the indium surface layer by evaporation. Even at room atmospheric pressure calculations showed the evaporation rate of indium at 500°C was 5×10^{-5} gms/day/unit area. Therefore, for an evaporated layer of weight 10^{-4} gm, two days would be required to remove the complete layer. The deleterious effects of an even more rapid evaporation rate at lower pressures could be avoided in practice by covering the active indium film with an overlayer of gold.

For the investigations in transport in thin films, for reasons to be discussed, it was decided to heat the whole specimen to

$\pm$ 5°C, whereas for temperatures above this value, and using water cooling of the clamps holding the tube, long-term variations of up to $\pm$ 15°C were recorded.

For these experiments a vacuum system was constructed and the counting system mounted on the base plate. This allowed the annealing procedures to be carried out in an inert atmosphere or, if required, under varying degrees of vacuum. The water and electrical supplies were brought into the system using vacuum-tight couplings and electrodes. It was found that, for a given current level, the reduction in convective cooling associated with evacuation resulted in the attainment of a wide range of temperatures for a given current level. However, the temperature stability of sample was found to be a sensitive residual pressure and this increased the inaccuracy of the temperature measurement. In addition, precautions were required in order to prevent depletion of the indium surface layer by evaporation. Even at room atmospheric pressure calculations showed the evaporation rate of indium at 500°C was 5×10^{-5} gms/day/unit area. Therefore, for an evaporated layer of weight 10^{-4}gm, two days would be required to remove the complete layer. The deleterious effects of an even more rapid evaporation rate at lower pressures could be avoided in practice by covering the active indium film with an overlayer of gold.

For the investigations in transport in thin films, for reasons to be discussed, it was decided to heat the whole specimen to

an elevated temperature during the application of the electric field. This necessitated removing the specimen from the counting apparatus and placing it in a vacuum furnace during the actual electrotransport experiment. The furnace used had a uniform temperature zone in excess of the specimen length, and a controller maintained the temperature of this zone within $\pm\frac{1}{2}$°C of the prescribed value over periods of one week. In all experiments the vacuum capability of the furnace was not utilised apart from an initial evacuation to pressures of 10^{-6} mm Hg before introducing oxygen-free nitrogen into the chamber.

In the experiments on thin films current densities in excess of 10^4A/cm^2 were readily achieved using conventional power supplies, or batteries, capable of delivering up to one amp at several volts. The resulting current stability was dramatically improved in comparison with experiments on bulk specimens. Also, in addition to monitoring the current by measuring the potential developed across a standard resistor, the combined effect of any variations in temperature and current could be detected by monitoring the specimen resistivity.

Indium Evaporation

In the indium evaporations a conventional vacuum system was used. Special evaporation jigs were constructed to contain the excess evaporating material. In the majority of experiments the specimen (either gold tube or glass slide) was mounted

on the top surface of an enclosed box 3" above a resistively-heated molybdenum filament containing the active indium. An aperture in the roof of the box defined the deposition area. The evaporations were normally conducted at pressures of 10^{-5} mm Hg. Subsequent to the evaporation, the evaporation jig was committed to an activity-storage area. (It was estimated that 10^{-3} of the initial indium charge was deposited on the specimen.)

4.2 Electrotransport of In^{114m} in Solid Gold

Preliminary Experiments

In a preliminary experiment to test the operation of the counting system, an active indium film of thickness 2000Å and area $3mm^2$ was deposited on the surface of 1 mm diameter gold tube.

With the tube in position beneath the 4mm thick lead shield the settings of the photomultiplier E.H.T. pulse amplifier and discriminator were adjusted to obtain the optimum combination of source counting rate and source:background discrimination ratio; the aperture in the shield was 50 microns. The experiment was then repeated with the NaI scintillator and lead shield replaced by an aluminum shield and plastic scintillator with a high β-absorption cross-section. The results obtained with this latter system were superior and acceptable counting rates and ratios were readily obtained. For the gamma counting system it proved difficult to obtain a useful source counting rate and concomitantly an acceptable source:background ratio.

This was attributed to the several other gamma disintegrations of In^{114m}. These range in energy from 0.2 to 1.3 MeV and, taking a weighted average, a lead shield of thickness 4.7 cm would be required to reduce the background to an acceptable level. Unfortunately, the geometrical attenuation factor resulting from the use of a narrow slit in conjunction with this thickness of shield was calculated to be greater than the absorption attenuation of the shield itself. This system, was, therefore, impractical. In all subsequent experiments the counting system designed for the 2 MeV beta radiation was used.

The same specimen was also used to check the reproducibility of the measurement of the activity distribution. Using the micrometer drive the active region was moved under the detector and a count taken at each 100 micron increment. A total of 10,000 counts (± 1%) was taken at each position with the active region beneath the slit and 1000 counts (± 3%) for the background regions. The measurement was repeated several times. Next, the realignment accuracy of the photomultiplier and bridge assemblies was tested by remeasuring the activity distribution after these items were removed and replaced. The counting rates were then calculated from the results, normalised to allow for the decay of the isotope, and compared. With the error in counting rate determined on the basis of 95% confidence limits, the positions of the distributions were found to be in agreement within experimental error.

Diffusion at 127°C

After some further preliminary experiments to calibrate the temperature-current characteristic of the tubular gold specimens and to determine the current stability and accuracy of the temperature measurement, the electrotransport investigations were initiated.

Prior to evaporating the film of In^{114m} on the tube, microhardness indentations were made in the centre regions and at the ends of the tube. As discussed previously, measurement of the positions of these indentations before and after transport was expected to reveal any shift of the hot zone which might result from gold electrotransport. The positions of the markers were measured within ± 10 microns using a Cambridge measuring microscope.

The evaporation on the tube of a 3mm x 3mm area of active indium followed the previously described procedure. The specimen was then mounted in the counting system and a chromel-alumel thermocouple positioned inside the tube, with the extremity of the thermocouple in the centre region directly below the active zone. To prevent any asymmetry of the temperature distribution in the samples a dummy thermocouple was inserted at the opposite end of the tube. The vacuum system in which the apparatus was mounted was evacuated and filled with oxygen-free nitrogen. Heating of the sample by an a.c. current of 12 amps (current density 3×10^3 A/cm^2) for a period of 24 hours facilitated

diffusion of the indium film into the surface layer of the tube. (Since, at this time, no information was available on the diffusion of indium in gold the choice of diffusion conditions was arbitrary). This pre-treatment was intended to result in the formation of an alloy phase in the surface layers of the tube. Consideration of the phase diagram of the gold-indium system (Fig.4.2) showed a wide existence region of the phase $AuIn_2$. Therefore, at lower temperatures and with predominant formation of this phase or an indium solid solution, the activity distribution might not be significantly affected by phase segregation. (Powell and Braun (1964) subsequently showed, from experiments in the temperature range 140° to 152°C, that a widely distributed $AuIn_2$ phase was the major component in the diffusion zone.)

The activity distribution of the sample was counted twice using micrometer increments of 100 microns. The specimen was moved a total distance of 1.2 cm. No assymetrical effects were observed which could be attributed to transport at thermal gradients.

Using the bridge rectifier system a current of 17.5 A (current density $7 \times 10^3 A/cm^2$) was passed for a period of 16 hours. The temperature registered by the specimen was recorded on a Sefram potentiometric recorder. For the above current density the centre section of the specimen attained a temperature of 127°C ± 5°C. At the completion of the experiment the initial

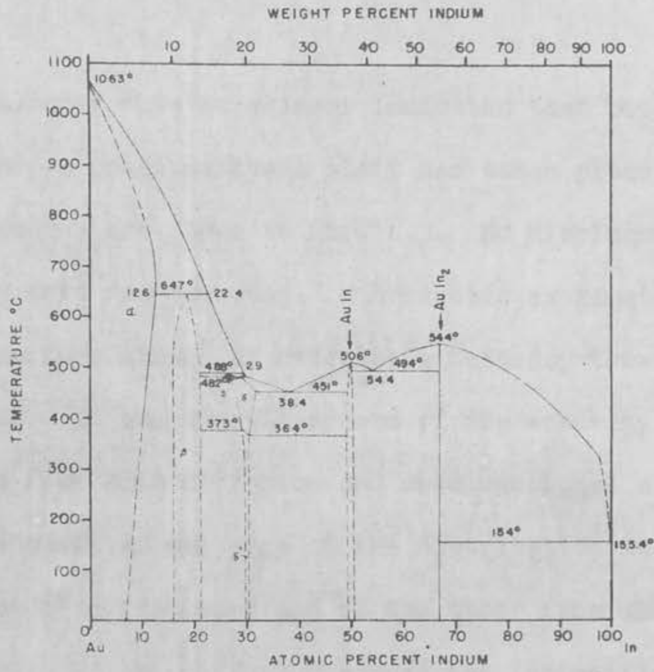

FIGURE 4.2 Equilibrium phase diagram for the gold-indium system.

and final activity distributions were normalised and compared. The carriage was then removed from the counting system and the positions of the marker identations remeasured.

The results of this experiment indicated that both diffusion spread and a unidirectional shift had taken place. The two distributions are shown in Fig. 4.3. No displacement of the inert markers was detected. Microscopic examination of the sample surface showed no detectable tendency towards pore formation. If the overall spread of the activity distribution resulted from both diffusion and unidirectional electrotransport, then the shift of one edge of the distribution must result from diffusion plus transport and of the other from diffusion minus transport. If the diffusion spread was insignificant, i.e. no pronounced alteration in the shape of the active region, then the shift can be determined from the lateral movement of this edge. In the presence of diffusion spread, however, an estimate of the shifts involved can be made by comparing the "normalised coordinates" which are associated with a counting rate of $((N_P-N_B)/e + N_B)$ where N_P and N_B are the counting rates for the maximum of the distribution and for the background respectively. (This presumes the volume diffusion equation for an infinite source to be applicable). The position coordinates corresponding to these counting rates were determined for both edges of the initial and final activity distributions. The difference between the edge-displacements can be taken as x_D+x_T

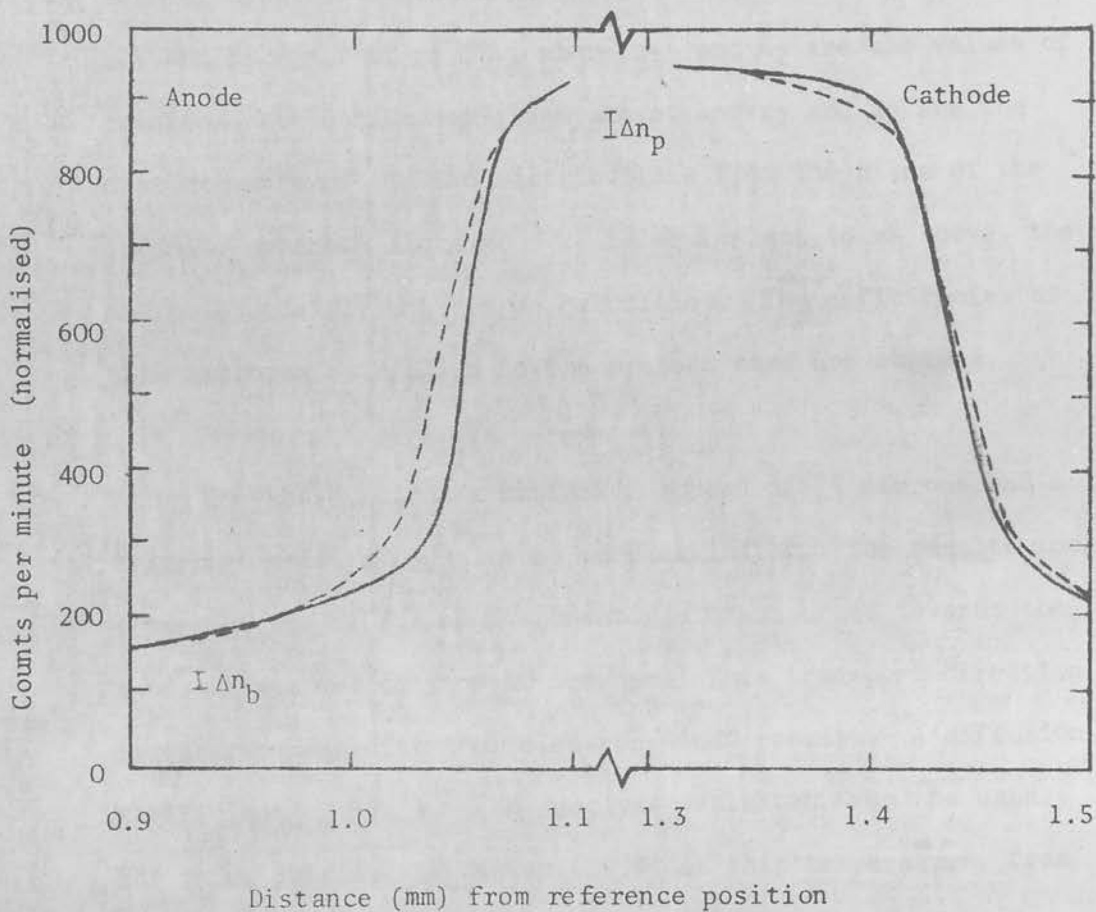

FIGURE 4.3 Schematic representation of activating distribution; initial distribution - solid curve final distribution after diffusion for 16 hrs at 127°C - dashed curve (Δn, error in counting rate for 95% confidence limits)

for the larger displacement and $x_D - x_T$ for the smaller, thus giving the diffusion displacement x_D and the transport displacement x_T. An estimate of the diffusion coefficient can also be obtained from the results. In a rudimentary approach, the displacement of the two distributions, assumed to be described by the Gaussian error curve evolved from a step function, infinite source, distribution, are given by the equations $n_1 = n_o \exp{-x_1^2/4Dt}$ and $n_2 = n_o \exp{-x_2^2/4Dt}$, where n_1 and n_2 are the values of counting rate derived as given above, and x_1 and x_2 are the displacements of the two distributions from the plane of the infinite source. Since $x_1 - x_2$ is equivalent to x_D above, the diffusion coefficient can be calculated. The deficiencies of this approach as applied to the present case are obvious.

Using the above method a diffusion spread of 75 microns and a transport shift of 50 microns were estimated. The results indicate that the diffusing component was transported towards the anode with a velocity of 10^{-7} cm/sec. This transport direction is in agreement with the "electron wind" concept. A diffusion coefficient of 5×10^{-10} cm^2/sec was evaluated from the data. The value obtained by Dickey (1959) at this temperature, from measurements of self-diffusion of In^{114m} in single crystal indium, was 2×10^{-10} cm^2/sec. However, Powell and Braun found that the intrinsic diffusion coefficient of indium in the phase $AuIn_2$ was only 3×10^{-11} cm^2/sec at 141°C. The experimental result is therefore closer to the value for volume self-diffusion.

If the transport phenomena is rate controlled by surface kinetics a larger diffusion coefficient than that found by Dickey would be expected.

Inserting the values obtained for the transport velocity and diffusion coefficient in Huntington's modification of the Nernst-Einstein equation (section 2.1.3)

$$\frac{v}{j} = \frac{\alpha D}{f} \frac{\rho_o}{kT} e Z_i^o \qquad (4.1)$$

and taking the resistivity at 127°C as 1.3×10^{-5} ohm-cm (Kurnakow and Zemczunzy, 1909), the correlation factor f as 0.78, and α as unity, a value of -65 was obtained for the effective valence Z_i^o. Also, using equation (2.63)

$$Z_i^o = (Z_i - \tfrac{1}{2}\overline{Z} \frac{\Delta\rho_d}{\rho_o} \frac{N}{N_d} \frac{m^*}{|m^*|}) \qquad (4.2)$$

and taking $Z_i = \overline{Z} = 3$, m^* positive, and ρ_o as given above, the "specific resistivity" per percent defect $\Delta\rho_d \, N/N_d$ was obtained as 6 micro-ohm-cm/% defect.

These values of effective valence and specific resistivity are high in comparison to values obtained for self-electrotransport in indium. At 127°C Lodding (1965) evaluated the transport velocity as 3×10^{-8} cm/sec and obtained values of -8.2 and 1.1 micro-ohm.cm/% defect for the effective charge and specific resistivity respectively. The higher values obtained here may be ascribed to the elevated transport rates of indium in solid solutions. Despite reservations concerning the validity of the

theoretical treatment in application to this complex system and the accuracy of the various estimated parameters, the foregoing nevertheless demonstrates one qualitative approach to tha analysis of data obtained from such experiments.

Diffusion at 240°C

As it was anticipated that the solid phase $AuIn_2$ would be maintained at temperatures of up to 300° C, a second experiment was performed at a temperature of 240°C. The current density required to raise the centre section of the specimen to this temperature was 7×10^3 A/cm^2 and the run was conducted for a period of 40 hours.

On comparison of the activity distributions before and after transport the resulting diffusion spread and transport shift were estimated as 140 and 260 microns respectively. The transport velocity was, therefore, 2×10^{-6} cm and the diffusion coefficient estimated as discussed previously, 2×10^{-9} cm^2/sec. Substituting these high values in eqs. (4.1) and (4.2) gave an effective valence of -80 and a specific resistivity of 11 micro-ohm.cm/% defect.

On raising the temperature to 265°C the specimen melted in the region of the centre of the tube. This was no doubt due to the creation, by diffusion of indium through the wall thickness of the tube, of a lower melting point

component of the phase $AuIn_2$ associated with a large atomic percentage of indium. In the subsequent experiments the thickness of the evaporated indium film was reduced by a factor of five.

Diffusion at Temperatures of 400°C

In this next set of experiments In films of thickness 400Å were evaporated onto the gold tube.

In order to achieve a more restricted temperature distribution modified water-cooled clamps were substituted for those used in the previous experiments. For temperatures in the range 200-400°C the use of water-cooled clamps reduced the maximum temperature of the specimen for a given current level by approximately 4%. Once again microhardness indentations were made at the end and centre regions of the specimen and the distance between the markers measured. As stated previously, the long-term temperature variations using this modified system were of the order of ± 15°C.

Subsequent to an initial a.c. diffusion aneal of 24 hours at 200°C the activity distribution was measured and the current level increased to 36 amps, the maximum output of the step-down transformer (current density $10^4 A/cm^2$). This produced a maximum temperature in the centre region of the sample of 400°C. The duration of the experiment was 20 hours. Unfortunately,

no useful comparison could be made between the two activity distributions due to distortions produced in the gold tube. It was found that the tube was quite malleable and easily bent. As the apparatus incorporated fixed specimen supports, stresses generated in the gold tube were not relieved; in diffusion at elevated temperatures this resulted in specimen deformation. In comparison with marker motion experiments, where it is possible to introduce correction factors for such effects by observing the displacements of individual markers, in radiotracer methods such corrections cannot readily be made.

It was therefore apparent that to continue experiments with this system would require redesign of the apparatus to reduce the stresses imposed on the specimens. This would probably have necessitated floating one, or both, of the clamping electrodes in a mercury bath. In addition, specimens of larger cross-sectional area would be required, necessitating the construction of a power supply capable of maintaining considerably higher current levels. Also, there was a requirement for improved current stability to reduce the temperature fluctuations from the high level observed in the previous experiment. In consideration of these factors it was decided that these requirements could best be met by the use of both materials in thin film form. Investigations based on thin films were considered to have the further advantage that current densities

of the same order as those used in the above experiments would be developed at considerably reduced current levels.

4.3 Electrotransport of In^{114m} in Thin Gold Films

These experiments required some minor modifications to the apparatus. Principally, the height of the bridge supports was reduced to locate the shield 0.25mm above the surface of a glass substrate positioned on the carriage. The carriage itself was also modified to accommodate the substrate and registration and clamping strips provided for accurate and positive alignment.

The main distinction in experimental technique between the investigations using bulk and thin film gold, was that, for the latter, the diffusions were conducted in a separate furnace. In this part of the experiment the specimen was removed from the counting system and, as described in section 4.1, the electrotransport experiment conducted in a vacuum furnace. At the completion of the experiment the slide was removed and remounted on the counting system for the measurement of the activity distribution. This technique had certain positive advantages; (1) the temperature of the specimen was accurately measured and was stabilised within $\pm \frac{1}{2}^{o}C$ over the duration of the run, (2) the current through the specimen was also accurately measured and maintained within precise limits by the use of batteries in conjunction with precision components, (3) the resistivity of the specimen could be monitored throughout the duration of the run, (4) the possible complicating effects of thermal transport

at temperature gradients were eliminated by maintaining the whole specimen at a uniform temperature (this implies that the applied current density does not raise the temperature of the specimen significantly above the ambient level), and (5) the frame of reference for electrotransport shift measurements could be taken, for convenience, at the ends of the specimen.

The last two points in the above require further amplification. With reference to point (4), it is obvious that, for current densities in the range where electrotransport may result, the temperature in certain parts of the specimen is raised above the ambient value. The actual temperature increase for a given current density depends on a number of parameters. The temperature increase between the centre and end of the specimen can be calculated from the formulation

$$\int_{T_1}^{T_2} \frac{K}{\sigma} \, dT = \frac{1}{8} (V_3 - V_1)^2 \qquad (4.3)$$

where T_1 and T_2 are the temperatures at the end centre regions respectively, K is the thermal conductivity, σ the electrical conductivity and V_1 and V_3 are the potentials at either end of the specimen (the potential at the centre is assumed to be $(V_1+V_3)/2$). Taking the values of the various parameters as those of gold at 150°C, an increase of 10 deg.C in the temperature of the mid-section of a specimen of width 1.9 cm and thickness 2000Å was calculated to result for a current density of 4×10^{3} A/cm^{2}.

This temperature rise was considered acceptable, and the current density within the range where transport effects should be observable in an experiment of sufficient duration. For a film of the above dimensions this current density is associated with a current of only 50mA. For a gold film of the above dimensions the actual temperature rise measured with a thermocouple attached to the surface of the film was 3 deg.C; deviations from the calculated value would be anticipated for a number of reasons, included the use of bulk values of thermal and electrical conductivity.

Recalling the discussion in the section on previous work regarding the choice of reference system to be used in the measurement of electrotransport of tracer ions, it was indicated that a marker would be required in the hot zone in order to measure the correct transport velocity of the migrating component. In the type of experiment described here the whole specimen is positioned in a uniform temperature zone. Therefore, if this method is used for an experiment on self-electrotransport the marker is not required and the frame of reference can conveniently be taken at the ends of the specimen. For the case of alloy transport, the additional use of an inert marker is still necessary to allow for possible migration of the solvent; however, the location of this marker is not critical.

Preliminary Experiments

The preliminary experiments were designed to permit resetting

of the counting system, evaluation of the accuracy of the specimen realignment system, and determination of the suitability of the vacuum furnace in this application.

Using high-purity gold a film of thickness approximately 2000Å, as measured by interferometry techniques, was deposited on a clean 3" x 1" Pyrex glass slide. Next, a film of In^{114m} of thickness 1000Å was deposited in a strip 12mm wide by 3mm long on the surface of the gold film by evaporating a 40mg chip of the isotope. An evaporation jig identical to that described in section 4.1 was used. The long side of the indium strip was parallel to the ends of the slide.

The sample was then positioned on the modified carriage and the settings of the electronic equipment altered to reoptimise the counting conditions. The activity distribution was then measured and the resetability of the alignment system checked. This was found to be satisfactory.

A number of pure diffusion runs were conducted to ascertain the temperatures at which phase segregation in this system became pronounced. The specimen was placed in the copper box of the diffusion furnace which evacuated and repressurised with oxygen-free nitrogen. (This latter step was merely a precaution as solid indium does not react with oxygen and the formation of

the nitride is slight (Ludwick,(1950)). The activity distributions were measured at the completion of each experiment and compared with the previous distribution. A Pt-Pt13%Rh thermocouple connected to a Sefram potentiometric recorder was used to monitor the temperature of the furnace. Over periods of 100 hours the temperature remained constant within $\pm$ 1deg.C.

The first experiment was conducted for a period of 94 hours at 100°C. No diffusion spread was detected. When the experiment was repeated at 133°C for a duration of 180 hours the activity distribution showed a spread of approximately 200 microns for each edge. Unfortunately, a point of inflexion was observed on the slope of the distribution which was taken as an indication of the presence of a phase boundary. Applying the previous considerations to the section of the distributions corresponding to the phase adjacent to the initial active zone a value of $10^{-9}cm^2/sec$ was qualitatively estimated for the diffusion coefficient.

Increasing the temperature to 143°C and heating for 100 hours resulted in an overall spread of 250 microns and the distribution indicated the presence of three phases. These can be seen in the photographs of the specimen shown in Plate 4.1. For comparison purposes the plot of the initial activity distribution and that obtained at the completion of the above diffusion run are shown in Fig. 4.4.

Finally the specimen was diffused for a period of 85 hours at

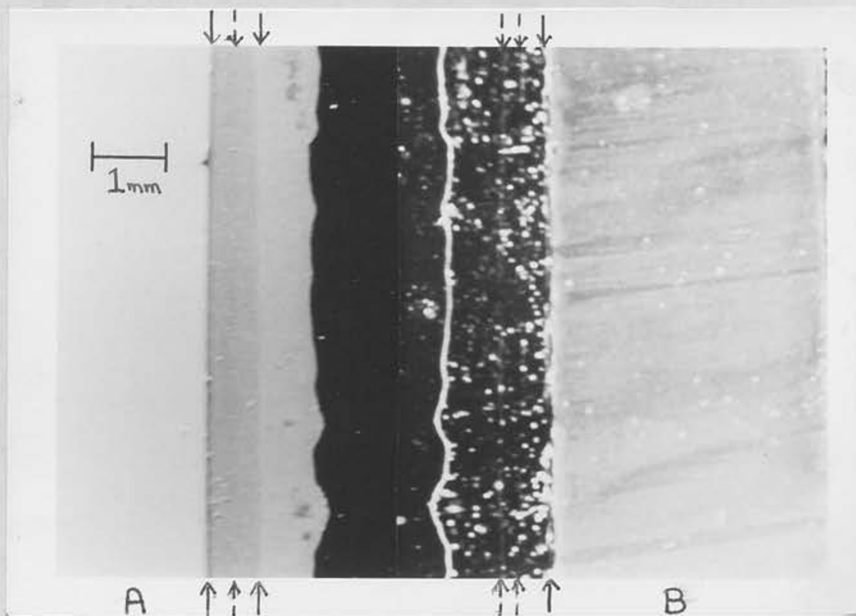

Diffusion zone of In^{114m} in a thin gold film.

(Distribution photographed after heating for a total of 94 hours at 100°C plus 180 hours at 133°C plus 100 hours at 143°C.)

A. Viewed on upper face of film.

B. Viewed through glass substrate.

Inter-phase boundaries are indicated.

Plate 4.1.

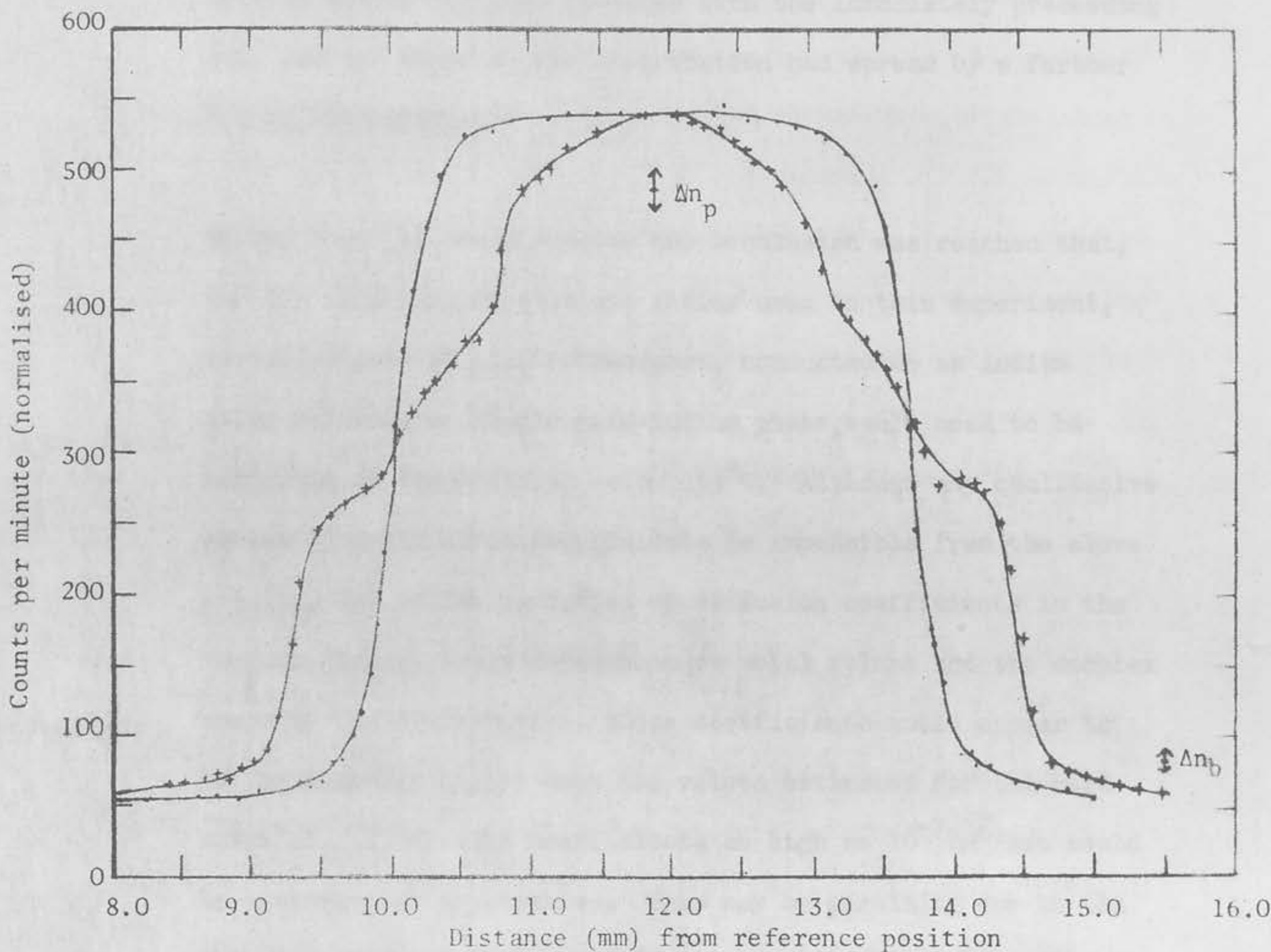

FIGURE 4.4 Activity distribution of In^{114m} in Au film

(A) initial distribution.

(B) distribution after heating for a total of 94 hrs at 100°C plus 180 hrs at 133°C plus 100 hrs at 143°C. The errors in counting rate (95% confidence limits) and position in peak and background regions are indicated by Δn_p and Δn_b respectively.

153°C. In this case a pronounced change was observed in the shape of the profile. The centre section was reduced in amplitude by almost 50% when compared with the immediately preceeding run, and the edges of the distribution had spread by a further 650 to 800 microns.

On the basis of these results the conclusion was reached that, for the thickness of gold and indium used in this experiment, investigations of electrotransport, conducted on an indium solid solution or single gold-indium phase, would need to be performed at temperatures below 133°C. Although any qualitative estimate of diffusion coefficients is impossible from the above results, due to the variation of diffusion coefficients in the various phases, their dependence on molal volume and the complex shape of the distribution, these coefficients would appear to be considerably higher than the values estimated for the bulk material. (Diffusion coefficients as high as 10^{-7} cm^{2}/sec could be envisaged as applicable). This may be partially due to the thin film form of the materials and may also be linked with surface diffusion effects.

Diffusion at 106°C

This electrotransport experiment was intended to investigate possible electrotransport at temperatures where the phase segregation described above was not pronounced. To further facilitate the maintenance of the $AuIn_2$ phase, the thickness of the active

In film was doubled from 1000Å to 2000Å. To allow the connection of current leads to the sample a contact pad was formed at each end of the slide by causing molten indium to flow over the glass. The gold films (area 8.5 x 1.9 cm) were evaporated to partially cover these areas and electrical contact was made by attaching nickel wires to the pads using indium solder. For the gold films the inert marker was provided by masking-off a V-shaped area at one edge of the film. With the specimen mounted on the carriage the position of this marker relative to a second marker on the carriage itself, was measured using a travelling microscope. The accuracy of this measurement, allowing for repositioning the specimen on the carriage, was ± 20 microns.

After annealing the specimen for 24 hours with an a.c. current of 50 mA, the initial activity distribution was measured. The sample was then removed from the counting system, positioned in the vacuum-furnace, and the temperature set for approximately 105°C. The current supply consisted of a set of 2V batteries. The current leads were introduced into the vacuum system through glass-to-metal seals. Using a potential divider the current through the film, determined by measuring the potential drop across a 1 ohm standard resistor, was set at 100 mA. The associated current density was $2 \times 10^3 A/cm^2$. The overall resistance of the specimen was determined by measuring the potential drop across it using a potentiometer. (In the calculation of the specimen resistivity, the value obtained from this potential

difference corresponds to the composite film and, therefore, was nearer to the resistivity of gold. Since the thickness of the indium film would be rapidly reduced once diffusion commenced the thickness of the gold film was used in the resistivity calculation.)

Heating of the sample continued for a period of 210 hours. During this time the actual temperature of the sample was 106°C with an overall temperature variation of ± 1°C. The current through the sample remained constant within 0.5%.

Measurement of the position of the activity distribution at the completion of the experiment, as anticipated from the results of the preliminary experiments, showed, within the error of the measurement, no detectable diffusion spread. (Evidence for at least limited diffusion was noted when viewing the underside of the gold film through the glass substrate; the area defined by the initial indium evaporation had acquired a silver colouration). However, a transport shift of 135 ± 20 microns was found to have taken place in the anode direction. No shift of the gold film marker was detected. The transport velocity corresponding to the above shift was $1.8 \pm 0.2 \times 10^{-8}$ cm/sec. The absence of a value for the intrinsic diffusion coefficient of indium in the gold-indium alloy at this temperature restricts utilisation of this result in the determination of effective valence and specific resistivity. Some indication of possible values of these parameters can, however, be obtained by selection

of diffusion coefficients from the literature. The previous results on the electrotransport of indium in solid gold showed the estimated diffusion coefficient more closely approximated the self-diffusion coefficient of indium reported by Dickey (1959), than the intrinsic diffusion coefficient of indium in indium solid solution, or $AuIn_2$, phases reported by Powell and Braun (1964). The results of the former author give a self-diffusion coefficient of $4.5 \times 10^{-11} cm^2/sec$ at 106°C (averaged for the two orthogonal diffusion directions in single crystal indium), whereas, at the minimum temperature investigated by the latter authors, 142°C, the intrinsic diffusion coefficient of indium was $2.4 \times 10^{-11} cm^2/sec$ in an indium solid solution and $2.9 \times 10^{-11} cm^2/sec$ in $AuIn_2$. The initial estimate of effective charge and specific resistivity for the present experiment was therefore based on the diffusion coefficient of $4.5 \times 10^{-11} cm^2/sec$. Values of these parameters calculated from the diffusion coefficients of Powell and Braun would necessarily be lower. The resistivity value for the composite film, as calculated from the experimental results, was 8×10^{-6} ohm-cm. The error in this result is difficult to estimate since there are a number of contributing factors. These include errors in the electrical measurements and in the determination of the physical dimensions. (The latter consist of not only measurement errors, which may be as high as ± 10% for the interferometric thickness measurement, but also the effects of voids in the film). Also an error may be associated by assuming the resistivity of the lattice in the region to be given by the value for the composite film.

Using the values quoted above, the effective valence was calculated from the correlated Einstein equation (eq. 4.1) as -63 and the specific resistivity from Huntington's theory as 3.4 micro-ohm.cm/% defects. Although the effective charge has a similar value to the previous result for electrotransport this may be fortuitous, since the specific resistivity is significantly different. Obviously both these results are critically dependent on the choice of diffusion coefficient and errors in the estimated resistivity. Once again, the electrotransport appears to be anode-directed hence indicating that scattering of the conduction electrons at the activated diffusion complex is responsible for the observed mass transport. The result of the effective valence calculation shows that the electron wind force on the migrating ion is about 20 times larger than the electrostatic force.

Diffusion at 122°C

The results of the preceeding experiment appeared encouraging and a second diffusion run was conducted on the same specimen. For this experiment a temperature of 122°C was used and a diffusion time of 182 hours; the current through the specimen was maintained at 117 mA. It was hoped that at this temperature some diffusion effects would be observable, therefore allowing an independent estimate of the diffusion coefficient.

Unfortunately, examination of the specimen at the completion of the run showed that the gold film had disintegrated in the region where it joined the gold-indium alloy film. This occurence is difficult to explain, especially as no such effect

was apparent in the preliminary diffusion experiments which were conducted over a wide range of temperature. It is conceivable that the gold film may have absorbed moisture. Due to the relatively poor adhesion of gold to glass, this may have induced peeling in localised areas during heat treatment. This might be expected to occur preferentially in a stressed region such as the junction of the two films. Alternative explanations would appear to be associated with the indium deposition procedure. As the indium film evaporated on this specimen was thicker than that deposited in the preliminary experiments, the heat transported to the gold underlayer would therefore be greater, perhaps creating stresses at the junction which adversely affected the adhesion properties of the film during lengthy diffusion runs. The adhesion of the gold film could be improved by depositing an initial evaporated layer of silicon monoxide on the glass substrate. This would also alleviate the affects of absorbed moisture. For complete protection against moisture absorption the composite film would require to be overcoated with a second silicon monoxide layer.

At this stage in the investigations the numerous disadvantages attendant upon investigations of electrotransport in the indium-gold system were quite apparent. Apart from the experimental difficulties, which may have been resolved by improvements in technique, the experimental results indicated that, for the observation of pronounced transport in an experiment of

reasonable duration, the investigations would require to be conducted at higher temperatures. At these temperatures the occurrence of phase segregation rendered any analysis of the results extremely complex. For the various phases the molal-volume dependent diffusion coefficient would take on different values and, associated with this, the transport velocity in one phase might be dependent on the diffusion coefficients in adjacent phases. Therefore, any quantitative evaluation of diffusion coefficients in the various zones would be complicated. Also, as a result of uni-directional electrotransport and the dependence of the transport velocity on the diffusion coefficient, the activity distribution after transport would be asymmetrical with respect to the centre line of the initial active zone and might possibly have exhibited maxima and minima. Such distributions would prohibit the measurement of transport displacements and the separation of diffusion and electrotransport contributions. The maximum temperature where phase segregation was not apparent was some tens of degrees lower than the melting point of indium (i.e. the limiting temperature for measurements of self-electrotransport in this metal).

The theoretical analysis applied to the reduction of the data may be of limited validity in application to such a complex system. The problems of accurately evaluating diffusion coefficients have been discussed in some detail and the analysis

may also require to take into account possible variations between the effective charge on an activated ion and the mean effective charge on an ion of the lattice. It may also be necessary to differentiate between the scattering cross-section of solvent ions, the scattering cross-section of the activated ion complex, and the average scattering cross-section for charge carriers in the material.

Due to the disadvantages associated with these experiments, the decision was made to progress to the next phase of the programme, namely the investigation of self-electrotransport in indium films.

4.4 Self-electrotransport of In^{114m} in Thin Indium Films

The experimental procedure used in this group of experiments was similar to that described in the previous section. In this case, a layer of high purity indium was evaporated on the glass substrate prior to the deposition of the active material. The evaporation conditions, i.e. source current, pressure, and evaporation rate, were identical for both films. Slight variations in the quantity of material evaporated resulted in an indium underlayer of thickness 2000Å ± 150Å and an active indium film of thickness 1800Å ± 150Å. The dimensions of the active area were 12mm by 3mm.

The diffusion experiments were conducted at temperatures ranging from 100°C to 143°C, with applied current levels of 100 to 500mA and diffusion times of the order of one week. The techniques of

temperature and current control and measurement were as described in section 4.3, these parameters were stable within ± 1% over periods of one week.

Before the commencement of the experiment and the measurement of the initial position of the activity distribution, the specimen was diffused for a period of 24 hours at a temperature of 75°C. The normal procedure for aligning the specimen in the counting system and recording the activity distribution was followed.

The main alteration in this experiment relates to the method of data analysis. The method used in all the preceeding experiments utilised only the minor portion of the recorded information on the activity distribution . In particular, for the determination of transport and diffusion shifts, the counting rates over the regions corresponding to the edge of the activity distributions were of primary importance. More restricted information on counting rates from the background and peak regions of the active zone was also used. Therefore, in order to fully utilise the available data, and to improve the accuracy of the analysis, a computer programme was drawn up whereby the displacement of the distribution resulting from electrotransport was determined from a curve fitting routine known as a "Pearson fit". In applying this programme it was possible to compensate for the resolution of the counting system and therefore to eliminate the spread imposed on any measurement of a sharp-edged distribution by the

finite slit-width. In essence the Pearson-fit routine compared the distributions before and after each run. By calculating several of the moments (1-4) of each distribution, and thereafter subtracting them, parameters were obtained from which the displacement in the position of the mean of each pair of distributions could be determined. This programme also incorporated a sub-programme which normalised the counting rate measured at each position for the decay of the isotope. The computations were performed using the Manchester University Atlas computer.

For these measurements of self-electrotransport in an extended uniform temperature zone it was not necessary to incorporate an inert lattice marker. The reference system used was chosen, for convenience, as one end of the glass substrate. Microscopic examination of the specimen failed to reveal any pore formation which, if present, might have indicated the occurrence of dimensional changes.

The values of diffusion coefficient, estimated from the spread of the activity distributions at the various temperatures were of the same order as those reported by Dickey (1959) for volume diffusion of the isotope in single crystal indium. (Qualitative estimates of the diffusion coefficient are in the range 10^{-10} cm^2/sec. For experiments of one week's duration the spread of the activity distribution resulting from diffusion was readily observable.)
As Lodding (1965), in his investigations of electrotransport in solid indium, utilised the diffusion coefficients obtained by

Dickey in the derivation of transport parameters, the same procedure has been adopted here to allow comparison of results.

In Table 4.1, shown below, the results of this set of experiments are presented. The resistivities of the films were calculated from the measured resistance and physical dimensions of the composite film. The transport velocities are based on the transport shifts obtained from the computer results.

Despite the restricted nature of the results extracted from these experiments, they present some interesting features. Unfortunately the diffusion conducted at 144°C was not successfully completed as it was found that during transport the indium had melted and flowed over the surface of the substrate. This was not detected during the experiment due to the maintenance of electrical continuity. This occurrence was considered to result either from temperature variations within the vacuum oven, which resulted in the specimen being at a temperature 11 deg.C higher than indicated by the measuring thermocouple, or else from an increase in current level which raised the temperature of a localised region of the specimen above the melting point. The former explanation was considered unlikely and this was verified by subsequent experiments which showed the maximum variation between the tempera-

TABLE 4.1

SELF-ELECTROTRANSPORT OF IN^{114m} IN THIN INDIUM FILMS

Run No	Temperature °K	Current Density A/cm^2	Time Hours	Resistivity ohm-cm	Transport Velocity cm/sec	Diffusion Coefficient cm^2/sec (Dickey, 1959)	Effective Valence Z°	Specific Resistivity micro-ohm.cm /% defects	Remarks
1	293	-	-	4×10^{-6}	-	-	-	-	Initial distribution - nc transport
2	373	2.0×10^3	169	4.2×10^{-6}	-	3.5×10^{-11}	-	-	Transport shift not resolved.
3	393	2.03×10^3	168	3.6×10^{-6}	2.8×10^{-9}	1.2×10^{-10}	-4.5	0.18	
4	406	9.6×10^3	168	4.6×10^{-6}	1.26×10^{-8}	2.6×10^{-10}	-2.0	0.16	
5	417	2.02×10^3	168	4.8×10^{-6}	-	5.1×10^{-10}	-	-	Specimen melted (see text

tures of the specimen and thermocouple was 1.5 deg.C. The second explanation was considered more tenable. A separate experiment showed that, at an ambient temperature of 144°C, the temperature in the centre section of the film rose above the melting point for a current density of 750mA. This result was correlated with the addition of an extra battery to the current supply during the course of the experiment; the necessary increased current may have been present during readjustment of the current-controlling potential divider. Due to the destruction of the specimen this run could not be repeated.

Returning to the results presented in the table, it is interesting to compare these with the data reported by Lodding (1965) for electrotransport in solid indium. The theoretical treatments indicate that transport velocities at a given temperature should be proportional to current density. For Lodding's experiments the ratios of transport velocity to current density at 120°C and 130°C were $5.4 \times 10^{-13} cm^3/A.sec.$ and $1.43 \times 10^{-12} cm^3/A.sec.$ respectively. (This calculation takes into account the factor of 1/3 allowing for isotropic dimension changes). The corresponding values for the present experiments were $1.37 \times 10^{-12} cm^3/A.sec.$ and $1.30 \times 10^{-12} cm^3/A.sec.$ The values for the higher temperature are in fair agreement. It should be pointed out that the data obtained from the computer programme indicated a probable error of 12% in the the magnitude of the shift at the higher temperature and a 50% error at the lower temperature. If

the former transport velocity was reduced by this amount the result would be in correspondence with that obtained by Lodding. Taking into account the limited accuracy of the present experiments, the variations in experimental method, and, in particular, the disparity between the structural forms of the material, any agreement is perhaps fortuitous, and, therefore, possible correspondence of the results does not merit detailed discussion. Greater disparity is seen in comparisons of the effective valence and defect resistivity. The values of these parameters obtained by Lodding were -8.4 and 1.07 micro-ohm.cm/% defects at 120°C and -10.3 and 1.34 micro-ohm.cm/% defects at 133°C. The electron:ion interaction force is on the basis of the present results, of similar magnitude, but oppositely directed, to the electrostatic field force on a natural ion of the lattice (the valence of an indium ion in the lattice is taken as + 3.0e). The defect resistivity reported by Lodding is an order of magnitude higher than that obtained for the thin films. This is a reflection of the lower values of the resistivity of these films in comparison with the values calculated by Lodding from the data of Kurnakow and Zemczuzny (1909). This result is anomalous when it is considered that the more pronounced defect structure of the metal in this film form is frequently associated with an increased value of resistivity due to the increased contribution from defect scattering. This argument has been extended on a hypothetical basis (Ghate, 1967) to other processes involving scattering and therefore might be expected to result in an increased transport velocity. This has not been

confirmed by the present restricted results. The effective valence values are in closer agreement but are also affected by the resistivity variation. (Here also the resistivity was calculated on the assumption of an overall film thickness of 2000Å; i.e. no allowance was made for possible deviations in resistivity in the active zone.)

Derivation of the electrotransport parameters assumed the applicability of the volume diffusion coefficient for bulk, single crystal, indium. The results are critically dependent on the choice of diffusion coefficient. The mechanisms of diffusion and electrotransport in the thin film may be considered in terms of a bulk process, a surface process, or a combination of these. Thus, apart from any distinctions which may be drawn between diffusion processes in thin films and the bulk material, it must be established whether the kinetics of the process are volume or surface dominated. In experiments on volume diffusion through thin films of a number of metals, Brown (1961) found that the diffusion coefficients were similar to the bulk values.

The limited results of these experiments did not permit the definitive analysis of transport velocities over a range of temperatures. This would have provided an indication of the activation energy for the electromigration process in indium films. Similarly it was not possible to test the validity of the theory for the thin film structure as this also would have

required the evaluation of the effective valence and defect resistivity over a larger selection of temperatures. However, the results obtained indicate that further investigation of electrotransport in this system is warranted.

5. CONCLUSIONS

This report has been concerned with the phenomenon of electrotransport, the directed displacement of a diffusing species under the influence of an applied electric field. Some of the theoretical aspects of this subject have been reviewed with accentuation on the treatments pertaining to electrotransport in the solid metals, and, in particular, those which have found application to the analysis of experimental results. The previous experimental work on electrotransport in solid metals has also been discussed.

The experimental results of an investigation of the electrotransport properties of the radioactive isotope In^{114m} in thin films of indium and in both thin film and bulk forms of the indium-gold system have been described. The experimental technique consisted of measuring the position of a radioactive zone of In^{114m} deposited on the surface of the material in which electrotransport was to be investigated, using a scintillation-type counting system. This system was considered to have advantages over inert marker-motion experiments as the velocity of the migrating component could be measured directly and also the activity distribution was determined in a non-destructive fashion, thus allowing the same specimen to be used for a number of separate investigations -for example, at different temperatures or applied current densities.

The experiments on thin films of gold and indium are believed to be the first investigation of electrotransport in this structural form of the materials. The first reports of electrotransport in thin films have only recently appeared in the literature and are purely qualitative in nature. In the present experiments the thin film form of the material was used to eliminate one disadvantage of experiments conducted on bulk material, namely the possible effects of mass transport at temperature gradients (the Sôret effect). This was achieved by conducting the electrotransport experiment under a uniform ambient temperature in the diffusion range, using sufficiently low current levels to prevent localised heating of the specimen; the current densities, 10^3-10^4A/cm^2, were still of sufficient magnitude for electrotransport effects to be observable and were comparable with the values used in experiments on the bulk material. This allowed a considerable improvement in temperature stability, and also in current stability, since the current levels required were low in comparison with the requirements of bulk specimens. Adversely, however, this experimental approach negates one potential advantage of thin film studies, namely, the capability of this form of the material to accommodate much higher current densities than can be sustained by bulk specimens. Since the mass transport is expected to exhibit a linear dependence on current density, then it would be anticipated that electrotransport effects would be more pronounced than observed in the bulk material at similar temperatures. Thus, this aspect of investigations on thin films offers two approaches each having advantages over bulk material

experiments, Firstly, for the non-uniform temperatures typical of the bulk, extra high-current densities will be achieved in thin films, and secondly, uniform externally induced temperature distributions can be maintained at moderate current densities. Also, due to the increased grain size and defect structure of thin films such investigations might reveal more pronounced effects of vacancy creation and annihilation resulting from the transport process. (In the literature pronounced and rapid void formation has been reported at high current densities in aluminium thin films (Ghate, 1967).) Thus, thin films might prove to be particularly useful for studies of vacancy kinetics and formation processes, and, concomitantly, may provide an alternative insight into scattering processing in metals resulting from the interaction of current carriers with the activated complex of the diffusion species.

The results of the experimental investigations are, to a large degree, inconclusive. Due to the experimental difficulties encountered, it has not proved possible to extensively analyse the results nor to test the validity of the chosen theoretical treatment in its application to electrotransport in thin films. This would require investigations to be conducted reproducibly over a range of temperatures, current densities and isotope concentrations using both uniform and non-uniform temperature distributions. Nevertheless, the limited results obtained show that, in all investigations where directed mass transport was

observed, the transport direction was towards the anode. This is in agreement with the concept of scattering of conduction electrons in these negative Hall coefficient materials at the activated diffusing complex. This effect can be ascribed to the electron friction or electron:ion interaction force termed descriptively the "electron wind".

The parameters descriptive of the electron:ion friction force and the defect resistivity resulting from scattering processes were evaluated from Huntington's theoretical treatment. Investigations on the gold-indium system in both solid and thin film form showed that the effective valence, which is a measure of the magnitude of the electron:ion interaction force, was considerably larger than the corresponding valence found in investigations of electro-transport in bulk samples of gold or indium. This may be a manifestation of increased transport rates in the alloy system. In a number of alloy systems (Kalinovich et al., 1960) the transport velocity of one component has been found to be high, resulting in large values of effective valence. For the investigations on the thin film system, the large values of effective valence may be partially attributable to increased transport rates in this type of structure. Similarly, in both forms of material the specific resistivity values of the activated defect complex were higher than obtained for the pure bulk materials. However, in view of the inconclusive nature of the experimental results any detailed discussion of their origin is speculative.

The restricted results obtained for self-electrotransport in thin indium films showed some correlation with those obtained by Lodding (1965) for measurements on bulk indium. In particular, the values of transport velocity per unit current density were of the same order and this could be taken as an indication that the "activation energy" for self-transport in the thin film is similar to that of the bulk material.

From the temperature dependence of the transport velocity in solid indium, Lodding (1965) derived an activation energy for electrotransport which agreed closely with the activation energy for volume diffusion reported by Dickey (1959). The tenuous agreement of the present results with those of Lodding may therefore be an indication of a similarity between diffusion processes in thin film and solid indium, and that these are volume dominated. The effective valence and defect resistivity values derived for diffusion of In^{114m} in thin film indium were appreciably lower than the corresponding transport parameters of this isotope in gold.

One of the main conclusions reached as a result of these experimental investigations is that the experimental approach is both useful and valid for the investigation of the electrotransport of radioactive tracers in thin films. The design of apparatus and the experimental techniques require refinement in order to match the accuracy and resolution attainable in more

sophisticated inert marker experiments. However, there appears to be no dubiety concerning the validity of this method of determining transport velocities. The positive advantages of this non-destructive and direct method of analysis render it particularly suitable for this type of investigation. It is considered that, with little improvement in the alignment of specimen and counting systems and also by the use of a more accurate micrometer drive system, the accuracy attainable could match that of inert marker systems. In the limit, an experiment is envisaged in which the specimen alignment and traversing systems would be interferometrically controlled. Redesign of the counting and shielding systems should permit measurement of electrotransport of radioactive isotopes in a wide range of metals and alloys.

In the present form of the experiment the measurement of the activity distribution profile is a relatively lengthy and repetitive process. However, this type of counting experiment lends itself readily to automation and had the results proved satisfactory, the present system could readily have been converted to automatically advance the micrometer drive at a preset total count and to record the associated counting rate.

Experiments of the type described in this report are considered to be of importance due to possible ramifications of electrotransport effects in the applications of thin film technology to microelectronic components. More fundamentally, electro-

transport investigations, as a result of their dependency on the electron:ion interaction and scattering effects at the activated diffusion complex provide an alternative insight into diffusion and electrical conduction processes and also into the kinetics of vacancy formation and annihilation. For these reasons the investigation of this phenomena in thin films is considered to justify further detailed investigation.

REFERENCES

Babikova, Yu. F., and P. L. Gruzin, 1957, Physics Metals Metallography 5, (2), 57.

Baranowski, B., 1955, Roczniki Chem. 29, 129.

Bardeen, J., and C. Herring, 1951, Atom Movements, Cleveland (Amer. Soc. Metals).

Belashenko, D. K., and A. A. Zhukovitsky, 1961, Russ. J. Phys. Chem. 35, 944.

Berry, R. W., G. M. Bouton, W. C. Ellis, and D. E. Engling, 1966, Appl. Phys. Letters 9, 263.

Bressler, S. E., amd G. E. Pikus, 1958, Soviet Phys. - Tech. Physics 3, 2094.

Bosvieuz, C. and J. Friedel, 1962, J. Phys. Chem. Solids 23, 123.

Brown, L. C., 1961, Ph.D. Thesis, University of Glasgow.

Brown, S. and S. J. Barnett, 1952, Phys. Rev. 87, 601.

Claisse, F., and H. P. Koenig, 1956, Acta. Met. 4, 650.

Coehn, A., and W. Specht, Z. Physik 62, 1.

de Boer, J. H., and J. D. Fast, 1940, Recu. Trav. Chim. 59, 161.

de Gennes, P. G., 1956, J. Phys. Radium 17, 343.

Dickey, J. E., 1959, Acta. Met. 7, 350.

Drakin, S. I., 1953, Zhur. Fiz. Khim. 36, 2096.

Fiks, V. B., 1959(a), Soviet Phys. - Solid State 1, 14.

Fiks, V. B., 1959(b), ibid. 1, 1211.

Frantsevich, I. N., 1959, UNESCO/NS/RIC/29, (Pergamon Press, London).

Frantsevich, I. N., and I. I. Kovensky, 1961(a), Dopvidi Akad. Nauk Ukr. R.S.R. 9, 1169.

Frantsevich, I. N., and I. I. Kovensky, 1961(b), ibid. 11, 1471.

Frantsevich, I. N., D. F. Kalinovich, and I. I. Kovensky, 1959, Physics Metals Metallography 8 (4), 93.

Frantsevich, I. N., D. F. Kalinovich, I. I. Kovensky, and V. V. Pen'kovsky, 1958a, Ukrain. Fiz. Zhur. 3, 124.

Frantsevich, I. N., D. F. Kalinovich, I. I. Kovensky, and V. V. Pen'kovsky, 1958b, ibid. 3, 552.

Frantsevich, I. N., D. F. Kalinovich, I. I. Kovensky, and V. V. Pen'kovsky, 1961, ibid. 3, 124.

Frenkel,J., 1955, Kinetic Theory of Liquids (Dover Publications N.Y.).

Geradin, M., 1861, Compt. rend. 53, 727.

Ghate, P. B., 1967, Appl. Phys. Letters 11, 14.

Glinchuk, M. D., 1959, Ukrain. Fiz. Zhur. 4, 684.

Grone, A. R., 1961, J. Phys. Chem. Solids 20, 88.

Gruzin, P. L., Yu. F. Babikova, Yu. A. Polikarpov, and G. B. Fedorov, 1957, UNESCO/NS/RIC/28 (Pergamon Press, London).

Heumann, Th., 1959, The Physical Chemistry of Metallic Solutions and Intermetallic Compounds Vol.1, paper 2C (H.M. Stationery Office, London).

Ho, P. S., 1966, J. Phys. Chem. Solids 27, 1331.

Ho, S. C., and H. B. Huntington, 1966, ibid. 27, 1319.

Huntington, H. B., and A. R. Grone, 1961, ibid. 20, 76.

Huntington, H. B., and S. C. Ho, 1963, J. Phys. Soc. Jap. 18, Suppl.II, 202.

Jost, W., 1952, Diffusion in Solids, Liquids, and Gases (Academic Press, N.Y.).

Kalinovich, D. F., 1961, Soviet Phys. - Solid State 3, 812.

Khar'kov, E. I., and P. P. Kuz'menko, 1959, Ukrain. Fiz. Zhur. 4, 389.

Khar'kov, E. I., and P. P. Kuz'menko, 1960, ibid. 5, 428.

Klemm, A., 1953, Z. Naturforsch. (A), 8, 397.

Klemm, A., 1954, ibid. (A), 9, 1031.

Kubaschewski, O., and F. Weibke, 1938, Z. Elektrochem. 44, 870.

Kurnakow, N., and S. Zemczuzny, 1909, Z. anorg. Chem. 64, 152.

Kuz'menko, P. P., 1961, Ukrain, Fiz. Zhur. 6, 116.

Kuz'menko, P. P., 1962, ibid. 7, 117.

Kuz'menko, P. P., and V. S. Grom, 1961, ibid. 6, 140.

Kuz'menko, P. P., and E. I. Khar'kov, 1958, ibid. 3, 528.

Kuz'menko, P. P., and E. I. Khar'kov, 1959a, ibid. 4, 537.

Kuz'menko, P. P., and E. I. Khar'kov, 1959b, ibid. 4, 401.

Kuz'menko, P. P., and E. I. Khar'kov, 1960, ibid. 5, 430.

Kuz'menko, P. P., E. I. Khar'kov, and G. P. Grinevich, 1960, ibid. 5, 683.

Kuz'menko, P. P., and L. F. Ostrovsky, 1961, ibid. 6, 525.

Kuz'menko, P. P., L. F. Ostrovsky, and V. S. Koval'chuk, 1962, Soviet Phys. - Solid State 4, 356.

Laity, R. W., 1959, J. Phys. Chem. 63, 80.

LeClaire, A. D., and A. B. Lidiard, 1956, Phil. Mag., 1, 518.

Lewis, G. N., E. G. Adams, and E. H. Lamman, 1915, J. Amer. Chem. Soc. 37, 2656.

Lodding, A., 1961, Isotope Transport in Liquid Metals, Gothenburg Studies in Physics, No.1 (Almquist and Wiskell, Stockholm).

Lodding, A., 1965, J. Phys. Chem. Solids 26, 143.

Ludwick, M. T., 1950, Indium (The Indium Corporation of America).

Mangelsdorf, P. C., 1960, J. Chem. Phys. 33, 1151.

Mott, N. F., and R. W. Gurney, 1948, Electronic Processes in Ionic Crystals (Oxford University Press, Oxford).

Mott, N. F., and H. Jones, 1936, The Theory and Properties of Metals and Alloys (Clarendon Press, Oxford).

Mutter, W. E., 1967, Spring Meeting, Electrochemical Society, Dallas.

Onsager, L., 1945, Ann. N.Y. Acad. Sci. 46, 241.

Penney, R. V., 1964, J. Phys. Chem. Solids 25, 335.

Powell, G. W., and J. D. Braun, 1964, Trans. Met. Soc. A.I.M.E. 230, 694.

Schwarz, K., 1933, Z. physikal. Chem., (A) 164, 223.

Schwarz, K. E., 1940, Elektrolyfische Wanderung in flüssigen und festen Metallen (Johann Ambrosius Barth, Leipzig).

Seith, W., 1955, Diffusion in Metallen : Platzwechselreaktionien (Springer Verlag, Berlin).

Seith, W., and Th.Daur, 1938, Z.Elektrochem. 44, 256.

Seith, W., and H. Wever, 1953, ibid. 57, 891.

Skaupy, F., 1914, Verhandl. deut. Phys. Ges. 16, 156.

Skaupy, F., 1924, Z. techn. Physik. 5, 563.

Sullivan, G. A., 1967a, Phys. Rev. 154, 605.

Sullivan, G. A., 1967b, J. Phys. Chem. Solids, in press.

Verhoeven, J., 1963, Metall. Reviews 8, 311.

Wagner, C., 1933, Z. physikal. Chem. (A), 164, 231.

Wagner, C., and G. Heller, 1940, ibid. (B), 46, 242.

Wever, H., 1956, Z. Elektrochem. 60, 1170.

Wever, H., 1959, Phys. Chem. of Sol. Intermet Compounds, Vol. 1, paper 2L (H.M. Stationery Office, London).

Wever, H., and W. Seith, 1955, Z. Electrochem. 59, 942.

Williams, J. M., and C. L. Huffine, 1961, Nuclear Sci. Eng. 9, 500.

(ii)

ELECTROLUMINESCENCE IN ZINC TELLURIDE

1. INTRODUCTION

Luminescence is the phenomenon of emission of electromagnetic radiation in excess of thermal radiation. The radiation is located in the ultraviolet, visible, or infra-red regions of the electromagnetic spectrum. There exist a number of sources of input energy resulting in excitation of the luminescent substance. This dissertation is concerned with luminescence resulting from electronic stimulation of a material by means of an applied electric field or current. This form of excitation is termed electroluminescence. Electroluminescence may occur in gaseous, liquid or solid materials, but most practical applications, excluding electrical discharges in gases, involve crystalline solids.

The earliest observations of electroluminescence were made by Lossev (1923) over forty years ago, and related to the observation of luminescence in naturally occuring p-n junctions in SiC under the action of a directly applied electric field. Such phenomena, in which the luminescence is related to the direct current drawn, are described by the term Lossev effect. A second broad classification covers electroluminescence resulting from an alternating electric field applied to microcrystalline solids embedded in a dielectric medium and is termed the Destriau effect after the original investigator in this field (Destriau, 1936). Until recent years the main emphasis in investigations relating to the development of practical electroluminescent devices emitting in the visible region of the spectrum was on

the Destriau effect in ZnS microcrystalline powder phosphors. These phosphors permit the attainment of high brightness levels with emission occuring in several regions of the visible spectrum depending on the particular impurities incorporated in the host material. With such materials large area displays are quite feasible. The disadvantages of ZnS phosphors relate to the high applied voltages and frequencies required for satisfactory operation and to the restrictions on operating lifetime imposed by the reduction in emission intensities associated with ageing effects.

Although numerous applications have been found for powder phosphors and recent developments in thin film technology have indicated that large area thin film phosphor panels operating under significantly reduced fields are feasible, the emphasis in the field of solid-state electroluminescence has now shifted to investigations of electroluminesce in single crystals of various semiconducting elements and compounds.

Considerable impetus has been given to research in such materials by the observation in recent years of high efficiency stimulated emission from p-n junctions in a number of compounds from Group III and Group V of the periodic table and of efficient emission of a spontaneous nature from homojunctions and heterojunctions of III-V and II-VI compounds. Semiconducting light

sources covering a wide range of wavelengths from the near ultraviolet to far infrared have been fabricated. Such devices hold promise for application in areas where incandescent lamps are now commonly utilised and offer advantages of size, operating parameters and reliability over presently used sources. The application of a number of solid state materials as lasers, operating in the visible and infrared regions of the spectrum, offers a capability in the field of data transmission and communication.

An efficient semiconductor light source combines a suitable structure for the introduction of carriers in an excited state with a fast radiative recombination path for the recombination of a hole and an electron. There are a number of ways in which these conditions can be met. The most effective technique of carrier introduction is the injection of minority carriers across a p-n junction. Such p-n junction devices can be fabricated from many III-V materials. Of the II-VI materials, for reasons to be discussed, only CdTe can be made in both n and p-type form. The other compounds from these groups can normally only be made in one type of conductivity. This has resulted in a number of sophisticated device fabrication techniques by which minority carriers are introduced into a recombination zone. These have included the fabrication of p-n heterojunction structures utilising two compounds from Groups II and VI of opposite type conduct-

ivity - e.g. $ZnSe_xTe_{1-x}$. Other techniques have involved the creation of insulating regions where both injected holes and electrons can recombine or where highly energetic carriers can be created by collision processes. Carriers have also been introduced by field excitation over, or tunneling through, metal:semiconductor barriers. Many of the II-VI compounds have energy gaps in the visible region of the spectrum and hold promise as potentially useful emitters. The difficulty of fabricating p-n junctions in II-VI compounds has not deterred workers in this field. Investigations of electroluminescence in ZnS have been conducted for many years and recently efficient low temperature emission has been observed in a number of II-VI heterojunction and insulating layer devices.

The recombination process subsequent to the excitation process can involve a number of different types of transition depending on the band and defect structure of the crystal, the incorporated impurities and the energies of the carriers introduced. Possible transitions include

1. transitions involving chemical impurities or physical defects (lattice vacancies, etc.)
   a. conduction band to acceptor
   b. donor to valence band
   c. donor to acceptor (often called "pair emission").

2. Interband transitions

a. intrinsic or "edge emission" corresponding very closely to the band gap; phonons and/or excitons may be involved

b. higher energy emission involving energetic or "hot" carriers, sometimes called "avalanche emission".

3. Intraband transitions, involving energetic carriers; sometimes called "deceleration emission".

Not all electronic transitions are radiative. An efficient luminescent material is one in which radiative transitions predominate over non-radiative ones.

In addition to device properties information is presented on the related crystal growth and material properties of ZnTe, and also the results obtained by other workers investigating this material are considered. Heterojunctions and insulating barrier layer devices based on ZnTe have been reported in the literature to give efficient visible emission at low temperatures. The techniques of device fabrication to be described utilise relatively simple contacting and mounting procedures. The potential usefulness of ZnTe devices as a room temperature visible emitter is described. This dissertation is confined to considerations of the electroluminescent properties of devices based on one member of the Group II-VI compounds, namely ZnTe. No attempt will be made to discuss the literature relating to other II-VI electroluminescent compounds, but pertinent comparisons will be drawn between results reported hereinafter and similar results obtained from other II-VI and III-V compounds.

2. PREVIOUS WORK

Of the binary compounds formed by synthesis of elements from Groups II and VI of the periodic table, the most interesting, in terms of their electroluminescent properties, are the sulphides, selenides, and tellurides of zinc and cadmium. The physical and chemical properties of these compounds are closely similar. As stated in the introduction this report is primarily concerned with the electroluminescence and related properties of ZnTe; in a number of instances, however, it will be convenient to draw comparison between results obtained for this material and the other II-VI compounds as well as other electroluminescent materials.

In this chapter the results of previous investigations into electroluminescence in ZnTe will be described together with considerations of the mechanisms of excitation and radiative recombination advanced by various authors. In addition we report the available literature on synthesis of single crystals of ZnTe, and previous investigations of the relevant optical and electrical transport properties of the material are described.

The discovery of laser action and efficient spontaneous emission in GaAs and other binary III-V compounds awakened interest in the potential of II-VI compounds in similar applications. Several members of this group, ZnSe, ZnTe, CdS and CdSe, have

electronic band gap energies corresponding to wavelengths in the visible regions of the spectrum and these are generally considered on the basis of present information to be direct band gap materials (i.e. the highest maximum of the valence band and the lowest minimum of the conduction band occur at k=0 in momentum space). Although early investigations of electroluminesce in II-VI compounds were conducted on powder samples, principally of ZnS, investigations have extended to cover this compound and the other chalcogenides in single crystal form. In general it can be stated that the growth of single crystals of semiconducting binary compounds presents more problems than the case of the elementary semiconductors. In the latter case large single crystals can readily be grown from the melt. The materials technology of III-V compounds, e.g. GaAs, GaP, is less complicated than that of the II-VI compounds and small area platelets of the former materials can readily be grown by a variety of techniques; the growth of larger crystals presents considerably more difficulty. The fact that ZnTe has the lowest melting point of the zinc chalcogenides can be considered one advantageous feature of this material. The melting point of 1295°C is within the temperature range where quartz apparatus can be used in conjunctions with a near stoichiometric mix. Despite this advantage ZnTe has received relatively little attention compared to many other II-VI compounds - this is perhaps due to the fact that its behaviour as a photoconductor or a luminescent material

is not as pronounced as that of some other II-VI compounds.

A disadvantage of the II-VI compounds in application to electroluminescent devices is that the majority of these materials exhibit only one type of conductivity (an exception to this is CdTe which can be prepared in both n and p-type form). This lack of amphoteric conduction, which for the case of ZnTe is probably associated with compensation of any dissolved donors by singly or doubly charged Zn vacancies, means that electroluminescence resulting from the recombination of minority carriers injected across a p-n junction with majority carriers or luminescent centres is not possible. Several alternative techniques of excitation have been investigated. These include excitation over a metal:semiconductor barrier, tunneling and the fabrication of metal:insulator:semiconductor (m-i-p) structures. Similarly, the lack of amphoteric conduction can be overcome by the use of II-VI compounds having opposite type conductivity (e.g. $ZnSe_xTe_{1-x}$). Highly efficient emission has been reported in such structures at low temperatures.

The lack of amphoteric conduction in ZnTe has reduced the amount of information obtainable from electrical transport measurements. In particular, no detailed information is available on conduction band structure.

There are several reviews of the luminescent and electroluminescent

properties of solids which are relevant to this section (Henisch (1962), Ivey (1963), Goldberg (1966)). Many aspects of the physical, chemical and electroluminescent properties of II - VI compounds are discussed in a text edited by Aven and Prener (1967).

2.1 Structure and Crystal Growth

2.1.1 Crystallography

The crystallography of the II-VI compounds is somewhat complicated by their tendency to crystallise in a variety of polymorphic modifications. The principal structures are cubic zincblende (sphalerite) and hexagonal wurtzite. In the latter atoms are arranged tetrahedrally.

Crystals encountered in practice are usually non-ideal and contain imperfections and defects which often dictate the semiconducting properties of the material. Crystal defects can be arbitrarily classified into point defects, such as vacancies and impurity atoms, line or plane defects, such as dislocations and stacking faults, and complex defects which result from the interaction or coalescence of elementary defects. Because of the extensive polymorphism in these compounds, gross defect structures associated with intergrowths of several crystal forms frequently occur.

The II-VI compounds crystallise in structures in which the binding varies from "ionic" to "covalent". In "ionic" binding arrangement in crystals is more dominated by the coulombic forces due to charges on atoms or ions than by directional properties related to the nature of the chemical or homopolar bonding. In "covalent" binding the dependence is reversed.

The crystalline structure of the majority of II-VI compounds can be classified on the geometric basis of cations filling some of the interstitial positions in different sequences of close packed anions. All of these compounds form crystals of the zincblende or B3 arrangement and this is the common form of ZnTe. This structure, shown in Fig. 2.1, is based on the cubic space growth T_d^2 - $F\bar{4}3m$. In a unit cell there are four ZnTe molecules and all atoms occupy special positions with the coordinates: 4 Te in (a) 0,0,0; 0,1/2,1/2; 1/2,0,1/2; 1/2,1/2,0 and 4 Zn in (c) 1/4,1/4,1/4; 1/4,3/4,3/4; 3/4,1/4,3/4; 3/4,3/4,1/4. The point symmetry in the (a) and (c) sets of positions is $\bar{4}3m$ and every atom is surrounded tetrahedrally by four atoms of the other kind. Each Zn(Te) atom has four nearest neighbours of Te(Zn) at a distance of $1/4\sqrt{3}a$ at the corners of a regular tetrahedron (a is the cubic lattice parameter). There are twelve next-nearest neighbours of atoms of the same

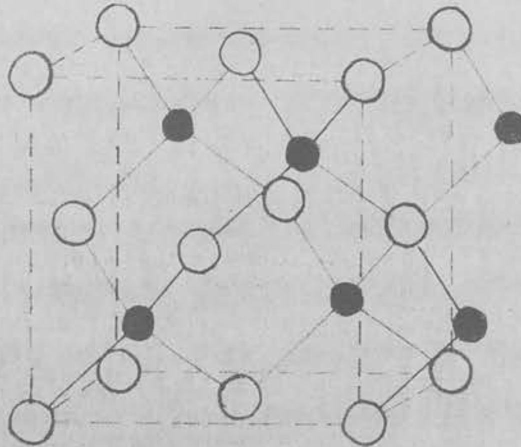

FIGURE 2.1 Zincblende. The arrangement of Zn atoms (filled circles) and Te atoms (open circles) in zincblende, the cubic form of ZnTe. (Pauling, 1960).

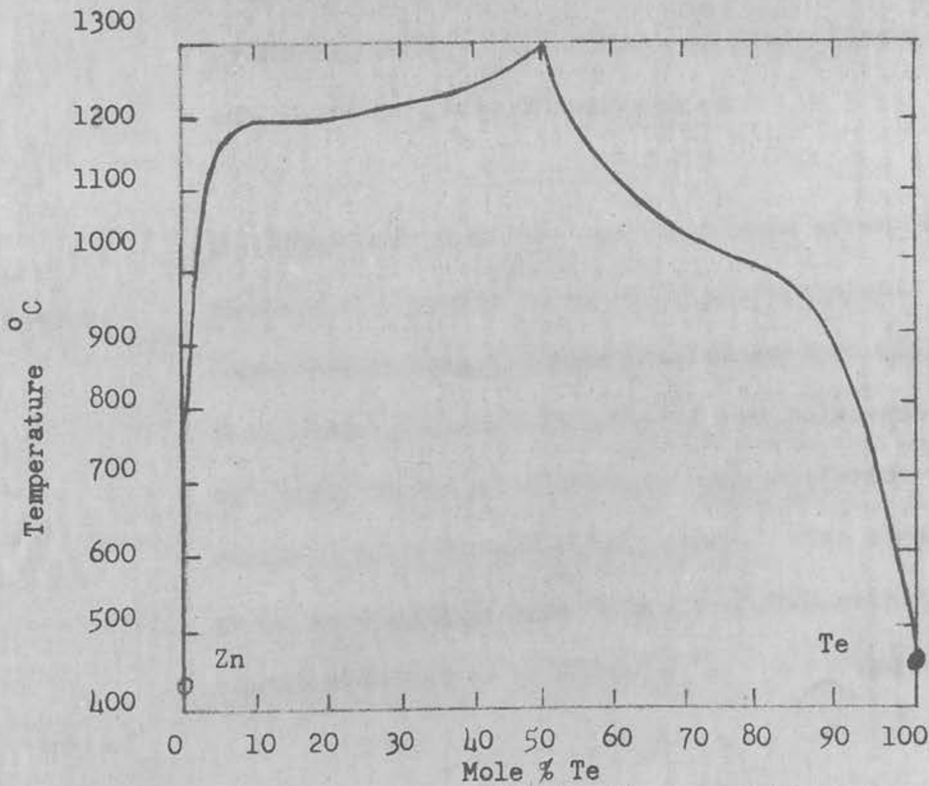

FIGURE 2.2 Phase diagram of ZnTe (Carides & Fischer, 1964).

kind at the distance $\frac{1}{2}\ \sqrt[2]{a}$. Six of these are distributed at the corners of a hexagon in the same plane as the original atom; the remaining six form a trigonal antiprism with three above and three below the plane of the hexagon

The lattice parameters of ZnTe are given in the literature as - 6.1037Å, d(Zn-Te) - 2.64Å, d(Zn-Zn) - 4.32Å (Larach et al., 1957). The occurrence of polytypes of ZnTe of hexagonal habit and reportedly 15R structure (Thiabault, 1944) have been reported by Pashinkin et al. (1960). (Polymorphs are different crystalline modifications of a substance, and the term polytype refers to a class of polymorphs for which there is a special structural relationship between the contents of the unit cells). Chistyakov and Krucheanu (1961) have detected the presence of wurtzite (hexagonal form) modifications in predominantly cubic crystals of ZnTe grown by sublimation.

One important aspect of the zincblende arrangement is the absence of a centre of symmetry or inversion. The Zn-Te layers have unique orientations along the <111> directions. As a result, zincblende crystals are polar and opposed (hkl) and $(\overline{hkl})$ faces and directions have different physical and chemical properties (Dillon, 1962). The directions of the polar axes in ZnTe have been correlated with the etching characteristics of the A and B (A^{II} B^{VI}) faces. (The

opposite polar faces of a zincblende crystal are termed A and B if they are parallel to the (111) planes and terminate with only A and B atoms respectively). (Eland 1960, 1962; Warekois et al. 1962; Aven and Garwacki, 1963).

As stated previously, the bonding in II-VI compounds is considered to be neither completely ionic nor completely covalent and is often described as "partly ionic". A pure ionic model does not satisfactorily explain the interatomic separations, as the distances between the II and VI atoms calculated from conventional atomic radii are significantly larger than those observed. If this is assumed to be due to covalent effects, the covalent shortening increases with increasing atomic number; this is not substantiated by experimental observations but the covalent bond in sphalerite compounds nevertheless play an important role. For ZnTe the observed spacing is 2.64Å, the calculated ionic spacing 2.81Å, and the calculated covalent spacing 2.63Å (Roth, 1967).

The effects of polytypism, point defects, dislocations and stacking faults, will have pronounced effects on the semiconducting properties of the II-VI compounds. Unfortunately little information is available in the literature on the perfection of ZnTe crystals, as the majority of such experiments have been concerned with ZnS. However,

it is anticipated that many of results obtained on this material be extended to ZnTe; this topic has been reviewed by Roth (1967)

2.1.2 Crystal Growth

Due to the high melting point of the II-VI compounds and pressures developed near the stoichiometric melting point, the majority of the techniques utilised to produce single crystals of these materials have involved vapour growth which allows the use of lower temperatures and pressures. This is in contrast to techniques used for elementary semiconductors, large crystals of which can readily be grown from the melt. The disadvantages of vapour growth relate to limitations in purity, crystal size and time required to produce sizeable crystals. This has resulted in recent work being directed toward the more difficult problem of growth from the melt. There are now available single crystals of all II-VI compounds but these cannot be compared in size or perfection to crystals of the elemental semiconductors.

The thermodynamic properties of II-VI compounds and the associated phase equilibria (solid, liquid and gas phases) have by no means been extensively studied. Relatively little information is available on temperature-pressure relationships, perhaps due to the temperatures and pres-

sures involved.

ZnTe can readily be prepared by melting the elements (Fischer, 1961). The reaction proceeds exothermically at the melting temperatures (Zn melting point - 420°C; Te melting point - 450°C; heat of formation at 298°K - 26Kcal/mole). The solid-liquid-vapour phase diagram for ZnTe is shown in Fig. 2.2. The melting point of the stoichiometric mix is 1295°C and minimum pressure of the compound at this temperature 0.64 atm. (The pressure - temperature phase diagram of ZnTe has been evaluated by Carides and Fischer (1964) and Kroger (1965)). Four categories of crystal growth are arbitrarily designated. These are (1) growth from a stoichiometric or near-stoichiometric melt, (2) growth from an off-stoichiometric melt, (3) vapour growth, (4) growth from a solution of an element other than one of the constituents of the compounds or utilising a flux.

One of the main drawbacks of stoichiometric melt growth of II-VI crystals, namely the high melting points of these compounds, is less pronounced for ZnTe. The melting temperature of 1295°C can be attained using conventional quartzware. Unfortunately in order to completely liquify the compound, temperatures in excess of the melting point are required and at such temperatures quartz

softens. As it is necessary to utilise a sealed system, the minimum pressure at temperatures above the melting point rapidly exceeds one atmosphere, resulting in expansion and possible rupture of the quartz container. Thus, although growth of ZnTe crystals from a stoichiometric mix is feasible, it is not normally attempted without special precautions being taken to reinforce the growth ampoule.

In order to obviate these difficulties growth at lower temperatures from off-stoichiometric mixes can be attempted. At first sight this technique would appear to be a most promising approach for II-VI compounds having even higher melting points than ZnTe. However, for the majority of II-VI compounds, the possibility of crystal growth by this method is also limited. First, there is basic shape of the T-x diagrams which show liquidus curves rising very steeply with temperature in the vicinity of the pure metals. Hence, growths at lower temperatures on the metal rich side are confined to very dilute solutions, which in general does not lead to large and well-formed crystals. For several compounds there are also other disadvantages associated with liquids rich in the group VI element. For example the vapour pressures of the sulphides are prohibitively high. Fortunately, these objections do not apply to the ZnTe system and the use of

off-stoichiometric melts is a useful growth technique for this compound.

Another disadvantage of stoichiometric growth is that, due to the high minimum pressure near the maximum melting point, mass transport occurs through the vapour phase to any cooler region of the system, unless the dissociation pressures are suppressed via one of the components or a high inert pressure. This tendency can be used to advantage in vapour growth. Since, for the II-VI compounds, the vapour pressures of the components are high, growth from the vapour phase can take place at significantly lower temperatures. In ZnTe the useful vapour growth temperature range is from 900°C upwards. Below this temperature the equilibrium pressure for the compound is small and growth takes place at a slower rate. In practice, this can be overcome by increasing the transport by a forced gas flow or by the inclusion of another component, which, through reaction, changes the equilibrium. Vapour growth techniques are therefore useful in application to the growth of ZnTe crystals.

The above summarised the crystal growth techniques which are considered applicable to the system Zn-Te. Actual growth procedures reported in the literature are now described.

2.1.2.1 Vapour Growth

The basic requirement for growth from the vapour phase is a continuous flow or supply of the group II-VI elements through the gas phase. The source of elemental components can be either dissociation of the preformed compound or the elements themselves. The gaseous species diffuse or flow to a region where they become supersaturated and growth takes place. Vapour growth can be subdivided into dynamic and static techniques according to whether or not a carrier gas is used and the system is in a continous state of externally induced flow.

The static method of vapour phase growth, in which transport occurs via diffusion through the gas phase, was originally devised by Reynolds and Czyzak (1950) and was later modified by Greene et al. (1958). In this method a powder charge was positioned midway between two seed plates,with the charge located in the hottest zone of a furnace. The system was filled with argon at a pressure of one atmosphere. This technique was successfully applied by Devlin et al. (1960) to the growth of ZnTe crystals. Typical growth runs extended over a period of 200hours at a temperature of 1250°C. Crystals weighing up to 15 gm were obtained. Lynch et al. (1963) also used a similar

vapour growth technique in which distillation took place from a polycrystalline mass held at 1090° in 1 atm. of helium with regrowth taking place in a cooler zone some 20° lower in temperature. In this case the product was a boule of several cm^3 from which single crystal regions of 0.1-1 cm^3 were obtained. Piper and Polich (1961) made significant modifications to the system of Greene et al. In this system the charge was placed in a quartz tube which had a conical end section. The initial position of the crucible was such that the conical tip was near the maximum temperature. The crucible was then pushed through the furnace so that the tip moved into a cooler region of the furnace at a rate of 0.3 - 1.5 mm/hr. As the tube moved supersaturation at the tip increased until nucleation occurred. This technique was used for ZnTe by Piper and Polich (1961) and Aven and Segall (1963). In the latter case the sintered charge was pulled at a rate of 0.2 mm/hr through a furnace heated to 1050°C. The product was a boule which contained single crystal regions up to 1 cm^3 in size. Shiozawa et al, (1964) successfully grew a large single crystal of ZnTe by modifying the above technique. In this case a single crystal seed was placed in an evacuated tube along with the source material. By keeping the temperature differ-

ence between source and seed small ($3^{o}C$) epitaxial growth was observed. This crystal was of large size (14gm) and was found to be twin free - an unusual result in the growth of a II-VI compound. The growth of ZnTe crystals by sublimation onto a silica substrate has been reported by Takahashi et al.(1966).

In a recent paper DeMeis and Fischer (1967) have reported a novel vapour transport technique which allows rapid growth of ZnTe crystals. In this method the compound was placed in an evacuated ampoule to which a long quartz capillary tube was attached. As shown in Fig.2.3 this capillary protruded beyond the movable furnace used to heat the ampoule. The use of a capillary tube allowed the minimum decomposition pressure of the compound to be attained by acting as a cold trap for the collection of excess volatile material. Thus the system adjusted automatically to the stoichiometric deviation corresponding to the minimum decomposition pressure. With the furnace maintained at a temperature of $1050^{o}C$ growth commenced in the hotter part of the capillary, sealing it off. The capillary acted as a nucleation tip for seed selection. The use of a growth speed of 0.5 mm per hour resulted in the production of large, regularly shaped, ZnTe boules; in common with results of the other experimenter these boules contained twinning planes,

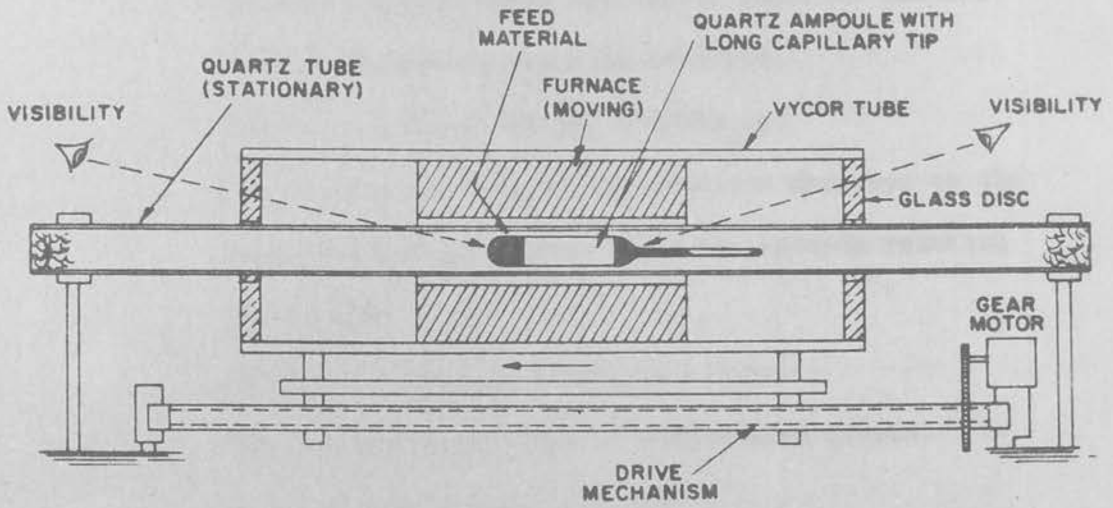

FIGURE 2.3 Vapour Phase Growth of ZnTe in Capillary-Tipped Ampoules (DeMeis & Fischer, 1967).

but large single crystal portions were obtained. This technique was amenable to the use of halogen gas in a chemical transport reaction. In the higher temperature zone where the source material was located the following reaction occurred:

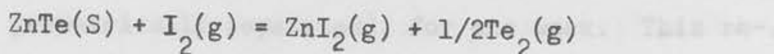

$$ZnTe(S) + I_2(g) = ZnI_2(g) + 1/2Te_2(g)$$

The gaseous products of the reaction diffused to the lower temperature region where the reverse reaction took place:

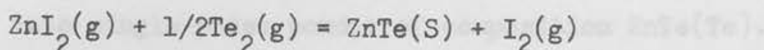

$$ZnI_2(g) + 1/2Te_2(g) = ZnTe(S) + I_2(g)$$

This technique resulted in accelerated growth.

These authors also used the capillary tip technique for the successful melt growth of ZnTe crystals at 1300°C. In this case it prevented the dilation of the soft quartz which otherwise resulted from the internal vapour pressure generated by an excess of one component.

A dynamic vapour growth technique for ZnTe has been described by Yamanaka and Shiraishi (1965). In this method a charge was placed in a tube having a pinhole at one end. Under a flow of N_2 gas sublimation from the charge held at 1250°C resulted in the growth of single crystals in the region of the pinhole maintained at 1100°C.

Albers and Aten (1965) (Albers, 1967) prepared ZnTe crystals without inclusions by an equilibrium vapour transport method in which a mixture of ZnTe(Te) + Te(Zn) and a second smaller mixture of ZnTe(Zn) + Zn(Te) were heated at 850°C in the same vessel (but geometrically separated), for one week. This resulted in a net transport of Te, via the vapour phase, from the former to the latter until equilibrium was reached and the ZnTe(Te)+Te(Zn) mix was converted into single-phase powder of composition ZnTe(Te). In this way, inclusion free, millimeter-size single crystals were grown in the ZnTe(Te) powder. These crystals were further enlarged by annealing this material at 850°C.

2.1.2.2 Melt Growth

It is normally considered that in order to obtain large volume single crystals the most useful technique involves growth from the melt. As discussed above, melt growth near the stoichiometric melting point in the II-VI compound presents problems due to the high temperatures required and high pressures encountered. Although ZnTe can be grown from such a melt without special precautions being taken, normally the quartz tube is placed in a thick-walled graphite sleeve so that the development of internal

pressure forces the soft quartz against the walls of the graphite bomb (Eastman, 1964, 1966). An alternative technique utilises a complex autoclave in which a high pressure of an inert gas prevents the induction of strains in the quartz ampoule (Fischer, 1963). This technique also eliminates another disadvantage of melt growth techniques, whereby dissociation of the compound takes place accompanied by mass transport through the vapour with subsequent recrystallization in low temperature regions. Growth from an off-stoichiometric melt allows growth to proceed at lower temperatures. ZnTe was grown by Title et al. (1964) from a melt containing 50 at% excess Te. This excess reduces the melting point to around 1200 ^{o}C (Figure 2.2). The actual procedure of growth from the melt normally involves a Bridgman technique or modifications thereof. In one method the melt is withdrawn at a slow rate from a high temperature zone into a second zone maintained at a lower temperature. In another technique a sharp temperature gradient is used, the "second zone" of the furnace often being at room temperature. The crystal growth furnaces use either conventional resistive elements or R.F. induction coils. Withdrawal rates range from 1-25 mm/hr. High withdrawal rates have one disadvantage due to the fact that the latent heat

of fusion of the compound liberated at the freezing zone can melt material crystallised beyond this point. This effect is less pronounced at slow withdrawal rates (<2 mm per hour).

ZnTe crystals used in the fabrication of electroluminescent devices are most commonly grown by the Bridgman techniques (Hinotani and Sugigami, 1965; Watanabe et al.,1964). This method has found particular application in the growth of doped material by the addition of phosphorus (Morehead and Mandel, 1964; Eastman et al., 1964; Miksic et al., 1964; Komatsu et al., 1964) and other impurities (Crowder et al.,1966; Crowder and Hammer, 1966) to the initial mixture.

In growth techniques in which the impurities are added to the constituents prior to crystal growth care must be taken to separate the effects of these impurities on the electrical properties (carrier concentration, mobility etc.) of the material from the values of these parameters that would have been obtained had impurities not been added. In a number of papers only the properties of doped materials are reported and the values of the various parameters are not quoted for undoped crystals, grown by an identical technique. It is anticipated that, in some cases, the major contribution

to the reported parameters arises from the intrinsic defect properties of the undoped crystals.

The feasibility of growing n-type crystals has been demonstrated by Fischer et al. (1964). ZnTe/Al crystals were grown in a pressure bomb under 30-50 atmospheres argon pressure by cooling a Zn-rich melt from 1280°-1100°C, followed by rapid quenching to room temperature.

2.1.2.3 Solution Growth

In essence growth from an off stoichiometric mix containing an excess of one component of the compound can be described as solution regrowth. The use of this phrase is, however, restricted to growth procedures in which crystals of a compound are grown by the technique of dissolving and subsequent freezing out of a compound from a solvent other than either of the components. The solubility temperature is determined by the relative weight percentages of the compound and the solvent element. These are normally chosen so that the compound commences to form the solid phase at temperatures below the stoichiometric melting point. As an example, the solubility of ZnTe in In and Ga is illustrated by the liquidus curve shown in Fig. 2.4

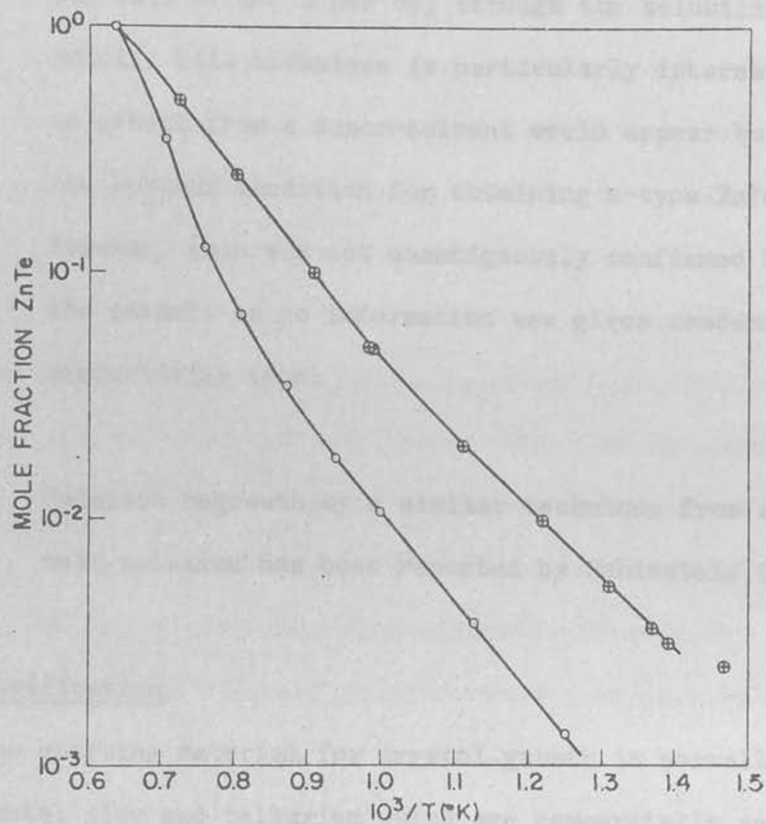

FIGURE 2.4 Liquidus curves for ZnTe-Ga(0) and ZnTe-In (θ) plotted as log mole fraction ZnTe versus 1/T (Wagner and Lorenz 1966).

The application of solution regrowth techniques to ZnTe crystals has recently been reported. Wagner and Lorentz (1966) have obtained good quality crystals of several mm^2 by dissolving ZnTe in a solution of In or Ga and slowly cooling the solution at the rate of $100^{o}C$ per day through the solubility point. This technique is particularly interesting as growth from a donor-solvent would appear to be the optimum condition for obtaining n-type ZnTe. However, this was not unambiguously confirmed by the authors as no information was given concerning conductivity type.

Solution regrowth by a similar technique from a bismuth solution has been reported by Rubinstein (1966).

2.1.3 Purification

The starting material for crystal growth is normally elemental zinc and tellurium which are commercially available at purity levels in excess of 99.999%. ZnTe is obtainable commercially in sintered polycrystalline form, although the available purity of the compound is slightly below that of the constituent elements. This situation renders any special purification techniques unnecessary; indeed it is quite possible that such procedures would have a deleterious effect on the overall purity level.

In some cases, however, purification may be justified in order to eliminate residual traces of a particular element. In the majority of procedures it is sufficient to reduce possible surface oxide layers by heating in an atmosphere of pure H_2.

In growth techniques using elemental Zn and Te the elements are usually combined prior to growth by melting them together under vacuum, inert gas, or reducer gas. (Shiozawa et al., 1962; Aven and Segall, 1963).

Unfortunately, the use of high purity starting material does not necessarily guarantee a high purity compound. Impurities may be introduced from containers used in the growth procedures and/or by handling procedures prior to synthesis. It is therefore advisable in practice to restrict purification procedures, when used at all, to treatment of the final compound.

In vapour growth by sublimation there is always some degree of purification because of the one step distillation process. In such procedures all impurities will be reduced to at least their solubility limit at the growth temperature. Therefore, this technique is effective in reducing the concentrations of impurities, particularly metals. The fact that the sublimation temperature is

higher than the condensation temperature means that crystals are grown from the vapour phase under non-equilibrium conditions and inclusions of a second phase (Zn or Te precipitates) may be expected. Thus, purification procedures may be required to remove both impurities and gross inclusions of a second phase. The use of a zone-refining technique, similar to that used in conventional semiconductor purification, has been reported by Thomas and Sadowski (1964) to reduce the concentrations of metal impurities by an order of magnitude. The high melting point of ZnTe places a restriction on the usefulness of this technique.

Aven and Woodbury (1962) successfully applied the technique of solvent-extraction to the purification of ZnTe crystals. The solvent used was the metal component of the crystal, i.e. Zn, and the extraction was carried out by sealing the crystal together with additional Zn under vacuum and heating for two days at a temperature of 900 - 1000°C in order to establish equilibrium between the solid and liquid phases. After cooling the crystal was separated from the Zn. This technique was particularly effective in removing column IB elements and also has the advantage that possible Zn inclusions remaining in the crystal are removed. Lynch et al. (1963) found that such inclusions could be removed by heating crystals for a few minutes in an atmosphere of Zn at

$1100^{\circ}C$ or by annealing at a lower temperature ($800-900^{\circ}C$) in an inert atmosphere.

In addition to the possibility of microscopic inclusions, variations in the concentrations of native defects arise due to the fact that the existence region of a semiconductor is often extremely small and has some maximum value at a temperature between the maximum melting point and $T=0^{\circ}K$. The existence region is the composition limits within which the pure compound exists. As a consequence compounds prepared at high temperatures by conventional vapour transport and melt-growth techniques generally contain small amounts of a native second phase. The presence of such precipitates will affect the physical properties of semiconducting devices prepared from the material. Albers and Aten (1965) utilised an equilibration technique to eliminate Te and also possible Zn inclusions by annealing ZnTe crystals first in a powder mixture of ZnTe + Zn and then in a second mixture of ZnTe + Te. The equilibration temperature was $850^{\circ}C$. After quenching, single phase ZnTe crystals were obtained at room temperature. By use of a more sophisticated equilibration procedure the native defect concentration of crystals can be stabilised (Albers, 1967) and the composition of the crystal adjusted to lie within the existence region over a wide range of temperatures. Apart from experiments carried out by the origin-

ators, this technique does not appear to have been applied by other investigators. It is anticipated that crystals grown by conventional techniques will contain residual native defects giving rise to shallow acceptor states (Aven and Segall, 1963).

2.2 MATERIAL PROPERTIES

In this section the optical and electrical transport properties of ZnTe are reviewed. Some theoretical aspects of the electronic band structure and optical properties of the II-VI compounds are presented in appendices.

Investigations of the electroluminescent properties of II-VI compounds provide information on the electronic band structure and energy levels associated with impurities and imperfections. This evidence is complementary to that obtained by other techniques widely employed in semiconductor research. These include optical absorption, electrical transport, and electron spin resonance measurements. Conversely, detailed theoretical knowledge of band structure and impurities and imperfections provides a basis for understanding the luminescent and other physical properties of these compounds. In the case of carrier injection electroluminescence, the theories of p-n and metal-semiconductor junctions require consideration, and for high-field excitation processes, these theories require extension to cover avalanche breakdown and field influenced trapping processes. It is not intended to discuss in detail the theoretical

quantum-mechanical and electronic band structure concepts relevant to the properties of the II-VI compounds detailed above. However, some results of theoretical considerations which appear relevant to ZnTe are presented in appendix 1 and reference is made to the sources of detailed analysis of these topics.

It would appear from the present state of knowledge that the general character of the electronic band structure of a material can be determined by theoretical methods, but that quantitative details are better determined from experiments, for example, by cyclotron resonance measurements. Theoretical aspects of the band structure of the II-VI compounds have been reviewed by Segall (1967).

Considerable advances in the understanding of the electronic band structure of the II-VI compounds have been made possible by the results of investigations into optical absorption and reflection spectra over a range of photon energies. Absorption spectra associated with the smallest energy gap have been studied extensively and allow elucidation of the symmetries and location in the Brillouin zone of the conduction and valence band extrema as well as the parameters associated with these band edges. There are several regions of interest in the absorption spectra of a typical II-VI compound. In the "low" energy region the absorption is relatively weak, highly temperature dependent, and impurity sensitive. From investigations on near infrared absorption in both doped and undoped ZnTe

Watanabe (1966; Watanabe and Usui, 1966) obtained information on possible intervalence band transitions, acceptor state radii, and light and heavy hole masses.

At high energies the optical properties of the compounds are frequently investigated in terms of reflectivity spectra. Much of the experimental work and associated theoretical interpretation in this field has been carried out by Cardona and his associates (Cardona and Greenaway, 1963; Cardona and Harbeke, 1965; Cardona 1965). In reflectivity measurements over a wide range of wavelengths extending into the far ultraviolet these authors studied interband transitions and the band structure of ZnTe. From these results effective masses associated with band edge extrema were determined and band parameters due to transitions from split-off valence bands to the top valence bands and acceptor states were evaluated.

The absorption spectra in the region where the absorption increases rapidly with increasing photon energy and the region extending over a fraction of an eV where the spectra can exhibit sharp maxima have received considerable attention due to the fact that in these regions transitions between the valence and conduction band extrema take place. These transitions involve exciton systems. In semiconductors and pure insulators electronic excitation states exist in addition to the energy bands which are responsible for charge transport by electrons or positive holes. The basic electronic excitation in a perfect

semiconductor at low temperature is the transfer of an electron from a filled valence band to an excited state, leaving behind a hole with which the electron interacts via a Coulombic attraction. This "two-particle" system - the interacting electron and hole, together with the remainder of the crystal - constitutes the exciton system. The excitons do not contribute to electrical conductivity; they do however have a significant influence on absorption processes and in some excitation mechanisms and radiative recombination processes.

The model for the exciton system appropriate to the II-VI compounds is found to be proposed by that of Wannier (1937). This model is discussed in some detail in appendix 2. The more theoretical considerations of the optical properties of II-VI compounds which allows distinction to be made between "direct" and "indirect" gap semiconductors are also discussed in this appendix.

2.2.1 Absorption Properties

As remarked in appendix 2 the absorption properties of ZnTe have not been thoroughly investigated to date and little experimentally derived data exists on parameters such as ground state exciton energies, binding energies and reduced masses.

In experimental measurements on the photon energy and

temperature dependence of the absorption properties of II-VI compounds in the "threshold" region many anomalous results have been obtained. This is due in part to the great sensitivity of the spectra to defects, impurities and sample inhomogeneity and also to the effects on absorption of various surface preparation techniques. The results of Loh and Newman (1961) are of interest in this connection. These authors obtained a reciprocal thickness dependence of the absorption coefficient for photon energies in the region where the absorption decreased rapidly as the photon energy was reduced. This was ascribed to surface damage and correlated with a "damage-depth" produced by mechanical polishing. The effects of surface preparation techniques on the absorption of other II-VI compounds are also pronounced (Segall and Marple, 1967). It has since been pointed out by Redfield (1965) that the presence of an exponential absorption, observed in numerous semi-conducting materials can, in theory, be accounted for by the effect of electric fields within the space-charge region near the charged surface of the solid. The defining relationship used for the evaluation of absorption coefficients:

$$\int_0^T \alpha(x)\, dx = \mathrm{Ln}\frac{I_o}{I_T} \qquad (2.1)$$

Where T is the sample thickness and I_T and I_o the transmitted and incident intensities respectively. In the

ordinary case of uniform bulk absorption α is not a function of x and the relationship can be directly integrated giving the standard relation $\alpha T = \mathrm{Ln}\frac{I_o}{I_T}$ However, in Redfield's theory α is a strong function of x and the use of the usual relationship gives rise to an apparent absorption coefficient $\alpha_{app} = T^{-1}\mathrm{Ln}(\frac{I_o}{I_T})$ since, in an otherwise ideal sample, absorption below the energy gap occurs only in the two surface regions, I_T will not vary with thickness. Therefore, α_{app} will have a reciprocal thickness dependence at fixed frequency. This approach can be used as an alternative explanation of the results of Loh and Newman.

In a number of semiconducting materials low energy tails are observed in the absorption spectra. These tails are similar in shape to those obtained for an indirect-gap material and this has in the past led to the erroneous interpretation of such effects in terms of indirect transition processes. As has been reported by Marple (1966) for the case of intrinsic absorption in CdTe, no satisfactory fit was obtained in these tail regions with the various equations satisfying indirect transition processes (eqs. A.22; A.23; A.24). From measurements on ZnTe, Aten et al. (1962), concluded that the lowest energy optical transition in ZnTe was indirect, and that the increase in slope of the absorption energy relationships at higher energies was associated with the onset of direct

transitions. Indirect transitions have also been proposed for two other II-VI compounds, CdTe and ZnO. The anomalous nature of these results has been discussed by Cardona and Harbeke, (1963) as it is at variance with other experimental evidence supporting the direct transition mechanism which, on the basis of the consensus of evidence, would appear to be common to all II-VI compounds. The presence of "tails" on the low energy side of the absorption edge is obtained in high-purity samples as well as in those where impurity effects would be anticipated. For the case of direct-transition material the presence of tails on the intrinsic absorption spectrum can be explained in terms of a phonon-assisted "direct" exciton absorption mechanism. This mechanism in no way invalidates the main tenets of the direct-transition theory. For a direct-transition material this phonon-assisted absorption provides an explanation for the tails observed in the absorption spectra. For an indirect transition material the phonon-assisted direct exciton absorption process may mask the indirect processes, resulting in the shape of the absorption spectrum in the band-edge region being dictated by the former. Phonon assisted direct transitions were first proposed by Dumke (1957) for a process involving free electron-hole pairs i.e. for band-to-band transitions. Dumke showed that, for a substance with conduction and valence band extrema at

the same point in k-space giving rise to absorption by direct transitions, indirect transitions can also take place between these extrema. In these transitions, the electrons must emit or absorb phonons of essentially zero wave vector and the absorption will consist of components equally spaced above and below the direct transition threshold by the energies of such phonons. Since, in this case, indirect transition absorption is much weaker than that associated with direct transition, then absorption processes involving the former and located at energies above the direct transition threshold will not be resolved. Therefore only those components of indirect transitions which begin at energies below this threshold will be seen. These components are due to transitions in which optical phonons with zero wave vector are absorbed, these being the only phonons with finite energy at zero wave vector. This absorption will therefore appear on the direct absorption curve as a tail of the same shape but differing in detailed phonon structure from that of an indirect transition material. This tail will tend to vanish at low temperatures.

The theoretical treatment for phonon assisted transitions involving excitons was first advanced by Thomas et al. (1960). In this case it is envisaged that in addition to the transitions without phonon participation, which

have already been discussed, "direct" (K=0) excitons can also be created by the simultaneous absorption of a photon and one or more phonons. In the single phonon case the absorption of a phonon of wave vector q and energy h_1 together with a photon of energy h produces an exciton in the final state with $E_{ex}(K) = h\nu + h\omega$ (appendix 2) and wave vector K=q via a lower energy intermediate state. The relevant phonons are those of the longitudinal optical (LO) mode since the electronic particles couple strongly with the dipole moment associated with these modes. The result of the theoretical treatment involving second order perturbation theory is that the absorption coefficient should be an essentially temperature independent function of $E_{exl}(T) - h\nu$ In the calculation it was assumed, for simplicity, that the only exciton state making an important contribution to sums over intermediate and final states was the n=1 band. The experimental data for CdTe was found to give a good fit with this theory (Segall 1966). It was found in these studies that the absorption by one phonon had a threshold, in agreement with energy conservation principles, at $E_{exl} - h\nu = \hbar\omega$; beyond this threshold, absorption resulted from processes involving one or more phonons.

As the temperature is increased the threshold for the one-phonon process gradually becomes indistinct and the

absorption coefficient acquires an exponential dependence on photon energy given by

$$\alpha(h\nu) = \alpha^{o}\exp\ (b(h\nu - h\nu_{o})(kT) \qquad (2.2)$$

which is Urbach's rule (Urbach, 1953). Here k represents Boltmann's constant and b and α_{o} are constants. This smoothing results in a large part from increased thermal width of the exciton line. Segall (1966) has advanced the theory that Urbachian behaviour in the II-VI compounds can be explained by an extension of the low temperature absorption mechanism of photon absorption through the creation of (unlocalised) excitons accompanied by the annihilation of a few LO phonons. As pointed out be Segall this is in contrast to previous discussions where Urbach behaviour is understood in terms of localised excitons, which, in the case of intrinsic excitons, are self-trapped. Regardless of the mechanism, Urbach behaviour effectively masks the typical relationships involving both direct and indirect transition processes in materials where it occurs. In CdTe (Marple 1966) this behaviour is observed at temperatures $\geqslant 130^{o}$K and in ZnTe (Loh and Newman) it was observed at temperatures extending down to 77°K. Some of the previous results obtained on ZnTe are shown in Fig.2.5. This figure illustrates the lack of agreement between the reported results. There was considerable variation in the sample preparation techniques used by the various authors.

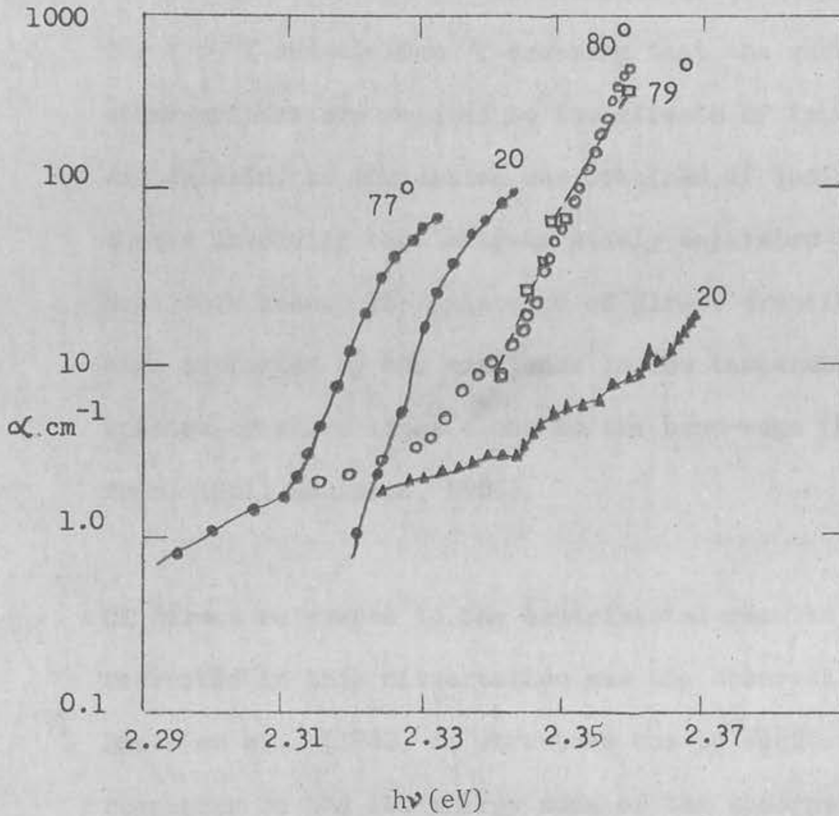

FIGURE 2.5 Absorption coefficient α, of ZnTe as a function of photon energy, $h\nu$, as reported for $T \approx 77°$ and $2°K$ o: Aten et al. (1962); o: Marple (1966); Δ: Marple (1966); □ : Loh and Newman (1961).

Aten et al. (1962) utilised "as grown" ZnTe platelets prepared by a sublimation method, Loh and Newman (1961) studied mechanically polished and etched crystals, Marple (1966) used vapour-phase grown crystals purified in Zn and mechanically polished. Marple (1966) has demonstrated that for high-purity crystals intrinsic exciton absorption is related to the LO phonon-assisted direct exciton process for $T > 65^{o}K$ and $\alpha > 10cm^{-1}$; assuming that the results of other authors are related to the effects of impurities and defects, no indication was obtained if indirect processes involving band extrema widely separated in the Brillouin zone. The existence of direct transitions is also supported by the existence in low temperature emission spectra of sharp lines close to the band-edge (Halsted and Aven, 1961; Redfield, 1965).

Of direct relevance to the experimental results to be described in this dissertation was the observation by Dietz et al. (1962) of structure due to exciton-defect complexes on the low energy side of the absorption edge. The centre involved was located 0.4 eV below the band-gap energy. Further absorption and fluorescent investigations of this centre by Hopfield et al. (1966) using ZnTe crystals grown from a melt containing quantities of ZnO, resulted in the conclusion that the centre was associated

with oxygen substituting isoelectronically for Te (i.e. oxygen is incorporated as an uncharged impurity centre). This isoelectric substituent, being significantly different from the atom it replaces was considered to act as a trap. This trap has the capability of attracting electrons by virtue of the local potential created by the lowering of the s and p orbitals of the substituent. Once the isoelectronic trap has captured an electron, a hole will bind to the long-range Coulomb potential in an acceptor-like wave function. This bound exciton state is termed an isoelectronic acceptor. As will be described later this centre can significantly affect the electroluminescent properties of ZnTe devices.

Photoluminescence in ZnTe is less easily stimulated than in the case of ZnS and is normally only observed at low temperatures. For doped crystals several peaks are usually observed in the range 2.26 - 2.36 eV (Watanabe, 1966), the most intense maxima for p-doped ZnTe being located at 2.326 eV. Photoconductivity measurements on high-resistivity crystals showed a peak in the spectral photoresponse at this same energy, whereas the maxima for low resistivity material lay at 2.23 eV (Takahashi et al., 1966).

Radiative recombination processes occurring within a few tenths of an eV of the band gap energy are referred to by the term "edge emission". These processes are pronounced in recombination spectra at low temperatures, and, in general, a band edge emission process is characterised by a set of "lines" separated by equal energy increments. The width and relative strength of the satellite lines in a set increase with displacement of the set from the band gap energy, until, at sufficient displacement, structureless broad emission bands are observed. The excited states for some of the dominant band edge emission processes can be semi-quantitatively described in terms of electron-hole pairs localised near ionised or neutral crystal defects and termed "bound exciton complexes". The subject of bound exciton complexes in the II-VI compounds and their properties has recently been reviewed by Halsted (1967). The possible combinations of aggregates comprising a charged defect and one or more electrons and holes are considered. These types of aggregates are known to provide, or could provide, bound states near the conduction and valence band edges which may participate in optical transitions. The primary experimental technique in such studies is the Zeeman effect. The theoretical treatments utilise simple hydrogenic models for bound exciton complexes and assumes valence and conduction bands centered on $k=0$. Such investigations provide information on both the energy levels

associated with defect complexes and the transition energies associated with the variety of possible defect complexes. In the case of phonon assisted transitions the occurrence of sets of lines equally spaced in energy allows evaluations of the energies of the phonons involved; for example, the dominant structure of edge emission in the II-VI compounds has been associated with the longitudinal optical mode lattice vibrations (Halsted et al., 1961). Other phonon energies have been evaluated from restrahl data and the study of lattice absorption bands in the infrared. Satellite emission peaks other than those due to LO phonons have also been observed in ZnTe (Dietz et al., 1962) and tentatively correlated with correlated with transverse accoustical $(TA)_1$, longitudinal accoustical (LA) and transverse optical (TO) phonons.

Although stimulated emission of radiation under electron beam excitation has been reported for a number of II-VI compounds such as CdSe, CdTe, ZnS and ZnO (Benoit a la Guillaume and Debever, 1965; Nicoll, 1966) lasing action action has, to date, not been observed in ZnTe.

2.2.2 Electrical Transport Properties

The electrical transport properties II-VI compounds provide valuable information on the kind and number of carriers, the band structure of the material and the

electron scattering mechanism which in turn allows elucidation of electron-phonon interactions and crystal imperfections. By comparison of experimental results with theoretical models, it is often possible to determine the numerical values of microscopic material parameters. Electrical transport measurements also provide an indication of the purity of the material.

On the basis of experimental results it would appear that geometrical defects do not have a significant influence on the transport properties of the II-VI compounds and that the most important defects are the vacancies and interstitials of the constituents. For ZnTe there has been little evidence that interstitial Te or Te vacancies are electrically active (Devlin, 1967). However it has been suggested that cation vacancies are electrically active as double acceptors (Aven and Segall 1963). The evidence covering the II-VI compounds in general as obtained from transport and other experimental data suggests that the concentration of isolated interstitials and vacancies in II-VI compounds is quite low with the possible exception of cation vacancies in the tellurides.

Although electrical transport measurements reveal details

of the band structure of compounds, this evidence is restricted to only those features within either a fraction of an eV of the bottom of the conduction band or the top of the valence band. Over this small energy range complete specification is obtained from relatively few parameters. These are the energy and location of minima and maxima in k-space, the effective mass, which is an indication of band curvature, and any warping due to degeneracy or non-parabolicity. Unfortunately, the relatively small amount of experimental work completed on transport properties and their possible anisotropy has contributed little to our knowledge of the band structure of these compounds. In most cases transport measurements have provided only weak confirmation of other experimental measurements and theoretical predictions. The determination of effective mass of holes in ZnTe is the sole exception to this - the only estimate available has been obtained from mobility measurements.

The quantum-mechanical treatment of defect states utilises the approach known as the effective mass approximation. This formulation is normally considered in terms of weakly bound impurity states, with the more deeply-bound states being treated as deviations from this result. For the weakly-bound states the assumptions made are: (1) the

derivation is made using the one electron approximation, (2) only a single band is involved, (3) only a small range of k about the extremum is required, and (4) that the perturbing potential can adequately be represented by the Coulomb energy $-q^2/\kappa_s r$. (κ_s is the static dielectric constant).

For the case of a simple substitutional donor the wave function for weak binding of the additional electron to the donor will be very extended and most of the probability density, $|\psi(r)|^2$, will be outside the cell containing the impurity. The electron is assumed bound to the donor by Coulomb attraction of the extra charge, and is envisaged as orbiting around the donor in undisturbed regions of the crystal. This motion is considered to be determined by the properties of the conduction band near the minimum, in particular, by the effective mass m^*. The description of this state is therefore based on the Bloch functions for k in the vicinity of the band edge. In the mathematical formulation the wave function of the donor state is expanded in terms of Bloch states (appendix 1).

Using the assumptions (1) - (4) above and considering only the k=o minimum in a cubic material it can be shown (Kohn 1957) that a Schrödinger-like equation described

as the "effective mass equation" for the donor is obtained. The resulting equation is very similar to that obtained for the hydrogen atom. The energy spectrum of the system can then be considered to consist of discrete levels and can be shown to be of the form (Segall, 1967)

$$_n = (E-E(o))_n = \frac{Ry}{K_s^2}\frac{m^*}{m}\frac{1}{n^2} = \frac{-E_D}{n^2} \qquad n = 1.2... \qquad (2.3)$$

and a continuum representing the ionised states. E_D is here the donor ionisation energy with Ry equivalent to the Rydberg (13.6 eV). Although this equation can be used to determine effective masses and impurity ionisation energies with considerable success in the elemental semiconductors, in application to II-VI compounds the agreement is less satisfactory. This is due to the tighter binding of the electrons in these compounds and to degeneracy of the band edge for the case of acceptor states. This latter condition requires consideration of more complex matrix differential equations. This consideration, and the extension of the effective mass approximation to more deeply bound states, is discussed by Kohn (1957).

The most useful experimental technique for determining donor and acceptor ionisation energies, and that which has been most widely applied, is measurement of the Hall

effect. It is normally adequate to evaluate Hall coefficients under the assumption that only one type of carrier is involved, and carrier concentrations are evaluated as $R_H e^{-1}$ where R_H is the Hall constant and e the electronic charge. This assumes that the ratio of the Hall mobility to the drift mobility of the current carriers, μ_H/μ_d is unity. R_H is evaluated in the conventional manner from the force exerted on the charge carriers by the combined electric and magnetic fields, i.e. for mutually orthogonal electric and magnetic fields

$$R_H = \frac{E_y}{J_x B_z} \qquad (2.4)$$

where J_x is the applied current density, E_y the Hall field developed and B_z the magnetic flux density. Considering a p-type material and assuming that only one major impurity is present and that it has only one ionisation level the carrier concentration data for compensated material can be analysed by the use of the expression (Blakemore, 1962)

$$p\,(p+N_D)/(N_A-N_D-p) = 2(2\pi m^* kT/h^2)^{3/2}\,(1/g)\exp\left(\frac{-E_A}{kT}\right) \qquad (2.5)$$

where p is the hole concentration, N_D the donor concentration, N_A the acceptor concentration and E_A the acceptor ionisation energy. The degeneracy factor, g, depends on

the nature of the impurity and the band edge involved. For four-fold degenerate valence band wave functions, impurities which are acceptors have a degeneracy factor of 4. (Teitler and Wallis,1960).

In the II-VI compounds there are several mechanisms of importance in considerations of interactions which result in carrier scattering. In these compounds it is considered that the polar nature of the semiconductors plays a major role in their transport properties. At least four scattering mechanisms require consideration; these are scattering by the piezoelectric activity of the acoustic modes, the deformation potential, and nonpolar and polar interactions with the optical modes. For all four mechanisms the mobility would be expected to fall with increasing temperature and comparison can be made between the experimental temperature dependence of the mobility and that predicted by the scattering mechanisms (Aven and Segall, 1963; Devlin, 1967).

The first mechanism arises from the electrostatic potential induced by the polarisation accompanying the acoustic phonons due to the piezoelectric effect. Since momentum conservation requires that only phonons of wave vector comparable to the electron wave vector can interact with

the electrons, the energy of these phonons is negligible except at low temperatures. The mobility of a carrier in a simple band with this interaction is

$$\mu_{piezo} = 1.05 \rho \langle u_l^2 \rangle K_s^2 \, e_{14}^{-2} (m^*/m)^{-3/2} T^{-1/2} \mathrm{cm^2/Vsec} \quad (2.6)$$

where K_s is the static dielectric constant, e_{14} the piezoelectric constant (in esu/cm^2), the density and $\langle u_l^2 \rangle$ is the square of the longitudinal sound velocity averaged over direction. The values of the various parameters in the above equation are known for the II-VI compounds. In the case of ZnTe and the majority of investigated impurities the correlation between the theoretical and experimental mobility dependence is poor.

Deformation potential (or acoustic mode) scattering by acoustic phonons is one of the most important scattering mechanisms in the elemental semiconductors. The mobility is given as

$$\mu_{dp} = 3.0 \times 10^{-5} (m^*/m)^{5/2} \rho \langle u_l^2 \rangle T^{-3/2} E_b^{-2} \mathrm{cm^2/Vsec} \quad (2.7)$$

where E_b denotes the deformation potential in eV for the relevant band edge. Despite uncertainty concerning the value of the deformation potential in ZnTe it would appear that this scattering mechanism is not of great significance for metal impurities of the type Au, Ag and Cu.

The expression for the scattering in degenerate p-like bands scattered by non-polar interaction with the optical phonons, μ_{npo}, follows from the derivation of Ehrenreich and Overhauser (1956).

$$\mu_{npo} = \frac{1.35\times10^{17}\rho a^2\theta^3}{C_4^{\,2}\ T^{5/2}}\left[\frac{m^{5/2}(m_1^{\,1/2}+m_2^{\,1/2})}{(m_1^{\,3/2}+m_2^{\,3/2})}\right]\int_0^\infty \frac{x\ \exp(-\theta T^{-1}x)dx}{\varphi(x^{-1})}\ cm^2/Vsec \qquad (2.8)$$

with $\varphi(t) = n(1+t)^{1/2}+(n+1)(1-t)^{1/2}$ for $t<1$

$= n(1+t)^{1/2}$ for $t>1$

Here n is the optical phonon occupation number given by $(\exp(\theta/T-1)^{-1}$, is the Debye temperature, m_1 and m_2 are the masses of the light and heavy hole (associated with the two valence bands) respectively, a is the lattice constant (in cm) and C_4 is the coupling constant (in eV). These coupling constants, or optical mode coupling parameters, are referred to by some authors as "optical and acoustic deformation potentials" (Devlin, 1967). It appears that valves of this parameter have not been directly evaluated for ZnTe and the values obtained for other semiconductors are frequently incorporated in the equation given above (Aven and Segall 1963). It would appear that this scattering mechanism is not operative in ZnTe at low temperatures, but could conceiv-

ably account for a portion of the scattering at room temperature and above.

The most important scattering in ZnTe is polar optical mode scattering and results from the interaction between the charge carriers and the electrical polarisation associated with the long wave longitudinal optical phonons; an electrostatic potential is induced by these phonons in the partially ionic lattice. The strength of the interaction is indicated by the polar coupling constant α which is

$$\alpha = (m^*/m)^{1/2} \, (Ry/\hbar\ )^{1/2} \, (K_\infty^{-1} - K_s^{-1}) \qquad (2.9)$$

where Ry is the Rydberg of energy, $\hbar\omega_l$ is the energy of the longitudinal optical mode for long wavelength, and K_∞ is the optical dielectric constant. For compounds where the interaction is relatively weak (i.e. the coupling constant $\alpha < 1$) second order perturbation theory can be used to calculate the transition probability $W_{k_q}^{k'}$ of a carrier being scattered from a state of wave vector k and energy E, to a state of wave vector k' and energy E' with the absorption of a photon of wave vector q and frequency ω (Ziman, 1960).

$$W_{k_q}^{k^1} = (2q^2 N(q)/\gamma\omega q^2) \, \delta\,(k'-k-q) \, \delta\,(E'-E-\hbar\omega) \qquad (2.10)$$

where q is the charge of the carrier, N(q) is the population of the q phonon mode. Here γ is obtained from $1/\gamma = {}^2(1/\mathcal{K}_\infty - 1/\mathcal{K}_s)$ and δ is the Dirac delta function. It can be shown (Devlin, 1967) that further derivation using this equation leads to an expression for the mobility

$$\mu_{polar} = \frac{0.870(m/m^*)}{\alpha \hbar \omega_l} \frac{e^Z - 1}{(Z^{1/2})} \quad G(Z)e^{-\xi} \ cm^2/Vsec \qquad (2.11)$$

where $Z = \hbar\omega_l/kT$, with $h\omega_l$ in eV, and $G(Z)e^{-\xi}$ is a tabulated function. This result does not allow for screening by the carriers, but this can be neglected in the case of ZnTe (Aven and Segall, 1963). For both intrinsic and p-type ZnTe this theoretical result gives good agreement with the experimental temperature dependence of the mobility and appears to be the dominant scattering mechanism.

Impurity scattering may be of importance in impure and nonstoichiometric compounds, especially at low temperatures. There is an absence of reference to impurity scattering in the literature on ZnTe. Such scattering might be expected to give rise to a mobility derivable from the Brooks-Herring formula (Brooks, 1955)

$$\mu_{is} = \frac{4(2/\pi)^{3/2} (kT)^{3/2} (4\pi\varepsilon_o\mathcal{K}_s)^2}{q^3 m^{*1/2} N_I[\ln (b) - 1]} \qquad (2.12)$$

where N_I is the concentration of ionised defects and b is given by

$$b \doteq \frac{6m^* (kT)^2 (4\pi \varepsilon_o K_s)}{\pi q^2 \hbar^2 n'}$$

It is required that $b \gg 1$. In p-type material in thermal equilibrium

$$n = p + (N_A - N_D - p)(p + N_D)/N_A$$

and $N_I = p + 2N_D$

The characteristic three-halves temperature dependence of the mobility predicted by the above equation may only be observed if N_I is temperature independent; this may only be true at low temperatures. Unionised impurities can also scatter carriers and can contribute to the mobility at low temperatures.

Use has been made of the various scattering mechanisms described above in the determination of the effective mass of holes. By correlating the theoretical mobility with that obtained from Hall measurements Aven and Segall (1963) and Shiozawa et al. (1964) obtained a value of 0.6 m.

The mobility of holes in ZnTe has been measured by several workers; Tubota et al. (1960), Tubota (1963); Aven and Segall (1963); Devlin et al. (1960); Shiozawa et al. (1962); and Thomas and Sadowski (1964). The reported results are in good agreement at room temperature and above (100 - 200 $cm^2/Vsec$). Below room temperature the results show significant variations between samples and this could be attributed to impurity scattering. Several authors noted that at temperatures below approximately 100°K the ohmic properties of the contacts (usually evaporated or electroplated Au plus In or In/Ag solder) were not retained. Tubota found that the mobility varied as $T^{-3/2}$ at higher temperature where impurity scattering could not be considered significant and interpreted this as being due to accoustical mode scattering. Measurements on crystals of higher purity (Aven and Segall, 1963; Shiozawa et al. 1964) allowed interpretation of the mobility results primarily in terms of interband polar scattering as described previously. Both Aven and Segall and Shiozawa found that piezoelectric scattering in ZnTe was negligible. The agreement in determination of the effective mass and coupling constant for interband scattering between these two sets of results in surprisingly good considering the simplified theoretical treatments used and the indirect methods which had to be applied due to the number of unknown band parameters.

Although a wide variety of dopants have been incorporated in ZnTe, there is little evidence to indicate that it is possible to obtain n-type conductivity in this material. Reported room temperature values for not intentionally doped material range from 0.5 - to 50 ohmΩ-cm with associated carrier concentrations of the order of $10^{16}/cm^3$ and mobilities of 200 $cm^2/Vsec$. As discussed above the native defect (acceptor) centre in this form of the material is generally accepted to be the Zn vacancy. Fisher et al. (1964), using the growth technique described earlier in section 2.2.2, report to have obtained Al doped n-type crystals with room temperature dark resistivities between 10^5 and 10^7 ohm-cm and electron mobilities of 340 $cm^2/Vsec$ under illumination. Wagner and Lorenz (1966) attempted to obtain n-type crystals by solution regrowth from a donor (In) solution. The resulting crystals had resistivities of 10^5 ohm-cm and electron mobilities of 70-350 $cm^2/Vsec$; it was not stated explicitly that n-type conductivity was obtained. Tubota et al. (1961) found that doping ZnTe with In did not result in n-type conductivity but in high-resistivity p-type material. Measurement of the variation of resistivity with temperature as $\exp(E_A/kT)$ allowed an estimate of the band gap energy to be made. The resulting energy was 2.12eV, a value which is within the range of room temperature band gap determinations made from optical measurements (2.1-2.3eV).

Aven and Segall doped crystals of ZnTe with Cu, Ag and Au. These impurities act as deep acceptors with ionisation energies of 0.15eV, 0.11eV and 0.22eV respectively. The 0.11eV level was previously reported by Bube and Lind (1957) and Devlin et al. (1960) but was attributed to Cu. A level at 0.24eV has been reported by Boltaks et al. (1955), but was not identified. Aven and Segall observed a native defect whose concentration varied with the pressure of Te vapour in which the crystal was heated. This defect had an ionisation energy of 0.048eV and was attributed to the first ionised state of the Zn vacancy. They found some evidence for a second ionisation of this defect at 0.14 ± 0.02eV. Thomas and Sadowski (1964) also identified a native acceptor as the Zn vacancy from measurements on the p-type conductivity of undoped ZnTe between 700 and 950°C at Zn pressures of between 10 and 400 mm Hg: The first ionisation state of a Zn vacancy was reported by Tubota (1963) at 0.033-0.035eV. This author also observed a deeper acceptor level at 0.22-0.27eV in crystals doped with In, I, Sb or Se. The first two impurities would be expected to introduce donor centres and the second pair acceptor centres. Tubota interpreted this level as the second ionised state of the Zn vacancy with the first level compensated. It is therefore obvious that a lack of agreement exists between the reported ionisation energies of the native defect in ZnTe. The ion-

isation energies obtained by Tubota for Cu and Ag are in agreement with those reported by Aven and Segall.

Although the most common dopant introduced into ZnTe crystals used for the fabrication of electroluminescent devices is P, few results have been presented on the electrical transport properties of P-doped crystals. Miksic et al. (1964) reported on investigations of ZnTe grown from an excess Te melt containing either 1% As or 1% P. The P dopant gave rise to room-temperature resistivities in the range 0.06-0.5 ohm-cm with associated carrier concentrations of 10^{17}-$10^{18}/cm^3$ and mobilities of 100-200 $cm^2/V.sec$. Watanabe and Usui (1965) reported the P level in ZnTe to have an ionisation energy of 0.04eV. Hinotani and Sugigami conducted experiments on nominally undoped ZnTe and analysed the current-voltage characteristics in terms of Lampert's (1956) theory of one-carrier space-charge-limited currents. The limited agreement obtained between theory and experiment indicated a hole trap depth of 0.13-0.17eV with a concentration of 10^{16}-$10^{17}/cm^3$. Crowder et al. (1966), reporting the highest low temperature efficiency yet observed in ZnTe devices, used crystals grown in an excess Te melt with between 0.5 and 1 mole % Li, and reported the room temperature resistivity hole concentration and mobility to be 0.29 ohm-cm, 2.2 x $10^{17}/cm^3$, and $97cm^2/V.sec$. respectively. At 77^oK these

values were 1.75 ohm-cm, $5.1 \times 10^{15}/cm^3$, and $630 cm^2/V.sec$. Diffusion of Al into the crystals changed the room temperature values of these parameters to 0.11 ohm-cm, $8.5 \times 10^{17}/cm^3$ and $70 cm^2/V.sec$, and the 77^oK values to 0.97 ohm-cm, $4.1 \times 10^{16}/cm^3$, and $160 cm^2/V.sec$. No information was given on ionisation energies associated with these impurities.

2.2.3 Electroluminescence

As stated in the introduction there are at least two general types of mechanisms by which electroluminescence can be produced in crystalline solids. The first is the injection of minority carriers across a potential barrier followed by radiative recombination with majority carriers either directly or at recombination centres. The methods of introducing minority carriers into the recombination region are varied and encompass injection over the reduced potential barrier of a p-n junction, injection over a forward biased metal:semiconductor junction, tunneling of minority carriers through naturally occuring or fabricated insulating layers between a metal contact and the semiconductor, and injection of minority carriers created by impact ionisation in the localised high-field of an insulating region. For the case of ZnTe, which can only be usefully made with p-type conductivity, the first of these

injection mechanisms has no direct application. In this connection, however, consideration must be given to the outstanding results obtained from p-n heterojunctions fabricated from ZnTe and other II-VI constituents exhibiting n-type conductivity, eg. $Zn_xCd_{1-x}Te$ and $ZnSe_xTe_{1-x}$ alloyed quasi-homojunctions, and CdS-ZnTe heterojunctions.

The second type of mechanism relates to the acceleration of majority carriers to sufficient energies to impact ionise either the lattice or a filled recombination centre by means of an applied electric field. These "hot" carriers or secondary carriers generated in the collision process can subsequently recombine with the opposite species either directly across the forbidden gap or at a recombination centre. The much higher than thermal energies of these accelerated carriers allow the possibility of some recombination radiations which exceed in photon energy that of the band gap. Such processes may take place in reverse biased p-n junctions where impact ionisation can occur in the high field region of the junction. This effect has been observed in both elemental semiconductors and the various forms of II-VI compound junction devices. The process can also take place in localised high field regions in metal: semiconductor devices. As a generalisation it can be stated that more efficient electroluminescence is obtained from

injection than from impact ionisation processes.

Regardless of the actual electroluminescence mechanism which is operative a number of different steps may take place between excitation and radiative recombination, involving the transport of the excitation energy from one site to another. These steps include trapping processes which may delay the recombination, exciton migration and capture at activator centres, the quantum mechanical processes of resonance transfer between luminescence systems, and Auger recombination in which recombination energy appears not as photons nor phonons but in the increased kinetic energy of the carriers. This section will discuss the mechanisms of the excitation processes which are relevant to ZnTe, including subsequent energy transport and recombination, and will conclude with a description of the results of previous studies of the electroluminescent properties of this material. No attempt will be made to review the electroluminescent properties of II-VI compounds in general, although the results obtained for alloyed heterojunctions of ZnTe with other II-VI compounds will be presented. As this report is primarily concerned with electroluminescence resulting from direct-current excitation, no consideration will be given to electroluminescence produced by alternating-field excitation.

(For the case of the compound ZnS, this latter phenomenon has been the subject of considerable investigation (Henisch, 1962; Ivey, 1963).)

2.2.3.1 Mechanisms of Electroluminescence

2.2.3.1.1 Minority Carrier Injection

Minority carrier injection is first considered. In order to stimulate the emission of radiation from a solid it is necessary to alter the equilibrium between holes and electrons in the material and thus produce radiative recombination in excess of that associated with thermally generated holes and electrons. The recombination radiation contributes to the thermal "black-body" radiation characteristic of the temperature and the material. If as a result of applying an electric field minority carriers are injected into a crystal, either at a metal contact which has an appropriate work function, or at a p-n junction, then the rate of recombination is considerably increased over the equilibrium value. Minority carrier injection is only one way of altering the existing equilibrium between holes and electrons, but its importance in terms of electroluminescent phenomena has resulted in the use of the terminology "injection-luminesence" to character-

ise such processes. A concomitant process is majority carrier extraction. This occurs at the same junction as the injection process and is of particular importance for the case of heterojunction, metal:semiconductor or metal:insulator:semiconductor devices, as it results in current flow without recombination and thereby reduces the quantum efficiency of the device. The suppression of the majority carrier extraction process is therefore desirable and for this purpose many forms of composite device structure of varying degrees of complexity have been proposed. (e.g. Fischer and Moss, 1963.)

p-n Junctions

Of the various mechanisms by which minority carrier injection can be achieved the simplest is that which occurs at a forward biased p-n junction. In this case the injection characteristics are controlled by the bulk properties of the semiconductor rather than by the complicated surface characteristics of the metal:semiconductor junction. Three types of p-n junction are of relevance to this discussion, the homojunction, the heterojunction and the quasi-homojunction. The first term refers to junctions

formed in an elemental semiconductor or compound at the boundary between two regions of opposite type conductivity. These junctions may be produced by alloying a donor(acceptor) impurity on the surface of a p (n)-type crystal at temperatures well below the melting point, by diffusing the appropriate n-or p-type dopant at elevated temperatures into the oppositely doped crystal, or by epitaxial deposition from the vapour or liquid phase of a layer of one conductivity type onto the surface of a substrate exhibiting the opposite type of conductivity. Of the II-VI compounds only CdTe appears to exhibit amphoteric (p- and n-type conductivity) conduction at conductivity levels suitable for application as a p-n homojunction device. The heterojunction is formed by contacting one type of semiconducting material with a chemically different material of opposite conductivity type. At the interface of the two materials the band structure is completely disrupted and there is a step in the band gaps (e.g. Cu_2S-ZnS, CdS-ZnTe). Experimental evidence indicates that the II-VI compounds form alloys, miscible in all proportions, of the type $ZnSe_xTe_{1-x}$ and $Zn_xCd_{1-x}Te$,

with the possible exceptions of the system ZnS-ZnTe and CdS-CdTe. Apart from the ZnSe-ZnTe and CdSe-CdTe systems, which posses minima, the variation of band gap with composition is monotonic. It is therefore possible by choosing compounds of opposite conductivity type to achieve amphoteric conduction in a II-VI alloy system. Junctions formed in such devices are described by the term quasi-homojunction and are of importance in the achievement of efficient injection luminescence.

In practice a variety of techniques are used to prepare such junctions. Two broad categories, in essence similar to the techniques applied to homojunctions, are the diffusion of an impurity into an alloy crystal grown with one type of conductivity, creating a region of opposite type conductivity (e.g. the diffusion of Al donors into p-type $ZnSe_xTe_{1-x}$), and alloying of a compound of one conductivity type by simultaneous diffusion of the alloying element and an impurity, resulting in a region of opposite conductivity type (e.g. the diffusion of Zn and P acceptors into n-type CdTe crystals). The fast Zn diffusion results in an n-type

$Zn_xCd_{1-x}Te$ alloyed crystal and the slower P diffusion produces a p-type layer within the alloy).

As stated previously in this dissertation, ZnTe normally exhibits only p-type conductivity. It is convenient at this stage to consider the factors which prevent the achievement of amphoteric conduction in the material and therefore prohibit the fabrication of p-n homojunctions. The fact that exposure of ZnTe crystals to high concentrations of donors is ineffectual in producing n-type conductivity is due to the effectiveness of self-compensation processes in this material. This self-compensation effect can be attributed to the presence of anion and cation vacancies which are normally present in appreciable concentrations even at room temperature. Under normal conditions, the presence of these vacancies does not affect the electrical conductivity of the material as the opposite types of vacancy annul each other by recombination of the donor electrons and acceptor holes. It therefore results that heating of a II-VI compound in an inert gas renders the material more insulating due to the tendency of anion and cation vacancies to be created in equal concentra-

tions. If, however, taking the example of ZnTe, the crystal is fired in an anion (Te) atmosphere, the excess concentration of cation (Zn) vacancies readily results in p-type "self-doped" conductivity. Paradoxically, due to self-compensation, firing in a Zn vapour only results in the production of a more insulating p-type crystal. Whether or not self-doping of a II-VI compound results in p- or n-type conductivity can be considered to be dependent on the relative cation and anion size. It is found that if the ratio of the cation radius, r_c, to anion radius, r_a, is > 1, n-type conductivity is normally obtained and conversely p-type conductivity results for $r_c/r_a < 1$. For the II-VI compounds in general, this relationship, and the occurrence of self-compensation, can be partially explained by considerations of the relative levels, in relation to the valence and conduction band edges, of native acceptors and donors. For ZnTe, these considerations appear to be the principle factor influencing self-compensation effects in the material. This behaviour can be explained in terms of a simple model presented by Mandel (1964). If the vacancy cavity is large, because of removal of a large atom, the wavelength of the ground state of the carrier

standing wave in the associated potential box is long; therefore, the energy is low and the carriers are mostly near the bottom of the potential box. This corresponds to a high ionisation energy of the vacancy. Conversely, if a small atom is removed, the small vacancy cavity is associated with a short standing wave, resulting in higher frequency and higher energy of the state, and the carriers are at a higher level in the potential box, corresponding to low ionisation energy. If the cavity is very small, the wave function of the carrier "spills over" into the band resulting in a "hydrogenic" centre. In ZnTe the cation is small and the anion large (r_c/r_a = 0.99); hence native donors are very deep, but native acceptors shallow. This explains the observed conductivity limitations. The relative levels of donors and acceptors can also be used to explain the influence of self-compensation on the conductivity produced by impurities. In compensation-prone materials the addition of donor impurities results in the formation of native acceptors, whereas the addition of acceptor impurities produces native donors. The tendency to form compensating vacancies can be ascertained from energy balance considerations; if the "compensation energy", E_c,

(the energy resulting from recombination of carriers associated with the impurity centre and those associated with the vacancy) exceeds the energy required to create the vacancy, E_V, then vacancy formation will predominate, and vice versa. The energy required to create a vacancy is dependent on the crystal cohesion energy, which increases as the bonds become less ionic and the atoms smaller. It is also the case that the energy gained by compensation is greater for energy displacements associated with impurity and vacancy levels widely separated in the band gap (ie. the tendency to compensation is greater for higher band gap materials). The added impurity is normally chosen to occupy a shallow level. Therefore, if the level of the compensating vacancy is also shallow, and E_c is greater than E_V, then compensation can take place. If the compensating vacancy has deep levels, the tendency is reversed. For ZnTe the anion vacancies (donors) have deep levels in accordance with the condition $r_c/r_a < 1$ and therefore doping with acceptor impurities results in little or no compensation, whereas donor impurities are fully compensated by shallow acceptor levels. For the majority of the other II-VI compounds n-type conductivity with concomitant acceptor compensation is generally observed. ($r_c/r_a > 1$). In the

case of CdTe, the fact that the cation and anion are similar in size, together with other considerations of vacancy formation energy and ionicity of bonding means that compensation is less than 100% effective for either donor or acceptor impurities, and amphoteric conduction can be obtained. On the basis of the above considerations there would appear to be little possibility of attaining useful n-type conductivity in ZnTe. Although it has been demonstrated by Fischer (1964) that it is possible, by a nonequilibrium process such as quenching, to produce n-type conductivity in ZnTe, the insulating nature of the crystals renders them unsuitable for application in homojunction devices.

The electrical characteristics of minority carrier injection at a p-n homojunction or quasi-homojunction can be described in terms of the conventional model shown in Fig. 2.6. At equilibrium and in the absence of an applied electric field the diffusion barrier or built-in potential, V_D, associated with the space charge region is, as shown in Fig.2.6 (a), equal to the difference in the Fermi levels on the two sides of the junction, i.e. $qV_D=E_G-E_{F_n}-E_{F_p}$ eV. The diffusion barrier is reduced and finally eliminated by application of a voltage in the forward direction

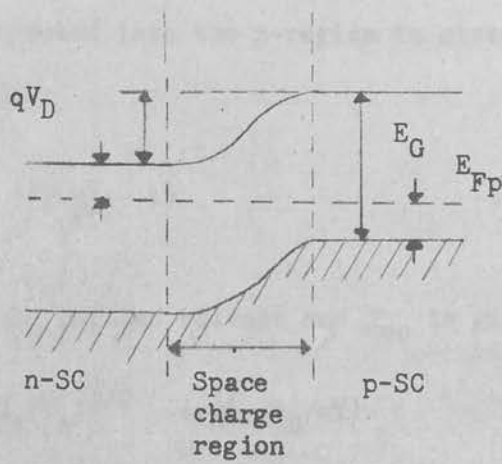

(a) Unbiased p-n junction.

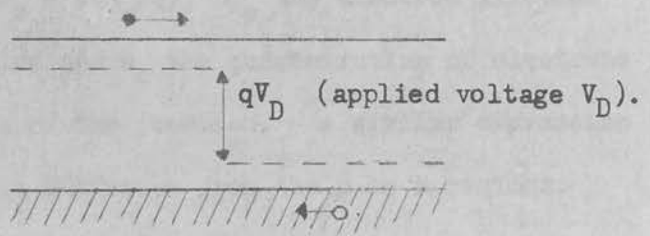

(b) Forward biased p-n junction.

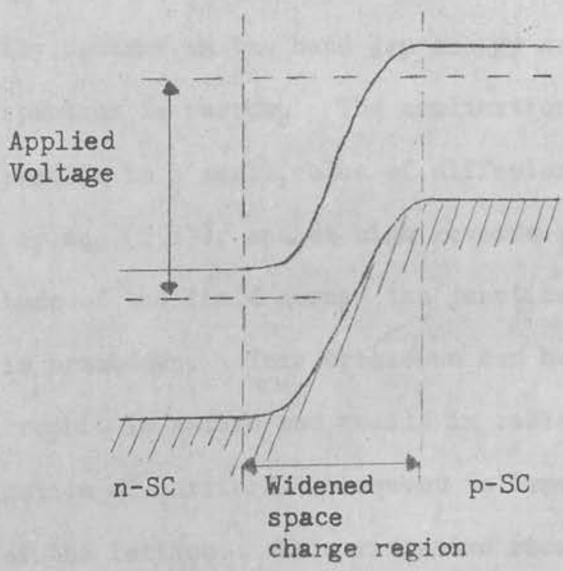

FIGURE 2.6 The p-n homojunction

and the diffusion current density resulting from electrons injected into the p-region is given by (Dekker, 1957)

$$j_e = j_{eo} \exp(\frac{qV}{kT} - 1) \qquad (2.13)$$

where V is the applied voltage and j_{eo} is given by

$$j_{eo} = q(D_e/\tau_e)^{1/2} \quad \exp(-qV_D/kT)$$

where D_e is the diffusion constant for electrons on the p-side ($D_e = kT\tau_e/q$), τ_e the electron lifetime in the p-region and n_o the concentration of electrons on the n-edge of the junction. A similar expression holds for hole diffusion from the p to n regions. Under suitable conditions the injected electrons and holes recombine radiatively in the region of the junction. The energy of the emitted radiation is normally centred on the band gap energy and the emission spectrum is narrow. The application of reverse bias results in a small value of diffusion current given by eq. (2.13), and at high reverse biases the magnitude of the field across the junction may result in breakdown. This breakdown can be non-catastrophic in nature and result in radiative recombination of carriers subsequent to impact ionisation of the lattice. This radiative recombina-

tion can take the form of a broad "avalanche-emission" spectrum which is perhaps centred on the band-gap energy due to the creation and subsequent recombination of free electron-hole pairs. Emission corresponding to energies greater than the band gap may be observed due to the creation of energetic carriers in the impact ionisation process (Henisch, 1962). The physical characteristics of the junction are reflected in the variation of the width of the space charge layer with applied voltage. For abrupt junctions, such as result from an alloying process, the layer-width is proportional to $V^{1/2}$, whereas for a linearly graded junction produced by diffusion processes the dependence is normally $V^{1/3}$. At sufficiently low voltages, and under forward bias, the current which is driven by recombination in the space charge region dominates that driven by diffusion. The variation of the recombination current with voltage is $\exp(qV/2kT)$. It is therefore to be anticipated that for devices operating by this mechanism and where the majority of the recombinations are radiative, the radiative recombination current (i.e. the emission intensity) will initially exhibit this dependence. The pre-exponential factor, j_{eo}, in the expression for the

recombination current density is $\sim q(w/\tau)n_i$, where w is the width of the space charge region, n_i the intrinsic concentration of carriers at the junction temperature, and τ the recombination lifetime in the space charge region. For larger applied potentials the narrowing of the space charge region results in domination by the diffusion current.

An extension of the concept of the simple p-n homojunction is the p-i-n junction shown in Fig.2.7. Such a device in effect possesses two junctions, one between the p-type semiconductor and the insulator and the other between the insulator and the n-type semiconductor. The resistance of the insulator may be reduced in operation either by double injection of holes and electrons from the semiconductor region with mutual space charge compensation (Lampert, 1962) or by photoconduction by absorption of the electroluminescence (Dumke, 1964). Both effects can give rise to a negative resistance regime and consequently a complicated I-V characteristic. For the p-i-n junction the forward current is controlled by recombination in the space charge or i-region rather than diffusion outside this region. For voltages large compared to V_D, the forward current through

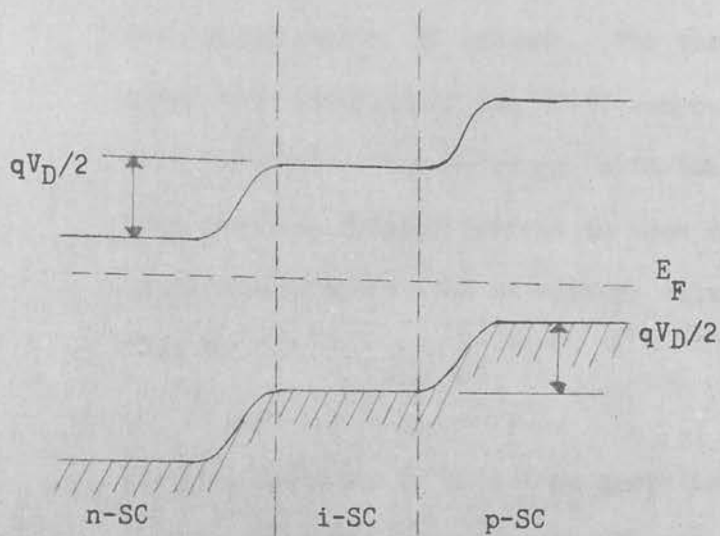

FIGURE 2.7 A p-i-n junction.

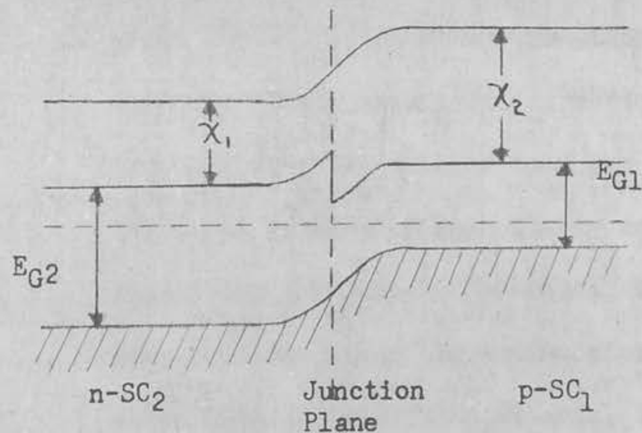

FIGURE 2.8 A p-n heterojunction. Electron affinity of p-type semiconductor denoted by χ_1 and n-type semiconductor by χ_2.

a junction is limited by the composite resistance of the semiconductor bulk, the contacts, and the insulating region, if present. For the case of quasi-homojunctions of the II-VI compounds these bulk resistances can be large, with the disadvantage that the forward current in some cases is resistance limited even at voltage values lower than V_D.

For homojunctions as described above there is no problem of competition between minority carrier injection and majority carrier extraction. The injection efficiency of holes or electrons is relevant only in the case where radiative recombination is much more efficient on one side of the junction than on the other. In a heterojunction, where the two sides of the junction are of chemically different materials, injection of minority carriers into the smaller band gap material from the wider is usually more likely under forward bias. For the cases of practical importance in the II-VI compounds, injection of minority carriers into the wider gap material is desirable for visible emission, as this material normally has a band gap energy lying within the visible

spectrum. For the material shown in Fig.2.8 the step between the valence bands permits the injection of relatively few holes. It therefore requires only a small applied potential in the forward direction to eliminate the diffusion barrier for electron extraction from the wide gap material, but a much higher potential to substantially enhance hole injection into the wide gap material. The situation can be somewhat improved by heavier doping of the smaller band gap material, which enhances hole injection, and also by the slight discontinuity in the conduction bands caused by the difference in electron affinities (χ) of the two materials which to some extent suppresses electron extraction from the wide gap material. A further disadvantage of the heterojunction device is the high density of interface states which produce non-radiative recombinations. In general this device has the same limitations on injection efficiency as the metal:semiconductor junctions to be discussed below. Fischer (1964) has discussed refinements in the structure of heterojunction devices using additional surface layers which may permit efficient hole injection in the type of device described above.

Schottky Emission

Minority carriers may be injected into a semiconductor over a potential barrier formed by a non-ohmic metal contact. The metal semiconductor contact is characterised by the work function of the metal ϕ_m, the electron affinity χ, the band gap E_G and the Fermi level E_F of the semiconductor. The work function of the semiconductor is given by $\phi_s = \chi + E_{F_n}$ for n-type and $\chi + E_G - E_{F_p}$ for p-type, where E_{F_n} is the energy separation of E_F from the conduction band and E_{F_p} from the valence band.

Contacts which are described as injecting or blocking are of high resistance, rectifying, and characterised by a large difference in ϕ_m and ϕ_s. This difference is given by

$qV_D = \chi + E_G - E_{F_p} - \phi m(eV)$ for a p-type semiconductor

and $qV_D = \phi m - \chi - E_{F_n}(eV)$ for an n-type semiconductor

i.e. a low work function metal is required for an injecting contact into a p-type material ($qV_D = \phi_s - \phi_m$) and a high work function metal for an n-type material ($qV_D = \phi_m - \phi_s$). Typical contacts are shown in Fig. 2.9.

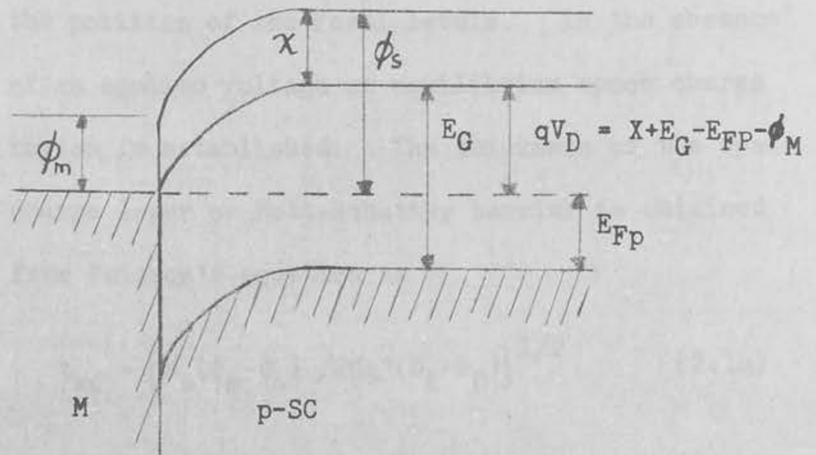

(a) Unbiased injection (or blocking) metal:semiconductor contact.

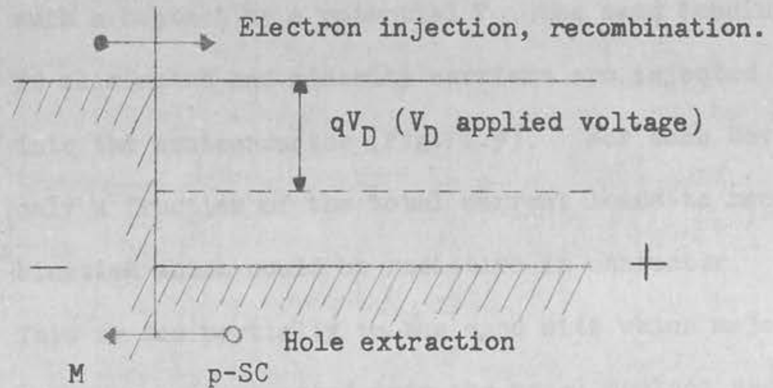

(b) Forward-biased blocking metal:semiconductor contact.

FIGURE 2.9

It is assumed here that surface states do not affect the position of the Fermi levels. In the absence of an applied voltage an equilibrium space charge region is established. The thickness of the space charge layer or Mott-Schottky barrier is obtained from Poisson's equation as

$$t_{sc} = \left[\mathcal{K}_s(\phi_m-\phi_s) / 2\pi q^2(N_A-N_D)\right]^{1/2} \qquad (2.14)$$

where N_D and N_A are the donor and acceptor concentrations in the semiconductor and $\mathcal{K}_s$ is the static dielectric constant. On forward biasing such a contact by a potential V_D, the band bending is eliminated and minority carriers are injected into the semiconductor (Fig. 2.9). For such devices only a fraction of the total current leads to recombination which could be radiative in character. This is due partially to the ease with which majority carriers are extracted into the metal contact and to the high density of interface states at which non-radiative recombination can occur.

In exceptional cases physical inversion layers can be created at metal contacts to semiconductors. For the case of a p-type semiconductor this could occur if a luminescent material of high electron affinity

is contacted by a highly conducting material of low work function. Again assuming that surface states do not influence determination of the Fermi levels, then the resulting depletion layer in the semiconducting phosphor can be so steep that a physical inversion layer is created; on forward bias minority carriers can be injected from this n-type region into the p-type semiconductor. For this to occur the relationship $V_D = \phi_m - \chi - E_G/2$ is fulfilled. The harmful effects of majority carrier extraction are also present in this case.

Tunneling

The efficiency of minority carrier injection over majority carrier extraction can be increased by the deposition of a thin insulating film of thickness 50-500Å and having a band gap intermediate between that of the metal and the semiconductor. (Fischer and Moss, 1963; Jaklevic et al., 1963). Fig.2.10 shows a schematic tunnel structure for a p-type semiconductor. Since the major part of the applied voltage is developed across the insulator, the potential barrier is altered so that carriers on one side are opposite holes or receiving states on the other side. The tunnel current can be shown

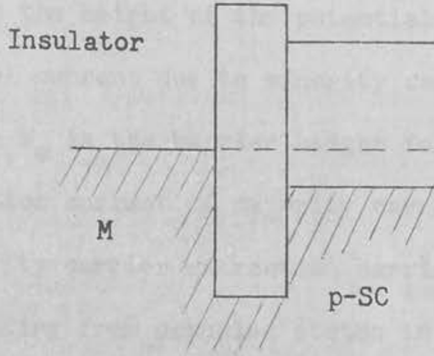

(a) Without Applied Voltage

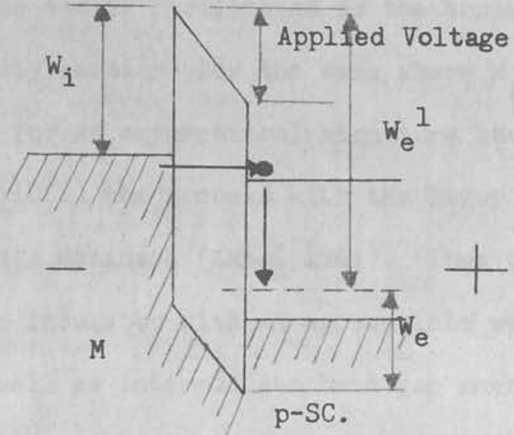

(b) With Applied Voltage

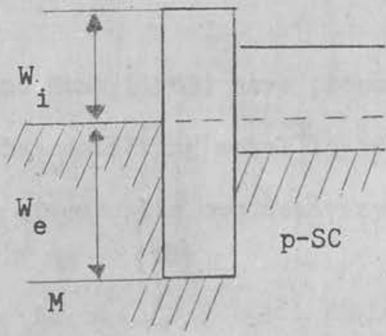

(c) Tunnel structure designed to block majority carrier extraction.

FIGURE 2.10 Metal:Insulator:Semiconductor Tunnel Contacts.

(Bohm, 1951) to be proportional to exp (-4d) where d is the thickness of the insulator. In the figure W_i is the height of the potential barrier for the tunnel current due to minority carrier injection while W_e is the barrier height for the tunnel extraction current of majority carriers. W_e' is the majority carrier extraction barrier for electrons tunneling from occupied states in the metal to opposite empty states in the forbidden gap of the semiconductor. Quantum mechanical considerations show that the tunnel extraction of majority carriers will be as easily facilitated as the tunnel injection of minority carriers for the case where $W_i \simeq W_e$. However, for an asymmetrical structure such as shown in Fig.2.10(c) the process with the lower barrier height will dominate (Kane, 1961). Thus the selection of an insulator with an appropriate work function as well as intermediate band gap energy is necessary for the effective suppression of majority carrier extraction; for a p-type semiconductor this requires an insulator of high work function.

Fischer and Moss (1963) have proposed the replacement of the contacting metal layer with a semiconductor layer of opposite conductivity and wider band gap

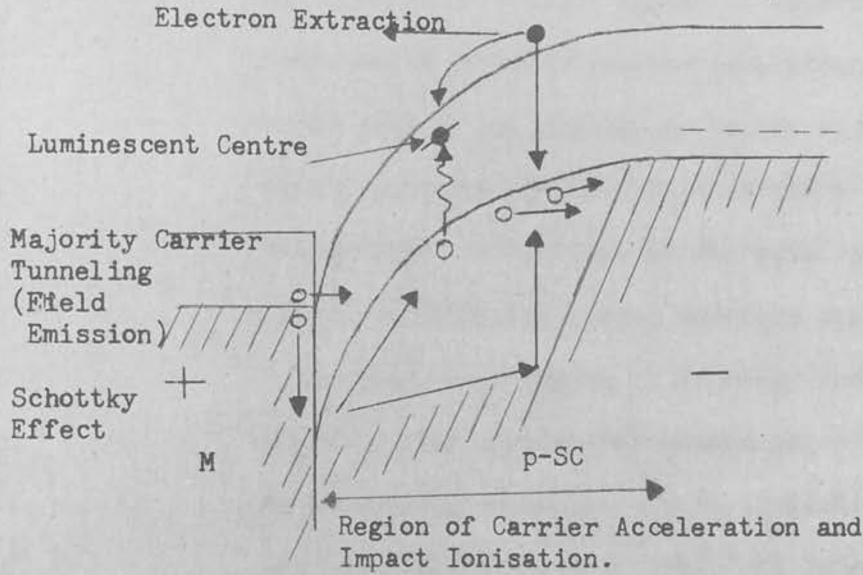

FIGURE 2.11 Reverse-biased metal:semiconductor blocking contact.

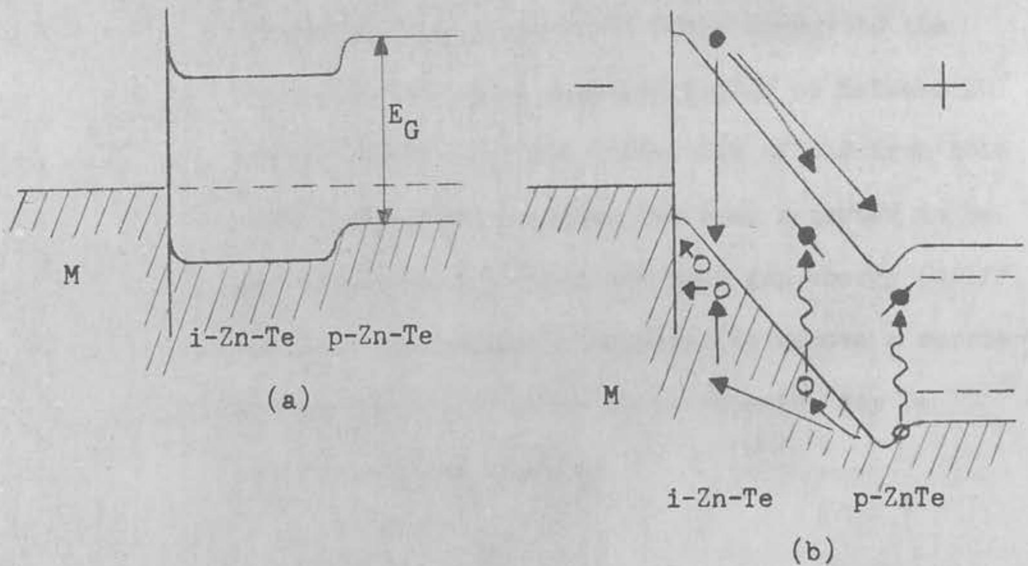

FIGURE 2.12 Metal-insulating ZnTe - p-type ZnTe structure.
(a) No voltage applied.
(b) Impact ionisation and avalanche injection forward bias.

cases the high field is produced by exhausting the junction or contact region of majority carriers, while minority carrier generation, either in the bulk of the crystal or in the space charge region, provides the source of carriers to be accelerated. In the case of the metal:semiconductor junction, additional carriers are supplied in the high field region by Schottky and field emission. The various mechanisms associated with carrier acceleration and impact ionisation have been reviewed by Henisch (1962) It is generally considered that this complex phenomena is related to dielectric breakdown of the crystal. To accelerate carriers to breakdown energies requires a field of sufficient magnitude so that the rate at which the carrier gains energy from the field exceeds the rate at which it loses energy to the phonon field. This reguires fields of between 10^5 and 10^6 V/cm. For the ionisation of electron hole pairs the energy required has been reported to be approximately 1.5 times the band gap energy (Wolff, 1954). Less energy is required to remove a carrier from an impurity centre since momentum may be absorbed by the impurity.

Subsequent to the creation of electron hole pairs by impact ionisation, the recombination of these carriers results in a broad spectrum which could include radiation of greater than band gap energy due to the presence of "hot" carriers (this term refers to the presence of carriers accelerated to energies in excess of the band gap value). In these reverse-biased processes the impacted generated electrons and holes are both extracted from the region where recombination takes place, and further, since the recombination of energetic carriers is less probable than that of thermalised carriers, the quantum efficiency of photon production is low. Higher quantum efficiencies are to be anticipated when the avalanche occurs in a thin insulating or localised high field region of a luminescent semiconductor in series with a conducting n- or p-type region of the same material. With the correct polarity, impact generated holes (electrons) can be swept into the low field n- (p-) region with the possibility of efficient radiative. Fischer (1964) demonstrated this principle with ZnSe. This avalanche injection of holes from a microplasma near the cathode of a ZnTe cry-

stal is shown diagramatically in Fig.2.12. High quantum efficiencies at $77^{\circ}K$ have been found in ZnTe M-i-p structures operating under this avalanche injection mechanism (Crowder et al., 1966) and similar avalanche injection from localised high field regions in ZnTe has been described by Kennedy and Russ (1967a, 1967b). The electrical characteristics of the device, and the spectral distribution of the emitted radiation normally allows a clear distinction to be made between this mechanism and that of "ohmic" minority carrier injection which could occur under identical polarity conditions.

From experiments on electroluminescence in ZnSe crystals using a wide variety of contacting and surface preparation techniques, Fischer (1964) has correlated the experimentally observed electrical and emission characteristics of ZnSe devices with particular mechanisms. Devices operating under the majority of the above described mechanisms were fabricated.

2.2.3.2 Electroluminescence in ZnTe

In this section we present details of the results obtained by previous investigators relating to the

fabrication of ZnTe devices, the electroluminescence of these devices, and the associated mechanisms of excitation and recombination considered to be operative. The majority of the mechanisms found to be applicable to ZnTe devices have been described in some detail in the preceeding section.

The majority of experiments utilised either nominally undoped crystals, in which the p-type conductivity characteristic of ZnTe results from self-doping by shallow Zn acceptors, or crystals heavily doped with P (carrier concentrations $> 10^{18}/cm^3$). In all cases the resistivity of crystals used in device fabrication was low (<5 ohm-cm). The common form of device fabrication technique can broadly be described as the alloying of a contact material, normally of low work function such as In or an In alloy, to produce a non-ohmic surface region. The variation in the blocking nature of the metal:semiconductor junction as influenced by the contacting techniques has a major influence on the resulting device, and several preparation techniques resulted in insulating (M-i-p) or semi-insulating (M-si-p) structures. In some cases blocking contacts were attached to both faces of the crystal but in others an alloyed or electroless-plated noble metal

was used to form an ohmic contact to one face. For the majority of devices the electroluminescent properties were found to be dependent on the nature of the contact used. Exceptions to this are the contacting of mixed crystal p-n quasi-homojunction and heterojunction devices whose electroluminescent properties are not related to the type of contact used, and also devices which have a thick semi-insulating region whose electroluminescent properties are primarily dependent on the semi-insulator and semiconductor regions and their interface.

The majority of reports describe electroluminescence observed at liquid nitrogen temperatures. At these temperatures efficient emission has been observed from ZnTe devices. The term "efficient emission" is normally applied to values of external quantum efficiencies in excess of 1%. In this context, the external efficiency is defined as the ratio of the number of externally observed photons to the number of electrons flowing through the device. Due to the high refractive indices of the II-VI compounds a large proportion of the internally emitted radiation can be lost due to total internal reflection. Also, if the emission peak is located near the band edge of the material, the effects of self-absorption can reduce

the intensity of the observed emission. The internal quantum efficiency can therefore be considerably greater than the external value. Another parameter frequently used in efficiency determinations is the power efficiency. This is defined as the ratio of the emission output power to the electrical input power. This value is normally less than the external quantum efficiency. For low resistivity p-n junction devices where injection occurs at low voltage levels the reduction may be insignificant; however, for higher resistance structures, or for devices operating under high field conditions requiring large applied voltages, the power efficiency may be a factor of 10-100 less than the external quantum efficiency.

The first observations of electroluminescence in ZnTe were reported in 1964 (Watanabe et al., Miksic et al., Komatsu et al., Eastman et al.).

Watanabe et al. fabricated devices from nominally undoped p-type crystals of conductivity 5 ohm-cm by alloying In and Ag contacts. At 293°K electroluminescence peaking at 6500Å was observed at the negative In contact. This polarity is consistent with the proposed mechanism of injection from the metal contact or an inversion layer. The authors assumed that the surface

layer was converted to n-type ZnTe by being doped with In. This would appear to be doubtful due to the previously discussed difficulties of obtaining n-type conductivity in ZnTe. The broad emission band was considered to result from recombinations involving localised states associated with In centres introduced during the contacting process. The efficiency of the emission process was not stated.

Komatsu et al. fabricated devices from nominally undoped vapour grown crystals utilising In contacts to one face of the crystal and electroless Au plus In alloy as the ohmic contact to the other face. Emission was observed at 77°K in the region of the In contact and extended into the bulk of the crystal for the forward direction of current flow. Emission was restricted to isolated areas in the region of the Au contact for the reverse direction. Three emission peaks at 5400, 5900 and 6200Å were observed. The authors considered that the emission resulted from the injection of minority carriers from the In and Au contacts; however, the high voltages applied to these devices and the occurrence of a negative resistance region in the I-V characteristic permits consideration of the possible existence of an insulating region

in the neighbourhood of the contacts, emission resulting from impact ionisation in the high field region at the insulating layer. The observation of emission extending into the bulk of the crystal could be taken as evidence for subsequent avalanche injection of minority carriers into the semiconductor. The efficiency of the devices was not reported.

The report of Miksic et al. is concerned with two types of device. For the first type In and Au contacts were attached to P-doped degenerately conducting crystals. Under forward bias emission was obtained in a narrow band (50Å) centred on 5340Å at 77°K and 5590Å at room temperature. The emission was observed at 77°K was measured as 0.8% but this required high-current pulsed excitation of 5×10^4 A/cm^2. The device resistances of 50 ohm may have influenced the overall efficiency due to power losses. The authors concluded from the marked temperature dependence of I-V characteristic and the polarity dependence of the emission that Schottky emission over a thermal barrier at the metal:semiconductor contact was the dominant mechanism. From photoluminescence measurements Morehead (1965) later confirmed that the emission of ZnTe crystals doped with P, Li and Na dopants was centred on a narrow band at 5340 Å. These

dopants were believed to be incorporated as shallow acceptor levels and produce a reduction the resistivty of the material. It has not been confirmed that these dopants participate in the radiative recombination processes. The measured PL and EL peaks have photon energies close to the band gap value. In the second type of device a 100Å thick SiO film was interposed between the In electrode and the crystal. The same narrow green line was obtained, the quantum efficiency being improved to 2%. This could possibly be attributed to partial suppression of majority carrier extraction. For this second device the authors still favoured the mechanism of Schottky emission rather than tunnel injection through the insulating layer.

Similar results to those above were obtained by Eastman et al. Using P-doped crystals contacted by In and Au electrodes emission was normally obtained for a positive potential applied to the In contact, ie. the reverse biased direction of the In:ZnTe junction. It was found that if both faces of the crystal were contacted by In electrodes the emission switched from one face of the crystal to the other as the polarity was reversed. The emission spectrum at 77°K consisted of a narrow band of half-width 60Å at 5375Å, while at

room temperature the emission peak shifted to 5650Å. These emission spectra are similar to those obtained by Miksic et al. and would again indicate that this spectrum results from near band gap radiation. The authors reject the conventional mechanism of impact ionisation in the high field region of the depletion layer as being inconsistent with the observation of monochromatic emission occurring linearly along the junction plane. A mechanism of double tunnel injection across the bandgap of the semiconductor at the depletion layer was considered to be a more satisfactory mechanism. The practicality of this mechanism has been questioned by Fischer (1966) as the electron-hole pairs created in this way would be separated by the intense field and the tendency would be for the electrons to be accelerated and extracted into the In contact. The possibility exists that the broad continuum spectrum of inter- and intraband transitions from recombination of hot carriers common to impact ionisation spectra was present, but at levels below the sensitivity limits of the measurement. For some devices emission was observed at the In contact with a negative potential applied. This was attributed to the presence of an insulating layer either formed during etching of the crystals or resulting from a poorly soldered electrode contact.

The mechanism of emission in these M-i-s devices was considered to be tunnel injection of minority carriers through this insulating layer. The degenerate nature of the semiconductor, as indicated by the lack of temperature dependence of the conductivity, was considered to favour a tunneling rather than Schottky emission mechanism. Comparing the results of these authors with those of Miksic et al, it is interesting to note that, despite the use of crystals prepared by similar techniques and the adoption of almost identical device fabrication techniques, the quantum efficiencies obtained by Eastman et al. were a factor of 10^{-3} less than those of the latter authors for devices operating under similar excitation conditions. Eastman et al. are the only authors who present details of switching time of ZnTe devices. It was reported that the time for emission to reach full intensity and to decay on the application and removal of a steep voltage pulse was 5×10^{-9} sec.

Subsequent to the initial reports of electroluminescence in ZnTe described above, four other papers devoted to this topic have appeared in the literature.

Kot et al. (1965) obtained electroluminescence for

the forward direction of current flow in ZnTe devices. Emission was obtained at both $77^{\circ}K$ and $300^{\circ}K$ and the emission spectra at the lower temperature peaked at 5800Å. No details were given of the impurity content of crystals used for device fabrication, the contacting technique, and the efficiency of the emission process.

More detailed results of the experiments conducted by Komatsu et al. were presented by Hinotani and Sugigami (1965). In this case melt-grown, nominally undoped crystals, were contacted by the same technique as reported previously, namely In and electroless Au. The authors assumed that ZnTe was soluble in In at the temperatures used in applying the contact and that a semi-insulating layer having n type conductivity was formed. Reverse bias capacitance measurements confirmed the existence of an insulating layer and the layer thickness was calculated as 1μm. As before, emission was obtained at $77^{\circ}K$ for both directions of current flow, with the emission located in the region of the In contact for one direction of current flow and in the form of isolated spots at the Au contact for the opposite polarity. The main emission peak was again located at 6200Å with a secondary

peak at 5900Å. The excitation mechanism was considered in terms of a M-si-s structure with electron injection from the metal contact. This is the only paper which contains details of the current-voltage relationship observed in ZnTe devices. This characteristic consists of several regions in which the dependence of current on voltage obeys exponential, linear, square-law, and higher power relationships. The onset of emission was found to coincide with the start of a square-law region. The shape of the I-V characteristic together with the identification of an insulating layer between the metal and the semiconductor prompted the authors to consider their results in the light of Lampert's (1956) theory of single-carrier space-charge-limited-currents. This theory predicts the shape of a current-voltage characteristic for one type of carrier in a semi-insulating region of a semiconductor. From the values of applied voltages at which sudden transitions occur in the characteristic it is possible to calculate the density of trapping centres in the semi-insulating region and also their energy levels. By analysis of their results Hinotani and Sugigami obtained trap densities and depths of 10^{16} - 10^{17} cm^{-3} and 0.13-0.17eV respectively. Unfortunately the analysis of other regions of the I-V characteristic in terms of the predictions of Lampert's theory these results were not confirmed. The fact that the emission intensity was observed to increase

linearly with current at voltages corresponding to a square law region of the I-V characteristic was considered to indicate the presence of both free holes and electrons. The radiative recombination of these carriers through In "donor" levels or traps was suggested as the explanation of the observed emission peak at 6200Å. The theory of one carrier S.C.L. currents could therefore not be applied throughout the experimental range of voltage and current. At high voltage levels the onset of a negative resistance region was observed. It is possible that an alternative explanation of the observed results in this metal:semi-insulator:semiconductor structure might again be the impact ionisation of minority carriers in the high field of the semi-insulating region, with subsequent injection of these carriers into the bulk of the semiconductor. Although observation of a negative resistance region in a current-voltage characteristic is frequently considered indicative of the onset of double-injection in a semi-insulating region, it can result from "avalanche injection" processes, apart from such completely separate considerations as sample heating and photoconductive effects induced by reabsorption of the emitted radiation.

The preliminary results obtained by Watanabe and described above, were extended in a later paper (Watanabe, 1966). These experiments were again concerned with P-doped crystals. In device fabrication one contact consisted of a film of evaporated In on which a pellet of In was alloyed for a few seconds at temperatures of 400-800°C, and a conventional electroless Au layer formed the other contact. From capacitance-voltage, blocking potential and resistance measurements it was confirmed that the alloying of the In contact produced a semi-insulating region at the surface of the crystal. The thickness of this region increased with alloying temperature and extended from $\sim$ 0.2 to 1 micron. Measurements were conducted at liquid nitrogen temperatures and emission was observed under both forward and reverse bias. This consisted of two bands - a narrow green band of width 60Å located at 5400Å and a broad red band extending from 5800 - 7000Å. The former emission was associated with the recombination of minority carriers with holes located on phosphorus acceptors. Photoluminescence measurements confirmed this finding, and detailed structure noted in the electroluminescent spectrum was associated with longitudinal optical phonon lines. The position of this green

emission peak is in agreement with the results of other authors. The broad red band was attributed to recombinations of electrons on deep In impurity donor levels with holes in the valence band or at shallow acceptor states. The excitation mechanism for the forward-biased case was again considered to result from the injection of minority carriers into the M-si-s structure. Variations were observed in the dependence of emission intensity on forward bias current for different alloying conditions. This was attributed to there being a dependence on the thickness and resistivity of the semi-insulating layer on the alloying conditions which therefore influenced the kinetics of the carrier injection process. For the reverse-bias emission an impact ionisation mechanism was favoured. Minor variations in the emission spectrum for the two directions of current flow substantiated this postulate; for the reverse-biased emission the red emission band was broader and extended to longer wavelengths and an extra emission band appeared at shorter wavelengths. These results were in agreement with an impact ionisation mechanism whereby a broad emission band corresponding to inter- and intraband transitions would be anticipated and the presence of "hot" carriers could result in higher energy transitions

(ie. shorter wavelength emission). The authors gave no details of the operating levels of current and voltage, and once again no statement was made concerning emission efficiencies.

The most efficient emission observed to date in ZnTe devices was reported by Crowder et al. (1966). The crystals used in these experiments were commonly doped with Li. This dopant was found to be the most successful in attaining efficient emission. Devices fabricated using Na, Sn, Ag and also no intentionally added dopants were found to be inefficient; the use of P-doped crystals occasionally resulted in an efficient device. It has been reported (Crowder and Hammer, 1966) that Li, like P, produces shallow hydrogenic like acceptors in ZnTe (ie. the ionisation energy of the acceptor levels decreases with increasing acceptor concentration approximately as the cube root of the average ionised-acceptor concentration). A semi-insulating region was created in the Li-doped crystals by the diffusion of an evaporated Al film into the substrate at a temperature of 850°C. The properties of the resulting devices were found to be independent of the material used to form the contacts, and electroless Au was commonly used. It was found that at 77°K the

current-voltage characteristic of efficient devices exhibited a "breakdown voltage" of 15-20 V in forward bias (bulk p-region positive), followed by a negative resistance region with a minimum sustaining voltage of 8-15V. The light output was found to be a linear function of current and external quantum efficiencies of 2% were obtained. The spectral output consisted of a narrow line at 5380Å characteristic of photoluminescence from Al-doped ZnTe. The fact that the green photoluminescence was observed to be located in the bulk of the crystal was taken as an indication that carriers generated in the high-resistivity region were injected into the bulk of the semiconductor. The excitation mechanism was considered to be the avalanche injection of minority carriers, generated by impact ionisation in the high-resistivity region, into the p-region of the semiconductor. As discussed previously, this mechanism has an advantage over reverse bias impact ionisation in that impact ionised electrons are swept into the p-region under the action of the applied field. It is of interest to note that these authors consider the observation of a narrow emission band to be compatible with an impact ionisation mechanism, whereas Eastman et al. rejected the possibility of such a mechanism explaining the narrow

emission band observed in their experiments.
At room temperature the resistance of the insulating region necessary for avalanche injection was considered inadequate to sustain efficient minority carrier injection. The existence of a semi-insulating region, the observation of negative resistance and hysterysis effects in the current-voltage characteristics, is a further example of experimental results which permit consideration of double injection effects in the semi-insulating layer with the possibility of the creating of additional carriers by field ionisation of traps. Such an analysis, however, would require detailed knowledge of the current-voltage characteristic.

Finally, electroluminescence reported from heterojunction and homojunction structures associated with ZnTe is described.

Aven and Garwacki (1963) epitaxially deposited a CdS film of controlled conductivity on the 111-Zn face of a Cu-doped, p-type, ZnTe crystal. Long wavelength, visible emission characteristic of CdS was observed at room temperatures; the quantum efficiency was low (10^{-6} photons/electron). A negative resistance regime

was observed and the mechanism assumed to be double injection in a compensated CdS zone of width approximately 4 microns. The low efficiency of the electroluminescence was attributed to the fact that CdS has poor luminescent characteristics at room temperature and also the dominance of recombination at non-radiative interface states. As discussed previously it is anticipated that a heterojunction device of this type will exhibit poor injection efficiency due to the fact that the injecting semiconductor is of lower band gap than the other component of the junction in which one hopes to achieve electroluminescence.

Morehead and Mandel (1965) obtained efficient emission at $77^{\circ}K$ in an alloyed quasi-homojunction device. The preparation of junctions in $Zn_xCd_{1-x}Te$ was carried out by simultaneous diffusion of Zn and P into an Al-doped crystal of CdTe under a Cd atmosphere at $850^{\circ}C$. This resulted in a P-doped p-type region and an Al-doped n-type region. The ratio of Cd to Zn in the sealed ampoule containing the constituents determined the composition of the resulting $Zn_xCd_{1-x}Te$ layer formed at the surface and in the region of the junction. Diodes fabricated from this solid solution had a peak emission in the region of 7200Å, corresponding to X=0.4.

The external quantum efficiency at 77°K was 6% dropping to 10^{-4} at 300°K. The reduction in efficiency with increasing temperature was accompanied by the usual shift in the emission peak to longer wavelengths. (The reduction in band gap energy as the temperature is raised is reflected in the shift of the emission peak to longer wavelengths). For this particular device the room temperature emission peak was located in the near infra-red, which eliminates these devices as useful visible emitters.

For applications requiring visible emitters, the results obtained by Aven (1965) on the crystal system $ZnSe_xTe_{1-x}$ are of greater interest. Electroluminescent diodes were prepared by the diffusion of Al into as grown p-type crystal of the mixed system. The use of material with x=0.36 yielded electroluminescent emission which at 77°K consisted mainly of a band of half-width 380Å and 6250Å. The lowest threshold for visually observable emission was 2.7V at a current density of 5×10^{-7} A/cm^2. The light intensity increased slightly super-linearly with current and at 10^{-2} A/cm2 and 70°K the external quantum efficiency attained the value of 18%. The observation of this high external quantum efficiency in planar structures suggested that internally one quantum of visible light was produced for every

carrier passing through the junction. Above liquid nitrogen temperatures the light intensity decreased exponentially with decreasing reciprocal temperature, and this was attributed to the thermal ionisation of holes out of the ground state of the shallow (0.06eV) luminescent centre and the transfer of these holes to killer centres. Attempts to improve the room temperature performance in these and other II-VI homojunction (CdTe) and quasi-homojunction devices by increasing the carrier concentrations at the junction has met with little success. For example for the system $ZnSe_xTe_{1-x}$, electron and hole concentrations of approximately $10^{15}/cm^3$ are usually obtained for compositions in the range $0.3 < x < 0.6$. The associated electron and hole mobilities are $100 cm^2/V.sec$ and $10 cm^2/V.sec$.

Fischer (1964) has prepared light emitting diodes of $ZnSe_xTe_{1-x}$ using a different technique to that of Aven. An epitaxial layer of $ZnSe_xTe_{1-x}$ of graded composition is produced on an n-type, Al-doped, melt-grown ZnSe crystal by firing the latter at 900^oC in contact with ZnTe:P powder in an atmosphere containing Cl and Zn. At room temperature a broad emission band of half-width 1200Å and peak position 6300Å was observed under forward bias. The operating voltage was in the range 1.8-5V. The low value of external quantum efficiency obtained from this

heterojunction device was attributed to the dominance of non-radiative transitions in the disordered and strained region between the ZnSe crystal and the $ZnSe_xTe_{1-x}$ film.

Despite the disappointing results in achieving room temperature visible emission, $ZnSe_xTe_{1-x}$ would appear to be the most promising member of the II-VI compound solid solution systems for this application.

In this section we have reviewed the growth and material properties of ZnTe crystals, the properties of ZnTe electroluminescent devices, and the mechanisms of excitation and recombination applicable to such devices. ZnTe, in common with a number of other II-VI compounds having large direct band gaps, has considerable potential as an efficient electroluminescent material. This potential has been realised at low temperatures, but efficient emission has yet to be achieved at room temperature.

Two distinct lines of experimental investigation can be recognised. The first is concerned with materials exhibiting amphoteric conduction. For reasons discussed above, it would appear that it is not possible, by existing materials technology, to prepare n-type ZnTe crystals of useful conductivity. This has resulted in investigations of solid solutions of ZnTe with other

II-VI compounds. Outstanding results have been attained at low temperatures with quasi-homojunctions in these alloy systems. The attainment of room temperature emission would appear to require improvement in crystal growth and device preparation techniques. In particular it will be necessary to obtain higher carrier concentrations and concentration gradients at the junctions in such devices and eliminate the effects of non-radiative impurity centres. Reduction in contact resistances and the resistance of the bulk semiconductor is also desirable. The second line of investigation is applicable to non-amphoteric semiconductors, and involves the imitation of p-n junctions by the construction of metal: semiconductor, metal:insulator:semiconductor, or metal:semi-insulator:semiconductor injection devices. Such structures have also resulted in efficient low-temperature electroluminescence, but again inferior results have been obtained at room temperature. The problem here would appear to be principally concerned with the fabrication of a "contact" region having efficient injection characteristics at room temperature, and which effectively suppresses the deleterious influence of majority carrier extraction and recombination at interface states. At the present time it is debatable which line of investigation will be the more successful. Although the effects of the presence of non-radiative centres located in the bulk of the crystal have a considerable influence on thermal quenching of the emission for the "injecting-contact" case these effects do not appear to be as pronounced in ZnTe as in the alloyed crystal systems. The effects of such non-radiative

centres may be significantly reduced by the use of other recombination centres located at deep levels and which are associated with longer wavelength emission. As described in the experimental results to be presented hereinafter, the thermal quenching of electroluminescence associated with such centres is less pronounced than that of shallower levels. Such centres could possible be utilised advantageously in both amphoteric and non-amphoteric systems. In the literature on electroluminescence in II-VI compounds, it has been reported (Morehead, 1967) that of the various excitation techniques impact ionisation processes exhibit the least temperature dependence of the emission efficiency. From these considerations, and on the basis of trends indicated by previous results and those to be presented here, it may prove that devices fabricated from material incorporating deep recombination centres, or alternatively material in which non-radiative centres have been eliminated, and operating under an impact ionisation cum avalanche injection mechanism, may permit the attainment of efficient, room-temperature, visible emission.

In the remaining sections of this dissertation details are presented of an experimental program principally directed towards the evaluation of the electroluminescent properties of ZnTe devices. In addition, details of experiments conducted on the growth of ZnTe crystals of suitable quality for device fabrication will be described and the results of measurements of the optical and electrical transport properties of these crystals presented. The electroluminescent properties of three distinct forms of ZnTe crystals will be considered. These are nominally undoped ZnTe crystals, oxygen doped ZnTe crystals, and polycrystalline ZnTe. In all cases relatively simple device fabrication and contacting procedures were used.

3. CRYSTAL GROWTH

In this section the techniques and apparatus used in the preparation of ZnTe crystals are described.

The growth techniques are divided into three main categories:

1. Bridgman Growth
2. Vapour-Phase Growth
3. Solution Regrowth

It will become apparent from the presentation of results that many of the crystal preparation procedures do not strictly fall into any one of the above categories. The separation of the procedures into these classes is, to some extent, a matter of con-

venience. It is therefore in order to consider the interpretation of this classification system as used in the present context.

Bridgman-type crystallation normally refers to a particular technique of growth from the liquid phase, recrystallisation taking place as the container containing the melt passes through a temperature gradient. In this context, the term covers all growth techniques in which a melt of ZnTe was passed through a temperature gradient and includes preparation procedures in which the withdrawal of the ampoule through a temperature gradient was simulated by using a stationary ampoule and reducing the temperature of the hot zone. In the majority of experiments the ampoule containing the melt was withdrawn from a stationary furnace in either the horizontal or vertical plane. As discussed in the previous section, the growth of ZnTe crystals from a stoichiometric melt presents difficulties due to the high temperatures required and vapour pressures encountered. To obviate these difficulties the growth techniques normally employed utilised an excess of one component. Thus crystals were, in effect, grown from a solution of this component; the solution temperature of the quantity of ZnTe contained in the melt being significantly lower than the stoichiometric melting point. Concomitantly, the vapour pressures of any of the components at the temperatures commonly used were well within the limits that quartz tube can withstand at these temperatures.

In vapour growth the ampoule containing the melt is positioned in a non-uniform temperature distribution, growth taking place from the gaseous phase by condensation and recrystallisation in in the region of the ampoule maintained at a lower temperature. In the present context it includes procedures in which non-stoichiometric melts were used. In a number of cases vapour-phase growth resulted when an ampoule was withdrawn through a temperature gradient; in many such cases in addition to growth from the vapour recrystallisation of the melt took place. For convenience, any procedures which resulted in the production of vapour grown crystals are included in this classification.

The term solution regrowth applies to all growth techniques in which the compound to be recrystallised is dissolved in another element. The correct use of this term therefore includes growth from a non-stoichiometric melt having an excess of one component. In the present context, however, solution regrowth refers to dissolution of ZnTe in an element other than either of the components.

The majority of the experimental growth runs completed during the course of this investigation are detailed in Table 3.1. This table lists the growth runs in three groups corresponding to the above classification. The numbering system used does not correspond exactly with the chronological order in which

TABLE 3.1 ZnTe GROWTH EXPERIMENTS

Growth No.	Starting Material	Temperature Data	Soak Time	Growth Technique
		1. Bridgman		
1(B)	80wt%Te 45wt%Zn Constituents reacted together in reducing atmosphere prior to growth.	1100°C constant along length of ampoule	3 hrs.	Horizontal Bridgman Withdrawal rate 0.6cm/hr for first 4 1/2 hrs then 17.5cm/hr.
2(B)	As (1)	1150°C constant along length of ampoule	1 hr	As (1), but withdrawal rate maintained at 0.6cm/hr.
6(B)	90wt%Te 10wt%Zn Constituents pre-reacted as (1)	1125°C	18 hrs.	As (1) withdrawal rate maintained at 17.5cm/hr.
7(B)	75wt%Te 25wt%Zn Constituents pre-reacted as (1).	1200°C	16 hrs.	As (6)
8(B)	Sections of boule from growth runs (4) and (5)	Constituents at 1270°C. Opposite end of ampoule at 1150°C.	1 hr.	Furnace temp.reduced to 1200°C and ampoule withdrawn at 7.5cm/hr.
9(B)	80wt%Te 20wt%Zn Constituents not reacted prior to growth.	1150°C	6 hrs Furnace failed	No withdrawal. Ampoule cooled at natural cooling rate of furnace.
10(B)	As (9)	1150°C	Brought up to temp. slowly and held for 5 hrs.	Using vertical furnace. Ampoule cooled at natural cooling rate of furnace.
11(B)	Stoichiometric mix of Te and Zn. Constituents not reacted	1250°C	4 hrs.	As (1) Withdrawal rate 15cm/hr.
14(B)	Stoichiometric mix as (11)	1300°C	-	-

TABLE 3.1 ZnTe GROWTH EXPERIMENTS

Quantity	Results and Comments	Growth No.
	1. Bridgman	
12.8gm	Polycrystalline boule. Good quality surface layer, but bulk of boule porous. Small single crystals of useful size extracted from boule.	1
13 gm	Results similar to (1). Larger crystals obtained from "front" section of boule.	2
15 gm	Metallic Te with small included volumes of ZnTe of unuseable size.	6
20 gm	Good quality surface layer. ZnTe crystals superior to (6) but still of unuseable size.	7
5 gm	Highly porous boule. ZnTe crystals contained large Te inclusions.	8
5 gm	Similar to 8, but some useful ZnTe platelets. Porosity not as pronounced as previous runs.	9
5 gm	Porous boule with some small platelets. Inferior to (9)	10
5 gm	Poor quality polycrystalline boule. Ampoule reheated and withdrawn without improvement in crystal quality.	11
5 gm	Ampoule exploded	14

TABLE 3.1 ZnTe GROWTH EXPERIMENTS

Growth No.	Starting Material	Temperature Data	Soak Time	Growth Techniques
		1. Bridgman		
15(B)	Sections of boule from growth run (2) + 2gms B_2O_3 flux	1150°C	3 hrs.	Ampoule removed after 3 hrs.
16(B)	40wt%Te 60wt%Zn Constituents not reacted prior to growth - 4gms B_2O_3 flux added to mix.	1150°C	-	-
20(B)	Harshaw ZnTe (as supplied)	1300°C	-	R.F. generator used to heat graphite crucible containing constituents.
21(B)	85wt% Te 15wt%Zn pre-reacted.	1300°C	-	R.F. generator used to heat ampoule held in graphite sleeve.
22(B)	Stoichiometric mix pre-reacted	>1300°C	-	Ampoule placed in soapstone cylinder
23(B)	As (21)	1100°C	-	Vertical furnace. Ampoule dropped through temperature zone at rate of 30cm/hr. When ampoule at 900°C quenched to room temperature
24(B)	As (21)	1100°C	17 hrs	Vertical furnace. Withdrawal rate of 0.75cm/hr for first 5 hrs then 6cm/hr
25(B)	As (21)	1120°C	17 hrs	As (22) but withdrawal rate maintained at 0.75cm/hr for 24hrs.
26(B)	78wt%Te, 22wt% Zn pre-reacted	1100°C	64 hrs	Horizontal furnace. Ampoule removed after 64 hrs.

TABLE 3.1 ZnTe GROWTH EXPERIMENTS

Quantity	Results and Comments	Growth No.
	1. Bridgman	
3 gm	No improvement on quality of original material	15
5 gm	Tube exploded. Attributed to weak seal.	16
5 gm	Ampoule ruptured	20
10 gm	Graphite sleeve fractured and ampoule ruptures.	21
10 gm	Soapstone expanded permitting rupture of ampoule. Attributed to inadequate heat treatment of soapstone.	22
20 gm	Small crystallites containing Te inclusions.	23
20 gm	Boule containing single crystal regions of volume 0.25cm^3 showing some porosity and inclusions.	24
10 gm	Results similar to (24) but larger single crystals of volume 0.5 cm^3 obtained.	25
15 gm	Boule contained crystals of inferior quality to run (25).	26

TABLE 3.1 ZnTe GROWTH EXPERIMENTS

Growth No.	Starting Material	Temperature Data	Soak Time	Growth Techniques
		1. Bridgman		
27(B)	As (26)	1100°C	125 hrs	Horizontal furnace. Ampoule stationary, furnace pulled on horizontal track
28(B)	As (26)	1120°C	85 hrs	As (27)
		2. Vapour		
3(V)	As (1)	As (1)	16 Hrs	As (1) but withdrawal rate of 17.5cm/hr
4(V)	Harshaw chemical Co. ZnTe sintered at 800°C prior to growth	1250°C constant along length of ampoule	16 hrs	As (3)
5(V)	As (4)	1270°C constant along length of ampoule	16 hrs	As (1) but withdrawal rate of 7.5 cm/hr
12(V)	Harshaw ZnTe (As supplied)	Constituents at 1200°C. Opposite end of ampoule at 1100°C	65 hrs	Ampoule removed after 65 hrs.
13(V)	55 wt% Te 45 wt% Zn. Constituents not reacted prior to growth.	Constituents at 1200°C. Necked down region of ampoule at 900°C	24 hrs	See text. Ampoule cooled at natural cooling rate of surface. Residual atmosphere of N_2 plus O_2.
17(V)	As (16) but 45 wt% Te 55 wt% Zn	Constituents at 1000°C. Opposite end of ampoule at 900°C.	4 hrs	Ampoule not sealed. Stream of reducer gas passed over orifice with ampoule inclined at angle of 15° to horizontal.
18(V)	As (17) but 71 wt% Te 29 wt% Zn	Constituents at 1150°C. Opposite end of ampoule at 900°C.	2.5 hrs.	As (17). After 2.5hrs ampoule cooled at natural cooling rate of furnace.
19(V)	As (18)	As (18)	As (18)	As (18)

TABLE 3.1 ZnTe GROWTH EXPERIMENTS

Quantity	Results and Comments	Growth No.
	1. Bridgman	
10 gm	Crystals similar to run 25, but concentration if inclusions and degree of porosity significantly reduced.	27
10 gm	This charge was subjected to two identical heat soaking and withdrawal cycles. In comparison with the results of run (27) a further improvement in crystal size and quality was obtained	28
	2. Vapour	
19.3 gm	First cm of boule contained good quality crystals beneath surface layer. Remainder polycrystalline and porous. Some vapour phase growth of useful quality platelets.	3
1 gm	Vapour phase growth of good quality crystals toward the lower temperature end of the ampoule.	4
1.2 gm	Vapour growth as in (4). Crystals coated with Te.	5
5 gm	Good quality vapour grown platelets.	12
5 gm	Large polycrystalline boule containing nonporous single crystal regions, free of inclusions and of volume 0.5cm^3. These crystals were O_2 doped and translucent red in appearance.	13
10 gm	Poor quality polycrystalline boule.	17
10 gm	Good quality vapour grown crystals.	18
10 gm	Vapour grown boule of volume 5 cm^3. Contained good quality single crystals.	19

TABLE 3.1 ZnTe GROWTH EXPERIMENTS

Growth No.	Starting Material	Temperature Data	Soak Time	Growth Techniques
		2. Vapour		
29(V)	Boat No.1 80wt%Te 20wt%Zn(20 gm) Boat No.2 57wt%Te 43wt%Zn (2gm). Constituents pre-reacted.	850°C	188 hrs	Boats placed in sealed evacuated ampoule in common temperature zone and annealed for one week.
32(V)	Stoichiometric mix not pre-reacted	Annealed at 1080°C Evaporated - constituents at 950°C. Condensation at 950>T>RT	15 hrs 2 hrs	Constituents annealed in sealed ampoule at 1080°C for 15 hrs, and then heated at 950°C for 2 hrs under running vacuum.
		3. Solution		
30(S)	Harshaw ZnTe (sintered) 0.1 mole fraction ZnTe in In .	875°C	-	ZnTe soluble in In at 800°C. Ampoule cooled at natural cooling rate of furnace. Initial rate 300°C/hr.
31(S)	Harshaw ZnTe (sintered) 0.1 mole fraction ZnTe in Bi.	950°C	-	ZnTe soluble in Bi at 910°C. Ampoule cooled as (30).

TABLE 3.1 ZnTe GROWTH EXPERIMENTS

Quantity	Results and Comments	Growth No.
	2. Vapour	
-	This technique of equilibrium vapour transport was used to prepare good quality microcrystalline ZnTe for use as starting material (see text)	29
20 gm	Vapour grown polycrystalline ZnTe (grain size 10^{-3} - 5 x 10^{-2} cm) (see text)	32
	3. Solution	
1.78 gm ZnTe +10.54 gm In	Solution regrowth of thin (10^{-2} cm) ZnTe platelets free of inclusions and of area 0.25 cm^2	30
-	Solution regrowth of ZnTe platelets similar to those obtained in run (30)	31

the experiments were performed. This is due to the fact that, in a number of cases, growth runs were conducted in parallel in order to fully utilise the available furnaces.

In the succeeding sections more information is presented on the various growth techniques employed and detailed descriptions are given of representative growth runs selected from Table 3.1. At the end of this section crystal preparation techniques which do not fall into the three categories listed above, and also experiments on the purification of crystals and the preparation of starting material, are described.

Description of Apparatus and Preparation Procedures

Before discussing the results of selected growth runs, the apparatus used and the preparation procedures normally adopted are described.

The furnaces used in the crystal growth procedures are shown in Plate 3.1.

In the B.T.U. furnace a uniform temperature zone 12" in length was maintained by the use of two separately controllable end zones which, when set up to provide a uniform distribution, were coupled to the main zone controller. The accuracy and stability of this unit was within ± 1/2°C along the length of the uniform zone. The second furnace used in these experiments was constructed

(a) B.T.U. diffusion furnace.

(b) Kanthal furnace and puller.
A. Drive system.
B. Furnace.

(c) 500 Kc/s R.F. Generator.

Plate 3.1.

from Kanthal A-1 resistance heating elements. As the length of the element in this furnace was 8" the plateau region was short and the shape of the temperature profile could be drastically altered if the insulating plugs, normally inserted in the open ends of the furnace tube, were removed. The natural temperature profiles of these furnaces are shown in Fig. 3.1. In a number of cases the variation in temperature along the length of the melt as it was withdrawn from the unifrom temperature zone, $\delta T/\delta l$, was considered to be too gradual, and a more planar freezing front, with a temperature gradient more closely approximating to a step function, was created by the use of a separately wound heater coil which protruded beyond the hot zone. The maximum temperature at which both furnaces could be operated for long periods was 1280°C, and the majority of growth runs were conducted in the temperature range 1050-1250°C. The pulling mechanism used in conjunction with the B.T.U. furnace was synchronous motor/gearbox system which allowed the choice of a variety of final drive gears and associated withdrawal rates ranging from 0.5cm to 30cm per hour. The withdrawal system used in conjunction with the Kanthal furnace consisted of the variable speed gearbox/drive shaft system shown in Plate 3.1. This system offered the capability of driving either the furnace itself or the container holding the constituents; both techniques were used during the course of the experimental growth runs.

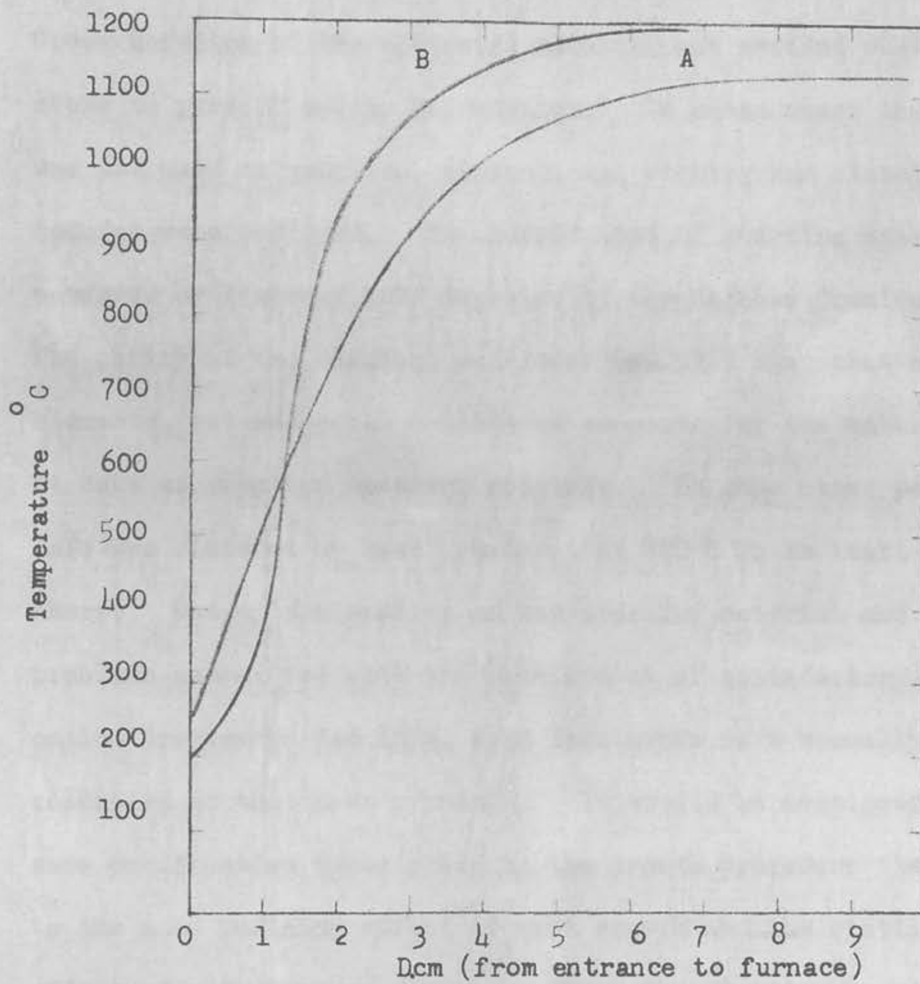

FIGURE 3.1 A. Temperature Profile B.T.U. Furnace

B. Temperature Profile Kanthal Furnace.

As a general procedure all silica tubing and crucibles used in these experiments were cleaned in aqua regia, washed in distilled water and dried with ethyl alcohol. Two forms of starting material were used. The first was Cominco Zn and Te of 99.999% purity. Undue handling of the elemental material was avoided wherever possible to prevent purity degradation. In cases where the material was not used as supplied, conventional etching and cleaning procedures were employed. The second type of starting material was powdered or sintered ZnTe supplied by the Harshaw Chemical Company. The purity of the compound was lower (99.99%) than that of the elements, but was still considered adequate for the material to be used as supplied wherever possible. In some cases powdered ZnTe was sintered by heat treatment at 800°C in an inert atmosphere. Due to the quality of the starting material and the problems associated with the development of satisfactory purification treatments for ZnTe, such treatments were normally only conducted on the grown crystals. It should be mentioned that some purification takes place in the growth procedure itself, due to the zone refining effect of melt growth and the distillation effect of vapour phase growth. These purification problems were previously discussed in section 2.1.3. In some of the growth runs using elemental material, the components were reacted in an inert or reducing atmosphere before being transferred to the container in which growth was to take place. (Zn and Te form in an exothermic reaction at approximately 600°C. The heat of

formation of ZnTe at 298°K was reported by Goldfinger and Jeunhomme (1963) to be 26 Kcal/mole.) In other cases the elements were sealed in the growth ampoule and the reaction allowed to proceed as the temperature of the ampoule was raised within the furnace. No definite experimental evidence, in terms of the quality of the resulting crystals, was obtained to indicate the superiority of either of these approaches; however, the former technique was found to be more convenient in practice. In the majority of experiments, and in particular all those in which the growth ampoules were withdrawn through a temperature gradient, the constituents were sealed in evacuated silica tubes at pressures of approximately 10^{-4} - 10^{-5} mm Hg.

3.1 Bridgman Growth

As stated previously the majority of experiments were conducted using an excess of one component, normally Te. The solution temperatures required for given amounts of ZnTe and Te were determined from the liquidus curves previously described and shown in Fig. 2.2. For example, in growth experiment No.1 it was desired to obtain recrystallisation at a temperature of 1050°C. From the liquidus curves the correct ratios of Te and Zn were determined to be 80 wt% and 20 wt% respectively. (A stoichiometric melt contains 66 wt% Te and 34 wt%Zn.) The use of a maximum temperature of 1100°C ensured that no ZnTe remained undissolved. The preferential use of excess Te in growth proced-

ures was instigated for several reasons. Firstly, as the majority of experiments into the electroluminescence of ZnTe crystals were to be concerned with crystals containing no deliberately introduced foreign impurities, it was considered that the p-type conductivity of the crystals would be enhanced by the incorporation of Zn vacancies. As discussed in section 2.2.3.1.1. the possibility of obtaining n-type conductivity crystals by growth from an excess Zn solution was considered to be extremely remote, and therefore the effects of such growth techniques would be expected to, at best, reduce the conductivity of the p-type crystals, thus producing more insulating crystals unsuitable for application as electroluminescent devices. In addition Fig. 2.2 shows that the rate of solidification from an excess Zn melt as the temperature is reduced is considerably more rapid than from a corresponding excess Te melt. Such rapid and relatively uncontrollable crystallisation would be expected to result from an excess Te melt under similar growth conditions. This latter consideration is not applicable to growth from the vapour phase. As shown in Table 3.1 constituent ratios varying from stoichiometric to 90 wt% excess Te were utilised in attempts to improve crystal quality and size.

In the initial growth runs it was found that the melt grown boule was covered with a crystalline skin of ZnTe. Beneath this skin the boule was porous in structure and comprised of polycrystalline ZnTe plus Te inclusions. The region of the boule which first

entered the temperature gradient contained the better quality single crystal regions and less inclusions. The concentration of inclusions increased towards the other end of the boule and at this end the excess elemental Te was located. The degree of porosity was found to be significantly reduced if the ampoule containing the constituents remained for a considerable length of time in the high temperature zone before withdrawal was initiated (heat soaking times of up to one week were used). Similarly the quality of the crystals and the distribution of inclusions improved as the withdrawal rate was reduced. Under slow withdrawal rates there was more tendency for the majority of the excess Te to freeze at the "high temperature" end of the ampoule. It was found that the quality of the crystals was not significantly influenced by the use of excess Te concentrations in the range 70-80 wt%. For values above 85 wt% the concentration of the inclusions increased and there was a general tendency for the complete boule to contain large segregated Te regions in which the ZnTe crystals were contained as small included volumes. In these cases difficulty was experienced in finding a satisfactory chemical agent capable of removing the elemental Te without attacking the ZnTe crystals; all of the etch solutions investigated attacked the ZnTe crystals as readily as the Te.

A number of experiments were performed in the Kanthal furnace in which the ampoule was raised or lowered vertically through the high temperature zone. This technique was used in runs 23, 24

and 25. In two of these runs good quality crystals of reasonable volume were obtained. In run No.10 recrystallisation was allowed to take place at the natural cooling rate of the furnace ($200^{o}C$ per hour) and as would be expected from such a rapid rate of temperature reduction, the quality of the resulting crystals was poor. For run No.23 the ampoule was withdrawn from the furnace at the rapid rate of 30 cm/hr. This is again equivalent to a high rate of temperature reduction and this was reflected in the poor quality of the resultant crystals. Runs 24 and 25, however, benefited from the use of slow withdrawal rates of 0.75 cm per hour, and the quality of the crystals obtained showed significant improvement. The use of B_2O_3, a highly stable compound, as a flux has been reported to produce improved ZnTe crystals (Eastman, 1966). In the present experiments the use of this flux did not result in any significant improvement in crystal size or quality.

Some of the most satisfactory results of this investigation into ZnTe crystal growth were obtained by the use of a moving furnace (Runs 27 and 28). In these experiments the growth ampoule was placed in a quartz tube which was then positioned horizontally in the centre of the furnace and suspended independently of the furnace mountings and drive mechanism. During growth recrystallisation, the zone was moved along the length of the melt by pulling the furnace along a horizontal drive shaft. Any possible movements and vibrations which may have arisen in systems where

the ampoule itself was withdrawn from the furnace were thereby eliminated. As in these experiments the heat soaking time was also significantly increased over the times used in previous experiments, it is therefore not possible to unambiguously associate any improvement in crystal size and quality with this particular modification. From the results of the other experiments it is almost certain that the improvements are mainly attributable to the extension in annealing time.

3.2 Vapour Growth

As stated previously, some of the best quality crystals obtained in these experiments resulted from vapour-phase growth. The size of crystals thus obtained were generally smaller than those that could be sectioned from the melt-grown boules, but were perfectly adequate for the fabrication of electroluminescent devices.

In growth runs specially designed to encourage growth from the vapour phase the ampoule containing the constituents was positioned in the furnace so that the end of the ampoule distant from the constituents was at a lower temperature. Although the normal technique of vapour phase growth utilised stoichiometric mixes, some of the best quality crystals (Run No.18) were obtained from mixtures containing an excess of one component. In such cases the constituents entered the vapour from the liquid phase and growth took place under an overpressure of this component. This

resulted in some cases with the crystals being covered by a layer of, say, Te caused by condensation of the element as the temperature was reduced. In a number of growth runs utilising withdrawal techniques vapour phase crystals were also obtained. (Nos. 3, 4, 5). In these cases it is understandable how this type of growth could be initiated, since the ampoule was withdrawn into a cooler region of the furnace. However such vapour grown crystals were not obtained consistently even in superficially similar runs.

In comparison to the Bridgman experiments not all the vapour growth runs were conducted using sealed, evacuated, ampoules. Several of these experiments are described in more detail as they are particularly relevant to the experimental measurements of electroluminescence in ZnTe.

In growth run No. 18 the constituents which included excess Te, were placed in a quartz ampoule necked down to leave an orifice of approximately 1 mm diameter at one end. During this process the ampoule was evacuated and flushed with reducer gas. It was then placed in the furnace at an angle of 15° to the horizontal and positioned so that the constituents would attain a temperature of $1150^{\circ}C$ while the temperature of the orifice situated beyond the uniform temperature zone would be $900^{\circ}C$. The ampoule was maintained at temperature for 2.5 hours during which time

a stream of reducer gas was passed along the furnace. The ampoule was then cooled over a further 2.5 hours at the natural cooling rate of the furnace. This technique resulted in a vapour grown boule which appeared to have nucleated initially in the region of the orifice; good quality crystals were extracted from this boule.

In experiment No. 13 a charge containing excess Zn was placed in an ampoule which was then inserted in a furnace maintained at 1200°C. A short capillary tube extended from the ampoule into a second temperature zone. By use of an auxiliary coil this zone was maintained at 900°C. From within this temperature zone a tube of larger diameter connected the capillary tube to an externally located reservior containing inert gas plus 5% oxygen. The growth run extended over a period of 24 hours and resulted in the growth of a boule of ZnTe and an additional quantity of white crystals; these latter crystals were identified by X-ray powder diffraction analysis to be ZnO. ZnTe crystals of approximate volume 0.4 cm^3 were extracted from the boule. These crystals exhibited a red colouration when viewed in transmission. A vacuum spark mass spectrographic analysis of these crystals, kindly arranged by Mr. R. K. Willardson of the Bell and Howell Research Center, qualitatively identified oxygen to be present in concentrations of approximately 10^{18} atoms/cm^3. Thus, in this experiment, vapour growth permitted the production of

reasonable quality crystals of a size comparable with those obtained by Bridgman techniques, and incorporating a dopant which will be shown to have a pronounced effect on the electroluminescent properties of devices fabricated from this material.

Vapour growth techniques were used in experiment No.32 to prepare polycrystalline ZnTe. This material was also the subject of extensive investigations in the form of electroluminescent devices. In this experiment high purity Zn and Te in approximately stoichiometric quantities were placed in an evacuated quartz ampoule and annealed for 15 hours at 1080°C. The resulting ZnTe excluding the remaining excess elemental material was placed in a quartz tube and inserted in a furnace maintained at 950°C. This tube extended from the furnace into the room and was connected to a running vacuum. After a period of two hours the ZnTe (20 gm) had evaporated and recondensed further along the tube at a position corresponding to a temperature of between 600°C and 700°C. The form of this condensate was hard packed polycrystalline material of grain size 10^{-3} - 5×10^{-2} cm. A photomicrograph of a polished slice of this material is shown in Plate 3.2. At a position further along the tube and corresponding to a lower temperature excess elemental material had condensed.

The equilibrium vapour transport technique of Albers and Aten, previously discussed in section 2.1.2.1., was used to prepare

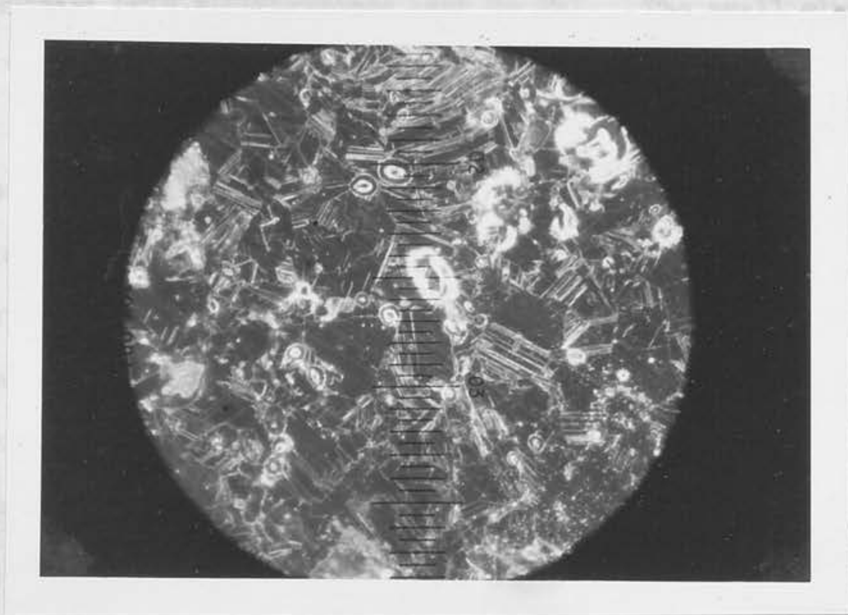

(a) Polycrystalline ZnTe. Scale - Thousandths of inch.

(b) Boule of ZnTe. Scale - Inches.

Plate 3.2.

good quality ZnTe microcrystals (Run No.29). The small size of these crystals renders them suitable for use as starting material only. In this experiment two mixtures, one containing excess Te and the other excess Zn, were pre-reacted, placed in separate fused silica boats and inserted in a quartz tube which was subsequently evacuated and sealed. The combination was annealed for one week at 850°C. This process resulted in the growth in inclusion free microcrystals in the excess Te boat. Another application of this technique is in the purification of grown crystals containing inclusions.

3.3 Solution Regrowth

Two experiments on solution regrowth from elements other than components of the compound were conducted. These are considered important, not because of the results obtained, which were inferior to the other growth techniques described above, but because it is considered that by use of slow rates of temperature reduction, good quality crystals of suitable size for device fabrication could be grown easily, and reproducibly, by this technique.

In the first experiment, No.30, 10.5 gms of In and 1.8 gms of ZnTe (i.e. 0.1 mole fraction of ZnTe) were placed in a sealed, evacuated, quartz ampoule. This ampoule was placed in a muffle oven and the temperature raised to 875°C. From Fig. 2.4 it was

determined that the solution temperature of this mole fraction was 800°C. The selected temperature ensured that all the ZnTe entered solution. The ampoule was then cooled at the natural cooling rate of the muffle oven, which initially corresponded to a rate of 300°C/hour. The ZnTe platelets grown by this technique were separated from the In by amalgamating the latter with Hg and heating this mixture in a running vacuum to drive off the metal components which were collected in a cold trap. The crystals obtained by this technique were extremely thin (10^{-2}cm) and of small area ($0.25cm^2$) but were of good quality and free of inclusions. It is therefore anticipated, that, by the use of considerably slower rates of temperature reduction, crystals of useful size and thickness could be obtained. One particularly interesting aspect of this technique is the relatively low temperatures at which regrowth can take place. Regrowth from an In solution has additional significance, as there exists the slim possibility that such crystals may acquire n-type conductivity by exposure to the donor-type solvent. Regardless of the conductivity type, the crystals would be expected to contain incorporated In, which, from the literature, reputedly gives rise to a characteristic electroluminescent emission spectrum (Watanabe, 1965). In a second experiment, No.31, ZnTe crystals were grown from a Bi solution by the same technique. The physical size of the crystals was very similar to that obtained from the In solution, except that the crystals regrown in In had a slightly more reddish

appearance when viewed in transmission.

Crystals grown by the techniques outlined in this chapter are shown in Plate 3.2.

To conclude this section it should be stated that several experiments were conducted at temperatures near the stoichiometric melting point (1300°C.). None were successful. As anticipated, it was found that unsupported quartz could not withstand this temperature and the associated vapour pressures. The use of graphite containers in conjunction with 10KW R.F. generator was found to be unsatisfactory due to the tendency of the graphite to fracture during cooling. In such techniques the quartz ampoule softened and expanded against the walls of the graphite cylinder. The tendency of the graphite to fracture can be attributed to the use of graphite cylinders of incorrect wall thickness which were unable to withstand the tensile stresses generated by the dissimilar contraction rates of graphite and quartz.

3.4 Crystal Purification

Two techniques were used to purify crystals grown by the various techniques described above. The success of the techniques was normally judged on the macroscopic scale by their capability to remove inclusions. The actual success either technique may have had in removing dissolved impurities was not investigated.

In the first technique, the crystal to be purified was placed in an evacuated and sealed quartz tube with a quantity of high purity Zn metal. Annealing ZnTe crystals in liquid Zn, or Zn vapour, has been reported in the literature to be a useful technique for the removal of inclusions and shallow acceptors such as Cu. (Aven and Segall, 1963; Shiozawa, 1962). The annealing was conducted for one week at a temperature of 800°C. This technique was effective in removing some near-surface inclusions. A more successful technique, from this standpoint, was the use of the equilibrium vapour transport method of Albers and Aten (1965) discussed in sections 2.1.2.1. and 3.2. In this case the crystal to be purified was placed in an ampoule together with a silica boat containing polycrystalline ZnTe plus Zn metal. The evacuated and sealed ampoule was annealed at 800°C for one week. This method was found to be quite successful and significantly reduced the size and concentration of inclusions in the ZnTe crystal.

3.5 Conclusions

Several conclusions concerning ZnTe crystal growth can be reached on the basis of the results of the above experiments.

The growth procedures did not result in the production of large-volume single crystals of ZnTe. At best crystals of volume 0.5 to 1 cm^3 were obtained. It should be stated, however, that such

crystals compare favourably in size with those reported by other investigators who used similar methods of preparation.

For the case of Bridgman growth, the best results were obtained by the use of extended annealing times and slow withdrawal rates. The results obtained probably do not represent the limit of what can be achieved by such techniques. The use of extended annealing times is quite feasible, and improvement would also be anticipated from the use of slower withdrawal rates, since even the slowest rates used in the above experiments are still an order of magnitude greater than those employed by several previous investigators. One of the main problems encountered in growth from a melt was the high degree of porosity and significant concentration of inclusions in the resulting boules. These conditions were also alleviated by growth techniques in which the melt was subjected to long-term heat soaking and slow recrystallisation. (For the grown crystals, equilibrium vapour transport purification treatments proved to be useful in the elimination of pores and inclusions.)

The most acceptable results were obtained by the vapour growth technique, as some of the best quality crystals, although limited in size, were produced by this method. The technique used for

growth run No.1 is similar in several respects to that recently reported by De Meis and Fischer (1967). These authors described an apparatus which also used a capillary tube extending from the high temperature zone. On the basis of this report and the results of the present experiments it would appear perfectly feasible to grow large ZnTe crystals from the vapour phase by such methods. The advantage of vapour growth from a sealed ampoule which extends beyond the high temperature zone is that excess volatile material collects in the colder region until the decomposition pressure in the ampoule reaches a minimum. Growth progresses under the optimum conditions which exist at slight deviations from stoichiometry corresponding to the minimum decomposition pressure; vapour growth techniques accomodate this adjustment. A second advantage of the method is that even at high temperatures dilation of the quartz is prevented as the excess pressure associated with either component is not generated.

Solution regrowth of ZnTe has received little attention in the past. In the restricted experiments conducted on this preparation technique good quality crystals were obtained; however, due to the high cooling rates employed, these crystals grew in the form of thin, small area, platelets. This method has considerable potential; as well as offering a convenient and reliable method for the growth of good quality crystals of useful size, it offers the advantages, which have been widely exploited in application to the III-V compounds, of permitting the introduc-

tion into the melt of a wide range of impurities which should be capable of incorporation in high concentrations.

4. MATERIAL PROPERTIES

4.1 Material Evaluation

4.1.1 Optical

Optical examinations were made on each batch of crystals in order to make comparisons between the various growth techniques.

Lapping and etching of representative samples from each growth run revealed considerable variations in crystallite size, larger single crystals being obtained from the Bridgman growth techniques. These crystals had, in a number of cases, a tendency towards porosity and thus the size of available single crystals was limited. The largest crystals thus obtained were in the range 0.5 to $1cm^3$ with segments commonly used for device fabrication being cut from single crystals of volume $0.25cm^3$. By examination under polarised light, it was found that crystals grown from the vapour showed more evidence of internal strains than those grown by Bridgman techniques. Crystals grown from solution were found to be free of the above flaws; however, crystals grown by this technique were of much smaller volume ($5 \times 10^{-3} cm^3$) than those grown by other methods. These crystals, several millimetres on edge, are still sufficient size for device fabrication, but in practice, a limitation on their usefulness is imposed by the thinness, and associated fragility, of the

platelets.

Inclusions were positively identified in representative crystals from a number of runs. These opaque areas were assumed to be formed by excess Te aggregation. This was confirmed by comparison of crystals showing inclusions before and after annealing in molten Zn or with a ZnTe powder mix containing excess Zn. These extraction, or "reaction", experiments resulted in a reduction of the concentration of inclusions, the latter technique proving the more effective. Crystals grown from solution or from starting mixtures containing excess Zn were notably free of inclusions. In appearance crystals grown by most techniques were orange in colour when viewed in transmission. Exceptions were those grown in an oxygenated atmosphere (No.13) and from an In solution (No.30); these crystals were more absorbent and appeared red in transmission.

4.1.2 X-Ray

Powder diffraction analyses were made of crystals from several growth runs. Such analysis would be expected to reveal only large concentrations of impurities (> 2%). It was anticipated that variations in the powder patterns would be found for material containing included regions, or material in which oxygen had been incorporated with the possible formation of zinc or tellurium oxides. The only

growth runs in which this latter effect could occur would be those which were grown in adequately evacuated ampoules or ampoules in which the seal had failed during growth. In the case of growth run No. 13 the deliberate use of an oxygenated atmosphere may have resulted in the growth of ZnO crystals and the possible formation of a mixed crystal system.

With the co-operation of the Defence Research Board a General Electric recording diffractometer was used to compare the powder diffraction patterns of material from growth runs Nos. 1, 12, 13 and 18. Cu, $K_{\alpha 1}$ radiation was used in these analyses. For all batches, comparison with the A.S.T.M. index revealed that the reflections obtained corresponded in position and approximate intensity with the ZnTe pattern. If portions of crystal mainly consisting of included regions were selected, then extraneous lines were found to be present. As anticipated, these lines qualitatively matched the A.S.T.M. index for Te. For run No. 13 ZnO was not present in detectable concentrations. The fact that the observed lines corresponded to the ZnTe pattern eliminated the possible existence of a mixed crystal system.

Although in growth run No.13 the ampoule containing the constituents had been connected via a capillary tube to a

vessel containing inert gas plus oxygen, doubt existed as to whether the oxygen present had back-diffused into the ampoule and become incorporated in the crystals. It was therefore of interest to analyse the white crystals which had grown from the vapour in the ampoule. For this analysis a Debye-Scherrer powder pattern was photographed using a Philips x-ray unit and Cu filtered, tungsten, $L_{\alpha 1,2}$ radiation. The use of 57.54 cm diameter Debye-Scherrer camera permitted only qualitative comparison with the A.S.T.M. index; however, the reflections corresponded, without ambiguity, to the ZnO pattern. This therefore confirmed that oxygen was present in the ampoule during crystal growth.

The Philips unit was also used to obtain a back reflection Laue pattern from the polycrystalline ZnTe of growth run No.32. The radiation used was again W, and a Polaroid, Type R1, X-ray camera (Plate 4.1) was used to record the back reflection pattern. In Plate 4.1 the polycrystalline nature of the specimen is shown by the multiplicity of reflections and by their tendency to lie on Debye rings. For comparison purposes a Laue pattern of a single ZnTe crystal from run No.12 is also shown in this plate.

4.1.3 Chemical

As the electroluminescence of the majority of ZnTe devices

(a) X-Ray Unit.

A. Polaroid Camera.
B. Debye- Scherrer Camera.

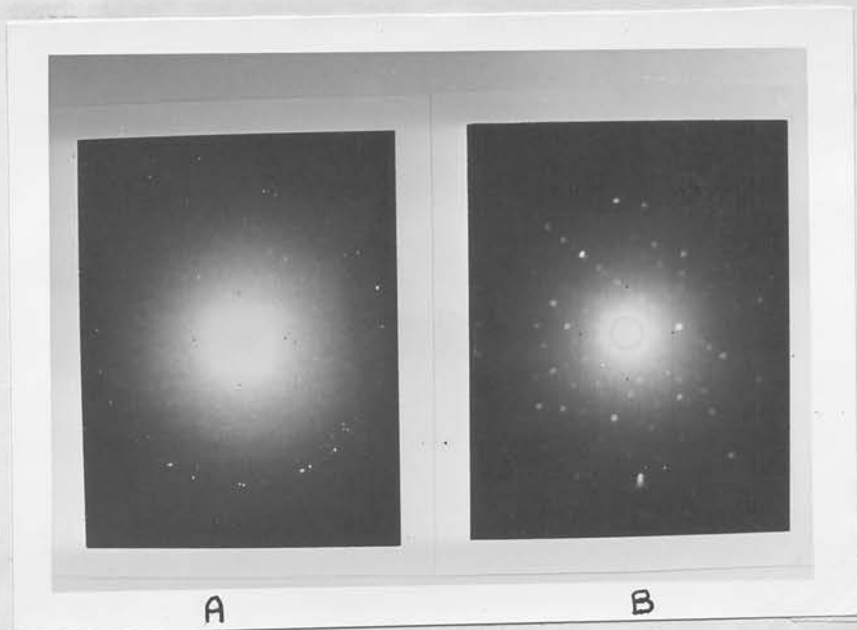

(b) Polaroid back-reflection Laue patterns of ZnTe crystals.

A. Polycrystalline ZnTe.
B. Twinned ZnTe crystal.

Plate 4.1.

to be described herein is associated with deviations from stoichiometric composition, analysis procedures capable of detecting stoichiometric deviations associated with concentrations of constituent vacancies or interstitials were investigated. The concentrations of these defects although low from the viewpoint of chemical analysis, may be of significance in affecting the semiconducting and electroluminescent properties of the material. The Department of Mines and Technical Surveys, as part of its programme on mineral analysis, has investigated compositional variations in a number of the II-VI compounds by techniques of chemical analysis. To date, however, the sensitivity of such analysis procedures is not adequate to detect stoichiometric deviations in ZnTe associated with "semiconduction" concentrations of native defects, ie. concentrations of the order of parts per million or less.

As discussed above in the section on X-ray analysis, ZnTe and dendritic ZnO crystals were identified as being present in run No.13. The presence of these latter crystals indicated that oxygen had probably also been incorporated as in impurity in the ZnTe crystals. To further investigate this hypothesis a vacuum spark source spectrographic analysis of these crystals was conducted at the Bell and Howell Research Center. The results of this analysis are shown in Table 4.1. Consideration must be given to the levels of

TABLE 4.1 IMPURITY CONCENTRATIONS IN ZINC TELLURIDE No.13 (IN PARTS PER MILLION ATOMIC)

Element(a)	Detection Limit(b)	ZnTe 116-A
H	0.05	10
Li	0.005	0.14
C	0.03	10-63
N	0.03	7.1
O	0.1	13
F	0.03	20*
Na	0.005	2.2-12
Al	0.01	0.40
Si	0.05	6.1
Cl	0.1	1.9
K	0.005	1.3-13
Ca	0.01	0.43
Ti	0.05	0.13
V	0.03	0.03
Cr	0.03	0.047
Fe	0.05	1.6
Ni	0.05	0.41
Se	0.07	0.92

(a) No analysis is given for tantalum or gold since tantalum slits were used in the mass spectrometer and the sample was sparked against an ultrahigh purity gold probe. Residuals in the instrument interfere with analysis for Ga, As, and Cd. Other impurities not listed were not detected and have concentrations less than 0.1 ppma except P, Cu, and I, analyses of which are interefered with by background lines of the matrix.

(b) Determined for 1 x 10^{-7} coulomb exposure.

* Seen on only one exposure.

__ Most representative value.

carbon, nitrogen, oxygen, sodium, potassium and silicon detected. The high level of carbon can be attributed to the use of organic chemicals for cleaning the silica ware used in crystal preparation. The levels of silicon, sodium and potassium can likewise be traced to the use of silica ware for crystal preparation. These impurities could, therefore, be considered to be present in all crystals although their concentrations may well be dependent on such crystal growth parameters as anneal time etc. The levels of iron and silicon are well below those given in the purity specifications for the starting material used, and are therefore expected to be present in all crystals. The levels of nitrogen and oxygen require further consideration. As nitrogen was used as the flushing gas and was also present in the residual atmosphere during growth, this could explain its incorporation in the lattice. The important feature of this analysis is that it confirms the presence of significant concentrations of oxygen in the ZnTe crystals. The two impurities, nitrogen and oxygen, would be expected to be peculiar to this growth run, and their presence in appreciable concentrations would not be expected in the other growth procedures.

4.2 Absorption

The optical absorption characteristics of ZnTe crystals were

measured using either a Beckman DK2-A prism spectrophotometer or a Jarrell-Ash 250 mm diffraction grating monochromator with a tungsten lamp as source. These instruments are shown in Plate 4.2. In the performance of the measurements, both instruments measured the intensity of light transmitted by the specimen crystal as a function of wavelength. The spectrophotometer could be used in a "transmittance" mode in which the beam leaving the monochromator passed through a beam splitter and, by means of a mechanical shutter driven by a sychronous motor, was directed alternately the sample and through a reference aperture containing a sample of the material on which the crystal was mounted (normally a glass microslide); the two components of the beam were directed onto the detector, again in an alternate fashion, by a second shutter which rotated in phase with the first. The detector circuit was coupled via a servo amplifier to a motor driving the exit aperture of the monochromator. Thus, when the beam was passed through the same material in both the "sample" and "reference" chambers then a constant 100% line was obtained across a wide range of wavelengths, the spectral response of the source and detector being compensated by automatic variation of the width of the exit aperture. This system had the disadvantage that, in addition to the variation of band-width, or resolution, introduced by the dispersion of the prism, a further variation was introduced by the servoing of the exit aperture. A second, and more serious

(a) Beckman DK-2A spectrophotometer.

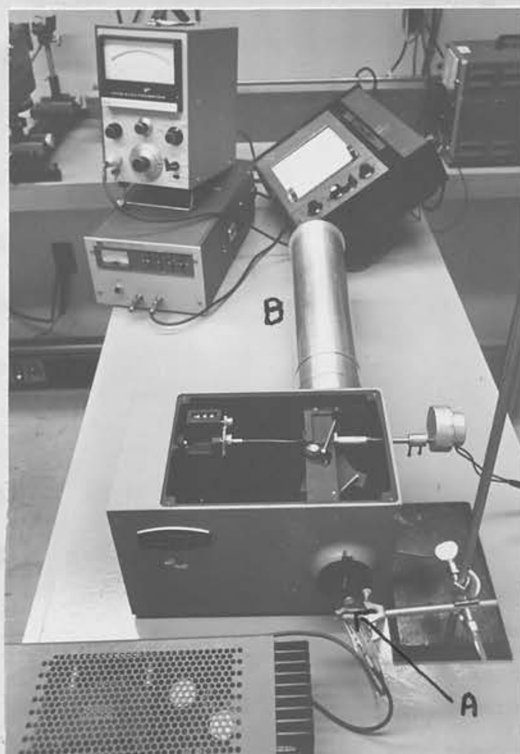

(b) Jarrell-Ash 250mm monochromator and associated equipment.

A. ZnTe electroluminescent device.
B. Photomultiplier.

Plate 4.2.

disadvantage in absorption spectra measurements, was that the range of transmittance scales available in this mode of operation were such that, having set up a 100% reference level, transmittance values of less than a few percent could not be measured with any degree of accuracy. It was found necessary, in the case of other than the thinnest crystals, to use the instrument in the "energy" mode in which the intensity of the light transmitted by the specimen is measured directly and displayed as a function of wavelength. For absorption spectra measured in this manner a separate spectrum was obtained of the relative spectral sensitivity of the detector to the emission of the source in the wavelength range of interest. This establishes the shape of the "incident illumination" spectrum. The transmittance can then be determined as the ratio of the amplitude of the signal obtained at a particular wavelength with the crystal positioned in the beam, to that obtained with the crystal removed. The detector used in the spectrophotometer was an RCA IP28 photomultiplier having a S-5 cathode response (ie. a spectral sensitivity peaking at 5200Å and falling to very low values at 6500Å). The monochromator was operated in an identical fashion to the spectrophotometer in the "energy" mode. This instrument had the advantage, however, of linear dispersion across the spectrum; also the photomultiplier used, an RCA 7265, had an S-20 cathode response of improved red sensitivity extending to 7500Å.

Radiation transmitted through a crystal is attenuated not only by absorption, but also by reflection at the crystal surfaces. With normal incidence on a parallel sided sample the measured transmitted beam contains multiply reflected components. When these are included, and provided interference effects are unimportant, the transmittance, T, is given by (McMahon, 1950)

$$T = \frac{(1-R)^2 e^{-\alpha d}}{1-R^2 e^{-2\alpha d}} \qquad (4.1)$$

where R is the normal-incidence reflectance at the air:sample interface, α is the absorption coefficient, and d the sample thickness. R is given in terms of the refractive index, n, and extinction coefficient, k, ($k = \alpha\lambda/4\pi$) as, (Stern 1963)

$$R = \frac{(n-1)^2 + k^2}{(n+1)^2 + k^2} \qquad (4.2)$$

In the measurements conducted on ZnTe crystals it was assumed that the spectral dependence of R was relatively unimportant compared with that of α, so that it could be considered as a constant in the calculation of α from T using eq. 4.1. The value of R to be used was determined by measuring the transmittance at long wavelengths far removed from the vicinity of the absorption edge; i.e. in a region of negligible absorption. The reflectivity is then obtained as

$$R = (1-T) \qquad (4.3)$$

assuming the absorbance is zero. This treatment is one that

is commonly used in the evaluation of absorption coefficients of semiconducting materials (Marple, 1966). For the majority of the ZnTe crystals used in absorption spectra measurements, the value of R was found to lie between 20 and 35%. The calculated absorption coefficients were in the range $10 < \alpha < 10^{3}$ cm^{-1} for thickness values, d, in the range $3 \times 10^{-3} < d < 10^{-1}$ cm.

The results of measurements on crystals from growth runs Nos. 12 and 13 are shown in a semi-log plot of absorption coefficient versus photon energy in Fig.4.1. Crystals from the majority of growth runs had absorption characteristics essentially identical to No.12, with minor variations in the shape of the absorption tail below 1.9 eV; in several specimens there was a definite tendency for the absorption coefficient to increase as the incident photon energy was decreased below 1.9 eV. Crystals from batch No.13 possessed a unique absorption spectrum extending over a wide range of energies and possessing several maxima. These results raise questions concerning the energy band structure and absorption processes in ZnTe and the possible effects of impurities on the absorption edge.

Although, as discussed in chapter 2 and appendices 1 and 2, there is little doubt that ZnTe is a direct gap material, the results of optical absorption measurements do not unambiguously show whether the lowest energy optical transition is direct or indirect, i.e. whether the conduction and valence band extrema are

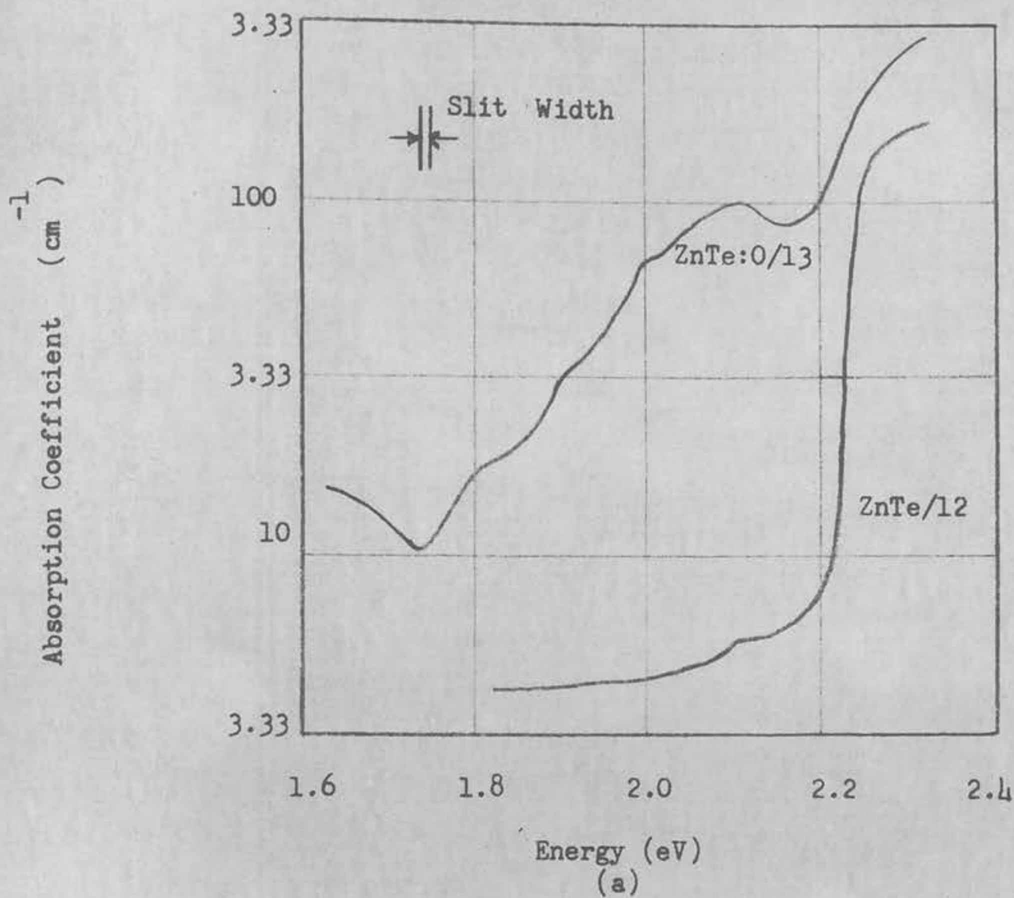

(a)

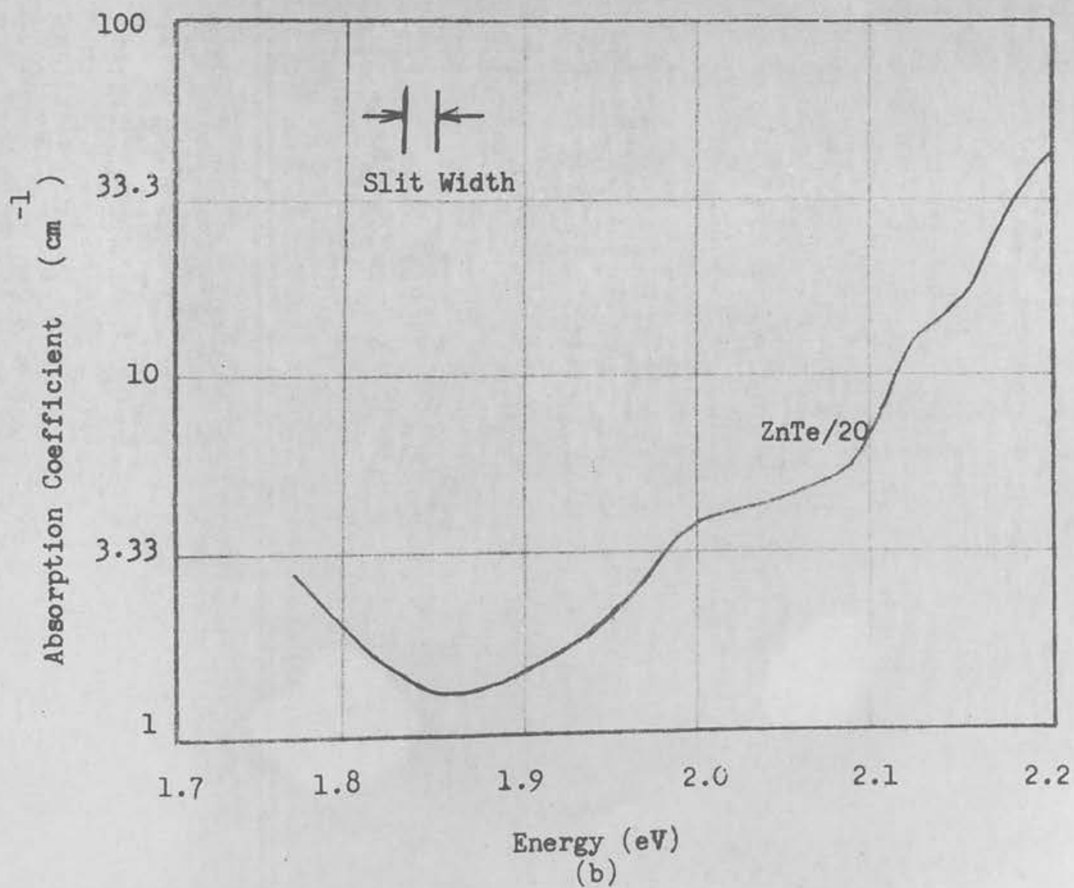

(b)

FIGURE 4.1 Absorption coefficient versus photon energy for ZnTe crystals at 293° K.

located at k=0. For example, Aten et al., on the basis of measurements of absorption coefficients in the range $5<\alpha<10^{-2}$ cm^{-1}, concluded that the lowest energy optical transition in ZnTe was indirect. Indirect transitions have also been proposed for other II-VI compounds (eg. CdTe, ZnO; Cardona and Harbeke, 1964). As discussed in appendix No.2, absorption band tails having a dependence of absorption coefficient on energy given by

$$\alpha \sim (h\nu - E_G + \hbar\omega)^2 \qquad (4.3)$$

$$\alpha \sim (h\nu - E_G + \hbar\omega)^3 \qquad (4.4)$$

are normally associated with indirect transitions. Here $h\nu$ is the photon energy, E_G the band gap energy and $\hbar\omega$ the energy of the phonon created or annihilated in the transition. Thus, in an indirect transition material the lowest energy transition would be expected to obey such a relationship; at higher energies where excitation can occur vertically across the band gap a relationship indicative of direct transitions would be followed. In contrast to the results of Aten et al., Loh and Newman found the lowest energy transition to consist of a steep transition covering several decades of the absorption coefficient and exhibiting a sharp exciton peak at low temperatures (Section 2.2.1., Fig.2.5). The observed exponential dependence of the absorption coefficient on photon energy obeyed Urbach's rule

(Eq.2.2). As discussed in section 2.2.1 this dependence does not obey the selection rules for either direct or indirect transitions and in itself does not positively identify either transition process. Segall (1966) from evaluation of the absorption coefficient of CdTe which followed Urbach's Rule at temperatures greater than 150°K considered it to be a logical extension of the proposed mechanism of absorption in CdTe i.e. phonon assisted direct exciton absorption. From Fig.4.1. it is seen that the absorption coefficient of the material of Run No.12 is approximately linear over a limited range of absorption coefficient and could therefore be considered to be exhibiting Urbachian behaviour. Other possible explanations which have been advanced by other authors to explain exponential tails and interpret Urbachian behaviour were discussed in Section 2.2.1.

Direct transitions are frequently considered to have an energy dependence of the absorption coefficient of the form $(h - E_G)^{1/2}$ (appendix 1). Thus, in a direct transition material, the lowest energy optical transition should obey such a relationship. However, as discussed in section 2.2.1, even a direct transition material can exhibit absorption tails similar to those found in an indirect transition material. These tails can be attributed to exciton defect complexes associated with lattice disorders, impurity content, sample inhomogeity, impurity

fields, or electric fields associated with the surface states of the crystal. Even if the presumption is made that the crystals are of high-purity, exhibiting only intrinsic absorption, absorption tails can still be obtained. As explained previously these spectra can be correlated with the mechanism of LO phonon assisted "direct" exciton creation. This theory has been successfully applied by Marple and Segall (1966) to results obtained for CdTe and was considered by these authors also to be applicable to ZnTe.

In the absence of experimental results covering a wide range of temperatures, which would permit detailed evaluation of the phonon structure of the absorption spectra, it is not possible to make a quantitative evaluation of the absorption processes in terms of the theories of direct interband, direct exciton phonon- assisted, indirect interband or indirect exciton absorption. The experimental results described here were obtained at room temperature only and covered a limited range of absorption coefficients. No conclusions can therefore be drawn concerning the band structure of ZnTe, possible phonon and exciton energies, and associated transitions. The results are of importance, however, in permitting comparisons to be made between the quality of crystals obtained in various growth runs, indicating the possible existence of impurity complexes, and allowing qualitative estimation of room temp-

erature energy band gaps. The fact that absorption spectra essentially similar to run No.12 were obtained for a wide variety of growth runs and crystal thicknesses is taken as an indication that this spectrum is typical of intrinsic absorption in ZnTe. This infers that the growth techniques used resulted in the production of high-purity crystals. The variations between the results obtained by previous authors has been considered by Marple (1966) to indicate, in a number of cases the presence of extrinisc absorption associated with exciton-defect complexes.

For the absorption spectra described here, the sharp rise in the absorption coefficient around 2.2 eV found in the majority of crystals, is not strictly exponential in behaviour. Assuming direct transition considerations to be applicable the slope in this region was fitted to the equation $\alpha \propto (h - E_{Ex})^{1/2}$, where E_{Ex} is some possible direct exciton-transition. In plotting α^2 versus photon energy the value of the exciton energy gap E_{Ex} was taken as the energy corresponding to the lowest value of absorption coefficient where this relationship was obeyed. A value of 2.21 ± 0.01 eV was obtained for the majority of crystals. The onset of the steep absorption edge in the II-VI compounds is commonly associated with an exciton absorption process. The tendency for the absorption spectra to exhibit a broad peak at photon energies just above the absorption edge, could be

taken as evidence of this, although at room temperature excitons would normally be expected to be thermally dissociated. For such an exciton process the measured gap may correspond to the exciton energy gap given by $E_{Ex} = E_G - E_{ExB}$ where E_G is the direct gap and E_{xB} the unknown exciton binding energy; thus the estimated band gap energy may be lower than the actual value by a small amount. (In the literature, room temperature values of the direct gap in ZnTe as high as 2.35 eV have been reported (Cardona, 1964), and the exciton binding energy for the A series in ZnTe at 77°K has been estimated as 0.01 eV (Aten et al., 1962).)

Crystals from several growth runs exhibited absorption spectra having several maxima in the low energy range. An example of this for a crystal from growth run No.20 is shown in Fig.4.1(b).

The absorption spectrum shown in Fig.4.1(a) from material No.13 is particularly interesting. This broad absorption spectrum, not previously reported in ZnTe at room-temperature is attributed to the impurity complex incorporated in the crystal during growth. An absorption peak is located at 2.1 eV and it will be noted that, in the absorption spectrum of material No.12, there is also an indication of an increase in absorption at this value. Whether the same impurity is present in differing concentrations in both crystals is debatable. Also located on the absorption edge are two definite maxima located at 1.92 and 1.99eV.

At a lower energy a maximum exists at 1.8 eV followed by a steeper transition to a minima in the region of 1.75 eV. By plotting α^2 vs $h\nu$ for high energies the "direct" gap was found to be 2.205 ± 0.010eV. The slight shift to lower energy in comparison with the value obtained for undoped crystals could be attributed to the increased impurity concentration. This broad absorption spectrum could be explained in terms of an impurity complex in a manner analagous to the case of Mn in ZnS; that is, a defect complex characterised by several absorption bands. Alternatively, there exists the unlikely prospect of there being more than one impurity present in significant concentrations. Dietz et al. (1962) detected in ZnTe at 20 ^{o}K a transition located 0.4 eV below the band gap energy. This was later identified as an isoelectronic acceptor introduced by the substitutional incorporation of oxygen during crystal growth. The zero-phonon line was located 0.4 eV below the band gap and the peak of the associated broad absorption spectrum occurred at 2.10 eV. The absence of structure in the zero phonon lines was taken as an indication that the centre involved a simple point defect. The excited state of this centre consists of a hole and electron bound to the ionised donor. The energy of the excited state will be approximately the band gap energy minus the binding energy of the acceptor involved. Since the latter quantities are much greater than the exciton binding energy (found to be less than 0.02 eV in

ZnTe) these bound exciton states can be far removed from the intrinsic excitons. As discussed previously, material 13 is expected to contain oxygen impurities, and it is therefore postulated that the observed absorption spectrum is a thermally broadened peak in essence identical to that observed by Dietz et al. at low temperatures. If the centre is located at 0.4 eV above the valence band the zero-phonon transition would be expected to occur at about 1.8 eV. Figure 4.1(a) shows a maxima at 1.8 eV followed by a sharp decrease in absorption. The minor peaks and fine structure between 1.75 and 2.15 eV could be associated with phonon emission and absorption and possible exciton formation.

The broad transmittance spectrum in the absorption edge region associated with the lattice disorder of polycrystalline material from growth run No.32 is shown in Figure 4.2.

No significant absorption peaks associated with other possible impurities were detected in measurements covering the I.R. region of the spectrum. The extension of optical absorption measurements to low temperatures should provide further information concerning the band structure of ZnTe, the nature of possible exciton and phonon assisted transitions, and the fine structure of absorption spectra associated with impurities. The optical absorption characteristics of ZnTe described in this chapter will be further discussed in the section of this report concerned with emission spectra of ZnTe devices.

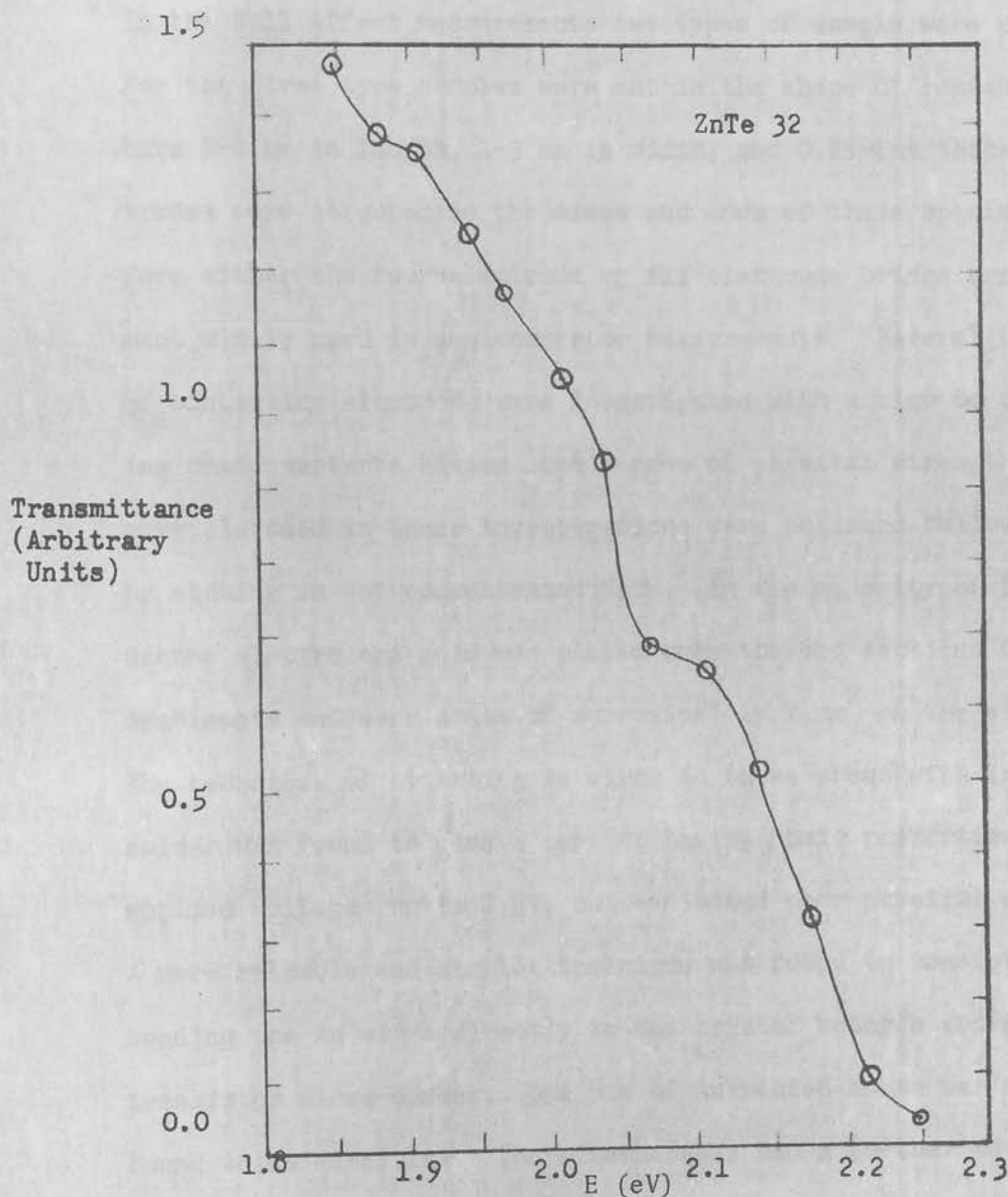

FIGURE 4.2 Transmittance versus Photon Energy of polycrystalline ZnTe from Growth Run No.32. Temperature 300°K.

4.3 ELECTRICAL TRANSPORT

Conductivity, Hall effect, and thermoelectric power measurements were conducted on representative crystals from the various growth runs.

In the Hall effect measurements two types of sample were used. For the first type samples were cut in the shape of rectangular bars 5-8 mm in length, 1-3 mm in width, and 0.25-1mm thick. Electrodes were attached to the sides and ends of these specimens to form either the four-electrode or six-electrode bridge arrangement widely used in semiconductor measurements. Several types of contacting electrode were investigated with a view to obtaining ohmic contacts having some degree of physical strength. All crystals used in these investigations were polished followed by etching in hot concentrated NaOH. In the majority of techniques electroless gold was plated over the end sections of the speciments and over areas of approximately 1 mm^2 on the sides. The technique of attaching Au wires to these areas with In/Ag solder was found to give a contact having ohmic properties at applied voltages up to 0.5V, but exhibited poor physical strength. A more reliable and simpler technique was found to consist of bonding the Au wires directly to the crystal using a conventional transistor micro-bonder. The use of Au-plated areas was not found to be essential. These techniques had a further advantage of permitting the use of small area contacts of similar size to

the wire used, typically 0.003" diameter. Some measurements were made with beryllium copper pressure contacts applied to the sides of the specimen and it was found that useful Hall measurements could be made despite high contact resistance. However, this contact resistance restricted the sensitivity of the Hall voltage measuring circuitry, thus significantly affecting the overall accuracy of the measurement.

Several problems were encountered in the preparation of satisfactory bridge-type specimens. The selection of good quality single crystals of adequate size to allow the fabrication of suitable specimen was limited; in the majority of cases the sample dimensions were smaller than those normally used in such measurements, (A.S.T.M. proposed standard, 1966), hence introducing the possibility of errors due to non-uniform current distribution. Also, in a number of the larger single crystals, the presence of inclusions adversely affected the reliability of the measurements. These inclusions could often be eliminated, or significantly reduced in size, by the application of annealing procedures such as those detailed in section 3.4.

Due to these disadvantages associated with bridge-type specimens the second type of sample used was the lamellar or van der Pauw specimen (van der Pauw, 1958). In this technique small regularly shaped sections of crystal, normally in the form of squares of side 3.0 - 5.0 mm were used. A typical specimen is shown in

Plate 4.3. Crystals of such restricted size are quite suitable for measurement by this technique and this permitted the selection of good quality single crystal regions, devoid of inclusions. The contacts were attached to the upper faces of the crystals as near as possible to the corners of the square. (In the van der Pauw method any shape of specimen and contact positioning can be used, but for greater convenience in reducing the variations in potential differences measured between the various electrodes, regularly shaped specimens are commonly employed). Contacting techniques were identical to those used with the bridge specimens.

The actual measurement of resistivity and Hall coefficient is slightly more complicated in the van der Pauw method due to the necessity of measuring potential differences between certain pairs of electrodes with current passing through the sample between various other pairs of electrodes, whereas, for bridge specimens, all potential measurements are performed with the current passing between the electrodes positioned at opposite ends of the specimen. The additional complexity of the van der Pauw method is accomodated by a modified contact switching procedure, and in practice relatively simple relationships exist between the specific resistivity and Hall coefficient of the material, and the various potential differences and currents measured. These relationships have been derived by van der Pauw by the application of conformal transformations.

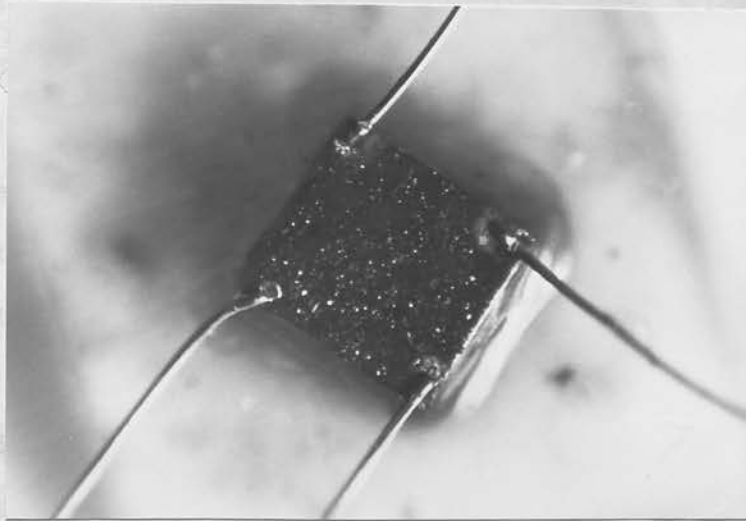

(a) Lamellar ZnTe Hall sample

(b) Hall-effect apparatus

Plate 4.3

Figures 4.3 and 4.4 show the electrical circuitry used in conjunction with bridge and van der Pauw specimens. The magnet system and power supply employed was capable of generating fields up to 12 kG and is shown in Plate 4.4. Current was supplied to the samples from a regulated d.c. power supply and the Hall e.m.f's and other potential differences were measured either using a potentiometer in conjunction with a galvanometer or electrometer, or an electrometer directly. The resistivities and Hall coefficients of the two types of sample were calculated by the "averaging" relationships given below. The voltages designated by the various subscripts are measured between the contacts indicated in the figures.

(1) <u>Bridge-Type or Parallel-piped Specimen</u>

(a) <u>Resistivity</u>

Two values of ρ are obtained at two positions.

$$\rho_A = 1/2 \left(\frac{V_2(+I)}{V_1(+I)} + \frac{V\ (-I)}{V_1(-I)}\right) \frac{R_{std} w_s t_s}{d_1'} \text{ ohm-cm} \qquad (4.5)$$

$$\rho_B = 1/2 \left(\frac{V_4(+I)}{V_1(+I)} + \frac{V_4(-I)}{V_1(-I)} \right. \frac{R_{std} w_s t_s}{d_2} \text{ ohm-cm} \qquad (4.6)$$

where the units of voltage are volts, R_{std} is in ohms, w_s is the specimen width, t_s the thickness parallel to the field direction, d_1 and d_2 are the separations of the side contacts. (All dimensions are in cm.) Voltages measured under reversed current are indicated by V(-I). The two resistivities normally agree within ± 10% for a homogeneous sample.

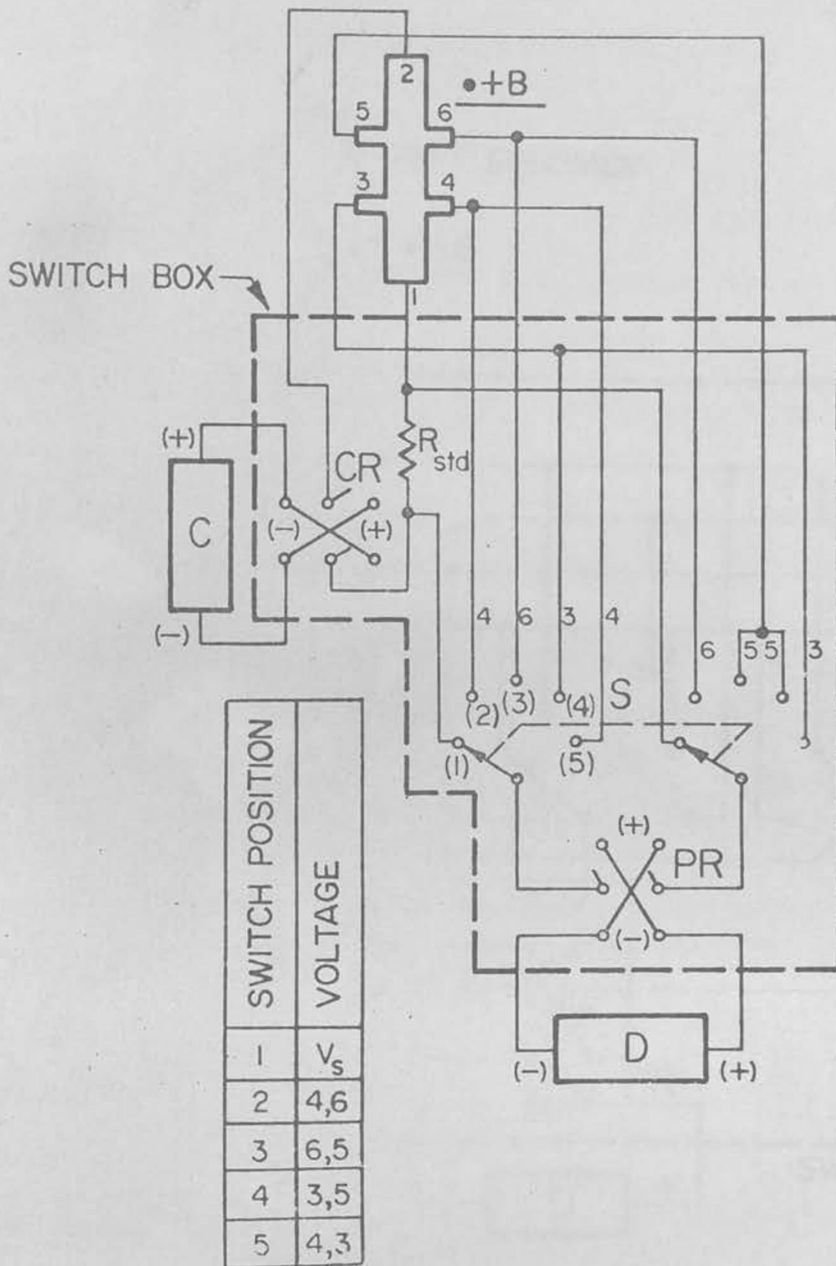

SWITCH POSITION	VOLTAGE
1	V_s
2	4,6
3	6,5
4	3,5
5	4,3

FIGURE 4.3 Test circuit for measurement of resistivity and Hall coefficient of a bridge-type specimen.

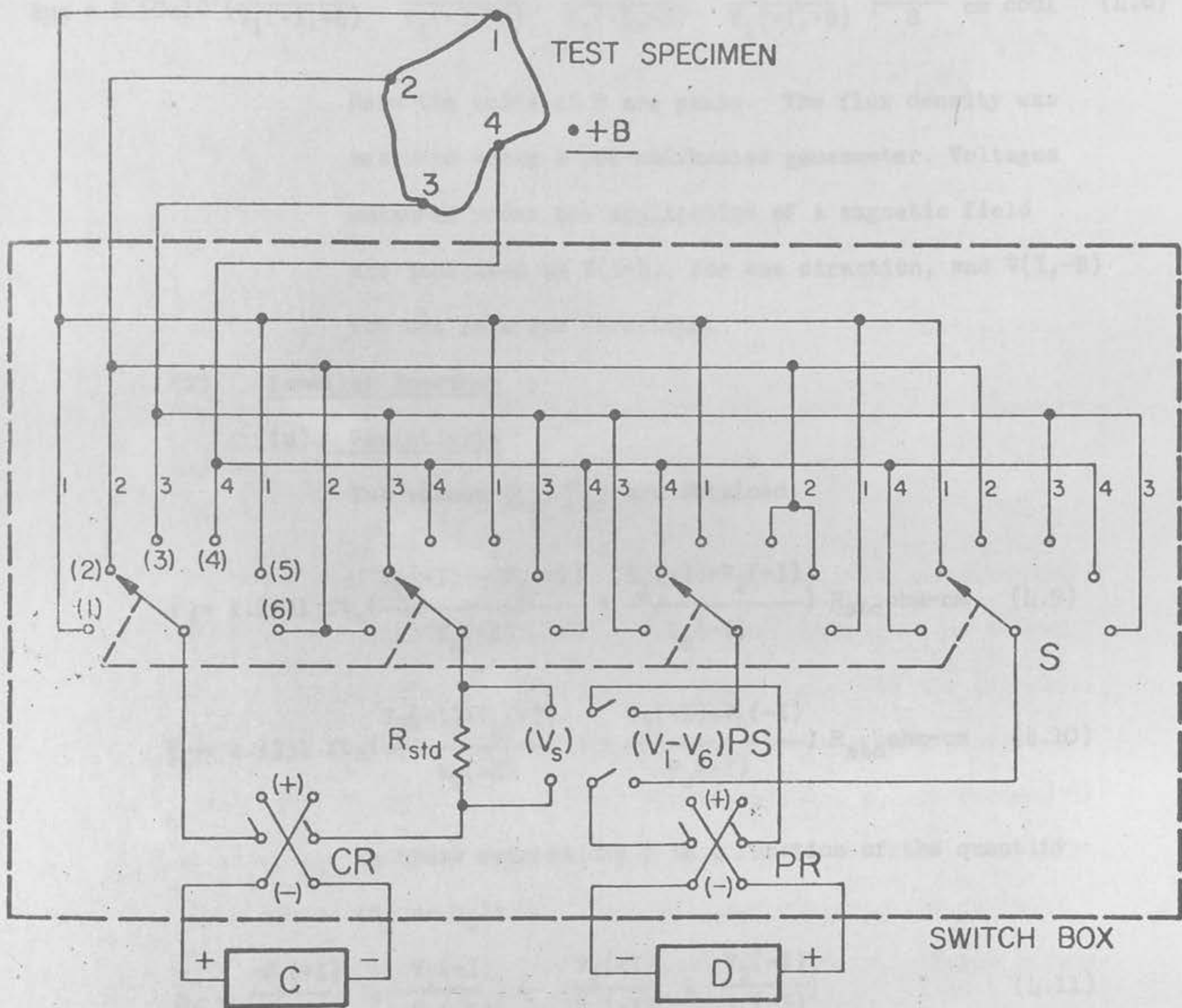

FIGURE 4.4 Test circuit for measurement of resistivity and Hall coefficient of a lamellar (Van der Pauw) specimen.

(b) Hall Coefficient

This is given by

$$R_{H3} = 2.50\times10^{7}\left(\frac{V_3(+I,+B)}{V_1(+I,+B)} - \frac{V_3(-I,+B)}{V_1(-I,+B)} + \frac{V_3(-I,-B)}{V_1(-I,-B)} - \frac{V_3(+I,-B)}{V_1(+I,-B)}\right)\frac{R_{std}}{B}\ \mathrm{cm}^3\,\mathrm{coul}^{-1} \quad (4.8)$$

Here the units of B are gauss. The flux density was measured using a pre-calibrated gaussmeter. Voltages measured under the application of a magnetic field are indicated as $V(I+B)$, for one direction, and $V(I,-B)$ for the reversed direction.

(2) Lamellar Specimen

(a) Resistivity

Two values (ρ_A, ρ_B) are obtained;

$$\rho_A = 1.1331\ f t_s\left(\frac{V_1(+I) + V_2(+I)}{V_s(+I)} + \frac{V_1(-I)+V_2(-I)}{V_s(-I)}\right) R_{std}\ \text{ohm-cm} \quad (4.9)$$

$$\rho_B = 1.1331\ f t_s\left(\frac{V_3(+I)+V_4(+I)}{V_s(+I)} + \frac{V_3(-I)+V_4(-I)}{V_s(-I)}\right) R_{std}\ \text{ohm-cm} \quad (4.10)$$

In these expressions f is a function of the quantity (Q_A or Q_B):

$$Q_A = \left(\frac{V_1(+I)}{V_s(+I)} + \frac{V_1(-I)}{V_s(-I)}\right) \div \left(\frac{V_2(+I)}{V_s(+I)} + \frac{V_2(-I)}{V_s(-I)}\right) \quad (4.11)$$

and Q_B substitutes V_3 and V_4 for V_1 and V_2.

The factor f is related to Q_A and Q_B by

$$Q_A,\ Q_B = f \operatorname{arc\,cosh} \frac{\exp(\ln 2/f)}{2} \quad (4.12)$$

The value of f is obtained from tabulated values of this function.

(b) Hall Coefficient

Two values (R_{HC}, R_{HD}) are obtained

$$R_{HC} = 2.50\text{x}10^7 \left(\frac{V_5(+I,+B)}{V_s(+I,+B)} - \frac{V_5(-I,+B)}{V_s(-I,+B)} + \frac{V_5(-I,B)}{V_s(-I,-B)} - \frac{V_5(+I,-B)}{V_s(+I,-B)} \right) R_{std} t_s \text{ cm}^3 \text{ coul}^{-1} \tag{4.13}$$

and R_{HD} substitutes V_6 for V_5. For an acceptably homogeneous specimen the two values of Hall coefficient should agree within ± 10%.

The Hall mobility, μ_H, is obtained from the commonly used expression for a single carrier system $\mu_H = |R_H| / \rho$ (4.14)

The results of room-temperature Hall and conductivity measurements on selected crystals, prepared by the growth techniques described in the previous section, are given in Table 4.2. In the calculations leading to the results given in this table a single carrier system was assumed. The carrier concentrations, p, are assumed to be given by $R_H e^{-1}$ for simplicity, where R_H is the Hall coefficient and e the electronic charge. The factor $r = \mu_H/\mu_d$, the ratio of Hall to drift mobilities, is thus taken to be unity. These assumptions are those commonly made in such electrical transport measurements. The orientation of the various samples was random. Measurements were made through a range of values within the limits of the potential drop and Hall voltage remaining linear functions of the current through the crystal.

Crystal Batch	R_H cm^3/coulomb	P cm^{-3}	ρ ohm-cm	μ cm^2/V-sec
1	4.0×10^6	2.5×10^{12}	2.5×10^4	100
13	3.4×10^2	2.0×10^{16}	8.0	42
26	1.0×10^3	6.2×10^{15}	20.0	55
27	1.2×10^2	5.0×10^{16}	14.0	10
32	8.2×10^2	1.3×10^{16}	3.9×10^5	2.1×10^{-3}

TABLE 4.2 Representative Values of Material Parameters at 300°K

In the absence of extended data on Hall coefficients over a wide temperature range, little information can be extracted from the above data on donor and acceptor concentrations, or ionisation energies of incorporated native defects and impurities; evaluations of possible scattering mechanisms are also prohibited.

The high resistivity and Hall coefficient obtained for run No.1 are high in terms of the values obtained for the other crystals; in the absence of more complete data, however, any evaluation of the origin of these results is speculative. This is particularly interesting as there was little apparent variation between the growth conditions of these crystals and several of the others investigated. The semi-insulating nature of these crystals could be associated with the presence of deep acceptor or compensated donor levels and possibly combinations of impurities resulting in more complex impurity level distributions; the native defect in

ZnTe is considered to be a shallow acceptor (0.048eV) associated with the Zn vacancy.. The incorporation of impurities which could give rise to such conditions is considered unlikely under the controlled preparation conditions used. It is conceivable that due to the technique of reacting the constituents, these combined in proportions other than those anticipated from the initial quantities, and that subsequent recombination of the additional constituents did not occur. Thus the deviation from stoichiometry of the melt could possibly have varied from that prescribed. Aven and Segall (1963) showed that growth conditions resulting in deviations from stoichiometry could produce significant variations in the resistivity and Hall coefficient of ZnTe crystals.

It should be stated that no further attempts were made either to repeat the conditions of growth run No.1, or to deliberately grow further quantities of insulating crystals. (ZnTe crystals having resistivities of 10^{10} ohm-cm were grown by Takahashi et al.(1966).) The measured p-type conductivity of the crystals excludes the possibility of the formation of n-type material which would be expected to exhibit high resistivity.

The variations in the electrical transport parameters between crystals from runs 26 and 27 could be attributed to alterations in the growth conditions which would result in a decrease in the partial pressure of Te in the latter case, with a concomitant variation in

carrier concentration. Unfortunately, the crystals from run 27 were subsequently purified by the vapour transport process and this would tend to increase the effective carrier concentration; the effect of these two variations cannot be separated. Material 13 was grown by a special technique and impurities of a different nature to those existing in the other crystals are considered to have been incorporated. In order to differentiate between the various effects described briefly above, and to fully categorise the electrical characteristics of the various forms of the material, Hall measurements would require to be made over a wide range of temperatures. Table 4.2 also includes the "effective" parameters for a sample of polycrystalline ZnTe.

Qualitative measurements of conductivity type were frequently performed using a thermoelectric hot probe technique. In this technique two probes, one of which was heated by a resistance element, were attached to a galvanometer. Embedding the probes in the surface of the crystal produces a thermoelectric or Seebeck e.m.f. as a result of the majority carriers acquiring sufficient thermal energy to surmount the metal:semiconductor junction at the hot probe and diffuse towards the colder regions of the crystal. The sign of this e.m.f. indicates the crystal conductivity type. Crystals from the majority of growth runs were tested in this way and

and all crystals exhibited p-type conductivity. It was hoped that this technique would have indicated the conductivity type of crystals regrown from Bi and In solutions as these crystals were too fragile and of inadequate area to be mounted as Hall samples. However, the fragility of the crystals also precluded the accomplishment of a thermoelectric measurement. Attempts to attach contacts to these crystals were, however, successful. The resistivity estimated in this manner was of the order of 10^6 ohm-cm; this is similar to the value obtained by Wagner and Lorentz (1966), who inferred that crystals regrown from a donor (In) solution were of n-type conductivity.

5. DEVICES

The objective of the experimental programme described in this report was the determination of the electroluminescent properties of devices fabricated from the various forms of ZnTe crystals and associated with metal:semiconductor junctions and barrier regions. The room-temperature emission properties of these devices were of primary interest, in order to evaluate the potential of ZnTe as an efficient room-temperature visible emitting material. With this objective in view, a total of some two hundred devices were fabricated. In a number of cases a relatively large number of devices were made from material obtained in particular growth run, and in other cases only a few devices, sufficient to allow comparison between the electroluminescent properties of these crystals and those obtained from other similar growth procedures, were constructed. Devices which were utilised in detailed investigations of the electroluminescent properties of ZnTe, and fabricated using relatively simple contacting procedures, are divided into four groups, corresponding to the number of distinct forms of the material considered to be produced by the growth procedures described in section 3. These are,

(1) Devices fabricated from semi-insulating ZnTe - i.e. from crystals obtained by growth procedure No.1.

(2) Devices fabricated from nominally undoped ZnTe - this covers devices prepared by several similar growth procedures.

(3) Devices prepared from ZnTe crystals incorporating oxygen - i.e. growth procedure No.13.

(4) Devices prepared from polycrystalline ZnTe - i.e. growth procedure No.32.

An additional sub-section describes the properties of devices fabricated from crystals which were obtained by various growth techniques and subsequently subjected to more complex processing procedures, such as the diffusion into the crystals of evaporated metal layers, with the intention of creating localised regions having specific resistivity values significantly different from that of the bulk material.

5.1 Device Fabrication

The majority of crystals obtained from the various growth procedures were not subjected to additional processing procedures before being used for device fabrication. This statement excludes such procedures as crystal purification, and the etching, polishing and shaping of crystals to device format.

Since it was anticipated that the electroluminescent properties of the devices would be critically dependent on the nature of the metal:semiconductor contact, special precautions were taken to standardise the crystal processing and contacting procedures. In essence the observed electroluminescence can be associated

with the blocking or rectifying properties of the metal semiconductor contact, and with the formation of semi-insulating or inversion layers at the metal:semiconductor interface.

In the normal routine used for device preparation inclusion free single crystal regions of random orientation were sawed or cleaved to give regularly shaped chips of area 1-6 mm^2. These chips were then ground, using several grades of Buehler alumina ranging from 5 to 0.03 micron particle size, to a final thickness of between 0.1 and 1.0 mm. In the initial experiments crystals received no further surface treatments beyond washing in de-ionised, distilled water and alcohol vapour degreasing. However, some of the more interesting results were obtained from crystals which were in addition etched in a solution of 4 parts HNO_3, 1 part HF, 3 parts Br and 3 parts distilled H_2O. (This etch is commonly known as CP-4).

Regardless of the particular form of crystal and the contacting technique used, standard preparation and processing conditions were used wherever possible in order to achieve uniformity for that particular type of contact. Many of the procedures used were typical of convential semiconductor process control techniques, however, due to the critical influence of the metal contacts, special precautions were taken in the surface preparation

of the semiconductor and the contacting metal. The surface preparation procedures, the duration and temperature of the contacting process, the quantity and purity of the material used for the metal contact were standardised, and all contactting procedures were conducted at a forced-draught clean bench. Care was taken to protect the materials from the ambient atmosphere in transport from one processing station to the next, and crystals and devices were stored in a clean, dry atmosphere.

The prepared crystals were usually mounted on conventional 6mm diameter transistor headers. These headers were either Au or Kovar plated. The bottom face of the crystal was contacted to the header itself and a gold wire 0.003" in diameter was attached from one of the header feedthroughs to a contact pad on the upper face of the crystal. The second feedthrough was connected to the header. A mounted device is shown in Plate 5.1. A variety of techniques were used to form the contacts to the upper and lower faces of the crystals. These are summarised in Table. 5.1, the techniques giving rise to electroluminescence being indicated. Of these contacting procedures, the highest electroluminescent efficiencies were obtained for specimens having a semiconductor: header contact of In/10% Ag alloy and pure In for the upper contact pad. The crystal was attached to the header by causing a standard length of In/10% Ag alloy wire to melt and flow across

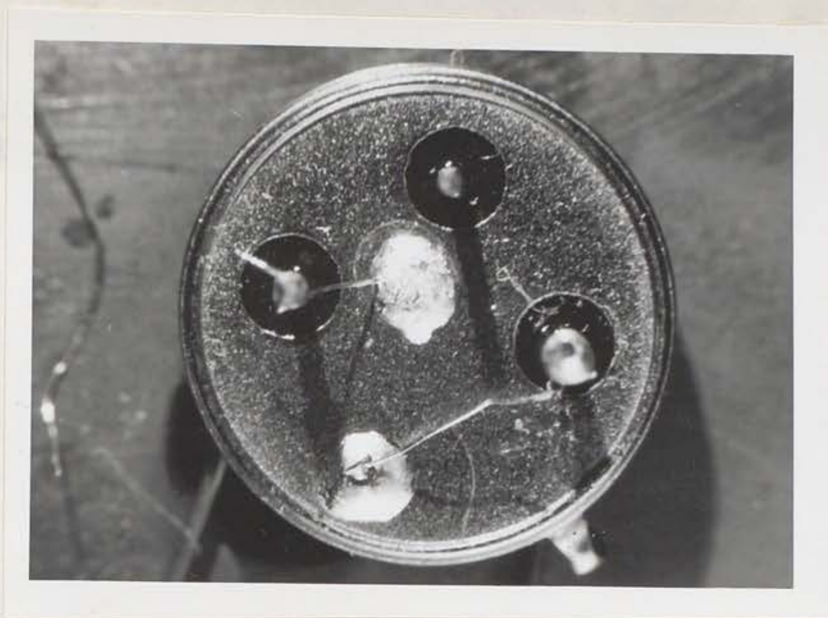

(a) ZnTe device mounted on TO-5 header.
(Diameter of header 8.5 mm).

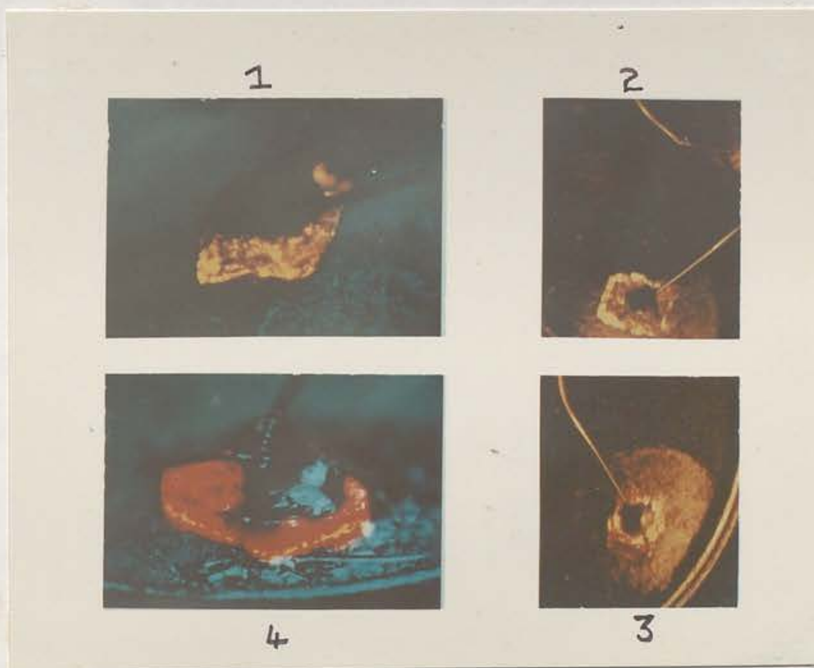

(b) Emission from ZnTe devices.

1. Semi-insulating ZnTe. Topcontact negative.
2. Nominally undoped ZnTe. Top contact positive.
3. Nominally undoped ZnTe. Top contact negative.
4. Oxygen doped ZnTe. Top contact positive.

Plate 5.1.

Contacting Technique No.	Top Contact	Bottom Contact	Emission Observed
1	In (soldered)	In/10% Ag soldered	Yes
2	In (vacuum melted)	In/10% Ag soldered	Yes
3	Point contact	Point contact	No
4	Point contact	In or In/10% Ag	Yes
5	Electroless Au + In (soldered)	Electroless Au + In/10% Ag (soldered)	No
6	In (soldered)	Electroless Au + In/10% Ag (soldered)	Yes
7	Electroless Ni + In (soldered)	Electroless Ni + In (soldered)	No
8	In (soldered)	Electroless Ni + In or In/10% Ag (soldered)	Yes
9	In (vacuum melted)	Electroless Au + In/10% Ag (soldered)	Yes
10	In (evaporated) + In (soldered)	Au (evaporated) + In (soldered)	Yes
11	Mn (evaporated & diffused) + pressure contact or In (soldered)	In (soldered)	Yes
12	Pressure contact or In (soldered)	Mn (evaporated & diffused + In (soldered)	No
13	Au (evaporated) + In solder	Al (evaporated + In solder)	Yes
14	Al (evaporated and diffused)+ In (soldered)	Au (evaporated and diffused) + In (soldered)	Yes
15	Au (evaporated and diffused) + In (soldered)	Al (evaporated and diffused) + In (soldered)	Yes

TABLE: 5.1

the surface of the header by application of a soldering iron; this pad was then cleaned of flux, remelted, and the crystal placed in the molten alloy. On solidification the crystal was firmly attached to the header. The upper In contact was made by placing a standard 20 mg piece of In wire on the upper surface of the crystal and causing this to wet and flow across the surface by direct application of a soldering iron. A section of this pad was next remelted to allow the attachment of the Au wire. It was not found necessary to carry out this contacting procedure in a reducing atmosphere.

Devices were also investigated in which the top contact pad was formed by heating the crystal under vacuum on a tantalum strip. In this technique a small piece of In was placed on the upper surface of the crystal. At a low temperature the In melted and formed a ball on the surface of the crystal. On increasing the temperature to 900°C the In flowed over the surface of the crystal. The molten In is considered to dissolve the ZnTe directly below the metal, and on cooling recrystallisation occurs with the possible incorporation of In atoms in the surface layer of the crystal. The crystal was normally held at the high temperature for five seconds. If the In was removed from the surface of the crystal, the dissolution of the ZnTe was confirmed by the presence (in the majority of cases) of a depression of up to 4×10^{-2} mm in depth in the surface of the crystal. There

is, of course, no definite evidence that the major proportion of the dissolved ZnTe recrystallised on the crystal surface, as this could have occurred throughout the molten In. Indeed, the presence of a depression could be taken as an indication that a quantity of the ZnTe did not recrystallise on the surface of the crystal. The possibility of limited penetration of In into the crystal by diffusion during the heating process cannot be excluded. Crystals with a contact pad attached to the upper face by this technique were attached to headers using, as before, In/10% Ag as the semiconductor-header contact.

In another fabrication technique attempts were made to form one ohmic contact to the crystals by the deposition of evaporated or electroless-plated Au or Ni layers. In/10% Ag solder was subsequently used to connect the plated face of the crystal to the header or to attach a Au wire. When used with either pure In, In/10% Ag, or vacuum-melted In as the opposite contact, frequently no electroluminescence was observed, and in those cases where electroluminescence was obtained it was generally weak in comparison with that observed in devices contacted by the other techniques described previously. In no case was electroluminescence observed if Au or Ni contacts were used on both faces of the crystal. Similar results were obtained if point contacts were used.

A small number of devices were fabricated in which an evaporated layer of Au, Al, In, or Mn was diffused into the crystal prior to contacting. In isolated cases weak electroluminescence having interesting emission characteristics was observed. All films were vapourised from molybenum evaporation sources at pressures of about 10^{-5} mm Hg. For contact technique No.10 the In and Au films were evaporated to a thickness of 2100Å and 1200Å respectively. No attempt was made to diffuse these layers into the crystal and contact was made to both faces of the crystal using In solder. For Nos.11 and 12 a 1200Å Mn film was evaporated onto one face of the crystal. In one procedure the Mn and Au films were diffused into the ZnTe by annealing in an argon atmosphere for 4 hours at 500°C. These specimens were mounted using both pressure and In soldered contacts. Devices incorporating evaporated Al films are of particular interest. It was the use of evaporated and diffused Al films in conjunction with Li doped ZnTe which gave rise to the highly efficient, low temperature electroluminescence reported by Crowder et al. (1966). For contacting techniques Nos. 13 to 15 the evaporated Al and Au films were of thickness 6000Å and 1700Å respectively. Several specimens were mounted without further treatment using In solder, whereas others were annealed at 625°C for 20 hours before mounting. Emission located in the green region of the spectrum was obtained for diffused Al specimens. This emission associated with transitions of greater than band gap energy is

difficult to explain and invokes considerations of the possible source of "hot" carriers.

Further details will be given of the various crystal processing, contacting, and mounting techniques for devices from the groups outlined at the introduction to this section, in the following section presenting the electro-optical characteristics of these devices.

5.2 Electro-Optical Characteristics

In the following sections the results of various measurements made on the several groups of devices presented above will be described. These measurements normally consisted of the evaluation of the current-voltage and emission intensity-current characteristics, the determination of the spectral distribution of the emission, and the estimation of the external quantum efficiency and power efficiency of the devices. In addition, for a number of devices, the dependence of the "junction" capacitance on applied voltage was measured. These measurements were frequently conducted at both room-temperature and 77°K. The performance of these measurements allows comparisons to be made between the electroluminescent properties of the various devices and permits some interpretation to be made of the excitation and recombination mechanisms. It will be found that broad similarities exist between a number of characteristics of the devices

and these can be linked to the type of metal semiconductor contacts used. Variations are considered to result from different forms of excitation mechanism associated with particular junctions and also the distinct radiative recombination properties of the various types of ZnTe crystals studied.

Before considering device properties in detail it is necessary to clarify the terminology used in the description of their electrical properties. The terms forward and reverse-biased junctions will frequently be encountered. In the present context, this is used in considering the polarity of a particular metal:semiconductor junction and has no relevance to the magnitude of the current flowing across the junction. This, however, in no way invalidates the usefulness of the terms. For the devices described here, both contacts to the semiconductor are blocking in nature and therefore, on voltage application, the junction at one face will be forward-biased and that at the opposite face reverse-biased. It is assumed that the semiconductor is p-type; hence, a forward-biased junction is associated with an applied voltage resulting in the metal contact being at a negative potential with respect to the semiconductor. This "device" terminology is mainly used either when the emission is associated with a particular contact or in discussion of excitation mechanisms. It should be stressed that the terminology is not intended to indicate the presence of a highly rectifying

junction. Frequently, in the discussion of the electrical properties of the composite device, the terms "high-current direction" or "low-current direction" will be used to describe the magnitude of the current through the device for a particular polarity and magnitude of applied voltage. In many cases the actual difference in the magnitude of these two currents may not be pronounced. On the basis of the above, it is quite feasible to discuss the emission properties associated with the particular metal:semiconductor junction which is, say, reverse-biased, although concomitantly this polarity is the high-current direction.

5.2.1 Semi-Insulating ZnTe

The characteristics of devices fabricated from the high-resistivity ZnTe crystals of growth run No.1 (Kennedy and Russ, 1967a) are first considered. The descriptions of the apparatus and measurement techniques contained in this subsection are applicable to all forms of ZnTe devices.

Contacting and mounting of these devices followed techniques Nos. 1, 2 and 6 of Table 5.1. Emission was observed for both directions of current flow, generally in the form of isolated spots located in the region of the contact to the header when a positive potential was applied to the top contact and in the region of the top contact with reversed polarity. The emission is therefore

associated with a forward-biased junction.

Emission Spectra

The room temperature emission was orange in colour and at liquid nitrogen temperatures shifted to shorter wavelengths, the energy associated with this shift corresponding closely with the reported variation of the band-gap with temperature (Cardona and Greenaway, 1963). In the initial experiments the DK-2A spectrophotometer was used to record the emission spectrum of the devices; however, due to the low sensitivity of the instrument in relation to the light output of the device, it was found necessary, for the majority of devices, to employ large slit widths associated with an average resolution of 600Å. This was sufficient to detect a broad peak at approximately 5800Å; however, no structural details could be resolved. Subsequently, a Jarrell-Ash 250 mm Ebert diffraction grating monochromator was used in conjunction with an RCA 7265 photomultiplier having an S-20 cathode response. This system was sensitive to considerably lower light levels than the DK-2A. Unfortunately, the diffraction grating supplied with the instrument (6000Å blaze) was found to possess an extremely oscillatory response in the wavelength range 7500-6000Å. This type of grating response, often referred to as "Woods anomalies", is associated

with defects in the ruling of the master grating. All spectra were therefore corrected for the response of the grating, the correction factors being determined by measuring the spectrum of a tungsten lamp in the wavelength range of interest utilising the DK-2A prism spectrophotometer, and comparing this spectrum with the output of the monochromator when using the same source; the same detector was used in both measurements. The majority of spectra presented in this report are therefore corrected not only for the response of the photomultiplier but also for that of the diffraction grating. Due to the sharp peaks in the response of the grating it was considered that, in comparisons between a measured spectrum and the known distribution of the grating, inaccuracies in estimating the wavelength of the measured spectrum could result in errors in correction factor selection. (The error in wavelength positioning during the recording of a spectrum was estimated to be ± 10Å). The measurement technique employed was normally to drive the monochromator grating at an effective scanning speed of 250Å/minute. Wavelengths were marked on a chart recorder by applying a potential to an auxiliary pen circuit causing one pen to make a slight excursion from the 100% position. The switch activating this circuit was depressed when the required wavelength was aligned with

the index line of the wavelength drive system. The main error in wavelength indexing was introduced by the pen-response time. Recently a replacement grating was obtained having a uniform response in the region of interest, thus reducing the magnitude of possible errors resulting from the application of an incorrect correction factor. The sensitivity of the photomultiplier system allowed the use of finer slits with concomitantly higher resolution. The 6000Å blazed diffraction grating of 1100 lines/inch had a dispersion of 30Å/mm. The range of slit widths routinely used were from 0.1 to 2.3 mm, equivalent to resolution values of 5 to 70Å.

The spectrum of a typical device measured at room temperature for the 'easy' direction of current flow and corrected for the response of the photomultiplier is shown in Fig. 5.1. It will be noted that the spectrum is extremely broad having a sharp cut-off at a wavelength around 5600Å corresponding to the absorption edge of ZnTe. A secondary maximum was noted at 6500Å in the red region of the spectrum. Watanabe et al. (1965-1966) have observed a broad spectrum located at 6500Å in nominally undoped ZnTe. This is the only reference in the literature to a ZnTe emission spectrum similar to that described here. Watanabe et al. associate the red emission spectrum with the presence

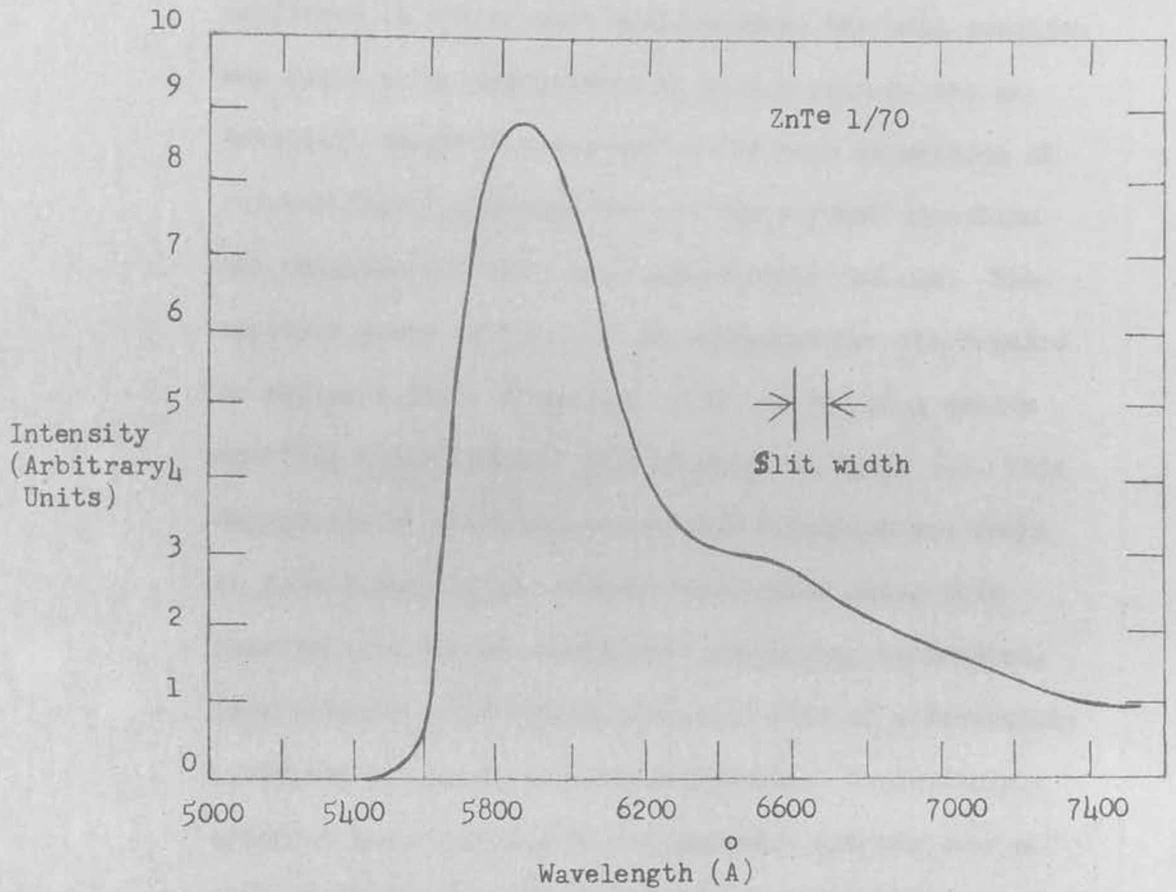

FIGURE 5.1 Room temperature emission spectrum of a semi-insulating ZnTe device (In-ZnTe-In/10% Ag).

of In donors. The experimental results obtained by these authors relating to the dependence of the peak position on the current flowing through the device, and the distinct variations between the spectra obtained for the two directions of current flow, were not confirmed in the present measurements; the peak position was found to be independent of device current and an identical spectrum was obtained for both directions of current flow - although for the low current direction the emission intensity was considerably reduced. The spectrum shown in Fig. 5.1 was obtained for the forward or higher current direction; a photograph of a device emitting under forward bias is shown in Plate 5.1. This dependence of intensity on current direction was found to hold generally for devices fabricated using this material and the aforementioned contacting techniques. This emission spectrum is characteristic of a reversible avalanche or impact ionisation process. Accordingly, emission generated within the material extends over a wide range of wavelengths from the infrared across the visible spectrum. The upper limit is not clearly defined due to the falling-off in the photomultiplier-response at long wavelengths; corrections are inaccurate beyond 8000Å. The actual extension of the spectrum into the infrared is therefore unknown. Similarly the

extension of the spectrum to wavelengths below 5600Å is masked by self-absorption. If emission is associated with an impact ionisation: carrier acceleration or reversible avalanche process, then there exists a finite probability that photons of energy greater than the band-gap value will be created. From the measured emission and known absorption spectrum of the material it is considered that the internal emission is maintained at wavelengths below the absorption edge.

It is reasonable to associate the various peaks contributing to the broad emission spectrum with recombinations at native defects and impurity centres. Under impact ionisation conditions, collisions involving minority carriers and the crystal lattice would result in the creation of electron-hole pairs; recombination involving free carriers would, therefore, be expected to result in an emission peak associated with the band gap energy of the material i.e. for the crystals used in these experiments 2.21 eV (5625Å). As discussed previously (section 2.2.3.1.2) recombinations involving carriers having a wide range of energies would be expected in such a process; however, it is anticipated that major peaks in the emission spectrum might result in recombinations involving specific recombination centres

(Kennedy and Russ, 1967b). For the case of ZnTe, the direct recombination of electron-hole pairs would result in emission located in the region of 5600Å. The first charge state of the Zn vacancy is located 0.048eV above the valence band edge; recombinations involving this centre would be located at 5750Å, a result which is in agreement with the observed emission spectrum. Considering the occurrence of possible secondary peaks in the emission spectrum, it is of interest that various authors have postulated the existence of localised gap states in the energy range 0.13 - 0.2 eV. These were considered to be associated with various defect or impurity states introduced during the device fabrication process. Hinotani and Sugigami (1965) postulated the existence of In donor levels introduced during the contacting process and located 0.2eV below the conduction band. This impurity could give rise to recombinations in the red region of the spectrum at 6200Å. Watanabe (1966) found a broad red emission peak in ZnTe which at 77°K was located at 6150Å for forward-biased devices and 6400Å for reverse-biased devices. (In Watanabe's terminology the terms forward-biased and reverse-biased are synonomous with "higher-current direction" and "lower-current direction" respectively). It was considered by these authors that the

shift in the emission spectrum to shorter wavelengths on the application of reverse bias was in agreement with the concept that, for this current direction, the impact ionised carriers would acquire higher energies. Taking into consideration the published data on the temperature dependence of the band gap in ZnTe (-6.0×10^{-4} eV/^{o}K) the position of these emission bands at room temperature is estimated at 6400Å and 6650Å.

Based on the results of experiments on devices fabricated from growth run No.13 crystals (section 5.2.3) the possibility of the incorporation of concentrations of oxygen centres in the ZnTe lattice cannot be precluded. Assuming that this centre is incorporated as an uncharged impurity centre substituting isoelectronically for Te and behaving as a deep isoelectronic acceptor located 0.4eV above the valence band, then an emission peak would be anticipated at 6850Å. From Fig.5.1 it will be seen that the secondary emission peak in the spectrum of the semi-insulating ZnTe is located at 6500Å. Due to the lack of experimental evidence on the possible impurities incorporated in these crystals and also to the possible inaccuracy in the determination of the room temperature absorption edge, (the edge is assumed to be located at the same wavelength position as that obtained for crystals

from other growth runs on which absorption measurements were performed) no definite statements can be made to link the observed emission spectrum with particular impurity centres. However, a qualitative comparison can be made between the peak observed in the red region of the spectrum and that considered by previous authors to be associated with In donors. The presence of this impurity has been considered to result in the creation of a more insulating p-type surface layer. Radiative recombinations involving In centres would therefore result in emission restricted to the semi-insulating region itself. The observation, for the present case, of emission extending into the bulk of the crystal at depths greater than could realistically be associated with the existence region of a semi-insulating layer, does not support this postulate.

Emission Intensities

Emission intensities were normally measured using a Photo Research Spot Meter. This instrument consists of a lens system, filters, photomultiplier, direct-current amplifier and output meter. The spectral sensitivity of the photomultiplier is modified by the filters to produce a response closely duplicating that of the human eye, and the output of the photomultiplier is indicated dir-

ectly in units of foot-Lamberts. A range switch allows the measurement of brightness levels from 0.001 ft.L to 1,000 ft.L. The instrument was pre-calibrated before use by means of a standard brightness source. For comparison purposes the spectral sensitivity of the eye is reproduced in Fig.5.2, together with that of a photomultiplier having an S-20 cathode response. In measurements of brightness levels, the source was focussed on the detector by means of a micro-lens. Using this instrument the emission intensities of typical devices for the higher-current direction were found to be 5 ft-Lamberts at current densities of 0.2 A/cm^2.

Emission Efficiencies

At this stage in the investigations the emission efficiencies of the devices were evaluated on the basis of the measured brightness levels and current densities. This approach involves an assumption of limited validity. In order to determine the total photon output of the device, a knowledge is required of the spatial origin of the emission. As ZnTe has a high refractive index, a large portion of the light produced within the bulk of the crystal suffers total internal reflection and the emission frequently appears to originate from the corners, edges and regions of surface inhomogeneity. Estimates

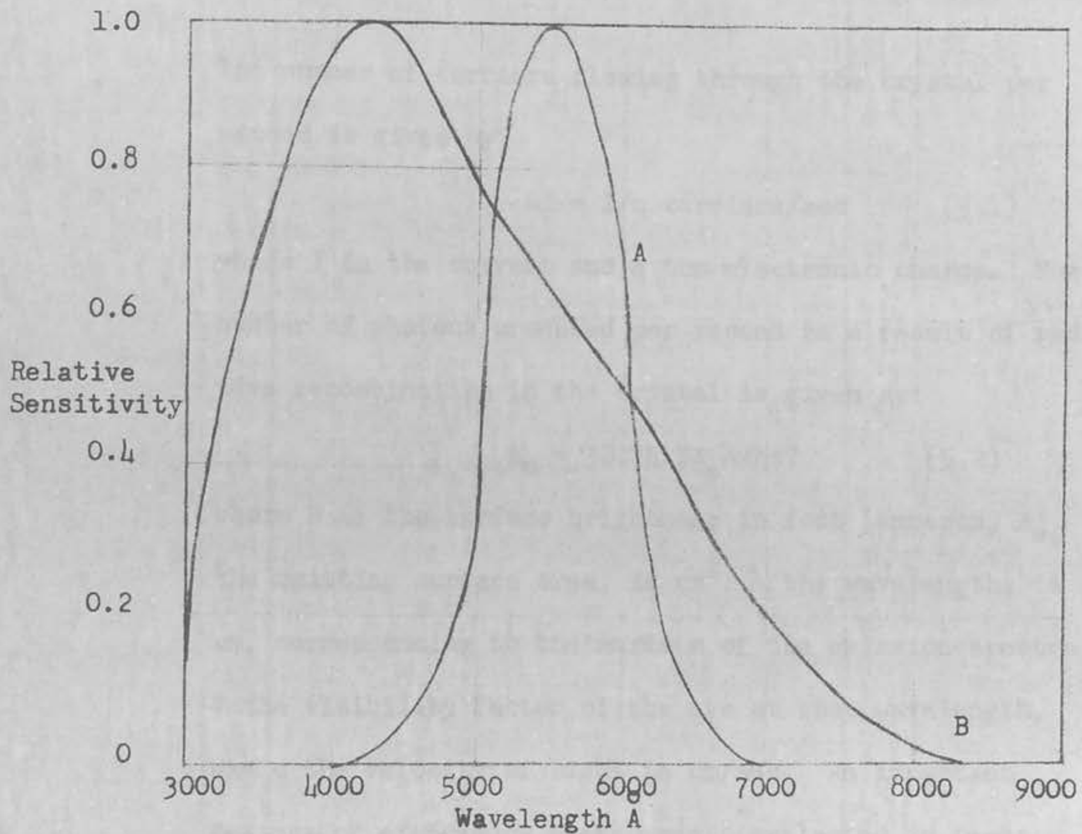

FIGURE 5.2 A. Spectral Sensitivity of the Eye.

B. Spectral Sensitivity of an S-20 photomultiplier Cathode.

of a total emitting area are therefore subject to error. Assuming, however, that the actual emission area is known, then the emission efficiency, that is, the ratio of photons detected externally to electrons passing through the crystal (section 2.2.3.2) can be evaluated as follows:-

The number of carriers flowing through the crystal per second is given by

$$n_c = I/q \text{ carriers/sec} \qquad (5.1)$$

where I is the current and q the electronic charge. The number of photons produced per second as a result of radiative recombination in the crystal is given by:

$$n_n = 30.74\, BA_e\lambda/hcV \qquad (5.2)$$

where B is the surface brightness in foot Lamberts, A_e the emitting surface area, in cm^2, λ the wavelength, in cm, corresponding to the maximum of the emission spectra, V the visibility factor of the eye at that wavelength, and c the velocity of light in cm/sec. An important feature of efficiency measurements evaluated in terms of surface brightness is the incorporation of a visibility factor. This factor is introduced to compensate for the fact that surface brightness is evaluated on the basis of the spectral sensitivity of the human eye. That is, if two sources operating under identical conditions are measured to have equal values of surface brightness, then

the quantum efficiency of the two sources will be equal only if the emission spectra are concentrated in the same region of the spectrum. For example, the quantum efficiency of a source emitting in the red region of the spectrum may be more than one hundred times greater than that of a green emitter having an identical value of surface brightness. For the devices considered here, the room temperature external quantum efficiences were estimated from the above relationships to be in the range 10^{-5} - 10^{-7} photons/electron.

Another estimate of the quantum efficiency, which is probably of limited validity for the complex structures considered here, can be made by comparing the transit time of the impact generated carriers, given by $t = d^2/\mu V$, (d is the width of the insulating layer, μ the hole mobility and V the applied voltage) to the recombination lifetime, τ ; an estimate of this latter parameter was obtained by measuring the time for the emission to reach maximum amplitude following the application of a voltage pulse, i.e. the switching time of the device. This was found to be of the order of 50μsecs. For the above equation t was determined to be 10^{-11} sec giving the efficiency t/τ as 2×10^{-7}. By application of the Einstein relationship the diffusion constant, D, was

evaluated as 2.5 cm^2/sec. Substituting this expression for D in the familiar equation $L = (D\tau)^{1/2}$ we obtain for L a remarkably high value of 10^{-2} cm.

As discussed in section 2.2.3.2, the internal quantum efficiency may be considerably greater than that detected externally due to the deleterious effects of total internal reflection and self-absorption. The external quantum efficiency could no doubt be improved by coating the surfaces of the device with a film of transparent material of refractive index and thickness selected to enhance the transmission of the emission. A similar technique would involve embedding the device in transparent material of spherical cross-section and having a refractive index intermediately between that of ZnTe and air.

The power efficiency, defined as the ratio of the optical power output to electrical power input, was a factor of $10^1 - 10^2$ less than the external quantum efficiency. This is a consequence of the magnitude of the voltage applied to the devices in order to obtain observable emission. In contrast, for devices operating by a pure injection mechanism, the applied voltages are commonly of the order of 1-2V, resulting in power efficiencies

little reduced from the external quantum efficiency. In succeeding descriptions of measurements performed on other types of ZnTe device, more accurate and simple methods of evaluating emission efficiencies will be described.

Current-Voltage Characteristics

Typical room temperature I-V characteristics are shown in Fig.5.3. Three separate regions can be distinguished, the first and second corresponding to ohmic and square-law behaviour respectively. In the third region the current rises as a higher power of the applied voltage. These devices exhibit slight rectification caused by variations in the blocking characteristics of the two contacts. In the majority of devices the onset of emission coincided with the deviation from the square-law region. Although the field across the whole specimen is low, the localized field created by the spreading resistance of the contact, or by semi-insulating regions, could be greater than 10^4V/cm. It was noted that in the square law and higher power regions illumination of the device resulted in an increase in current level of approximately 1%. This could be associated with release of carriers from traps. If this is the case then the observation of an increase in current level in the super square-

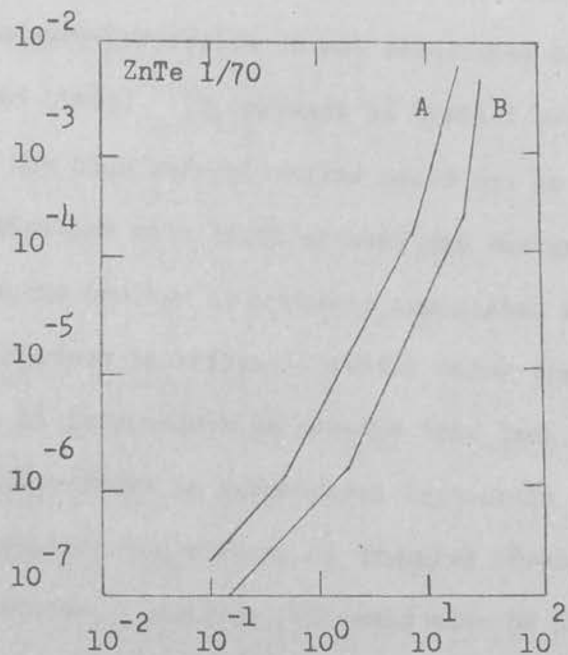

FIGURE 5.3 Room temperature current-voltage characteristic.

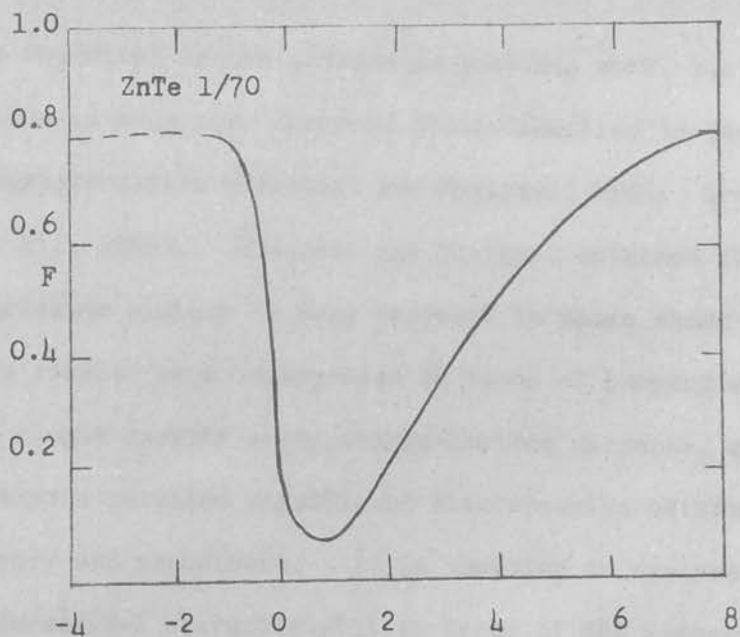

FIGURE 5.4 Capacitance versus voltage, Frequency 1 Kc/s.

law region is an indication that the transition from the square-law region is not associated with a traps-filled limit. In contrast to typical avalanche processes, the high current regime could not be initiated by illumination with light of band gap energy. As the avalanche process is probably associated with localised microplasmas in regions directly below the metal contact, it is possible to ascribe this lack of illumination dependence to geometrical factors in addition to the complicating effects of trapping levels and interface states. However, it could also be considered that the excitation mechanism may therefore involve a tunneling (Zener) process rather than true avalanche breakdown.

As described in the section on previous work, two previous authors have observed discontinuities in the V-I characteristics (Hinotani and Sugigami, 1965; Crowder et al., 1966). Hinotani and Sugigami obtained characteristics similar in many respects to those shown here. The results were interpreted in terms of Lampert's theory of single-carrier space-charge-limited currents, but analysis revealed significant discrepancies between theory and experiment. It is tempting to analyse the observed V-I characteristic in terms of the Lampert and

Rose theories of single-carrier S.C.L.C. Caution must be exercised in the application of these theories since they are derived for bulk effects, whereas for ZnTe devices impedance effects associated with barrier fields at the contacts can completely overide S.C.L.C. effects. For lower levels of barrier impedance, all voltage levels used in analysis must be reduced by an effective value required to overcome the contact potential-barrier and achieve injection of carriers into the space-charge region. Since the barrier resistance is non-linear, the total external voltage is shared between the barrier and other resistances (e.g. spreading resistance and the ohmic drop across the bulk material) in a manner which is itself voltage dependent. In practical devices the effects of interface states may also influence the injection process. This renders all relationships involving the total external voltage very complicated, particularly when one is dealing with more than a single contact as is the case for the devices studied here. Deviations from the basic theory would be expected for transitions to high current levels associated with either field ionisation of traps or the initiation of double injection, (space-charge compensation), rather than the achievement of a trap-filled limit predicted by single

carrier S.C.L.C. theory. Despite these reservations, it is still possible, by sophisticated experimental techniques, to evaluate the activation energies of traps; for example by the analysis of optically and/or thermally stimulated currents (Russ, 1962). Complex theoretical models describing double injection in insulators and semi-insulators have been derived by Lampert (1962) and Rose (1964). Consideration will be given later in this section to the validity of the Lampert theory, as applied to the present experiments.

Capacitance-Voltage Characteristics

Crowder et al. deliberately created a semi-insulating region in the device fabrication process by diffusion of an Al film into Li-doped ZnTe crystals to a depth of 10-20 . Hinotani and Sugigami considered that an insulating or semi-insulating layer, of thickness 1μ as determined by capacitance-voltage measurements, was formed at the surface of the crystal during the contacting process. Figure 5.4 shows the results of capacitance measurements on device No.1/70. These results were obtained using an impedance bridge with a.c. signals of 20mV peak-peak at a frequency of 1 Kc/s. Such capacitance characteristics are frequently used in semiconductor measurements to evaluate depletion layer widths, junction

voltages, and carrier concentrations. The graph shown here shows a minima in the forward bias region.

The explanation of such deviations requires recourse to considerations of surface charge states, possible insulating layers and the influence of injected minority carriers. The magnitude of these contributions are linked to the parameters used in the electrical measurement. The theoretical and experimental aspect of devices similar in characteristics to those described here have been discussed by Grove et al. (1965). The surface states charge may be due to a number of factors such as states introduced into the forbidden gap by irregularities associated with the metal-semiconductor, or insulator-semiconductor interfaces and impurity ions near the interface or within the insulating layer. It is assumed that surface states, however introduced, can be considered as due to charges located at the semiconductor interface. The analysis of Grove et al. does not permit consideration of fast surface states and assumes that all surface states are in poor electrical contact with the semiconductor, i.e. infinitely slow. Assuming the charge in these states to be constant and therefore the differential capacitance associated therwith is zero, then the capacitance of a m-i-s structure will be given by the series combination

of the capacitances of the insulating layer and space-charge region in the semiconductor:

$$C = \frac{1}{1/C_i + 1/C_s} \qquad (5.3)$$

where C_i and C_s are the insulating layer and space charge capacitances respectively.

The considerations of space charge capacitance are complicated by a frequency dependence which is due to a finite rate of carrier generation and recombination. In the case of low frequencies which are relevant to the experiments described here the minority as well as majority carriers will be able to follow the variation of the measurement signal. In this case the space charge capacitance is given by equilibrium theory as

$$C_s = K_s \varepsilon_o \frac{e(p_s - n_s + N_D - N_A)}{Q_s} \qquad (5.4)$$

where p_s and n_s denote carrier concentrations at the surface, K_s is the dielectric constant, ε_o the permitivity of free space and Q_s the net total charge within the semiconductor. For a given impurity concentration and known surface potential, Q_s can be obtained, thus allowing the estimation of C. The application of such equations can result in capacitance/voltage graphs of the shape shown in Fig. 5.4. At high negative bias voltages, i.e. in an accumulation region, the space charge capacitance is large due to the increased number of maj-

ority carriers near the surface, and the capacitance of the m-i-s structure approaches that of the insulating layer alone. With depletion of carriers from the surface C_s, and therefore C, drops. When the conduction and valence bands of the semiconductor insulator are sufficiently bent that inversion sets in minority carriers accumulate near the interface. At low frequencies these will follow variations in the measurement signal and contribute to the capacitance. Accordingly with increased inversion the capacitance rises and should again tend to the insulating layer value.

From a calculation based on the values of the capacitance in the high reverse-bias region, it is estimated that an insulating layer of thickness 10^{-4}cm could be considered to exist between the metal and semiconductor interfaces.

Mechanisms

Referring to the mechanisms of excitation and recombination in these devices, the observation of emission in the region of the top contact and through the bulk of the material with the polarity of the applied voltage such as to forward bias this metal:semiconductor junction is in agreement with an avalanche emission process in which minority carriers impact ionised in a localised high-field region are injected into the bulk of the

material. The emission energies corresponding to the rediative recombination processes extend from low energy collisions to lattice ionisation. The peaks observed in the emission spectrum can be associated with the predominance of recombinations involving defect and impurity centres. This excitation mechanism has been termed "avalanche injection" and is in essence identical to the more familiar occurrence of impact ionisation at a reverse-biased junction. The recombination kinetics of reverse bias impact ionisation are, however, less favourable, since impact-ionised minority carriers are constrained to the region of the metal: semiconductor junction. Although it was not found possible to stimulate the avalanche process by irradiating the devices with light of near band-gap energy, this is not considered a serious objection to the mechanism, due to the localisation of the avalanche regions and to the poor room-temperature photoconductive properties of the material. The observation that, for the opposite polarity, emission was observed to be localised in the region of the other metal:semiconductor junction, can be explained by the same mechanism, the reduction in emission intensity being associated with variations between the contacts and barrier layers for the two current directions.

Excitation and recombination processes involving minority

carrier injection have frequently been proposed to explain the emission characteristics of forward-biased junctions. This model is not considered to apply to the devices investigated here as several aspects of their electro-optical characteristics are not compatible with the predictions of such a model. Lack of correspondence between the observed results and those expected for minority carrier injection is found in the broad emission spectrum, the shape of the V-I characteristics, the high voltage, $eV>E_G$, required for the onset of emission, and the spread of the emission into the bulk of the crystal. Tunnel injection of minority carriers through the insulating region can also be considered as a possible mechanism. In this case it would be anticipated that a threshold voltage of $V = E_G/e$ would be required for the onset of emission. It would be expected, however, that in conjuction with the concomitant injection of majority carriers from the bulk of the semiconductor, a much narrower emission spectrum of more restricted spatial origin would be observed; the width of the insulating region is also several orders of magnitude greater than that normally associated with tunneling processes. Double injection in the insulating region is therefore rejected.

Considerations of Single-Carrier Space-Charge-Limited Currents

Due to the semi-insulating nature of the bulk crystal and the nature of the V-I characteristics the possibility of Lampert-type single carrier injection from the avalanching region into the bulk of the semiconductor cannot be neglected. As discussed above there are severe restrictions placed on the practical application of this analysis. Further resitrictions which apply will be indicated below. Several regions of the I-V characteristic are considered.

1. At low voltages where the injection of carriers into the semi-insulating layer is negligible, Ohm's law is obeyed and the slope of the I-V characteristic defines the resistivity of the layer as

$$\rho = pq\mu_p \tag{5.5}$$

   where p is the density of holes in the valence band at thermal equilibrium, and μ_p the hole mobility.

2. At some applied voltage, V_{TR}, the current begins to increase more rapidly than linearly with applied voltage.

$$V_{TR} = 4 \times 10^{12} q\, p_t d^2/\varepsilon \tag{5.6}$$

   where d is the thickness of the insulating layer, ε the dielectric constant and p_t is the density of trapped holes.

3. As the voltage is increased beyond V_{TR} additional holes are injected into the layer. If the Fermi level, which alters as injection occurs, is further from the top of the valence band than E_t, the trap depth of traps with density N_t, and moves in a region of the forbidden gap where the trap density is much less than N_t, then the ratio of free carriers, p, to trapped carriers, p_t, is constant and independent of applied voltage. In such a range the current density is given by

$$j = 10^{12} \mu_p \varepsilon \theta V^2/d^3 \quad (5.7)$$

where V is the applied voltage, and θ the ratio of the densities of free to trapped holes. Here θ is given by

$$\theta = p/p_t = N\nu/N_t \exp(-E_t/KT) \quad (5.8)$$

where $N\nu$ is the effective density of states in the valence band.

4. When the applied voltage further increases the square-law region of equation (5.7) will terminate in a steeply rising current which increases to meet the trap-free space-charge-limited currents given by

$$j = 10^{-13} \mu_p \varepsilon V^2/d^3 \quad (5.9)$$

The density of traps N_t can be determined from the voltage V_{TFL} at which the traps are filled and the currents rise sharply.

$$V_{TFL} = 4\pi \times 10^{12}\ q\ N_t\ d^2/\varepsilon \qquad (5.10)$$

The trap depth E_t is determined by inserting the value of N_t thus obtained, in eq. (5.8).

The determination of N_t and E_t by this method assumes that the discontinuity at the commencement of the rapid rise in current toward the trap-free curve always occurs when the traps are filled. Although this may sometimes be true, it is also possible for such a rapid rise to result from field ionisation of traps, or the onset of double-injection. Even if the latter effects occur, the trap depths and densities can be evaluated from eq.(5.8) provided the square-law portion of the curve is measured as a function of temperature so that a plot of ln vs 1/T is possible. E_t is then obtained from the slope of this curve and N_t from the intercept at 1/T = 0, without reference to the interpretation of V_{TFL}. The rapid rise in current can, of course, result from other effects such as an increase in the level of majority carrier extraction or the onset of avalanche multiplication processes. In practice a further inaccuracy in this analysis additional to those discussed earlier is the necessity of evaluating current densities, thus introducing possible errors due to the difficulty in determining the effective contact area. In all calculations involving

current densities the effective area is assumed equal to the area of the contact to the crystal. Also, errors can be introduced by inaccuracy in estimating the width of the insulating layer.

Applying this analysis to the characteristic of Fig. 5.3 gives, from eq. (5.10), $N_t = 5 \times 10^{15} cm^{-3}$; the thickness of the insulating layer was taken as 1 micron and the dielectric constant as 10.0 (Roberts and Marple, 1967). Using data from the square-law region of the characteristic in eq. (5.7) gave $\theta = 5 \times 10^{-5}$. The mobility value was taken from Table 4.2. Substitution of the values of N_t and θ in eq. (5.8) yielded the trap depth E_t as 0.44eV. It is of interest that, perhaps fortuitously, the trap depth thus calculated is approximately equal to the level associated with oxygen impurity centres (0.4 eV). If this analysis is applied to the case where the full width of the semi-insulating device is considered to act as an insulating region, i.e. $d = 5 \times 10^{-2} cm$, then the values of N_t and E_t obtained are 2.5×10^{10} and 0.74 eV respectively; this value of N_t is considered to be impractically low for a trap of depth 0.74 eV. In the absence of data on current-voltage characteristics for this material at other temperatures, eq. (5.8) cannot be used to directly test the validity of the interpretation placed on V_{TFL}.

From the I-V characteristic it is apparent that, at high current levels, consideration must be given to the effects of conductivity modulation in the bulk of the material. The reduction in overall resistivity may result from field-ionisation or optical stimulation of trapping levels or possibly from double-injection of carriers from the contact regions into the bulk of the crystal.

Figure 5.5 shows a schematic illustration of an approximate band model for the form of device considered in this section.

5.2.2 Nominally Undoped ZnTe

The results obtained from devices fabricated from crystals obtained from several growth runs having the common feature that no intentionally added dopants were incorporated during the growth procedure are next considered. Little variation was noted between the electrical transport or optical properties of crystals from the various batches.

Firstly, examples of the fabrication techniques used with crystals from the various growth runs, and the general characteristics of the electroluminescence will be described. Subsequently, the more detailed character-

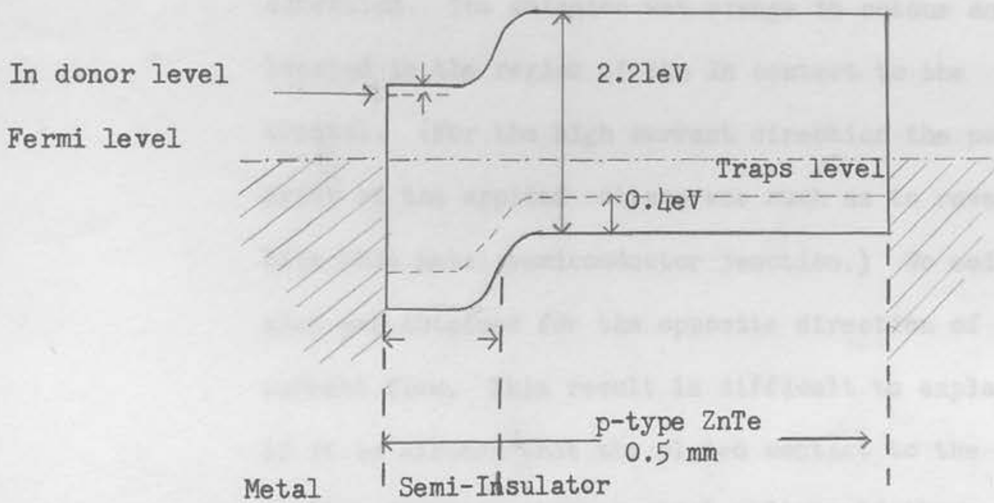

FIGURE 5.5 Approximate band model for Metal (In) - Semi-insulator (In + ZnTe) - Semiconductor (p-type ZnTe) structure.

istics of a number of devices will be presented.

General Emission Properties of Devices from Several Growth Runs

(a) Devices were fabricated from material of vapour growth run No.4 using contacting technique No.8. (Top contact In, bottom contact electroless Ni.) The physical dimensions of the devices were of the same order as those described previously. Electroluminescence was observed in devices contacted by the above technique for the high-current direction. The emission was orange in colour and located in the region of the In contact to the crystal. (For the high current direction the polarity of the applied voltage was such as to reverse bias this metal:semiconductor junction.) No emission was obtained for the opposite direction of current flow. This result is difficult to explain if it is assumed that the plated contact to the crystal forms an ohmic contact. It would therefore appear that here also two blocking contacts are created; in this case, however, the two junctions are dissimilar in nature.

(b) Crystals from vapour-growth run Nº.12 were cleaved into regularly shaped chips and mounted using contacting technique No.1. (Top contact In, bottom

contact In/10% Ag). Although no definite rectification properties were present in the electrical characteristics, the emission intensity for a positive potential applied to the top contact was much greater than that obtained for the opposite polarity. The electroluminescence usually appeared to be located around the upper face of the top contact at regions remote from the contact pad. It is therefore tentatively assumed that the emission is associated with the forward biased semiconductor: header junction, and is generated either in the region of that junction or in the bulk of the crystal. Due to the occurrence of total internal reflections the radiation appeared to be concentrated at the edges of crystal faces.

(c) Devices were fabricated from material of vapour-growth run No.18 using similar methods as in (b) above. In addition, however, devices were etched in a CP-4 solution prior to mounting. These devices were slightly rectifying, emission being obtained for both directions of current flow. With a positive potential applied to the top contact, the emission was observed to be located in the region of this contact. Conversely, for the opposite polarity the emitting area was defined by the semiconductor:

header contact. The clear distinction between the emitting areas for the two directions of current flow can be seen in Plate 5.1. The emission from the semiconductor:header junction, when viewed from above is transmitted through the edges of the upper face of the crystal. For these devices there exists no ambiguity in associating the emission with reverse-biased junctions.

Discussion of Variations in Emission Properties

The fact that emission for some fabrication techniques is associated with a forward-biased junction and for others a reverse-biased junction requires further consideration. For the purposes of this discussion the premise is made that impact ionisation:avalanche injection processes associated with a forward biased junction are a result of the creation, either during crystal processing or device fabrication, of an insulating or semi-insulating layer between the metal electrode and the bulk of the semiconductor.

For the semi-insulating crystals discussed in section 5.2.1. the techniques of creating the In contact layer apparently do not affect to any significant extent the resultant properties of the device. For the case of

soldered contacts formed in the absence of an inert or reducing atmosphere, the existence of a chemically produced surface layer, such as an oxide, may be all that is required to form the necessary insulating layer. Since, however, the material of (c) above, was contacted in supposedly the same manner as the semi-insulating ZnTe, and emission was associated with a reverse-biased junction for the former material and a forward-biased junction for the latter, consideration must be given to explanations involving the nature of the surface states in the semi-insulating material, which result in compensation conditions at variance with those operative in the case of the nominally undoped material, or, alternatively, the effects of undetected alterations in contacting procedure. Pursuant to this latter point it is of relevance that the investigations of the nominally undoped material were made at a later date than those conducted on the semi-insulating ZnTe, and it is possible that, despite the considerable efforts made to achieve uniformity of processing procedures, variations may have been introduced over a period of time, either in the processing and contacting procedures themselves, or in the materials and facilities used, which had a significant influence on the dynamics of insulating layer formation. The results detailed in (b) above give

little weight to either of the above possibilities, due to the doubt which exists concerning the junction with which the emission was associated for each current direction. This dubiety arose from the use of cleaved chips having irregularly shaped faces. However, it is considered that the appearence of the emission more closely resembled, in spatial origin, that associated with a forward-biased junction. Such a result would tend to favour the more conjectural arguments associated with the relationship between contacting and processing technique and insulating layer formation. The existence of minor variations in the properties of the various forms of nominally undoped bulk material are not considered to be of importance in this connection.

For the material of (a) the association of emission with a reverse-biased junction may involve additional considerations. The experimental evidence indicates that the electroplated metal contact to the crystals was blocking in nature. One is here again dealing with two junctions exhibiting variations in their blocking characteristics. Although the V-I characteristics for this material, Fig. 5.6, are not significantly different for the two directions of current flow, the possibility exists that the absence of electroluminescence for the

forward-biased In:ZnTe (or In:In-ZnTe:ZnTe), junction is due to the less blocking nature of the Ni:ZnTe junction for both current directions, thus preventing the onset of an impact ionisation regime at the forward-biased In:ZnTe junction. Alternatively, the nature of both junctions may permit the occurrence of impact-ionisation at reverse bias only, the excitation process at the Ni:ZnTe barrier being the less efficient.

In the above considerations we have excluded from consideration such mechanisms as that of carrier accumulation proposed by Henisch (1962). This mechanism relates to recombination procedures which occur at a particular contact to a device, the polarity being such that majority carriers accumulate at this contact following injection at the opposite contact. Although this model is theoretically feasible, there has been little evidence in the literature to support it.

Emission Spectra

The room temperature emission spectra of all devices fabricated from the nominally undoped crystals were essentially identical to that shown previously for devices fabricated from semi-insulating ZnTe. This would indicate that the excitation processes involved, whether originating from a reverse or forward-biased junction,

are associated with an impact ionisation mechanism. It is also indicated that no significant variation exists in the type of impurities incorporated in the semi-insulating and the various nominally undoped crystals. Minor variations between the emission spectra of devices from the different batches could be attributed to changes in the concentrations of native defect or impurity centres. For the case of the semi-insulating ZnTe there is no direct evidence that the impurity, or the more probable native defect, whose concentrations significantly affect the resistivity and carrier concentration in this material, is a centre which also participates in radiative recombinations.

It is of interest to compare the emission spectra typical of these devices with the room temperature absorption spectrum of Figs. 4.1 (a) and 4.1 (b). It is apparent that no definite comparisons can be made between the two spectra beyond the correlation between the absorption edge located at 2.2eV and the main emission peak at a wavelength associated with a slightly lower energy value; it is believed that this shift of the emission peak can be accounted for by the effects of self-absorption. In addition, the possibility exists that the secondary maxima occurring at low values of the absorption

coefficient can be correlated with similar peaks in the emission spectra.

Description of the Electrical Characteristics and Discussion of Possible Mechanisms for Devices of Groups (a) - (c)

The remainder of this section is devoted to the presentation of the detailed electrical properties of typical devices fabricated from nominally undoped crystals as described at the commencement of this section. Possible mechanisms of of excitation and radiative recombination in these devices are discussed.

(a)

Current-Voltage and Emission Intensity-Current Characteristics of Devices from Group (a)

The current-voltage and emission intensity-current characteristics of devices fabricated from vapour-grown crystals of growth run No.4 are shown in Figs. 5.6 and 5.7.

It will be noted that in the room temperature I-V characteristics the high current direction corresponds to a positive potential applied to the In contact at low currents and at high current levels to the opposite polarity, the change over taking place at a current level of 2×10^{-3}A. This "switching" effect was not found to

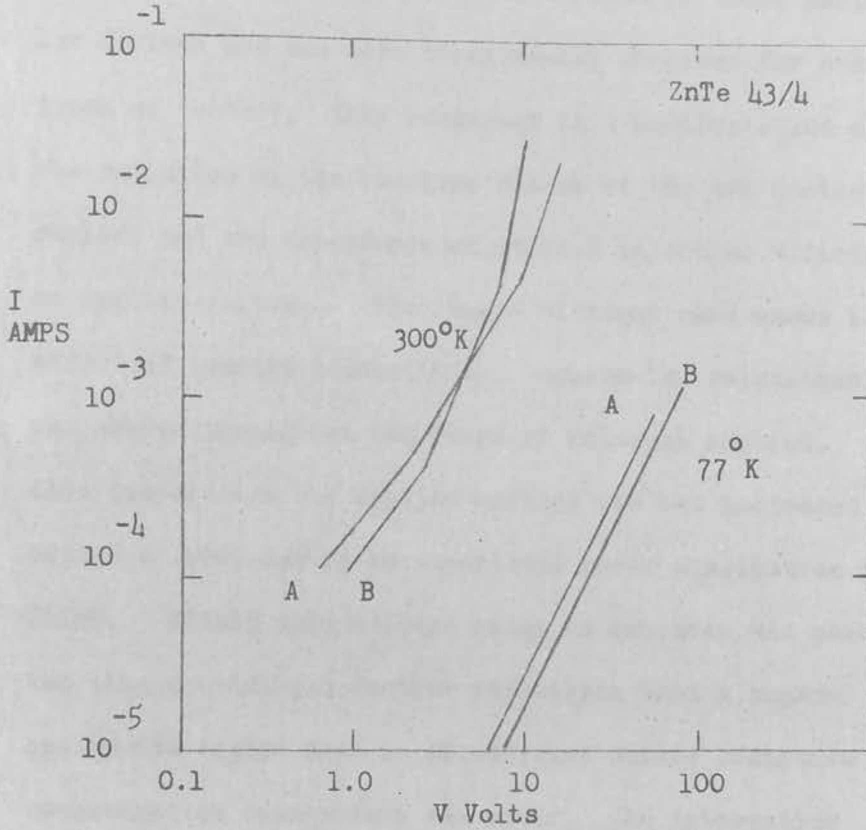

FIGURE 5.6 Current versus voltage. A Top contact Positive
B Top contact Negative

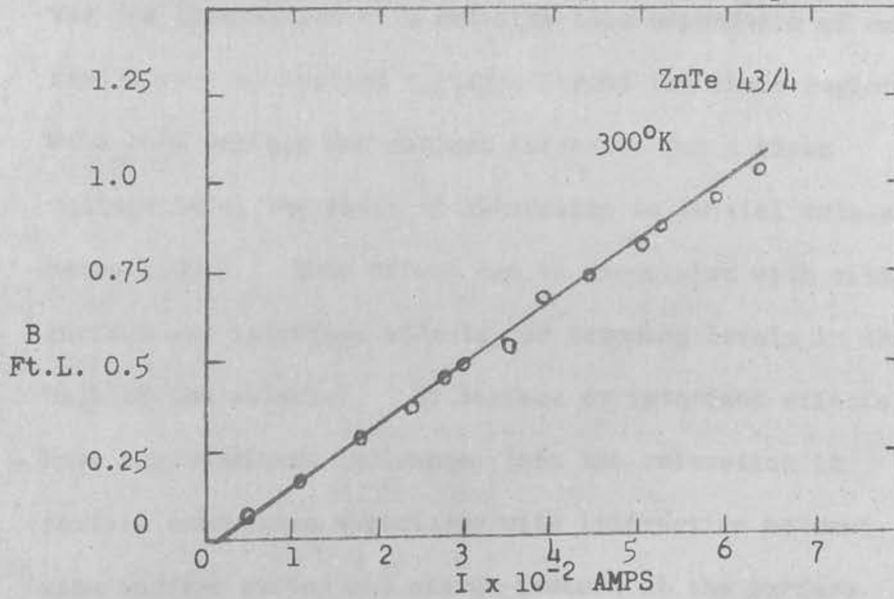

FIGURE 5.7 Emission Intensity versus Current.

be peculiar to the type of contacts used in these particular devices and was also occasionally observed for other types of contact; this behaviour is a manifestation of the variation in the blocking nature of the two contact regions and the dependence of overall injection efficiency on applied voltage. The liquid nitrogen case shows the effect of reduced conductivity; square-law relationship was obeyed throughout the range of voltages applied. At this temperature the applied voltage was not increased beyond a level having an associated power dissipation of 250mW. Within this voltage range no emission was observed thus providing a further indication that a super-square-law regime must be established before radiative recombination transitions can occur. An interesting feature of the room temperature electrical characteristics was the observation of a definite time dependence of current levels at applied voltages beyond the ohmic region. With both voltage and current increased for a given voltage level the ratio of saturation to initial values being 1.05:1. This effect can be associated with either surface and interface effects, or trapping levels in the bulk of the material. If surface or interface effects have a predominant influence, then the relaxation in surface conduction associated with interaction between slow surface states and charge induced at the surface

under the influence of the applied field could result in variations in overall current levels. If associated with bulk effects then release of current carriers from trapping levels under the influence of the field must be considered.

Figure 5.7 shows the variation in emission intensity with current for positive potential applied to the In contact. This curve obeys the relationship

$$B = K(I_o + I) \tag{5.11}$$

with $I_o = 1.5 \times 10^{-3}$ and $K = 16$. This linear dependence is frequently observed in impact ionisation processes (Ivey, 1963) and indicates that the current carriers contributing to the radiative recombination process increase in proportion to the total current.

The observed properties of these devices appear compatible with the proposed impact ionisation mechanism associated, for these particular devices, with a reverse-biased In:ZnTe junction. Tunnel injection mechanisms at the metal:semiconductor interface such as proposed by Eastman et al.(1964) could be operative at a reverse-biased junction. However, this particular model predicts monochromatic emission, high power dependence of emission intensity on total current, and temperature independent I-V characteristics; as these are at variance with the results obtained, this restricted

form of tunnel injection mechanism is rejected. A less restrictive model based on these considerations will be considered later in this section.

Since the emission of devices fabricated from group (b) could not be unambiguously associated with a particular contact region the I-V and B-I characteristics of these devices will not be discussed.

Current-Voltage and Emission Intensity-Current Characteristics of Devices from Group (c).

Finally in this section the I-V and B-I characteristics of devices from group (c) are presented. Figure 5.8 illustrates typical room temperature I-V characteristics and Fig.5.9 the B-I characteristics of the same device. In this latter figure two distinct slopes are shown obeying a relationship of the type

$$B = K(I_o + I^n) \qquad (5.12)$$

where K, I_o and n are constants. For the high current direction n takes the values 2.8 and 1.6 at low and high current levels respectively, with corresponding values for the low current direction of 2.0 and 1.0. The current levels corresponding to the change in slope of the B-I characteristic can be correlated to the current levels at which the I-V power-law relationship alters from a slope

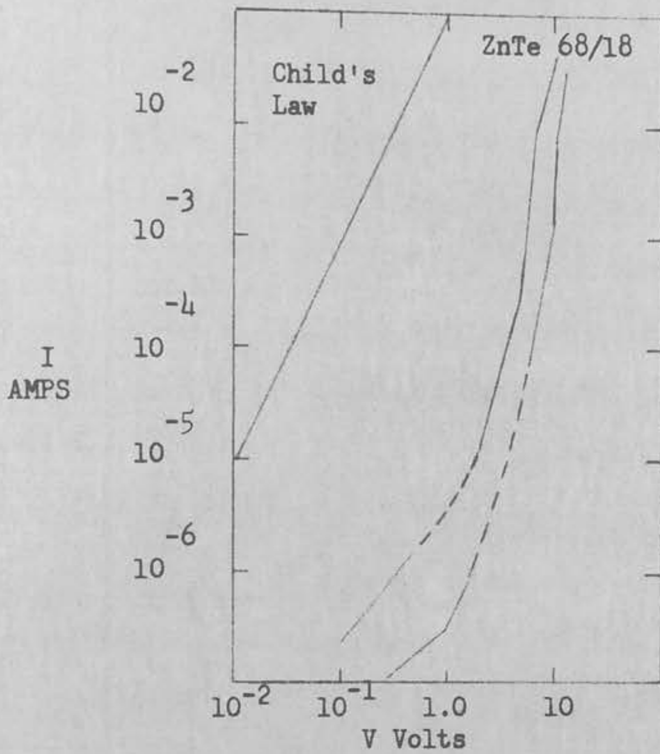

FIGURE 5.8 Current versus voltage
A Top contact positive
B Top contact negative

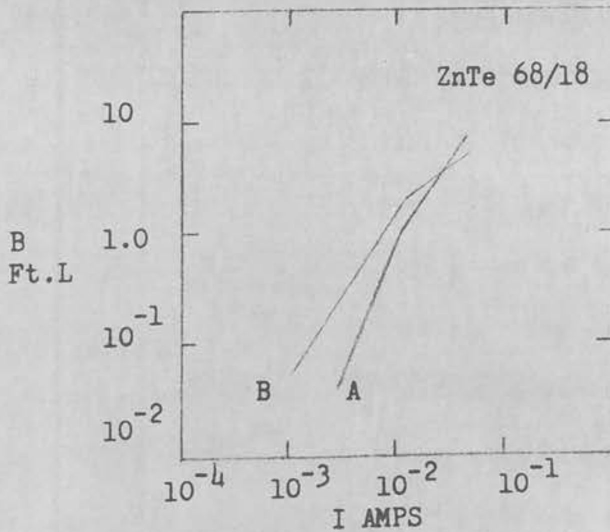

FIGURE 5.9 Emission Intensity versus current
A Top contact positive
B Top contact negative

corresponding to $I \propto V^{11}$ to $I \propto V^{6}$, also a reduction of approximately 2:1. The reduction in the power-law dependence of the I-V characteristic to a lower slope at high current levels could, from consideration of the composite device, be discussed in terms of the onset of trap-free conditions analagous to those observed at high current levels in space-charge-limited-current devices. However, if the characteristics are interpreted in terms of a contact-limited process, then the several regions of the I-V characteristic terminated by the high power-law regime can be regarded as being associated with the non-equilibrium excitation processes occurring in the barrier region. (Separate consideration can be given to the possible excitation mechanisms and associated radiative recombination processes). The final region could therefore be a manifestation of current limiting processes resulting from effects in the bulk semiconductor. These could possibly be interpreted in terms of the onset of space-charge or trapping effects. Also, the more complex effects of more than one trapping level being present in either the bulk semiconductor or contact region would be expected to result in a complex dependence of current on voltage. The reduced slope of this final region is also an indication that the preceeding high current regimes are in no way linked with the effects of sample heating. In order to prevent the occurrence of

resistive changes caused by sample heating, all devices operating at power levels in excess of 100mW were subjected to forced convection cooling, thus maintaining an ambient temperature close to that of the surroundings.

Further Considerations of Emission Intensity-Current Relationships

Square-law and linear B-I relationships have been frequently reported for electroluminescent p-n junction devices. In any analysis of the current dependence of the emission intensity of such structures it is relevant that the total junction current is generally the sum of several individual components such as injection current, majority carrier extraction current, surface leakage current and current resulting from trapping effects. Recently, appreciation of this fact has led a number of authors to the conclusion that it is more profitable to analyse the kinetics of radiative recombination at forward-biased junctions in terms of the dependence of light emission on bias voltage rather than on current. This, of course, presupposes a relatively low value of series resistance in the bulk crystal and in the contacts therefore allowing the potential across the junction itself to be measured. However, as these conditions cannot be met for the devices considered here, it was decided that

more useful information would be obtained by basing measurements on the dependence of light emission on current. Pertinent to this, semi-log B-V plots were not found to contain linear regions over extended voltage ranges.

It is not at all certain that the explanations advanced for the case of p-n junction devices are applicable to the complex impact-ionisation devices discussed here. The square law region signifies a non-linear dependence of "recombination current" on total current. This can be interpreted as an indication that the radiative recombination probability increases with increasing current due to saturation of non-radiative recombination centres. Alternatively, for an "injection" current of much smaller magnitude than the total current but suffering 100% radiative recombination, the ratio of "injected" to total current increases with increasing current. (For p-n junction devices the latter explanation is usually favoured. For example, if the emission intensity B was proportional to an injection current having a linear dependence on applied voltage and thus obeying the familiar relationship $B \sim \exp(eV/kT)$, and if the current-voltage characteristic is dominated by injection and recombination

in the space-charge layer so that the observed current I depends on bias as $I \propto \exp(eV/2kT)$, then it follows that $B \propto I^2$.) The transition to a region of lower slope can either be described in terms of the onset of non-radiative recombination processes, thus reducing the radiative portion of the "recombination" current, or, again considering the injection of a single type of carrier, high levels of injection could result in a minority carrier current of the same order as the majority carrier current. In this event, the recombination current, in the absence of non-radiative recombinations, would be proportional to the total current. Watanabe (1966), in investigation of forward-biased In-InZnTe devices, obtained B-I relationships of similar shape to those obtained here, and proposed an explanation based on the variation of injected minority carrier level with total current to be applicable.

For the particular devices considered in this section the correlation which exists between the reduction in the slope of the current-voltage and brightness-current plots at a particular current level is an indication that the alteration in the latter characteristic is related to changes in the concentration of current carriers in the device rather than the effects of an increase in the efficiency of non-radiative recombinations resulting from saturation of radiative recombination centres.

Consideration of Tunneling Mechanisms

As a number of devices possessed an exponential transition region in the current voltage characteristic, it was of interest to consider the results in terms of the relationship between current and voltage for a junction where the I-V characteristic is injection dominated and recombination occurs within the space-charge layer. An equation similar to (2.39) is applied

$$I = I_o(e^{eV/\beta kT} - 1) \qquad (5.13)$$

where I_o and β are constants. Typical results are shown in Fig.5.10. The values obtained were an order of magnitude greater than those normally obtained for p-n junction devices. High β values have been considered indicative of tunneling processes (Morgan, 1965). In the present case the β values obtained are no doubt in error since the distribution of the applied voltage across the device is unknown. It is, however, considered that in these devices the reverse-bias impact ionisation process could involve majority carriers tunneling through the cathode barrier, acquiring energy in the high field of the depletion layer, and subsequently causing impact ionisation of the lattice and/or luminescence centres (Fig.2.9). Intraband as well as interband transitions would be expected to result from such a tunneling process. The radiative recombinations associated with intraband transitions may have been self-absorbed by the crystal and therefore

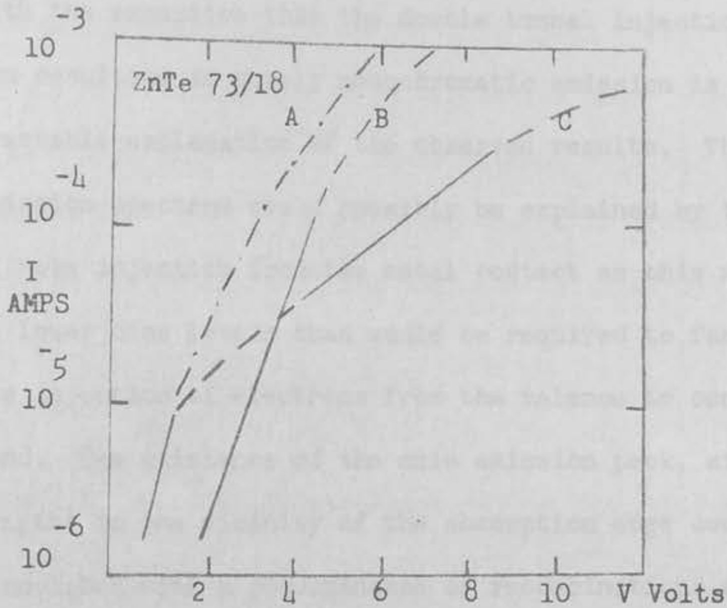

FIGURE 5.10 Current versus voltage.
A Top contact positive
B Top contact negative
C Point contact negative

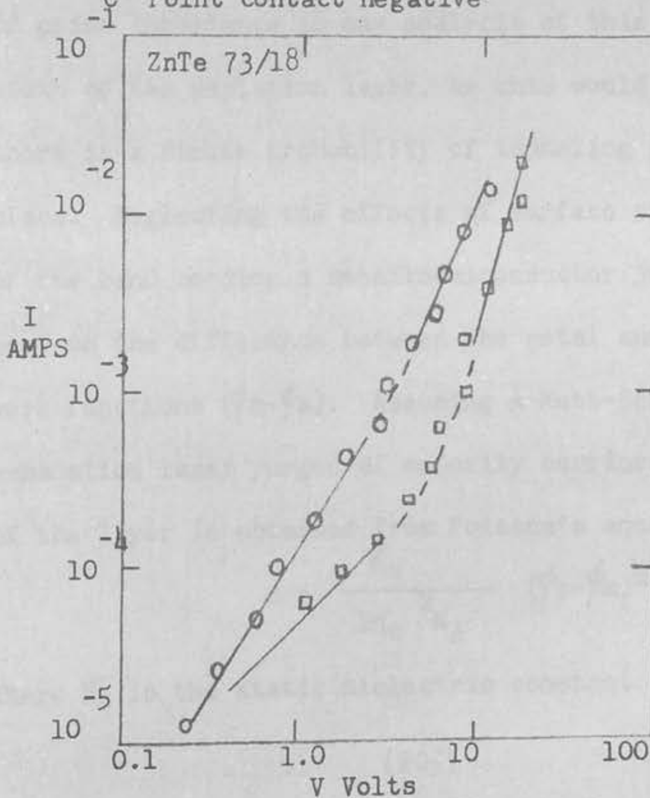

FIGURE 5.11 Current versus voltage
A Point contact positive
B Point contact negative.

were not detected in the emission spectrum. This mechanism is basically similar to that proposed by Eastman et al.(1964) with the exception that the double tunnel injection mechanism resulting in purely monochromatic emission is not a tractable explanation of the observed results. The broader emission spectrum could possibly be explained by the dominance of hole injection from the metal contact as this would occur at lower bias levels than would be required to facilitate the injection of electrons from the valence to conduction band. The existence of the main emission peak, at wavelengths in the vicinity of the absorption edge could be associated with a predominance of recombinations resulting from thermalised double-injected electrons and holes.

Of prime importance in any analysis of this type is the width of the depletion layer, as this would indicate whether there is a finite probability of tunneling processes taking place. Neglecting the effects of surface states, the extent of the band bonding a metal:semiconductor junction will depend on the difference between the metal and semiconductor work functions ($\phi_m - \phi_s$). Assuming a Mott-Schottky type of exhaustion layer purged of majority carriers, then the width of the layer is obtained from Poisson's equation as

$$d = \frac{K_s}{2\pi e^2 N_A} (\phi_s - \phi_m)^{\frac{1}{2}} \qquad (5.14)$$

where K_s is the static dielectric constant and N_A the acceptor

impurity density. For $K_s = 10$, $\phi_s - \phi_m = 1eV$ and $N_A = 5x10^{18}$ we obtain a minimum value for d of 150Å. This value is probably just within the thickness limits where current flow via tunneling is possible. Under reverse bias the energy bands deform as shown in Fig. 2.9 and the total width of the space charge region becomes, for the case of an abrupt junction,

$$d = \left[\frac{K_s}{2\pi e^2 N_A}(\phi_s - \phi_m + eV)\right]^{1/2} \qquad (5.15)$$

where V is the applied voltage. The fact that the width of the depletion layer increases as $V^{1/2}$ is compensated by the increase in field strength at the metal:semiconductor interface with increasing voltage; as a result of the accentuation of the band bending the junction field itself increases as $V^{1/2}$. For the case of a graded junction, (i.e. one in which the concentration of acceptors in excess of donors varies linearly with distance) the width of the exhaustion layer increases as $V^{1/3}$, and for a junction where an insulation layer exists is independent of V. The corresponding junction fields increase as $V^{2/3}$ and V^1 respectively. The theoretical dependence of current on voltage in a Mott-Schottky exhaustion layer of this type is complex (Henisch, 1962).

Point Contacts

Fig. 5.11 shows the room temperature V-I characteristic of the device ZnTe 73/18 which was used for the measurements

presented in Fig.5.10. For this measurement, however, the top contact was replaced by a point contact. Low level emission was observed for both directions of current flow. The location of the emission could not be accurately estimated. The V-I characteristic does not contain the high power regions found using two soldered In contacts, the relationships being linear, square-law and cubic. Current levels at a given voltage are approximately an order of magnitude less than those obtained for double indium contacts. This experiment illustrates the significant influence of the contacts on the emission processes.

Emission Efficiencies

The efficiencies of devices described in this section were measured by the technique described in section 5.2.1. The emission efficiencies for devices from groups (b) and (c) were similar to those obtained for devices fabricated from semi-insulating ZnTe, those from group (a) being a factor of ten lower (10^{-7} - 10^{-8}). This results from the lower emission intensities of these devices at the normal operating current levels as can be seen by comparison of Figs. 5.7 and 5.9.

5.2.3 ZnTe Incorporating Oxygen Centres

In this section we consider the properties of devices fabricated from crystals of growth run No.13. (Kennedy and Russ, 1967b). As discussed in sections 3 and 4 a number of pro-

perties of these crystals were significantly different from those of the other growth runs. Appraisal of these properties indicated that this material incorporated large concentrations of an impurity, believed to be oxygen.

Two forms of device were used for the majority of the investigations made on this material. Details of the fabrication techniques and relevant operating conditions of the devices are as follows.

(a) Device size chips of area approximately $1mm^2$ and thickness 0.5mm were cleaved from single crystal regions. The crystals were polished and mounted using contacting-technique No.1. (In soldered top contact, In/Ag soldered header contact). For this type of device emission having a red colouration at both room temperature and $77^{o}K$, was observed for a negative potential applied to the top contact, this being the low current direction for low levels of applied voltage. The emission normally appeared to be localised in the region of the reverse-biased junction.

(b) Regularly shaped chips $0.1mm^2$ x 0.5mm were cut from single crystal regions, etched in CP-4 and contacted using technique No.2. (In vacuum-melted top contact, In/Ag soldered bottom contact). For these devices it was found that emission was obtained for both directions of current flow, the more intense emission

being obtained for a negative potential applied to the top contact. This was normally the high current direction and for this polarity the emission was observed throughout the bulk of the crystal, whereas for the opposite current direction the emission was restricted to a broken line in the region of the semiconductor:header contact. Plate 5.1 shows the low-current direction emission for a device of this type. The regions from which the emission emanates are overexposed and have an orange colouration. On polarity reversal these localised emitting regions were not visible and the emission appeared to be generated within the bulk of the crystal.

Emission Spectra

The emission spectrum of a typical device is shown in Fig. 5.12. The 250 mm monochromator and a type 7265 photomultiplier were again used in these measurements. The spectra are corrected for the response of the photomultiplier. This emission spectrum was obtained for devices fabricated by various contacting techniques. For both current directions the emission spectra were identical. At 293°K the main emission peak was located at 6960Å. A secondary peak which had a relative intensity one-fiftieth of the main peak was located at a wavelength of 5750Å, i.e. just above the absorption edge of the undoped material. For oxygen-free

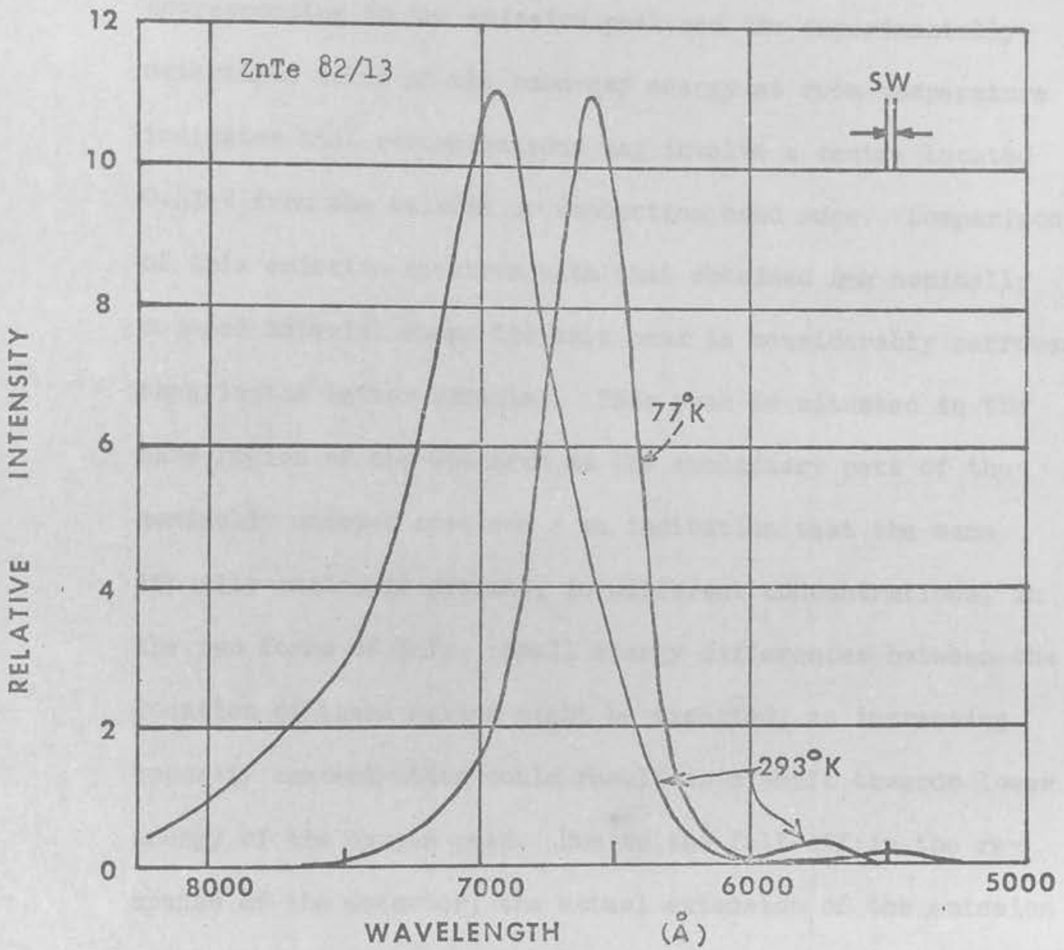

FIGURE 5.12 Emission Intensity versus wavelength for a ZnTe:O device at 293°K and 77°K.

crystals the main emission peak was located in the region of this wavelength. At 293°K no emission was detected at wavelengths below 5500Å. The difference between the energy corresponding to the emission peak and the experimentally determined value of the band-gap energy at room temperature indicates that recombinations may involve a centre located 0.43eV from the valence or conduction band edge. Comparison of this emission spectrum with that obtained from nominally undoped material shows the main peak is considerably narrower than in the latter material. This peak is situated in the same region of the spectrum as the subsidiary peak of the nominally undoped spectrum - an indication that the same impurity centre is present, in different concentrations, in the two forms of ZnTe. Small energy differences between the location of these maxima might be expected, as increasing impurity concentration could result in a shift towards lower energy of the oxygen peak. Due to the fall-off in the response of the detector, the actual extension of the emission spectrum of the oxygen-doped material into the infrared could not be determined.

At 77°K the main peak shifted to shorter wavelengths and was located at 6580Å, the half-width being reduced to 420Å. The shift in this peak between the two temperatures is in agreement with the reported temperature dependence of the band-gap (Cardona and Greenaway, 1963). In this case a secondary peak

was detected at 5400Å; the ratio of the intensity of this peak to that of the main peak was found to be 1:100. No emission was detected at wavelengths below 5230Å. At this temperature the limits of the emission spectrum in the near infrared could be evaluated; no emission was detected at wavelengths beyond 7800Å. As in the room temperature case the emission spectrum of nominally undoped crystals was found to exhibit an emission peak in the vicinity of this wavelength. The displacement of the main emission peak from the reported value of the band-gap energy at 77°K (Cardona and Greenaway, 1963) indicates that recombinations may involve a centre located 0.48eV from the valence or conduction band edge. The discrepancy between the values of this energy level at 293°K and 77°K possibly originates from errors in the selected values of the band-gap energies at these temperatures. It is possible that at both 293°K and 77°K the spectrum of the emitted radiation extends to shorter wavelengths than the values corresponding to the band-gap energies at these temperatures, but that the emission is internally absorbed. At both temperatures no detectable shifts of the emission peaks were observed for devices operating over a wide range of current levels; the apparatus used would have permitted the detection of a peak shift in excess of 10Å.

Comparison of the room temperature emission spectrum with

the absorption spectrum of Fig.4.1(a) shows that definite correlation can be made between the main emission peak corresponding to a photon energy of 1.78eV and the transition located at this energy in the absorption spectrum. The second transition at higher energies close to the band-gap value corresponds in energy value to the main emission peak located at 2.17eV. No correlation could be drawn between the other inflexions shown in the absorption spectrum and the shape of emission spectrum.

As discussed previously in chapter 2, Dietz et al. (1962) detected an extrinsic optical excitation in ZnTe located 0.4eV below the band-gap energy. In further investigations of this centre Hopfield et al.(1966) found that for crystals grown in the presence of oxygen the low temperature absorption of this centre was increased. Low temperature fluorescent spectra consisted of a zero-phonon doublet A,B followed at lower energies by phonon replicas. The zero-phonon doublet was formed by j-j coupling of a j=3/2 hole with a j=1/2 electron to produce the A level (J=1) and B level (J=2). The ΔJ=1 transitions from A to the ground state were allowed and ΔJ=2 transitions forbidden, with transition A in each case 1 to 3 meV above line B, so that thermalisation caused the intensity of the lines to change with temperature, line A being dominant at a higher temperature. The term isoelectronic trap was used to describe this situation where an atom

from the same group of the Periodic Table substitutes for the host atom. For the case of oxygen and tellurium this atom is sufficiently different from the host atom to provide a bound state for the hole-electron pair, or exciton. The trapping action of the uncharged impurity centre has been considered by Hopfield et al.(1966) to result from the local potential created by the substitution, which for the case of oxygen in ZnTe, attracts electrons in its vicinity; once an electron is captured a hole will bind to the long-range coulomb potential in an acceptor-like wave function. This bound exciton state might therefore be described as an isoelectronic acceptor.

Another optical transition which is of relevance to this discussion relates to Zn:O pair spectra. These have been observed in GaP and the detailed shape of the spectra, especially at room temperature, and also the position of the emission peak (Gershenzon et al., 1965) bear close resemblance to the results obtained for ZnTe:O. In this material the emission results from the recombination of an electron on an ionised oxygen donor with a hole on a Zn acceptor. It is possible that an undetermined impurity in ZnTe permits a similar radiative transition. (The Zn native defect acceptor level in ZnTe is located at 0.048eV (Aven and Segall, 1962)). Alternatively, recombinations could possibly take place between electrons trapped on a

isoelectronic oxygen impurity with holes on Zn acceptors.

In order to quantitatively evaluate the nature of the transitions involved, measurements of emission spectra would require to be made at lower temperatures, and ideally photoluminescent spectra of the material would also be required. From the detailed structure of these spectra it should be possible to elucidate the presence of either bound exciton and/or donor-acceptor transitions. Unfortunately, in the 77°K emission spectrum there were not present any minor peaks which could be unambiguously associated with the known energy levels of phonon replicas in ZnTe. The information which can be elucidated from the emission spectra is therefore restricted to the determination of a transition which could be associated with an impurity centre located 0.4 - 0.5eV from the valence or conduction band edge. The existence of a donor-acceptor type transition between a shallow acceptor and a donor level deeper than the above cannot be eliminated. Since in these crystals, the presence of high concentrations of oxygen is indicated, this is taken as evidence in favour of recombinations involving isoelectronic oxygen centres having a zero-phonon transition at approximately this energy displacement.

<u>Current-Voltage and Emission Intensity-Current Characteristics</u>

The 315°K and 77°K current-voltage characteristics of a

device fabricated using In soldered contacts as described in (a) above are shown in Fig. 5.13. The two graphs show regions of similar slope, the current level for a given applied voltage being much reduced at the lower temperature. It will be noted that the 77°K I-V plot has a region obeying the relationship $I \propto V^5$ followed at higher current levels to an approximate square-law region $I \propto V^{1.8}$; this is not exhibited in the higher temperature plot. At high current levels and at both temperatures the slight rectifying properties of the device disappear, the curves being identical for both directions of current flow. The emission intensity of this device at room temperature was measured using a spectra Spot Meter and is shown in Fig. 5.14; at low current levels a square-law relationship is obeyed with a transition to a linear dependence at a current level corresponding in the I-V characteristic to the commencement of a high power-law region.

Figure 5.15 shows the I-V characteristics of devices utilising the second type of contact described earlier in this section. The room temperature characteristics for both directions of current flow through the device were ohmic at low current levels with transitions to higher power law relationships as the voltage was increased. The 77°K characteristic shows the effect of reduced temperature on the resistivity of the material. The difference in the degree of recti-

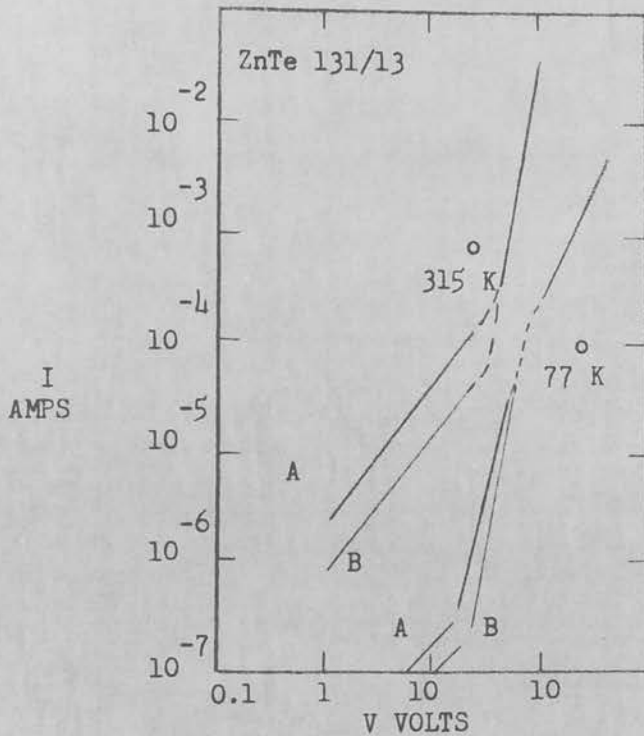

FIGURE 5.13 Current vs voltage

A Top Contact Positive
B Top Contact Negative

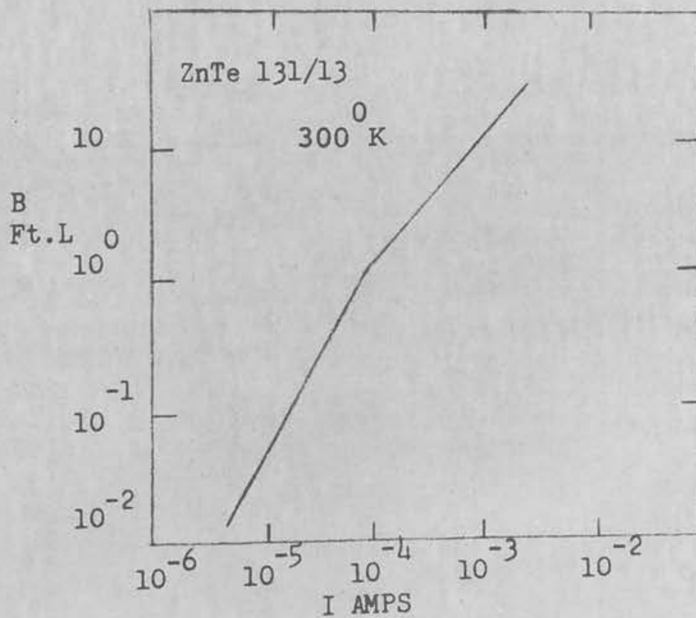

FIGURE 5.14 Emission Intensity vs Current
Top Contact Positive.

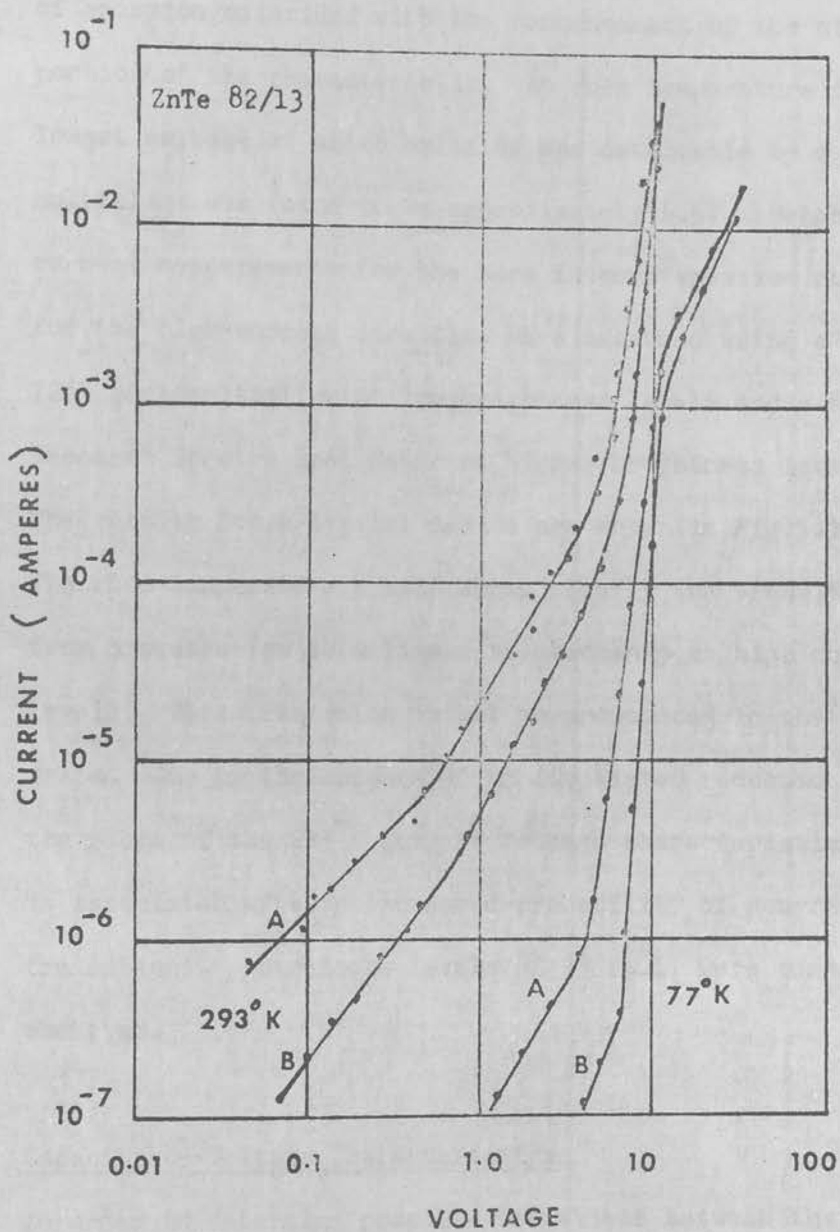

FIGURE 5.15 Current versus voltage for a ZnTe:O device at 293°K and 77°K.

(A) In diffused contact negative
(B) In diffused contact positive

fication of the two contacts was evidenced by displacement of the I-V plots for the two current directions. The onset of emission coincided with the commencement of the steep portion of the characteristic. At room temperature the lowest voltage at which emission was detectable by a photo-multiplier was found to be approximately 4.5V. Brightness-current measurements for the more intense emission obtained for the high-current direction were measured using a RCA 7265 photomultiplier at low brightness levels and a Photo Research Spectra Spot Meter at higher brightness levels. The results for a typical device are shown in Fig.5.16. The room-temperature result shows clearly the transition from a square-law to a linear relationship at high current levels. This transition is not so pronounced in the 77°K graph. Due to the absence of an associated reduction in the slope of the 293°K current voltage characteristic it is associated with an increased probability of non-radiative transitions. Brightness levels of 25 ft.L. were commonly observed.

Capacitance-Voltage Characteristics

In order to determine possible variations between the junctions formed by the two contacting techniques the dependence of junction capacitance on bias voltage was measured for representative devices. A Boonton direct-reading capacitance

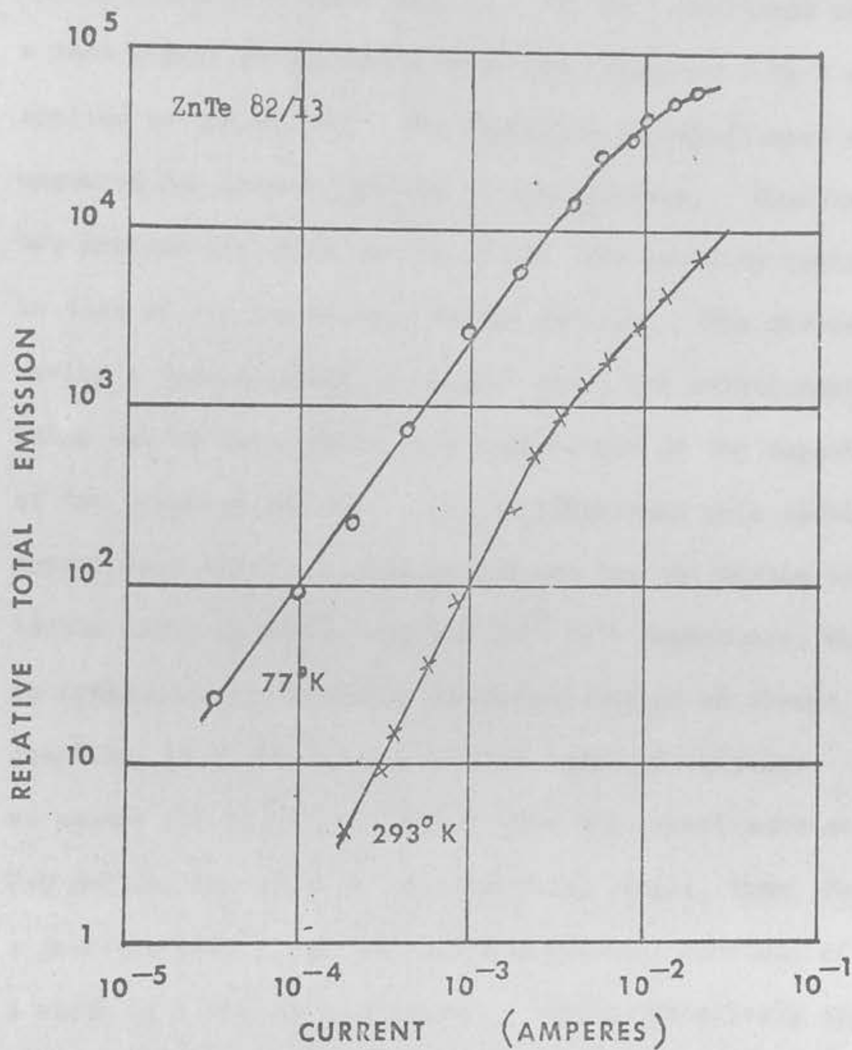

FIGURE 5.16 Brightness versus current and 77°K for a ZnTe:O device at 293°K
Structure - In (vacuum melted) - ZnTe - In/10% Ag.

meter was used in these measurements in conjunction with a highly stabilised power supply. In the capacitance meter a test signal of amplitude 20 mV and frequency 1 Mc/s was applied to the device. The variation in capacitance was measured for both directions of current flow. Results for two devices are shown in Fig. 5.17; the polarity indicated is that of the top contact to the devices. The device having a vacuum formed In contact has a C-V relationship which can be interpreted as a combination of the capacitance of two junction regions. On the other hand this double capacitance effect is less pronounced for the device contacted using In solder and the $1/C^2$ vs V dependence, which is frequently considered a characteristic of an abrupt junction, is obeyed over a limited range of voltages. If we assume for the former device that the capacitance at V=0 defines the width of an insulating region, then, for a junction area of $10^{-2}cm^2$ and a dielectric constant of 10, a width of 1 micron is obtained. Again tentatively applyint the S.C.L.C. theory contained in equation (5.7) to (5.10) indicates a trap located at 0.47 eV with a density of $2x10^{15}/cm^3$. As discussed previously the trap depth and density can be evaluated directly from the temperature dependence of Θ given in eq. (5.7). Evaluating Θ from the square-law regions of the 300^oK and 77^oK I-V characteristics, and assuming that these two values define a straight line, a graph is obtained of slope of $-E_t/k$ and intercept, for $1/T = 0$, of N_v/N_t.

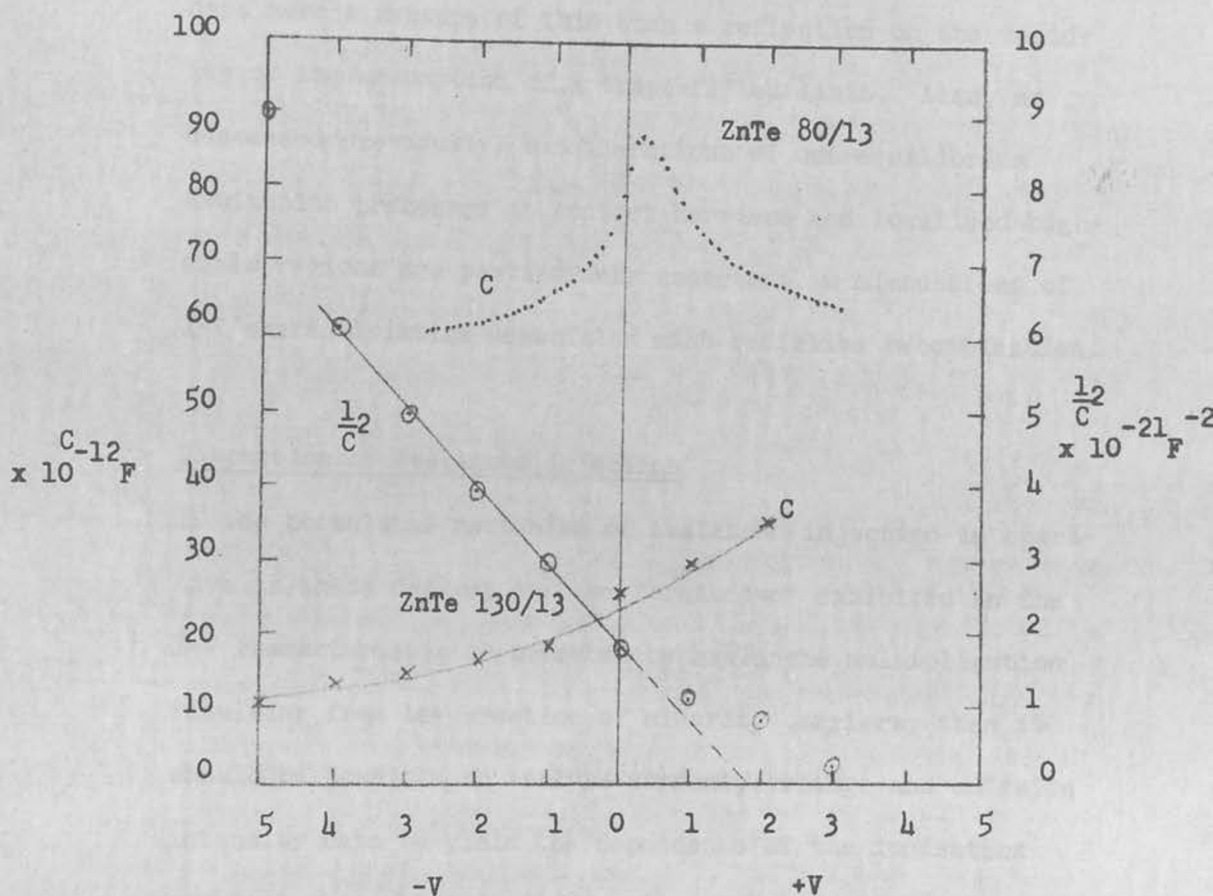

FIGURE 5.17 Capacitance-Voltage results for In(diffused)-ZnTe-In/Ag device (ZnTe 80/13) and In-ZnTe-In/Ag device (ZnTe 130/13). Voltage polarity shown refers to sign of the top contact to the device.

The application of this equation makes no assumption concerning the onset of a traps-filled limit at the transition voltage, V_{TFL}. The lack of sufficient data imposes severe restrictions on the accuracy of such a procedure, and the calculated values of E_t=0.05eV and $N_t = 10^{21}/cm^3$ are perhaps more a measure of this than a reflection on the validity of the assumption of a traps-filled limit. Also, as discussed previously, considerations of non-equilibrium excitation processes at contact barriers and localised high-field regions are particularly important in discussions of I-V characteristics associated with radiative recombination.

Discussion of Avalanche Injection

If the postulated mechanism of avalanche injection is operative in these devices and the "breakdown" exhibited in the I-V characteristic is produced by avalanche multiplication resulting from the creation of minority carriers, then it should be possible to analyse current, voltage and emission intensity data to yield the dependence of the ionisation constant α on electric field. One assumption implicit in the following analysis is that all electrons created by the avalanching process are swept out of the high-field region before recombining. From previous considerations of the spatial distribution of the emission it would appear that this is indeed the case. The analysis used is based on

that given by Moll (1964) for avalanche effects in Ge and Si in which the electron current i_n can be related to α by

$$\frac{di_n}{d_x} = \alpha_p i_p + \alpha_n i_n \qquad (5.16)$$

where α_p and i_p are the hole ionisation constant and current respectively and α_n and i_n are the corresponding quantities for electrons. Integrating this expression, assuming that at fields where avalanching is negligible, $i_p \gg i_n$ so that $i_p \approx i$, and taking $I = ai_n$ as a current associated with the emission intensity, gives

$$\frac{I}{i} = a\int_0^W \alpha_p \, dx \qquad (5.17)$$

where w is the width of the avalanching region, and a is an empirical factor combining the quantum efficiency of the device and the characteristics of the light detection system. The ionisation constant α_p depends on the field and cannot be taken out of the integral sign unless the field is constant throughout the avalanching region. Moll (1964) has shown, however, that the integral can be evaluated if depends exponentially upon the reciprocal field, $\alpha = \alpha_o \exp^{-b/E}$ where α_o and b are constants. If the field distribution is such that it can be expressed in the form $E = E_{max} f(x/w)$ where E_{max} is the maximum field in the avalanching region, then substitution of these equation (5.17) gives the result

$$\frac{I}{i} = a\alpha_o \exp(-b/E_{max}) W g(b/E_{max}) \qquad (5.18)$$

where g (b/E_{max}) is given by

$$\int_0^1 \left[\exp\frac{b}{E_{max}}\left(1 - \frac{1}{f(z)}\right)\right] dz$$

with $z = x/w$. The product Wg (b/E_{max}) can be called the effective width W_{eff}. The integral g b/E_{max} is available in tabulated form for several field distributions. For distributions of a linear or parabolic type the integral does not vary rapidly with b/E_{max}, typically by less than a factor of two for a corresponding change in applied voltage. In the devices investigated here the emission intensity alters by a much greater factor for a doubling of the applied voltage. Therefore from eq. (5.18) one should be able to plot log I/i vs. E_{max}^{-1}, and obtain a straight line over a fairly wide range in E_{max} without being concerned about variation in W_{eff}.

Equation (5.18) was applied to the results of emission intensity measurements for both directions of current flow through the crystal. The field distribution in the insulating layer was assumed to result in a maximum field given by $E_{max} = 1.5V/W$ (McKay, 1954; Weiser et al., 1967) and the abcissa taken as $W/1.5V$ with $W = 1$ micron. As the slopes of the resulting curves have a physical significance the scaling factor of the abcissa, i.e. the exact dependence of E on E_{max}, is important. Fortunately, the majority of field distributions commonly applied result in a dependence of E_{max} on applied voltage which dif-

fers at most by 30% from that chosen. The emission intensities, I, have arbitrary values, in this case the photomultiplier output current. It was found that a plot of log I/i vs $1/E_{max}$ was linear for the high-current, (a negative potential applied to the top contact) at applied voltage levels above 12V and extending to 28V. For the opposite current direction no linear correlation was found to exist. This latter occurrence is considered to be due to the fact that, in the low current direction, the minority carriers associated with the excitation process at the reverse-biased junction are extracted into the metal electrode or recombine in the high-field region, thus violating the basic assumption of this analysis that carriers are swept out of this region prior to recombination.

Three factors may be responsible for the failure of this dependence at voltage levels below 12V. These are: (1) variation in the factor $Wg(b/E_{max})$ of eq. (5.18), (2) at low voltage levels the emission intensity deviates from a linear dependence on current, (3) the inaccuracy in low voltage values of the abcissa due to the contribution to the total applied voltage of the potential dropped across the bulk of the crystal.

Above 12V in the forward direction the curves obeyed the relation α_p = Aexp-b/E. The slope of the graph yielded

a value of b of 7×10^5 cm/V. From Baraff's avalanching theory (1962) a dependence of α on E^{-1} of the form $\alpha = \alpha_0 \exp{-b/E}$ is expected on theoretical grounds. As in earlier theories, this treatment assumes that the energy of hot carriers is dissipated isotropically by the emission of optical phonons of constant energy E_r, and that this process is characterised by a mean free path λ. In theory, the slope of the semi-log plot, b, is equal to E_i/λ where E_i is the ionisation energy. Taking $b = 7 \times 10^5$ and $E_i = 1.5\ E_G$, where E_G is the band-gap energy (2.2eV at room temperature), gives $\lambda = 230$Å. This value is a factor of two to five times higher than obtained previously by Weiser et al.(1967) for electroluminescence associated with avalanche breakdown in GaAs. The assumption that $E_i = 1.5E_G$ is only valid if electron and hole masses are equal, which is not the case in ZnTe, since for p-type material the relevant hole mass must be taken at some distance from the valence band maximum in k-space, and the electron mass taken near the conduction band minimum (Hauser, 1966). The exponential dependence of ionisation constant on reciprocal field in the Baraff theory should hold up to fields of at least $E_r/e\lambda$. Taking E_r for ZnTe as 0.03eV, and λ as 230Å as obtained above, the limiting field is about 1.3×10^4V/cm. In the experimental results the linear dependence held to fields of 3×10^5V/cm.

Although it is obvious that the theory will not apply at full

scale breakdown where the avalanching process is carried out by both holes and electrons, the Baraff theory indicates that the application limit of this formulation is met at lower values of field, and the departure of the semi-log plot from a linear dependence at fields in excess of 3×10^5 V/cm is not necessarily an indication of the onset of full scale breakdown.

Emission Efficiencies

For ZnTe:O devices a simpler and more accurate method than that described previously was used to measure emission efficiencies. In these measurements a box of Si p-n solar cells was used to collect the light emitted from the device. The efficiency of the cells used was within close tolerance of a maximum value of 8%. The variation in efficiency of a typical cell across the relevant region of the visible spectrum was calibrated by comparison with a thermopile. In the efficiency measurement the short circuit current of the cells was measured using Keithley 601 electrometer. The device, η_D, efficiency is given by

$$\eta_D = I_c/I_D \, \eta_c \qquad (5.19)$$

where I_c and I_D are the output current from the cells and the input current to the device respectively, and η_c is the efficiency of the cells integrated over the emission spectrum of the device. Fortunately, since the spectral sensitivity of the cells shows little variation for large changes in wavelength, the value of η_c corresponding to

the peak of the device emission spectrum is usually sufficiently accurate for application in this equation.

The room temperature efficiency of the forward biased ZnTe devices measured using this technique was in the range 10^{-3} - 10^{-4} photons/electron, with the efficiency at 77°K a factor of ten higher. These results not only indicate that the emission efficiency in this form of ZnTe is at least a factor of 10^{2} greater than in devices fabricated from nominally undoped crystals, but also show that the thermal quenching of emission, which is a measure of dependence of the emission efficiency on temperature, is not pronounced. Normally for undoped material the room temperature emission efficiency is at least a factor of 10^{2} less than the 77°K value. These values are considered to be the highest room temperature efficiencies yet reported in ZnTe electroluminescent devices, and the 77°K value is within an order of magnitude of the efficiency reported by Crowder et al.(1966) for a ZnTe m-i-p device.

The maintenance of the radiative efficiency up to room temperature is a property of the deep impurity levels; carriers will remain trapped on these levels and ionisation will not take place until higher temperatures are attained. Recently Cuthbert and Thomas (1967), in investigations of the fluorescent decay times of excitons bound to isoelectronic

traps in oxygen-doped ZnTe, found the fluorescent efficiency to be roughly constant from $20^{o}K - 300^{o}K$. In terms of the isoelectronic-acceptor model for the centre, this was explained by the tight binding of the electron to the centre and weak Coulombic binding of the hole. As the temperature increases the weakly bound hole ionises first, (binding energy of hole to the centre = 5.7meV) leading to an increased radiative lifetime, the electron remaining unionised until room temperature is exceeded. Above this temperature the efficiency and decay times fell off rapidly, the latter with an activation energy of 0.4eV. It was assumed at these higher temperatures electtons and holes recombine non-radiatively. These authors determined the oscillator strength for the ZnTe:O transition to be 0.8. In the light of these results it would not appear unreasonable that the deep centre luminescence described above should retain its efficiency at high temperatures. The reduction in efficiency observed, may, therefore, be mainly attributable to the decrease in efficiency of the avalanche injection process with increasing temperature.

The electrical characteristics of these devices and the observation of emission in the bulk of the material allows consideration of an avalanche injection mechanism in which minority carriers impact ionised in a high-field region in the vicinity of the forward-biased metal:semiconductor junction are subsequently injected into the bulk of the semiconductor. The

high-field region may be created at a semi-insulating layer formed during the contacting process by the diffusion of In into the surface layers of the crystal. The experimental evidence is not sufficiently detailed to permit detailed elucidation of the recombination process, but it is considered that recombinations involve carriers trapped on oxygen atoms substituting isoelectronically for Te and located approximately 0.4eV above the valence band edge, electroluminescence resulting from recombinations between minority carriers bound to these centres and free carriers or holes located on shallow acceptor levels. The possibility of field or impact ionisation of these centres must be considered.

5.2.4 Polycrystalline ZnTe

The results obtained in investigations of polycrystalline ZnTe of growth run No.32 will now be presented (Kennedy and Russ, 1967c).

On the basis of the foregoing investigations it would appear that emission in ZnTe devices may result from high-field processes in the vicinity of the contacts. Since long-range order and high quality bulk material may not be essential for these processes to be operative it was of some importance to determine whether emission could be obtained from devices fabricated from polycrystalline material. Devices were fabricated using contacting techniques 1 (In top

contact, In/10%Ag bottom contact), 2 (In vacuum-alloyed top contact, In/10%Ag bottom contact), and 6 (In top contact, electroless Au bottom contact). The crystals were ground using grades 5, 0.3 and 0.1 micron alumina and cut to give regularly shaped chips of area 0.4 - 1mm^2. The surface layers of the crystals were subsequently removed by etching in CP-4 solution prior to contacting. Only technique No. 1 resulted in room-temperature emission of sufficient intensity to justify further investigation. Extremely weak emission was detected from the devices incorporating vacuum-melted In and electroplated Au contacts.

For the devices contacted by technique No.1, emission of a red-orange colouration was usually detected for both directions of current flow, the polarity and spatial distribution of the emission indicating that it was associated with a reverse-biased junction. The majority of the devices possessed definite rectification ratios under an applied voltage of 1.5V, and this manifestation of the variation in the blocking nature of the two contacts was confirmed by the observation that the emission intensity was generally higher for one direction of current flow than the other. Due to the high resistivity of this material (4×10^5 ohm-cm) the emission under a.c. conditions was investigated. It was anticipated that more intense emission might be obtained at similar voltage levels to those

used for d.c. excitation as the carriers generated by the impact-ionisation process, which is the mechanism considered to be operative at the reverse-biased junction, would tend to be swept into a low-field region on field reversal, thus permitting more efficient recombination in a manner analagous to the injection of impact-ionised carriers at a forward-biased junction. Although the emission intensities were found to be definitely higher under 4Kc/s a.c. excitation, the improvement was not outstanding.

Emission Spectra

The 300°K and 77°K emission spectra of a typical device are shown in Fig.5.18. The spectra were again recorded using a 250mm monochromator, using slits giving 70Å resolution, and an RCA 7265 photomultiplier; the spectra are shown corrected for the response of the photomultiplier. The room temperature spectrum was measured under direct current excitation, but due to the high resistivity of the material, it proved impossible to excite d.c. electroluminescence at 77°K, and the emission spectrum recorded at this temperature was obtained under 4Kc/s alternating field excitation. The room temperature spectrum is seen to consist of a broad peak centred on 6600Å with a width at half-maximum intensity of 1900Å. This broad spectrum substantiates the finding that the electroluminescence in these devices is associated with an impact ionisation pro-

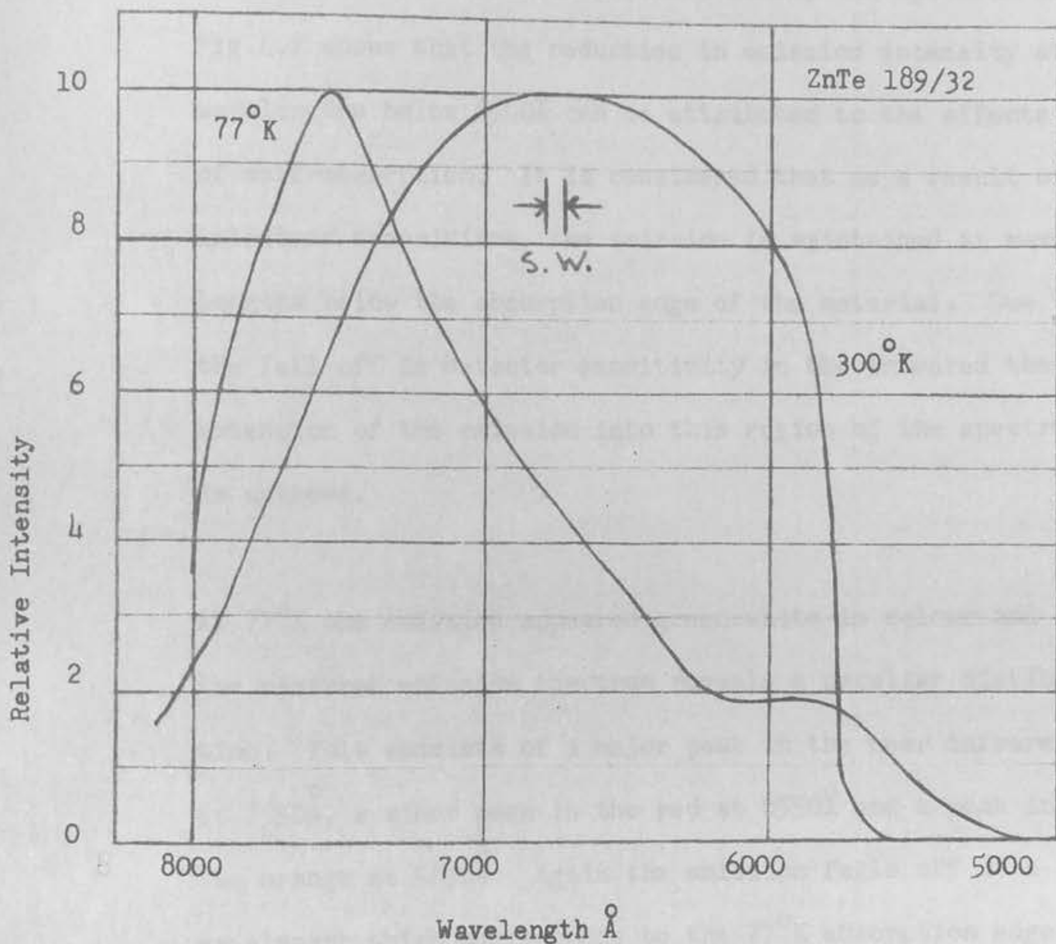

FIGURE 5.18 Emission intensity versus wavelength for polycrystalline ZnTe device at 300°K and 77°K.
Excitation 300°K d.c. 20V, 20mA
77°K 4Kc/s 200V, 2mA.

cess occuring at a reverse-biased junction. The spectrum exhibits a sharp cut-off in the region of the absorption edge of the material, and comparison of this emission spectrum with the room-temperature absorption spectrum of Fig.4.2 shows that the reduction in emission intensity at wavelengths below 6500Å can be attributed to the effects of self-absorption. It is considered that as a result of intraband transitions, the emission is maintained at wavelengths below the absorption edge of the material. Due to the fall-off in detector sensitivity in the infrared the extension of the emission into this region of the spectrum is unknown.

At 77°K the emission appeared green-white in colour and the measured emission spectrum reveals a peculiar distibution. This consists of a major peak in the near infrared at 7550Å, a minor peak in the red at 6550Å and a peak in the orange at 5850Å. Again the emission falls off at a wavelength which corresponds to the 77°K absorption edge of ZnTe, and the detailed shape of the shoulder on the main peak in the infrared region of the spectrum could not be accurately measured due to the sensitivity limitations of the detector. The spectral width at half-maximum intensity of the main peak was 1100Å. The occurrence of this peak is difficult to explain. It is not feasible that at 77°K the absorption spectrum of the material would extend to

to these wavelengths and cause a reduction in a broad impact ionisation spectrum - the converse would be expected. The symmetrical shape of the peak also refutes arguments based on absorption effects. It would therefore appear that this peak is associated with recombinations taking place either at a deep impurity level, or between two impurity levels. For this wavelength a transition involving an impurity level located 0.73eV from the valence or conduction band edge, or between two impurity levels having this energy separation must be envisaged. No evidence is available to remove from the realm of speculation any considerations of the nature of these centres. At room temperature it would be expected that the emission associated with the postulated impurity centre(s) would shift to longer wavelengths. Although the cathode sensitivity of the photomultiplier is considerably reduced at wavelengths approaching 8000Å it would be anticipated that the occurrence of a major peak would be detected. No such peak is shown in the recorded spectrum, although there is some indication of a minor peak in this wavelength range. It is therefore concluded that this emission band is virtually eliminated as a result of thermal quenching at the increased temperature. The minor peak located at 6550Å in the 77°K spectrum could again be attributed to the presence of isoelectronic oxygen centres introduced during the crystal growth procedure. There is

good correspondence between the location of this minor peak and the 6580Å maxima found in the 77°K emission spectrum of oxygen-doped ZnTe described in the previous section. The maxima of the broad room temperature emission spectrum is located at wavelengths corresponding to the location of such centres. Therefore a possible alternative explanation for the shape of this room temperature spectrum might be the predominance of recombinations involving oxygen centres. The 5800Å peak shown clearly in the 77°K spectrum is evidence of the recombination of hole-electron pairs of near band-gap energy, and would be expected in the impact ionisation spectrum of a direct-gap semiconductor.

Capacitance-Voltage Characteristics

The electrical characteristics of these devices are now considered. Fig. 5.19 shows the capacitance-voltage relationship for a polycrystalline ZnTe device. The measurement technique employed was described in the previous section. The graph illustrates the complex dependence of capacitance an applied bias found in these devices, the results not being readily interpreted in terms of conventional semiconductor C-V relationships. It would appear, however, that the shape of the characteristic for device

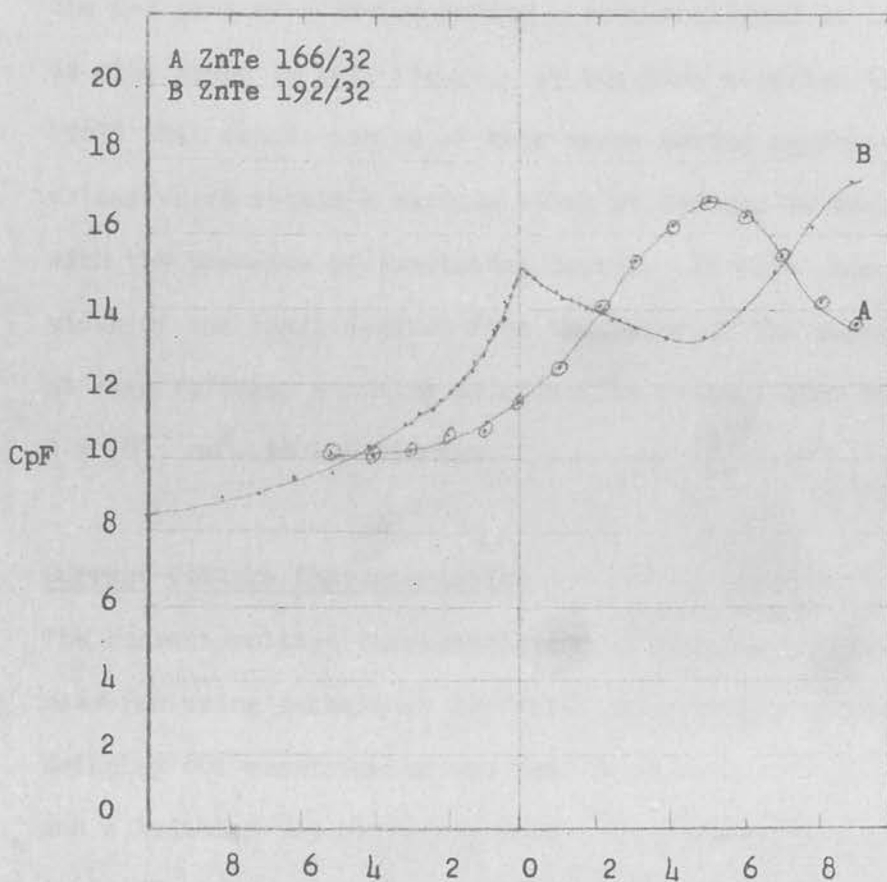

FIGURE 5.19 Capacitance vs. Voltage for polycrystalline ZnTe Devices. Polarity indicated is that of top contact to device.

No.192/32 is a result of the combination of the capacitance of the two junction regions, of which for a given polarity, one is forward-biased and the other reverse-biased. The sign of the applied voltages relates to the polarity applied to the top contact of the crystal. For comparison purposes the C-V plot of a device having a vacuum-alloyed In contact is also shown in this figure. It has been asserted (Fenner, 1967) that relationships of this shape having capacitance values which attain a maximum value at V=0 can be associated with the presence of insulating layers. In this case the width of the layer derived from the value of the capacitance at zero voltage, assuming an effective contact area of 3×10^{-3} cm^2, is 1.5 microns.

Current-Voltage Characteristics

The current-voltage characteristics of various devices were measured using techniques described previously in which a Keithley 601 electrometer was used to measure current levels and a Keithley 513 micro-voltmeter the corresponding potential difference across the device. Fig. 5.20 shows the results obtained for device 166/32. By the use of forced convection the device temperature was maintained at 293°K. For low voltage levels up to 1.0V a linear relationship exists between current and voltage. Above this voltage a transition occurs to a square-law region, rapidly followed

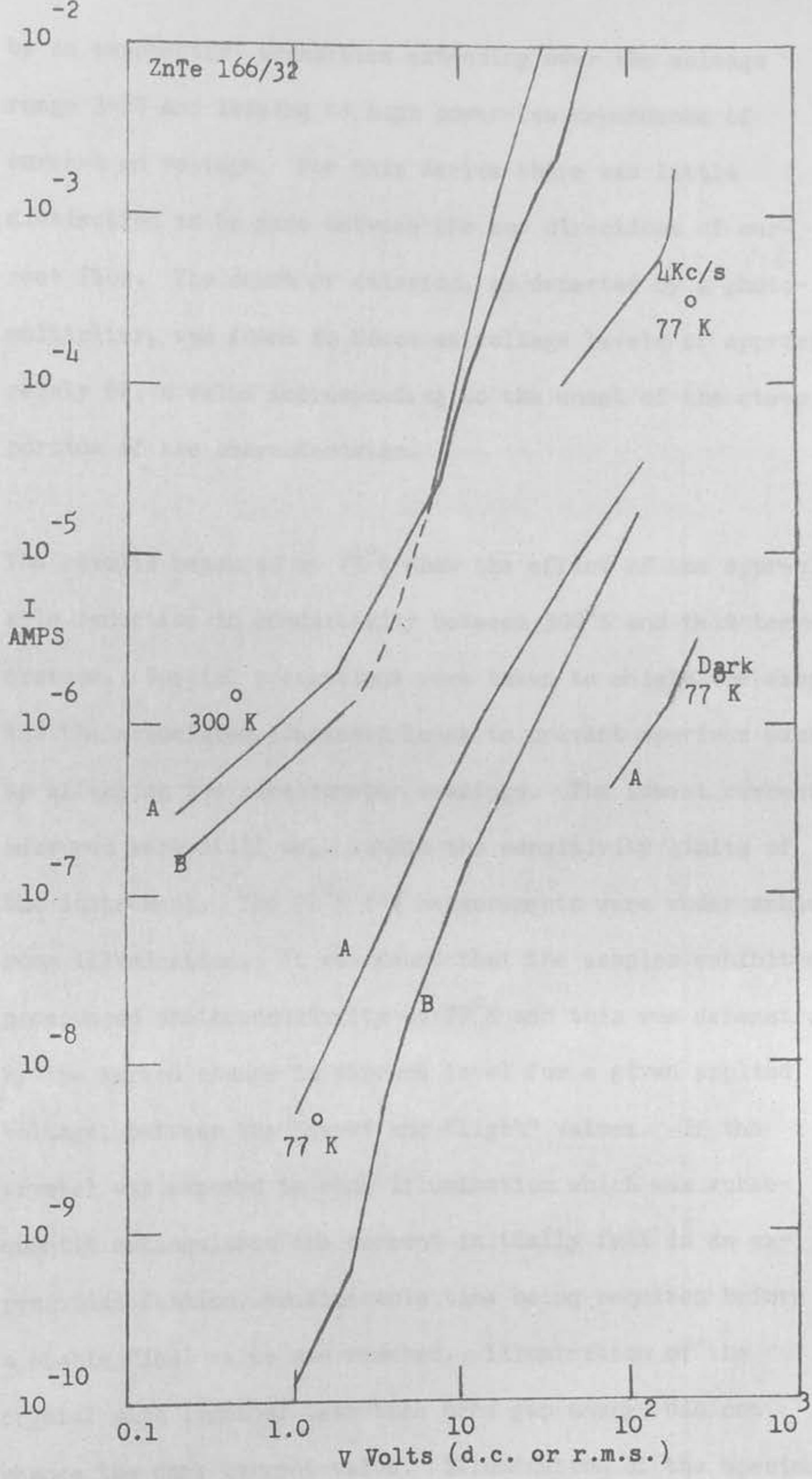

<u>FIGURE 5.20</u> Current versus voltage for a polycrystalline ZnTe device. Curves marked A or B measured under 120 ft.L. illumination.
A Top contact negative
B Top contact positive

by an exponential transition extending over the voltage range 3-8V and leading to high power-law dependence of current on voltage. For this device there was little distinction to be made between the two directions of current flow. The onset of emission, as detected by a photomultiplier, was found to occur at voltage levels of approximately 6V, a value corresponding to the onset of the steep portion of the characteristic.

The results measured at 77°K show the effect of the appreciable reduction in conductivity between 300°K and this temperature. Special precautions were taken to shield the sample and the associated connected leads to prevent spurious pick-up affecting the electrometer readings. The lowest currents measured were still well within the sensitivity limits of the instrument. The 77°K I-V measurements were under ambient room illumination. It was found that the samples exhibited pronounced photoconductivity at 77°K and this was demonstrated by the marked change in current level for a given applied voltage, between the "dark" and "light" values. If the crystal was exposed to room illumination which was subsequently extinguished the current initially fell in an exponential fashion, considerable time being required before a stable final value was reached. Illumination of the crystal with light of less than band gap energy did not change the dark current value. Illumination of the specimen

with light of ultraviolet wavelengths produced the most rapid and pronounced change in the dark current, the current level rising by a factor of 100. The increase obtained using light in the wavelength range 4000-6000Å did not match this, a factor of 10 increase being obtained; the radiant flux incident on the device from the two sources was approximately equal. It was noted that if a crystal which had been allowed to stabilise in room illumination was exposed to light in the 4000-6000Å band then the current was reduced. Also, exposure of the crystal to this illumination upon extinction of the room light resulted in a more rapid decrease in current than would otherwise have been obtained. These phenomona are not amenable to immediate interpretation, but are considered to indicate the presence of complex trapping levels. No detailed experiments were conducted into the low-temperature photoconductive properties of polycrystalline ZnTe although without doubt interesting results would be obtained from investigations of optically stimulated currents, and perhaps result in a more detailed understanding of the effects of trapping levels on the optical properties of this material. At room temperature the photoconductive properties were not at all pronounced, variations of less than 1% being obtained between the room illumination and dark current levels. Similarly photoconductive effects

were not apparent under alternating field excitation. Presumably at the frequencies used the trapping levels responsible for the reduced currents found under d.c. excitation are unoccupied. This may be considered an indication that the capture time of these centres is long in comparison to the period of the exciting waveform.

Due to the high resistivity of the material at liquid nitrogen temperature it proved impossible to obtain emission under direct-current excitation. This can be attributed to the reduction of bulk conductivity to a point where the conduction processes become limited by bulk effects such as the impedance of grain boundaries for example. Although the logarithmic graph does not exhibit linear regions of the type obtained at room temperature, the overall shape of the curve approximates to a square-law relationship. The reduced current levels obtained for one direction of current flow, in the absence of any illumination and over a limited range of voltage levels, are also shown in this figure. The current-voltage relationship obtained under 4Kc/s excitation shows a sharp increase in current at a voltage level corresponding to the onset of emission. This effect is similar to that observed at room temperature. It is possible that photoconductive effects induced in the crystal by the internally generated emission were responsible

in part, for the increase in current levels. However, this is considered unlikely, since at the frequency used, photo-conductivity could not be stimulated by external illumination. Under a.c. excitation it is not necessary for carriers to traverse the bulk of the material and charge transport within the surface and barrier layers can lead to a.c. current flow and, presumably, concomitant excitation and emission processes. As the actual location of the emission under low temperature alternating field excitation was not determined, it is, therefore, quite feasible that emission occurred throughout the bulk of the sample, and may have resulted from the existence of collision-acceleration phenomena occurring in the vicinity of structural defects and grain boundaries. It would be expected that at such imperfections localised fields of magnitude sufficient to permit the maintenance of these processes might exist. Similarly, by analogy with electroluminescent phenomena observed in II-VI compounds suspended in dielectric media, the effects of polarisation fields and the field-influenced release of carriers from trapping levels in this insulating material might have a dominant influence on the electroluminescent properties of the devices under alternating field excitation.

For this material the room temperature the I-V characteristics indicate the onset of conductivity modulation. Whether this originates in double injection effects, field ionisation of

trapping levels, or the optical stimulation of carriers as a result of self-induced photoconductivity is not apparent from the available experimental evidence.

Emission Intensity-Current Characteristics

The room temperature emission intensity as a function of current was measured using both d.c. and pulsed excitation and for both directions of current flow. Under d.c. excitation the onset of emission, as detected by the 7265 photomultiplier used in the measurements, coincided with a current level of 1.5×10^{-5} amps and emission intensities were recorded up to current levels of 8×10^{-3} amps. This current level was extended using pulse excitation, of repetition rate 50cps and width 5μsec, to 3×10^{-2} amps, corresponding to a current density of $30A/cm^2$. The response of a device to pulsed and a.c. excitation is shown in Plates 5.2 and 5.3 respectively. Pulses were obtained from a Hewlett Packard 214A pulse generator and the a.c. signal from a Hewlett Packard audio oscillator and power amplifier. The waveform applied to the devices together with the output obtained from the photomultiplier were displayed on a Hewlett Packard 175 dual-trace oscilloscope. The rise- and fall-time of the emission waveform as shown in Plate 5.2 is 2.5μsec. The a.c. response demonstrates clearly that a higher emission intensity is obtained for one direction of current flow, but that the shape of the emission waveform remains identical

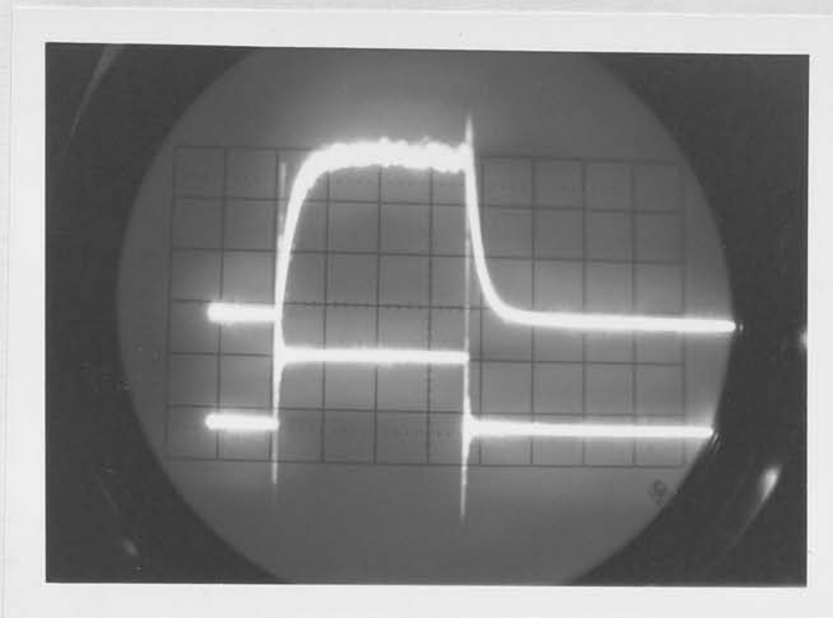

(a) Emission response of polycrystalline ZnTe device to pulsed excitation (pulse width 5 μ-sec, repetition rate 50 cps)

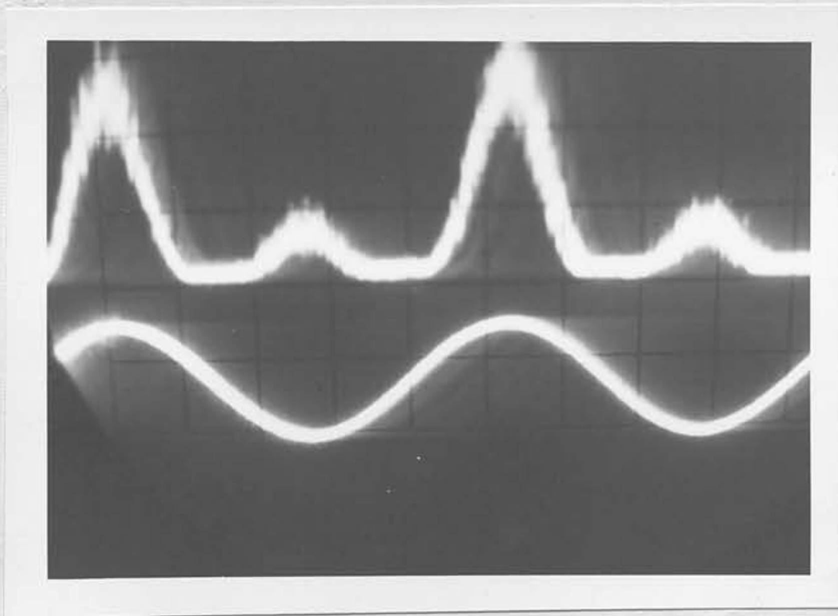

(b) Emission response of polycrystalline ZnTe device to a.c. excitation (frequency 4 Kc/s)

Plate 5.2

for the two current directions. The presence of noise on the photomultiplier output waveform is considered further evidence in support of an emission mechanism related to avalanche breakdown effects probably in the high-field regions of the reverse-biased metal:semiconductor contact.

Although for a number of other electroluminescent materials (e.g. GaP) it has been suggested that the emission efficiency is capable of improvement by the utilisation of crystals containing structural faults and grain boundaries, this was not found to be the case with this particular form of ZnTe. Due to the high resistivity of the material the voltage levels required to obtain emission were normally in excess of those required with monocrystalline material. In addition, the emission intensities were low, in general a factor of two or three less than values representative of electroluminescence observed at reverse-biased metal:semiconductor contacts in other ZnTe devices. External quantum efficiencies, as estimated from the observed emission intensities, were of the order of 10^{-6} to 10^{-7} photons/electron.

From the results of the investigations on this material the conclusion that electroluminescence results from impact ionisation or pair production processes at a reverse-biased junction appears justified. The spatial origin of the emission and its dependence on polarity, the broad emission

spectrum, and the linear dependence of emission intensity on current level are all factors which support this mechanism. It is feasible that the mechanism of tunnel injection proposed by Eastman et al. (1964) to explain the observed emission at reverse-biased In:ZnTe junctions is also operative in this material; however, the results appear adequately explained by the more familiar impact-ionisation model. The room temperature emission spectrum, when examined in conjunction with the absorption spectrum of the material, indicates the possible existence of intraband transitions. The 77°K spectrum reveals the presence of an impurity level of unknown origin and also indicates that other recombinations may involve isoelectronic oxygen centres. The excitation mechanism of majority carrier tunnel injection may also be operative in this material. Finally the experiments revealed some interesting low temperature photoconductive properties of the material.

5.2.5 Special Devices

Some investigations were conducted into the effects of evaporated and diffused impurity layers on electroluminescence in the various crystal types.

Manganese Films

Mn films were evaporated onto cleaved faces of crystals from growth run No.13. These layers, 1200Å thick, were

diffused for 24 hours at 500°C. Using pressure and indium soldered contacts no emission was observed if the Mn layer was interposed between the In contact and the crystal. Also, in this configuration the high-power law dependence of current on voltage was not observed and the I-V characteristic more closely approximated ohmic behaviour. This is an indication of the contact dependence of the emission process. Further investigations using this material are warranted, as there are relatively few materials which have found to make good ohmic contact to ZnTe.

Indium and Gold Films

In the use of undiffused In and Au films with this form of ZnTe, contact was made to the layers using In solder. Emission was observed in the high current direction; this originated from the region of the In layer. No emission associated with the Au contact was detected. These devices exhibited definite rectification characteristics which can be described by the term "poor diode". Typical current-voltage characteristics are shown in Fig. 5.21. For a minority carrier injection excitation mechanism, the I-V characteristic frequently obeys the diode equation, $I = I_o \exp(\frac{qV}{\beta kT} - 1)$, with a value of the constant of approximately 2. Applying this equation to the results of Fig.5.21 results in a β value of 40. This value is of the same order as that obtained from exponential regions observed in

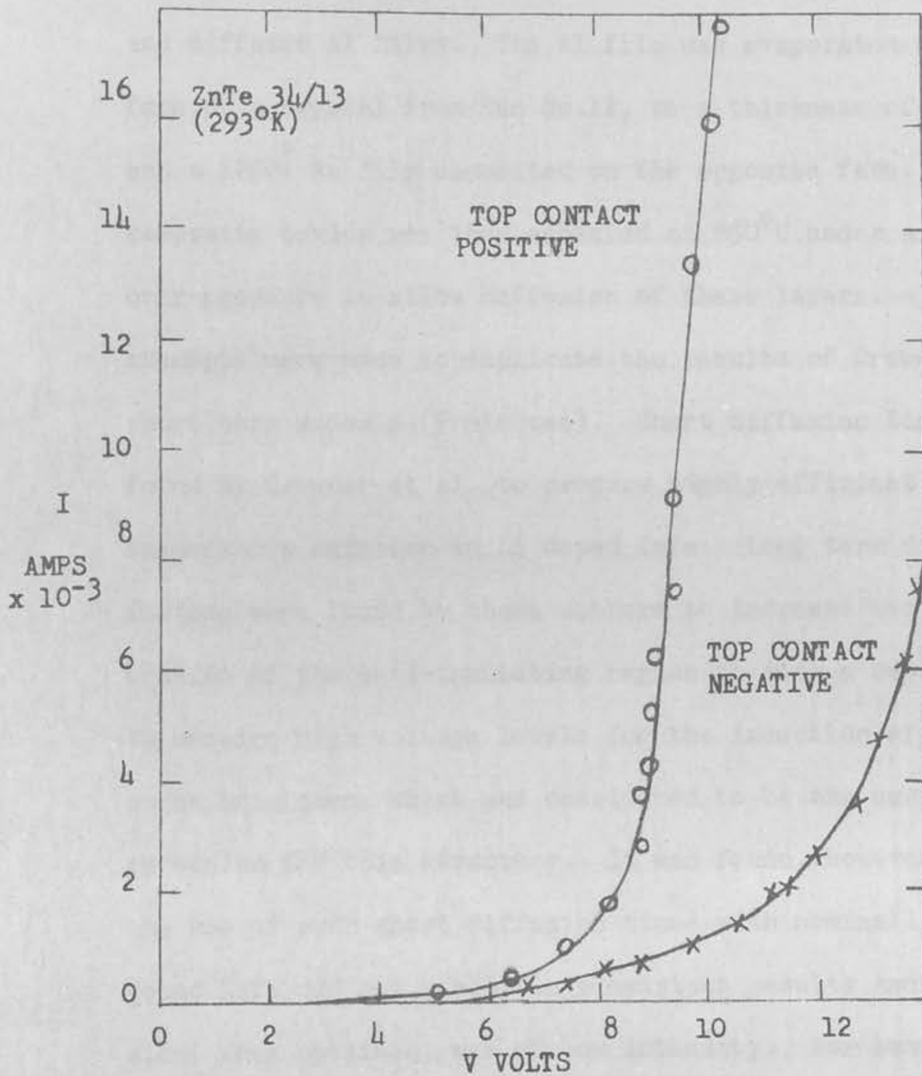

FIGURE 5.21 Current versus voltage for ZnTe device 34/13.
Top contact; evaporated and undiffused Au.
Bottom contact; evaporated and undiffused In.

the I-V characteristics of other ZnTe devices.

Aluminium Films

The most interesting results were found using evaporated and diffused Al films. The Al film was evaporated on one face of a crystal from Run No.12, to a thickness of 6000Å and a 1200Å Au film deposited on the opposite face. The composite device was then annealed at 850°C under a Zn over-pressure to allow diffusion of these layers. Initially attempts were made to duplicate the results of Crowder using short term anneals (5 minutes). Short diffusion times were found by Crowder et al. to produce highly efficient low temperature emission in Li doped ZnTe. Long term diffusions were found by these authors to increase the penetration of the semi-insulating region to such a depth as to require high voltage levels for the induction of avalanche breakdown, which was considered to be the excitation mechanism for this structure. It was found, however, that the use of such short diffusion times with nominally undoped ZnTe did not result in consistent results and emission, when obtained, was of low intensity. For succeeding specimens the diffusion conditions anneal times were altered from 5minutes at 850°C to 16 hours at 600°C. These devices showed no significant rectification properties, although slightly higher current levels were obtained for a positive potential applied to the Au film. Emission was

observed with a negative potential applied to the Au film. This emission was green in colour and formed a broken line around the edge of the crystal above the Al layer. At the same time reddish-orange emission was observed near the top Au contact. No emission was observed for the reversed polarity. The green emission line possibly marks the penetration depth of the semi-insulating Al layer. The emission intensity was found to increase linearly with current. This green emission can most readily be explained by the presence of recombinations involving energetic carriers. These "hot" carriers are envisaged to acquire energies in excess of the band-gap value as a result of impact ionisation, or perhaps majority carrier tunneling, processes taking place at the Al-ZnTe:ZnTe junction. The nature of the high-resistivity Al-doped ZnTe layer may be more conducive to energetic carrier formation than the semi-insulating layers representative of In contacts. Although the emission spectrum of these devices was not measured, the remaining characteristics are in keeping with an avalanche breakdown type of excitation process. Such a process would be expected to result in a broad emission spectrum extending to longer wavelengths. It is conceivable that the green emission corresponds to a secondary peak of this spectrum and appears prominent due to the sensitivity of the eye to wavelengths in this region. (The possibility of the formation during the annealing procedure of a green-emitting IV-VI compound (AlTe) is not

considered tenable.) If these recombinations take place throughout the plane of the Al:ZnTe junction, it is possible that the emission located in regions near the crystal faces will not be strongly absorbed. Under reverse bias, the impact generated electrons would be constrained to the junction region. Alternatively, the majority of carriers may tunnel through the contact barrier, becoming "hot" in the high field of the depletion layer. Some of these acquire sufficient energy to impact-ionise the lattice or possible luminescence centres. The impact generated electrons recombine either directly or via centres with other holes. Since the recombining holes are not at the top of the valence band the spectral shift to shorter wavelengths can be explained. The weak emission at the Au contact may be an indication that this contact is not ohmic at high current levels and that an inefficient form of injection occurs on the application of a negative potential to this electrode.

These experiments were repeated using single crystal material from run No.13. The electro-optical characteristics of these devices were similar to those described above for material No.12. The use of additional diffused layers did not result in any noticeable improvement in the electroluminescent efficiency of the devices.

More extensive investigations are necessary to fully evaluate the material and device properties resulting from processing procedures of the type described above.

6. DISCUSSION AND CONCLUSIONS

In the foregoing chapters the results of experiments conducted into the growth of ZnTe crystals, the electrical transport and optical properties of the material, and the electrical and optical characteristics of a variety of ZnTe electroluminescent devices have been presented. This section is devoted to an overall review and discussion of the experimental results.

Crystal Growth

There are several conclusions which can be drawn from the crystal growth experiments. As with all other semiconducting crystal growth procedures, the primary aim is to produce large volume, good quality crystals, preferably by a technique which permits the introduction of selected impurities while maintaining at a minimum the concentration of undesirable contaminants. The results obtained here, in common with many other growth procedures utilised in the production of compound semiconductor crystals, fell short of this ideal. In no crystal growth techniques were large volume single crystals obtained. However, from the majority of runs, single crystal regions could be selected of ample volume for device fabrication or the preparation of material analysis samples. With regard to dopant incorporation, the majority of growth procedures placed little restriction on the introduction of desired impurities. In only one growth run, however, was an impurity deliberately introduced; this refers to the incorporation of oxygen from the residual atmosphere maintained over the constituents. For the case of

solution regrowth dopants could be added to the melt, and for Bridgman growth either the liquid or vapour phase is suitable for this purpose. In the latter method the dopant can normally only be introduced from the vapour phase. The technique of solution regrowth is particularly useful in cases where large concentrations of dopants are required. The level of contaminants introduced during the majority of crystal growth procedures was not considered to be significant. It is indisputable, however, that the purity level of the starting material would be reduced by handling procedures and the introduction of the constituents into the growth ampoule. During the sealing-off of the ampoule the constituents would be exposed to Si vapour and other elements present in the quartz tubing. Further concentrations of these impurities would also be realised during the heating cycle, particularly the high temperature anneal.

The most successful growth techniques were those involving vapour phase growth or, in prolonged Bridgman techniques, heat soaking followed by slow withdrawal of the melt from the high temperature zone. The results obtained have indicated possible improvements in the crystal growth procedures used, and also other alternative procedures which should produce more satisfactory results. Firstly it is apparent that, in Bridgman growth, the quality and size of crystals produced is dependent on the withdrawal or recrystallisation rate. One major problem encountered was the formation of gaseous included volumes (voids)

in the recrystallised boule. From this it is concluded that the vapour pressure of ZnTe exceeds one atmosphere at the melting point and also under the normally off-stoichiometric excesses of Te used. It is considered that an overpressure of two to three atmospheres of an inert gas may result in effective suppression of bubbling in the melt, and result in the growth of larger, non-voided, crystalline regions. It would also appear necessary to maintain a sharp furnace profile, and this may best be attained by the use of an R.F. generator to heat a zone defined by the length of a graphite susceptor, in conjunction with a resistively heated secondary coil maintained at a temperature below the recrystallisation temperature of the melt. For the case of vapour phase growth, a significant improvement would no doubt be obtained by the provision of an initial nucleation site in the form of a capillary tip extending from the high temperature zone into cooler regions of the furnace. The additional use of a system for withdrawing the furnace past a stationary ampoule, thus preventing vibrational disturbances adversely affecting the nucleation procedure as the single crystal region increases in length and cross-section, would prove an asset. This technique has the further advantages that the capillary tip acts as a trap for excess elemental material, the composition can automatically adjust to the minimum decomposition pressure, and doping gases can be introduced through the capillary. In the growth of oxygen doped ZnTe crystals a technique broadly similar to that advocated was used, although no attempt was made to generate a nucleation front by movement of eitherthe ampoule or the furnace.

Solution regrowth of ZnTe is considered to present attractive possibilities. Such procedures have the advantage that growth can take place at relatively low temperatures. Although regrowth from either a Zn or Te solution presents difficulties due to the requirement of a selective etch for the elements, regrowth from a variety of other solvents is quite feasible. A further advantage is ease with which dopants can be incorporated in crystals grown by this method. Solution regrowth from donor solutions resulted in high resistivity crystals. The conductivity-type of these crystals was not determined; it is, however, considered unlikely that n-type crystals would be produced. This difficulty in achieving n-type conductivity in ZnTe, thus prohibiting the fabrication of p-n quasihomojunction devices, has been considered to result from self-compensation in the material. This situation is predominant in crystals with wide bandgap and low cohesion energy in which the energy gained by transition of carriers from an added doping ion into vacancy levels exceeds the formation energy of the vacancy. The differences in behaviour between ZnO, ZnS, ZnSe and CdS which tend to become n-type can be explained from the differences in the depths of the levels of the compensating vacancy of these materials, which in turn can qualitatively be understood from an argument involving the ratio of the cation to anion diameter. It would appear that the concentrations of vacancies in II-VI compounds is very high, of the order of 10^{19} - 10^{20} per cm^{-3}. Thus, any attempts to introduce donor dopants into ZnTe would require a growth technique which efficiently

suppressed vacancy formation. The only technique which has demonstrated any degree of success in the growth of n-type crystals utilised a high pressure autoclave and a growth procedure involving quenching of an excess Zn mix. This technique was considered to reduce the native defect concentration (Fischer, 1965). It would, therefore, be anticipated that crystals grown from an In solution would, at best, display highly resistive p-type conductivity. It is also probable that the carrier mobility of ZnTe crystals thus grown is low, thereby reducing the magnitude of thermoelectric voltages and rendering difficult measurements of conductivity-type by this method. The wide application of solution regrowth techniques to the preparation of single crystals used in the fabrication of high-efficiency GaP electroluminescent devices illustrates the merits of this type of growth procedure.

Devices

Devices were fabricated from crystals obtained in the majority of growth procedures, and results obtained from representative batches and also from crystals exhibiting special characteristics have been described in detail. Distinct variations were observed in the electrical and optical properties of devices representative of several growth runs. This is considered to be due partly to variations in the material properties and partly to other factors associated with crystal processing and subsequent device fabrication techniques to which the material was subjected. For example, in the semi-insulating ZnTe exhibiting at room temper-

ature relatively high resistivity and low carrier concentration, a significantly different degree of compensation must exist compared with the other forms of the material. Two separate compensating conditions can be envisaged which could result in material parameters of the order obtained. Firstly, for a weakly compensated material a model is considered in which the density of acceptor states, N_A, is much greater than the effective density of compensating donor states, N_D, which in turn is greater than p, the free hole concentration. With both p and n (the corresponding free electron concentration) small, the conventional semiconductor relationships pertaining to charge balance and donor and acceptor levels and their relationships with the carrier concentrations, activation energy of the defects, Fermi level, and temperature, indicate that, for $N_D = 10^{-2}N_A$, the Fermi level E_F lies nearer to the valence band than the acceptor levels and p and ρ have values of the order of those given in Table 4.2. Alternatively, these values could also be obtained if the material was strongly compensated, i.e. $N_A - N_D \ll N_A \approx N_D$ and $N_A \approx N_D \gg p$. With $N_A > 10^{14} cm^{-3}$ and $N_D = 0.99\ N_A$ and where p and n are again small, then similar values of carrier concentration and resistivity to those given above will result; in this case, however, the acceptor level will lie below the Fermi level. It is obvious that the former argument involving low concentrations of donors is more acceptable in terms of the known growth conditions. The other forms of ZnTe having lower values of resistivity and carrier concen-

trations in excess of $10^{16}/cm^3$, can again be considered in terms of a model for weakly compensated extrinsic material, $N_D \ll N_A$. In this case, either p is large but n is small, $N_D \ll p$, with E_F below E_A, or a similar situation can exist where the acceptors are fully ionised so that $p = N_A$ and the Fermi level lies above E_A. Values of $N_A = 10^{17}$ with $N_D < 10^{15}$ cm^{-3} would result in conductivity and resistivity values similar to those found in practice. For both the above crystal types the concentration of donor levels may be significantly increased in the surface layers of the crystal as a result of the contacting process. For example, if it is assumed that the initial linear slope in the room-temperature I-V characteristic of the oxygen-doped ZnTe (Fig.5.15) is indicative of the resistivity of an insulating layer of thickness 1 micron, as determined from capacitance-voltage measurements, then a resistivity of 10^5 ohm-cm is indicated. Taking as the hole mobility for the layer the value 40cm^2/Vsec found in the bulk material (Table 4.2) the estimated carrier concentration is 2×10^{12} cm^{-3}.

The majority of devices studied were contacted using In or In/Ag alloys for at least one of the contacts. The hypothesis has been advanced that variations existed in the nature of the metal:semiconductor junction which were dependent on the contact application technique. These variations were considered to result in different forms of excitation mechanism and differentiation has been made between electroluminescence associated with

forward and reverse-biased junctions.

The main emphasis in the experimental investigations has been on room-temperature electroluminescence, mainly for the reasons that few previous investigations into the electroluminescence of ZnTe devices had been made at these temperatures and in particular emission of useful brightness levels had not been reported at room temperature. It was therefore of considerable interest to evaluate the operating characteristics, emission spectra, brightness levels, and emission efficiencies of devices operating under these conditions; in short, an evaluation of the potential of ZnTe as a room-temperature emitter. Unfortunately, the majority of the previous results provide little information on the electroluminescent efficiency of ZnTe devices at low temperatures and in the remainder of the literature low temperature efficiencies ranging from 10^{-6} to 10^{-2} photons/electron have been reported. No information is available on room-temperature efficiencies. The results described here therefore represent the first evaluation of room temperature efficiencies of ZnTe devices and are combined with detailed considerations of other operating characteristics also previously unreported. For a considerable number of devices measurements were also conducted at 77°K, allowing more direct comparison with previously reported results. This comparison indicated that the low-temperature efficiencies of devices fabricated from nominally undoped material were considerably less than the optimum values

reported in the literature yet higher than the minimum values. The room temperature efficiencies were comparable with the lower range of efficiencies reported by other authors at low temperatures. It was noted that the temperature quenching of the electroluminescence, i.e. the reduction of emission efficiency with increasing temperature, was not so pronounced in nominally undoped ZnTe as the exponential dependence on temperature observed by previous authors for the case of II-VI p-n quasi-homojunction and heterojunction devices. Therefore, the temperature quenching of the "excitation efficiency" associated with impact ionisation processes may be less pronounced than that of minority carrier injection. This is considered to result from the fact that quenching of emission is less temperature sensitive for impact-ionisation than carrier injection excitation processes.

Outstanding results were obtained for devices fabricated from ZnTe crystals incorporating isoelectronic oxygen centres. The low temperature emission efficiencies were reduced by only an order of magnitude compared with the maximum low-temperature efficiency reported to date in ZnTe devices. The devices in which this was attained were fabricated from Li doped ZnTe, and, significantly, an impact-ionisation/avalanche injection mechanism was considered to be operative in these m-i-p structures (Crowder et al., 1966). In addition the room temperature

emission efficiency of oxygen-doped ZnTe was found to be only a factor of 10 less than the low temperature value. This result permits favourable comparisons to be drawn between the electroluminescent properties of ZnTe devices fabricated from this material and electroluminescent devices fabricated from other II-VI compounds either in the form of single-conductivity type devices or p-n quasi-homojunction and heterojunction structures. As discussed at length in section 5.3, this is primarily attributed to the maintenance over a wide range of temperature of the radiative efficiency associated with recombinations involving these deep oxygen levels. It is quite conceivable that the application of similarly doped material in device structures utilising improved blocking contacts, insulating barrier layers, or alloyed quasi-homojunctions, may result in efficient room temperature electroluminescence.

Although initial attempts to create m-i-p devices in oxygen-doped ZnTe by the in-diffusion of Al to form a semi-insulating region did not result in improved efficiency, it is considered that further investigations of this type of device structure are warranted. Such devices, by virtue of (1) the reduced temperature dependence of the emission efficiency resulting from impact ionisation excitation processes, (2) the increased recombination efficiency resulting from the injection of impact-ionised minority carriers into the bulk of the semiconductor,

and (3) the effective suppression of the deleterious effects of majority carrier extraction by the presence of an insulating layer, may provide an answer to the problem of achieving efficient injection luminescence in a material which can be usefully made in only one conductivity type. Moreover, for room temperature applications p-n quasihomojunction devices have two disadvantages which limit the emission efficiency - (1) the difficulty in achieving high carrier concentrations at the junction (2) the pronounced temperature quenching of the emission, normally attributed to the thermal ionisation of carriers from the ground state of the luminescence centre and their subsequent transfer to non-radiative centres. ZnTe:O m-i-p structures may therefore prove to be more efficient room temperature emitters than p-n quasi-homojunction fabricated from alloyed crystals of the type $ZnSe_xTe_{1-x}$. At present, the room temperature efficiencies of the ZnTe:O devices described in section 5.3 compare favourably with the values reported for $ZnSe_xTe_{1-x}$ quasi-homojunctions. In these studies no experiments were conducted at temperatures below 77°K. Investigations at temperatures in the liquid helium range are desirable since measurements of low temperature absorption, fluorescence, and emission spectra permit analysis of the nature of the impurity levels incorporated in the material and an understanding may be gained of the mechanisms of radiative recombination transitions in the material. In the case of ZnTe crystals believed to incorporate oxygen, such measurements would indicate whether the radiative recom-

binations involve an uncharged centre substituting isoelectronically for Te and acting as an electron trap, or whether donor-acceptor pair transitions occur between the native defect acceptor levels and ionised donor levels of unknown origin.

Emission Spectra

The emission spectra of devices fabricated from nominally undoped crystals exhibited a broad emission band typical of an impact-ionisation process involving carriers having a wide distribution of energies. The maxima of the emission spectrum occurred at wavelengths just above the absorption edge of the material. This so-called "edge emission" resulting from the recombination of electron-hole pairs produced by ionisation of the lattice is, in the absence of a high concentration if interband luminescence centres, statistically the most probable recombination. A minor peak located in the red region of the specrrum was tentatively identified as due to transitions resulting from ionisation of isoelectric oxygen acceptor centres (electron traps). These centres were presumed to be incorporated in the crystal in reduced concentrations either during growth or in the reaction of the elemental constituents.

For crystals incorporating large concentrations of oxygen in excess of 10^{18} cm^{-3}, pronounced emission peaks were observed in the red region of the spectrum at both $77^{o}K$ and $300^{o}K$. The position of the peaks indicated a centre located approximately 0.4eV from the valence or conduction band edge. One disadvantage

of ZnTe:O is that the room-temperature emission peaks at a wavelength of 6960Å. The ideal emitter would possess an emission peak in the same region of the spectrum as the maximum sensitivity of the eye, ie. 5400Å. Fortunately due to the broad nature of the spectrum in ZnTe:O, (680Å half width) the emission is maintained down to wavelengths clearly visible to the eye. In this emission spectrum the minority of recombinations involve near band-gap transitions. This is indicated by the presence of peaks at wavelengths just above the absorption edge of the material but drastically reduced in amplitude in comparison with the main emission peak. It was considered that in this case also the emission resulted from avalanche injection of impact-ionised minority carriers; however, for this material, the majority of recombinations involved carriers trapped on oxygen centres. Analysis of the current-voltage characteristics of typical ZnTe:O devices revealed the presence of a trap level 0.45eV from the valence band edge. Perhaps fortuitously, this corresponds to the location of the impurity level, assuming the position of the emission peak to be associated with transitions between the conduction band and this centre.

The emission spectrum of polycrystalline ZnTe devices indicated that at low temperature a large proportion of the recombinations involved a deep centre of unknown origin. The remainder of the spectrum possessed the characteristics of impact ionisation electroluminescence with a secondary peak located near the band-

gap energy of the material. Again a minor peak was observed at a wavelength which permitted correlation with the pre-determined isoelectronic oxygen level in ZnTe. For the room temperature emission the broad spectrum was again obtained, but in this case no structural detail could be resolved.

Mechanisms

The observed optical and electrical properties of the devices permit distinctions to be made between the various possible excitation mechanisms. The interpretation a number of the experimental results, particularly those relating to the electrical characteristics, is complicated by the fact that in many cases both contacts to the device are blocking in nature, and therefore the rectification properties of each contact has an influence on the form of the overall current-voltage characteristic. For example, if one contact to the device formed a metal: semiconductor Schottky barrier and the other incorporated an insulating surface layer then, for a given total voltage applied to the device, it would be difficult to predict the distribution of the electric field between the two junctions and the bulk of the semiconductor. Over certain ranges of voltage it would be expected that the characteristics of one of the contact junctions would have a dominant influence on the overall current level attained and high currents could probably only be achieved when the field developed across the reverse-biased junction was sufficient to cause breakdown. These arguments would be rendered

invalid, however, if tunnelling processes dominated the transfer of carriers across the reverse-biased junction, or if the diffusion length of minority carriers and the physical dimensions of the device were such that carriers entering the bulk of the semiconductor at the forward-biased junction reached the opposite junction before recombining. Another exception would arise if the characteristics of the composite device were controlled by space-charge-limited currents in a localised insulating region or in the bulk of a semi-insulating crystal. Alternatively, by extension of this latter consideration, the overall current levels may depend on double injection of carriers into a narrow insulating layer from the adjacent electrode and semiconductor regions or into the bulk of the semi-insulating crystal from the two contact junctions.

Restricting considerations of mechanisms to the particular junction with which the electroluminescence was associated facilitates analysis of the experimental results. Consideration can then be given to excitation and recombination processes occuring at several different forms of electrode-semiconductor junction. They comprise:

1. For forward-biased junctions -

(a) Injection at Schottky barriers and physical inversion layers (Fig.2.9)

(b) Tunnel injection electroluminescence at insulating (m-i-p) or semi-insulating (m-si-p) contact layers (Fig.2.10)

(c) Double injection in insulating or semi-insulating layers.

(d) Impact ionisation and avalanche injection in localised high field regions ((m-i-p) or (m-si-p)) (Fig.2.12).

2. For reverse-biased junctions.

(a) Impact ionisation in Schottky depletion layers (Fig.2.11) and m-i-p- or m-si-p contact layers.

(b) Tunnel injection at depletion layer barriers (2.11) or m-i-p contact layers.

(c) Impact ionisation at internal localised high-field regions (refers to a.c. electroluminescence in polycrystalline ZnTe).

As indicated above, illustrations of schematic models corresponding to a number of these processes have been presented previously (section 2.2.3.1).

For the case of electroluminescence at forward biased junctions, minority carrier injection at Schottky barriers and physical inversion layers is excluded as a possible mechanism, due to the lack of correlation between the predictions of this model and the observed electrical and optical characteristics of the devices.

The incidence of tunnel injection processes is dependent on the formation of an insulating or semi-insulating layer of thickness 50-500Å at the interface between the metal electrode and the bulk of the semiconductor. In addition to the thickness of the layer, and the energy-gap and work function of the insulator

are important factors in determining whether tunnelling is possible. As discussed previously, it is desirable in such processes for the insulator to have an energy gap and work-function which enhances the injection of minority carriers and suppresses the extraction of majority carriers. For a number of ZnTe devices it is considered that semi-insulating regions were created during the contacting process. Difficulties were encountered in confirming the presence of these layers by physical measurements. The measured dependence of junction capacitance on applied voltage was considered to be indicative of the presence of an insulating region and the layer thickness obtained therefrom. It should be stated, however, that in the absence of a complete analysis of capacitance-voltage characteristics for such complex double junction structures this interpretation remains unsubstantiated. The physical characteristics of the insulating layer also depend on whether it is formed from a material unrelated to both the metal electrode and the semiconductor, or whether it is created from the introduction of an impurity into the surface layer of the semiconductor thus rendering it insulating. In the majority of reports concerned with tunnel injection electroluminescence the former model is advocated. Nevertheless, tunnel injection processes could also be envisaged to take place at an insulating layer of the latter type. Further experiments utilising insulating films at the metal:semiconductor interface

and also compensated surface layers are necessary to fully elucidate the influence of tunnel-injection processes on the electroluminescence of ZnTe devices. Although it is possible to ascribe the electroluminescence observed under forward bias to tunnel injection processes, it would be anticipated that under these conditions emission would be observed at much lower applied voltage levels than were found in practice; this dependence is complicated by the presence of a second non-ohmic contact, which may effectively limit the current at low applied voltages. The effects of trapping levels and surface states are also of importance in this connection. The observed temperature dependence of the current-voltage characteristics could be considered to be another factor at variance with the tunnel-injection model. It would also be anticipated that the emission spectrum associated with the recombination of carriers introduced into the semiconductor by quantum mechanical tunneling would be relatively narrow, and, in the case of nominally undoped material, correspond to the band-gap energy. The fact that forward-biased electroluminescence was observed throughout the bulk of the crystal rather than in the region of the cathodic contact, as would be expected for tunnel injection, is a further objection to this mechanism. Although a tunnel injection process is not considered directly responsible for the observed electroluminescence, it is conceivable that the introduction of minority carriers into the crystal may be related to this process with radiative recombination

taking place subsequent to further excitation processes such as impact ionisation or volume controlled double-injection.

Next considered are possible mechanisms whereby emission results from recombinations occurring within the insulating or semi-insulating region itself, rather than as a result of recombination involving minority carriers which tunnel through the insulating layer as discussed in the preceeding paragraphs. This phenomena involves considerations of space-charge-limited currents resulting from the development of high voltages across thin insulating crystals or insulating regions within a crystal. CdS is the classic II-VI compound in which these effects have been observed. The current-voltage characteristics obtained for ZnTe devices are similar in many respects to those considered typical of SCLC injection processes. Analysis of the characteristics has indicated the presence of deep trapping levels having densities of the order of $10^{16}/cm^3$. The trap depth determined for a number of devices fabricated from crystals of several growth runs has a value (0.4eV) which can be correlated with the position of the major peak in ZnTe:O devices and minor peaks in a number of devices fabricated from nominally undoped and polycrystalline material. For the majority of crystals utilised in device fabrication the applied voltage levels when considered in conjunction with the physical dimensions of the devices result in fields of insufficient magnitude to allow realistic consideration of volume controlled injection processes.

That is, the injection of carriers from the contact regions with recombinations taking place throughout the bulk of the crystal. (A possible exception to this is the high resistivity ZnTe discussed in section 5.1). Considerations of these phenomena must be restricted to their occurrence in narrow semi-insulating layers. Once again recognition must be made of the influence of the non-ohmic contacts on these processes. For example, if the injection efficiency of the contact junction is low for one type of carrier, then the current levels obtained may be contact limited. Conversely, the contact resistance could decrease markedly with increasing field as in the case of field emission and Schottky emission (contact breakdown). It is, therefore, conceivable that the current could be contact limited at low voltages but become volume controlled at high voltages. Complications of this sort could be reflected in the I-V characteristics. With relevance to the observed results it could be argued that sudden increases in current level could result if one contact inefficiently injected minority carriers and these were trapped and stored in deep traps. If the trapped electrons have a long life-time then a situation arises analagous to that in a photoconductor. The trapped electrons alleviate the space-charge repulsion for hole flow, so that a higher hole current starts to flow. These carriers may transfer their energy to minority carriers as they reach the field of the cathode thus enabling the minority carriers to traverse the contact barrier, be injected and subsequently trapped. This regenerative condition

could lead to current instability. It has been shown by application of Lampert's single-carrier SCLC theory to ZnTe:O devices that the experimental I-V characteristics can be considered to represent, at high voltages, the onset of field ionisation of traps or the initiation of a double injection regime, resulting, at some critical field, in a decrease by several orders of magnitude in the resistance of the insulating layer. For the latter case the overlap of the space charge regions resulting from the injection of electrons and holes is referred to as mutual space-charge compensation. These effects could also be dependent on trapping effects as discussed above or on the creation of electron-hole pairs by self-absorption of the emitted radiation with the subsequent trapping of one carrier in photoconductivity centres and an increase in the current associated with the other carrier. If volume-controlled double injection were to occur in the bulk of the crystal, this could explain the observation of emission regions remote from the contact. The presence of a contact junction incorporating an insulating layer could prove beneficial in this case, due to the suppression of carrier extraction and accompanying increase in recombination efficiency.

It is apparent from the foregoing that the interpretation of the observed electroluminescence on the basis of SCLC and double injection effects requires ramification to account for the influence of non-ohmic contacts and the various other factors

which can additionally affect the injection properties and current voltage characteristics of devices. These considerations cannot be excluded since they explain, in a limited way, a number of the observed results. In terms of satisfactory explanation for the electroluminescence observed at forward-biased junctions this model, even with its attendant ambiguities, is considered to offer a feasible alternative to the favoured impact ionisation model discussed below. As stated previously, it is conceivable that these processes may take place in conjunction with other excitation mechanisms.

It is contended that the least complex and most suitable mechanism to explain the observed electroluminescence at forward-biased junctions is a process of impact ionisation occurring in localised high field region either associated with an interfacial insulating layer or a semi-insulating region created at the surface of the ZnTe crystal by the in-diffusion of compensating donor impurities during the contacting procedure (Fig. 2.12). The potential drop and field in these localised regions are considered to be adequate to accelerate carriers to energies where impact ionisation of luminescent centres, other levels, and the lattice is possible. A stationary microplasma of electrons and holes is formed in this high-field region at the cathodic contact. From this micro-plasma minority carriers are then injected into the bulk of the semiconductor, where

they recombine radiatively. The electrical and optical properties of the devices would appear to be consistent with this model. These included the sharp rise in current at critical fields, the lack of temperature dependence of the applied voltage at which the current increase was observed, and the broad emission spectrum. The presence of the insulating region is beneficial in restricting the outflow of majority carriers into the metal electrode. For the case of ZnTe:O the presence of an efficient luminescence centre results in a marked improvement in the efficiency of the devices. It is considered that a model based on the formation of a semi-insulating layer by compensation of the surface region of the semiconductor may have a higher radiative efficiency than models based on chemically distinct insulating layers, since the number of non-radiative surface and interfacial states would be expected to be greater in the latter.

For electroluminescence observed at reverse-biased junctions it is concluded that the observed results are, for the majority of cases, satisfactorily explained by an impact ionisation or pair production mechanism. In this case the high-field necessary for carrier acceleration is visualised as being developed at a Schottky type depletion layer or at an insulating layer interposed between the metal electrode and the bulk of the semiconductor. For this bias direction the impact generated

minority carriers are constrained to the region of the junction.

Quantum mechanical Zener tunneling of carriers through the barrier has been discussed previously and although this model could explain a number of the observed properties of the devices it is considered less satisfactory than the impact ionisation model. One disadvantage is that the electron-hole pairs created by tunneling through the barrier of the depletion layer would appear to be subjected to the intense field of the depletion layer and may therefore be separated, with the electrons being accelerated and extracted into the positive metal contact. This mechanism cannot be excluded, however, as it has been conclusively demonstrated to be responsible for the emission observed in elemental semiconductors (Henisch, 1962). One factor in its favour is that the impact ionisation, or avalanche, process is traditionally considered to result in a high level of electrical noise and concomitant pulsing of the emitted radiation. With the exception of polycrystalline ZnTe this was not observed in practice. Another is that avalanche breakdown is capable of initiation by optical stimulation. This was not found to be the case in ZnTe. However, this may be a result of the poor photoconductive properties ofthe material rather than an indication of a Zener breakdown process.

The electroluminescence observed in polycrystalline ZnTe devices under d.c. excitation is associated with an impact ionisation

process occurring at the reverse biased junction. Under a.c. excitation it is considered that the same mechanism may apply; however, due to the heterogeneous nature of the samples, the possibility of bulk excitation resulting from collision acceleration processes at multiple internal high-field regions cannot be excluded. The observation that the emission waveform duplicates the shape of the excitation waveform without the presence of phase changes or secondary peaks indicates that the mechanism in this material is less complicated than that of electroluminescence in polycrystalline ZnS devices.

The above discussion indicates that the electroluminescent properties of the devices investigated can be explained in terms of a single excitation mechanism. The complex nature of the devices and the form of the observed electro-optical characteristics allows considerations of alternative mechanisms or combinations of mechanisms which may be operative in the stimulation of electroluminescence in ZnTe. (For example, field emission processes have not been considered in detail.) The mechanism of impact ionisation is one of the most complicated, and least understood, phenomena arising from semiconductor junction processes, and it is therefore possible that the study of devices of the type considered in this dissertation may permit a deeper understanding of the kinetics of these processes.

In summary, the properties of a wide range of devices fabricated from ZnTe crystals prepared by a variety of growth procedures have been described and the results interpreted in terms of several mechanisms. The feasibility of attaining room temperature electroluminescence in ZnTe has been demonstrated and it has proved possible to significantly improve the quantum efficiency of the electroluminescence by the incorporation in the crystals of luminescent centres possissing high radiative efficiency over a wide range of temperatures. For devices operating by an impact ionisation mechanism operative at a forward-biased junction the radiative efficiency is considered to be further improved by the avalanche injection of impact-ionised minority carriers into the bulk of the semiconductor, and the suppression of majority carrier extraction by the use of metal-semi-insulator-semconductor, structures.

This type of device is one approach to the problem of achieving efficient room-temperature electroluminescence in wide-gap semiconductors which do not exhibit amphoteric conductivity. With the advance of materials technology and improvements in crystal growth techniques it may prove possible to develop efficient injection structures of the metal-semi-insulator-semiconductor type or to incorporate material containing efficient luminescent centres in p-n quasi-homojunctions devices prepared from alloyed II-VI compounds.

APPENDIX 1

THEORETICAL CONSIDERATIONS OF BAND STRUCTURE

As discussed in section 2.2 this appendix reviews some aspects of the theoretical background of the electronic band structure of solids. As the concepts involved are applicable to the field of solid state physics in general and are developed in detail in numerous texts, it is considered adequate to indicate the results of these treatments which appear relevant to the II-VI compounds in general and ZnTe in particular.

The theoretical development of the subject considers the idealised perfect crystal in the absence of lattice vibrations. By definition of a crystal lattice, translation by vectors

$$R_n = n_1 a_1 + n_2 a_2 + n_3 a_3 \qquad \text{(A.1)}$$

$$n_i = 0, \pm 1, \pm 2 \ldots\ldots,$$

results in an array identical to the original. Here a_1, a_2 and a_3 are called the primitive translation vectors, their three-dimensional indices depending on the crystal type under consideration. The crystal space is filled with unit cells centered on R_n.

Associated with R_n, and more specifically with the primitive translation vectors a_i are three independent vectors defined by

$$\kappa_i \cdot a_j = 2\pi \delta_{ij} \qquad \text{(A.2)}$$

where the Kronecker delta δ_{ij} has a value of 1 if i = j and is 0 if i ≠ j. These three vectors in turn determine another lattice K_n, termed the "reciprocal lattice" which possesses analagous translation vectors to eq. (A.1), and gives rise to the concept of k - space. The unit cell in k - space constructed for each reciprocal lattice is the Brillouin zone. For the case of a simple cubic lattice the Brillouin zone is a cube. For zinc blende crystals having the translational symmetry of the face-centered cubic lattice the primitive translation vectors are:

$$a_1 = 1/2\ a\ (1,1,0)\ a_2 = 1/2\ a\ (1,0,1)$$

$$a_3 = 1/2\ a\ (0,1,1) \text{ where a is a cube edge.}$$

The basis vector, that separating the anion and cation of the unit cell is b = 1/4 a (1,1,1). Using eq. (A.2) we find the primitive translation vectors for the reciprocal lattice which has the b.c.c structure, are:

$$\mathcal{K}_1 = 2\pi a^{-1}\ (1,1,-1)\ \mathcal{K}_2 = 2\pi a^{-1}\ (1,-1,1)$$

$$\mathcal{K}_3 = 2\pi a^{-1}\ (-1,1,1)$$

The Brillouin zone for this reciprocal lattice can be taken to be the truncated octahedron shown in Fig. (A.1). The points and lines of special symmetry are indicated with their conventional labels. As a result of the periodicity of all physical quantities (e.g. the electron density (r) at the position r, or the total potential energy V(r) must be invariant under the translation r → r + Rn

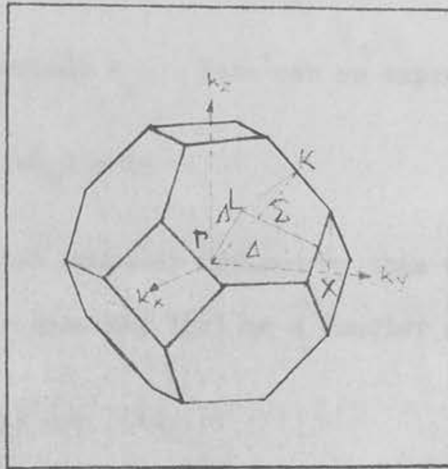

FIGURE A.1 The Brillouin zone for lattices with face-centred-cubic translational symmetry (i.e. the zincblende and diamond lattices) with lines and points of special symmetry.

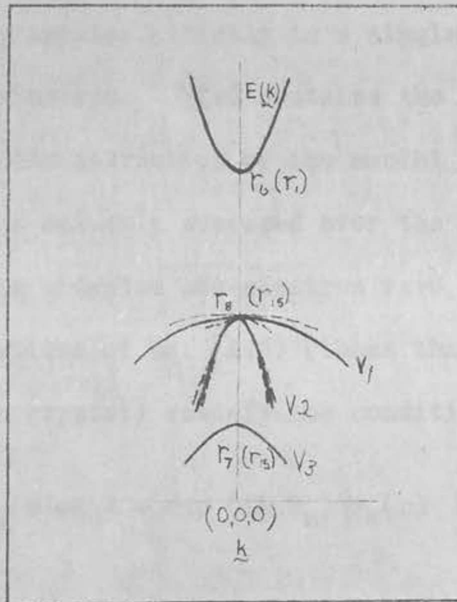

FIGURE A.2 The conduction and spin-orbit valence bands of a zincblende crystal. Irreducible representations for the group without spin are shown in parentheses. The others are for the double group. The effects of small linear terms resulting from the lack of inversion symmetry are shown schematically by the dashed curves.

i.e. are periodic with periods a_i. This can be expressed as:

$$T_n V(r) = V(r+R_n) = Vr \tag{A.3}$$

where T_n is the translation operator defined by this equation. Expansion of the periodic quantity V(r) as a Fourier series gives:

$$V(r) = \sum_n V(K_n) \exp (iK_n.r) \tag{A.4}$$

The time-independent Schrödinger equation for an electron in this potential well in terms of the electron wave function $\psi(r)$ is:

$$\mathcal{H}\psi(r) = -\hbar^2/2m\nabla^2\psi(r) + V(r)\psi(r) = E\psi(r) \tag{A.5}$$

Where $\mathcal{H}$ is the Hamiltonian operator and ∇^2 is the Laplacian operator. This equation only applies strictly to a single electron - the "one-electron" approximation. V(r) contains the sum of contributions corresponding to the attraction by the nuclei and the repulsion ofthe other electrons suitably averaged over the charge distribution derived from the occupied one-electron wave functions. The well-known Bloch solutions of eq. (A.5) (those that remain bounded throughout an infinite crystal) satisfy the condition.

$$T_n\psi (r) = \psi_k(r +R_n) + \exp (iR.R_n)\psi_k(r) \tag{A.6}$$

Here $\psi_k(r)$ has the form:

$$\psi_R(r) = \exp (ik.r)\, u_k(r) \tag{A.7}$$

where $u_k(r)$ is a periodic function of R_n. Thus k is a quantum number and $\hbar k$ is sometimes referred to a crystal momentum. There are ranges of E,(energy eigenvalues of the state ψ_k), or bands, in which

Bloch solutions exist, and forbidden bands, where they do not exist.

The finite size of the crystal under consideration results in a quasi-continuous spectrum of k values. Choosing periodic boundary conditions gives

$$\psi_k(r) = \psi_k (r + N_i a_i) \qquad (A.8)$$

where N_i (i = 1,2,3) is a finite but large integer so that $N_i a$ is of macroscopic dimensions. From these conditions result the fact that the total number of k values equals the number of unit cells in the volume V over which the periodic boundary conditions are applied.

Although the k-vector is defined by eq. (A.6) this equation does not uniquely define k since states with wave vectors k and $k + K_n$ behave "equivalently" under T_n as:

$$T_n \psi_{k + Kn} = \exp.\ (ik.R_n)\ (\psi_k + K_n) \text{ under eq. (A.2)}$$

k values within the first Brillouin zone can therefore be considered; any k outside the first zone could be replaced by an "equivalent" $k + K_n$ within the zone - this is termed the reduced zone scheme. For any given reduced wave vector k there will be a number of discrete eigenvalues E(k) illustrating that E(k) is a multi-valued function of k. It therefore results that in order to describe a state we must specify in addition to the quantum number a discrete quantum number μ so that the energy eigenvalues and Bloch functions are written:- $E_\mu(k)$ and $\psi_{k\mu}(r)$ respectively. The separation of

the eigenvalues is extremely small for a macroscopic crystal. The spectrum can be regarded as continuous and therefore each $E_{\mu}(k)$ as a continuous function of k. The energy bands are differential to all orders except at a k where there is a degeneracy.

Theoretical investigations of energy band structure frequently involve two limiting cases. These are the tight-binding and nearly-free electron limits. Both these methods are simplifications of the actual problem, but, with suitable modifications, they provide a useful insight into the electronic energy band structure of many materials.

The tight-binding approximation involves suitable linear combinations of localised functions, such as atomic orbitals $\varphi(r)$ which satisfy the Bloch condition of eq. (A.6).

$$\psi_k(r) = N^{-1/2} \sum_n \exp(ik.R_n)\, \varphi(r-R_n) \qquad (A.9)$$

where N is the number of identical atoms comprising the crystal. The expectation value of the energy comprises the atomic energy value plus k-dependent terms involving the overlap of atomic functions centred on different atoms. For tightly bound orbitals the overlap between nearest neighbours is all that has to be retained, leading, for the case of a simple cubic lattice and an

atomic s-state, to

$$E(k) = E_o + 2\ (\cos k_x a + \cos k_y a + \cos k_z a) \int \varphi^*(r) V(r) \varphi(r - a_1) d^3r \qquad (A.10)$$

The splitting of the energy arises from differences in the charge density in the region between the atoms for states of different k. For k=0 the amplitudes from neighbouring atoms add, whereas, at the zone boundary i.e. $k = \pi a^{-1}(0,0,1)$, the phase of the orbitals on the atoms at $(0,0,\pm a)$ is opposite that at $R_n = 0$, so that the charge density drops to zero midway between these atoms. If, as expected, V(r) is attractive in the region of large overlap, the integral in eq. (A.10) will be negative. This results in the frequently presented figure showing E(k) vs. k for k along one crystal axis (say (0,0,1)) with the s-band lowest at k=0 and highest at the zone boundary. Consideration of degenerate atomic levels e.g. p-states, results in modifications of eq. (A.10) and, due to complexity of analysis, are normally determined for particular crystal directions.

For the other limiting case, the nearly-free electron approximation, the V(r) are conveniently expressed in terms of its Fourier expansion, eq. (A.4). The relevant terms of the expansion are limited in this approximation, and the electrons have in the zeroth-order an energy $E^o(k) = \hbar^2 k^2/2m$ and a wave function $\psi_k^o = \mathcal{V}^{-1/2} \exp(ik.r)$. Correction to the energy due to the periodic potential $V(r) = \sum_n V(K_n) \exp(iK_n.r)$ are accounted for by perturbation theory. The energy

thus obtained is given by

$$E(k) = E^{o}(k) + (2m/\hbar^{2})\ V^{2}\ (100) \sum_{n}(k^{2}-(k + K_{n})^{2})^{-1} \qquad (A.11)$$

where the sum is over the vectors $K_n = 2\pi a^{-1}\ (1,0,0),\ 2\pi a^{-1}\ (0,1,0)$ etc. The second term is small except when k approaches the zone boundary at which point $E^{o}(k) = E^{o}(k + K_n)$ where the term becomes infinite. This is due to the energies of the unperturbed states of equivalent wave vectors k and k + K being sufficiently close that they become strongly intermixed even when the perturbation is weak. Simple perturbation theory is inadequate here and the Hamiltonian associated with the interaction matrix must be set up. This leads to an energy

$$E(k)=1/2(E^{o}(k)+E^{o}(k+K_{n})) \pm 1/2\ ((E^{o}(k)-E^{o}(k+K_{n}))^{2}+4V^{2}(K_{n}))^{1/2} \quad (A.12)$$

The energy gap at the zone boundary is $2V(K_n)$. The wave functions for the states k have the form

$$\psi_{k}(\pm) = (1+b(K_{n})^{2})^{-1/2}\ \exp(ik.r)\ (1\pm b(K_{n})\ \exp(iK_{n}.r)),$$

where the $b(K_n)$ determines the amount of the Bragg reflected wave that is mixed into the zeroth-order wave function. The term in brackets is periodic in R as required by the Bloch conditions. At

the zone boundary b = ±1 and the wave functions are simply cos k.r and sin k.r.

As a generalisation it can be said that the tight-binding methods are appropriate to insulators and large band-gap semiconductors, and the free-electron methods to metals and small band-gap semiconductors. The tight-binding picture would be expected to be applicable too for the core states and perhaps for deep valence bands. Since the free-electron model does not reflect the atomic character of $\psi(r)$ in the core region it is therefore a limited approximation. To describe the rapid atomic oscillations in V(r) and $\psi(r)$ for small r, K_n, large compared with the reciprocal of the core radius, must be included in their Fourier expansions. However, when the Bloch functions expressed in terms of a Fourier expansion are made orthogonal to the lower energy states of the same reduced k-vector as is required, certain "orthogonalisation" terms are introduced into the Schrödinger equations for the Fourier coefficients. In analysis it is found that these terms largely cancel the atomic potentials in the core region (Cohen and Heine, 1961). The net result is a quasi-Schrödinger equation for the slowly varying parts of ψ which contain a relatively weak residual potential and is the basis of the "pseudo-potential" method. Because of its simplicity and the fact that $V(K_n)$ are directly related to certain band gaps which can be determined experimentally the pseudo-potential method is useful as a phenomenological interpolation scheme. This method has been applied by Cohen and Bergstrasser (1965) to a variety of materials

including a number of II-VI compounds. The energy bands of ZnTe were empirically determined by these authors; in this work the maxima and minima of the valence and conduction band were located at k=0. The fact that there are other symmetry operations besides the translations which transform the crystal into itself (reflection, rotation, and inversion operations) has important ramifications on some of the properties of the energy bands. This subject requires the application of group theoretical techniques. For the case of crystals of the zinc blende form, detailed studies of the symmetry properties of the energy bands have been carried out by Dresselhaus (1955) and Parmenter (1955). The character table, selection rules and spin-orbit splittings for the group of k=0(T) are given in Table A.1. This table utilises the commonly accepted notation used for indexing the symmetry properties of states of a given k. At the head of each column the "classes" of symmetry operators are detailed, those associated with the symmetry properties of Bloch states with spin are denoted by bars over the corresponding rotations and reflections. The left-hand column indicates the possible types of symmetry states which are directly related to, or belong to, the "irreducible representations" considered in group theory. The first column indicates the degree of degeneracy of the various states. The "selection rules" from which it can be determined which states can make allowed transitions to a state belonging to a particular irreducible representation are also indicated, as are the extra representations associated with spin-orbit splitting. The conduct-

TABLE A.1 (after Segall, 1967)

Character table of the double group of Γ (i.e. k = 0) for zinc blende

Γ	E	$\bar{E}$	$6C_4^2$	$8C_3$	$8\bar{C}_3$	$6JC_4$	$6J\bar{C}_4$	$12JC_2$
Γ_1	1	1	1	1	1	1	1	1
Γ_2	1	1	1	1	1	-1	-1	-1
Γ_{12}	2	2	2	-1	-1	0	0	0
Γ_{15}	3	3	-1	0	0	-1	-1	1
Γ_{25}	3	3	-1	0	0	1	1	-1
Γ_6	2	-2	0	1	-1	$\sqrt{2}$	$-\sqrt{2}$	0
Γ_7	2	-2	0	1	-1	$-\sqrt{2}$	$\sqrt{2}$	0
Γ_8	4	-4	0	-1	1	0	0	0

Γ_i	Γ_1	Γ_2	Γ_{12}	Γ_{15}	Γ_{25}
$\Gamma_i \times \Gamma_{1/2}$	Γ_6	Γ_7	Γ_8	$\Gamma_7+\Gamma_8$	$\Gamma_6+\Gamma_8$

Selection rules

Γ_i	Γ_1	Γ_2	Γ_{12}	Γ_{15}	Γ_{25}	Γ_6	Γ_7	Γ_8
$\Gamma_i \times \Gamma_d (=\Gamma_{15})$	Γ_{15}	Γ_{25}	$\Gamma_{15}+\Gamma_{25}$	$\Gamma_i+\Gamma_{12}+\Gamma_{15}+\Gamma_{25}$	$\Gamma_2+\Gamma_{12}+\Gamma_{15}+\Gamma_{25}$	$\Gamma_7+\Gamma_8$	$\Gamma_6+\Gamma_8$	$\Gamma_6+\Gamma_7+2\Gamma_8$

ion and spin-orbit split valence bands of a zinc blende crystal around k=0 are shown in Fig.A.2. The band structure of the more complex wurtzite structure is not considered here.

In the majority of properties relating to the semiconducting nature of a compound the principal band edges (i.e. the bands in the vicinity of the absolute minimum of the conduction band and maximum of the valence band) are of primary importance. The majority of such information, or the verification of theoretical evaluation, relates to measurements made on the optical and electrical properties of the material. Less is known about the principal band edges of ZnTe than those of several other II-VI compounds. This is due, in part, to the fact that zinc telluride can only be made in p-type form (or high resistance n-type) and electrical measurements therefore only give information about the valence band. However, the results and conclusions drawn from the electrical measurements (Aven and Segall, 1963) are quite similar to those for p-type CdTe (i.e. they are in agreement with the theoretical band structure considerations in suggesting a k=0 maximum). The calculated electron g-factor, effective electron mass and effective hole mass are 0.17, 0.4 and 1.0 respectively. Recent piezoelectric studies (Sagar and Lehmann, 1965) also suggest that the valence band structure is of the type pictured in Fig.A.2. The optical properties have also not received detailed investigation but the intrinsic band edge absorption properties appear to be similar to those of CdTe and ZnSe. These optical properties

show sharp direct exciton lines in the immediate vicinity of the fundamental absorption edge. This also would indicate that ZnTe is a direct-gap material.

Information relating to energy bands at points and energies other than those for the principal extrema are of interest. A normal technique in evaluating band structure is the evaluation of band gaps at critical points in the zone, with subsequent interpolation between the remaining parts of the bands by various procedures (eg. pseudo-potentials). These investigations are mainly concerned with optical transitions such as reflectivity (transmission measurements are not easily applicable at energies lower than the band-gap energy), and photoemission. The effects of these higher energy transitions will not be considered further.

APPENDIX 2

THEORETICAL CONSIDERATIONS OF OPTICAL PROPERTIES

In this appendix the Wannier (1937) model for the exciton system considered appropriate to the II-VI compounds (Segall and Marple, 1967) is presented. Also considered are the theoretical aspects of the optical absorption properties of "direct" and "indirect" gap II-VI compounds. Use is made of the derivations presented in appendix 1.

The Wannier model is applicable to weak electron-hole interaction resulting from configurations where the electron and hole are on widely separated sites and execute large orbits about their centre of mass with motions determined by such properties of the conduction and valence band edges as the effective masses m_e^* and m_h^*. In many respects this system behaves like the hydrogen atom, i.e. it has a hydrogenic spectrum.

Wannier excitons are describable in terms of perturbed band states and therefore can be treated by effective-mass theory in a similar way as charged impurities in semiconductors (Segall, 1967). The exciton waveform is taken as a linear combination of band states, and since the electron-hole interaction is weak, only the lowest conduction band and highest valence band need be included in the expansion of Ψ so that

$$\Psi(r_e, r_h) = \sum_{k_e k_h} C(k_e, k_h) \psi^*_{c, k_e}(r_e) \psi_{v, k_h}(r_h) \qquad (A.13)$$

A quasi-kinetic energy operator is derived from the expression for the energy bands in the vicinity of the band extrema in terms of the difference $E_c(k_e) - E_v(k_h) - E_G$ (E_G band-gap). The Fourier transform for $C(k_e,k_h)$ then satisfies an "effective mass" equation of the type derived by Dresselhaus (1956). The simplest application of this effective-mass derivation is the case of simple spherical bands, those appropriate for a cubic material at k = 0. The problem has the same formulation as the hydrogen atom. The interaction depends on the relative position of hole and electron, $r = r_e - r_h$, and on relative momentum $k = 1/2\ (k_e - k_h)$ but not on the total momentum $K = k_e + k_h$. The solutions of the effective-mass equation are of the form

$$\Phi_{K,n} = \mathcal{V}^{-1/2} \exp(iK.R)\ \varphi_n(r) \qquad (A.14)$$

where Φ represents $C(k_e,k_h)$ and R is the transformation separating the centre of mass and internal motion;

$$R = (m_e^* + m_h^*)^{-1}\ (m_e^* r_e + m_h r_h)$$

In eq. (A.14) $\varphi_n(r)$ describes the state of internal motion and satisfies the Schrödinger equation.

$$(-(\hbar^2/2\mu)\nabla^2 - e^2/\mathcal{K}_s r)\varphi_n = \mathcal{E}_n\varphi_n \qquad (A.15)$$

Here the reduced mass μ is given by,

$$\mu^{-1} = m_e^{*-1} + m_h^{*-1}$$

$\mathcal{V}$ is the volume of the crystal and $\mathcal{K}$ is the appropriate dielectric constant. The $\varphi_n(r)$ can be identified with the atomic hydrogenic functions except that $a_{ex} = a_{o\ s}\ m/\mu$ replaces the Bohr atomic radius a_o. The resulting spectrum for the exciton energy $E_{exn}(K)$ is

$$E_{exn}(K) = E_G + 1/2\hbar^2K^2/M + \mathcal{E}_n, \qquad (A.16)$$

where $M = m_e^* + m_h^*$. This consists of the sum of the centre-of-mass kinetic energy and the K-independent internal energy

$$_n = -e^2/2\mathcal{K}_s a_{ex} n^2 = -G/n^2 \text{ or } \hbar^2K^2/2 \qquad (A.17)$$

for the discrete and continuous spectrum, respectively. Thus the exciton spectrum consists of a series of discrete parabolic bands below E_G at K=0 which merge into a continuium at higher energies, as shown in Fig. A.3. G is the binding energy of the hydrogenic spectrum.

One extremely important parameter in considerations of the electroluminescence materials relates to the interaction leading to absorption of photons and the criterion for characterising transitions. The interaction can be expressed as

$$q(nm)^{-1} A\ (\mathcal{k}) \sum_j \exp\ (i\mathcal{k} r_j)\ \xi_{\mathcal{k}} p_j$$

$$= \ q(nmc)^{-1}\ (\hbar/\nu)^{1/2}\ b_{\mathcal{k}} \sum_j \exp(i\mathcal{k} r_j)\ \xi_{\mathcal{k}} p_j \qquad (A.18)$$

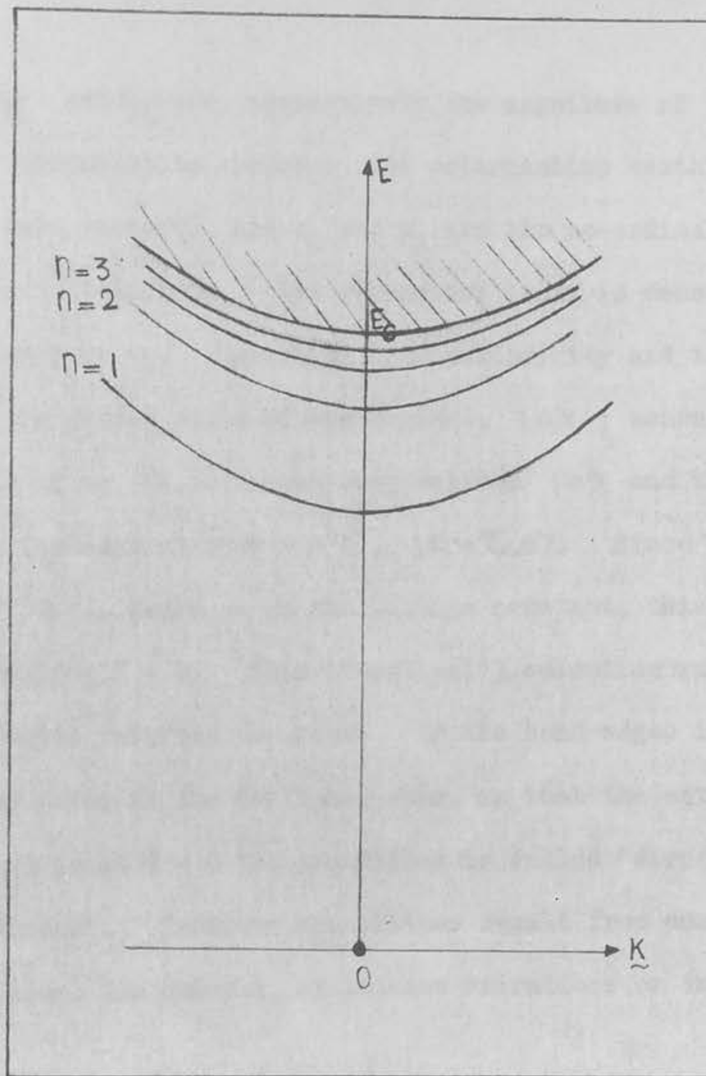

FIGURE A.3 Energy of the exciton bands, E_{exn}, for Wannier excitons as a function of exciton momentum K as given by eq. (A.17). The discrete "hydrogenic" states merge into the continuum for $E>E_G$. The point 0 represents the energy of the unexcited crystal.

where $A(\kappa)$, b_{κ} and $\xi_{\eta\kappa}$ are, respectively, the magnitude of the vector potential, the annihilation operator, and polarisation vector for the photon of wave vector κ, and r_j and p_j are the co-ordinate and momentum of the jth electron. The refractive index is denoted by n and the frequency by ν. Resulting from periodicity and the fact that K =0 for the ground state of the crystal, $|o\rangle$, nonvanishing matrix elements of eq. (A.18) occur only between $|o\rangle$ and those exciton states (in band n) with $K = \kappa$, $|K = \kappa, n\rangle$. Since κ is very small ($\kappa a/2\pi \sim 10^{-3}$), where a is the lattice constant, this condition amounts to requiring K = 0. This ("vertical") selection rule provides the criterion referred to above. If the band edges involved are at the same point in the Brillouin zone, so that the extremum of the exciton band is at K = 0 the transition is called "direct", otherwise "indirect". Indirect transitions result from destruction of crystal perfection, for example, by lattice vibrations or impurities.

The classification of a prospective electroluminescent material as either a "direct" or "indirect" emitter is of considerable relevance to the resulting properties of the device. In particular the stimulation of coherent emission can only be produced in a direct-gap material, and the characteristics of spontaneous emission in respect of the efficiency, radiative recombination processes, impurity band emission, and the effectiveness of non-radiative recombination centres are dependent on the form of the band-gap transition.

Optical absorption processes can be divided into at least two broad classes. The first is concerned with intrinsic absorption processes and the second with extrinsic absorption such as exciton-defect complexes. Investigation related to the fundamental band structure of a material are concerned primarily with intrinsic absorption and necessitate the use of high purity crystals. It would appear that a number of absorption effects attributed to intrinsic absorption can be explained by the presence of exciton defect complexes. One example of this is the postulation of indirect band-gaps in some of the II-VI compounds (e.g. CdTe) from the results of optical absorption measurements, which are not substantiated by subsequent measurements on higher-purity crystals.

Much of the theoretical background of intrinsic optical absorption by direct exciton processes has been contained in the publications of Elliot(1957), Dresselhaus (1957), and Hopfield (1960). Many aspects of optical absorption have been reviewed by Reynolds et al., (1965).

In the case of direct transitions, the transition rate between $|0\rangle$, a state of assumed zero energy, and the exciton state $|K,n\rangle$ can be evaluated from eq. (A.18), leading to an absorption constant obtained from

$$\alpha = n(cN_\nu(\mathrm{T}))^{-1}\sum_n R_n \qquad \text{(A.19)}$$

where R_n is the transition rate obtained from eq. (A.18) and $N(\Upsilon)$ is the density of photons of wave vector Υ. The summation is over all internal quantum numbers consistent with energy conservation. The use of equations used in the outline of exciton theory allows the development of the matrix element for these transitions and this is found to consist of a modulating envelope function incorporated with Bloch functions of "atomic" character. Selection rules for weakly bound excitons are arrived at by consideration of the matrix element, and these have been discussed by Hopfield (1960). Transitions can be classified as "allowed" or "forbidden" depending on whether or not the equation representing the matrix element vanishes as $\Upsilon \to 0$. In the simple and important case of $k = 0$ the electron and hole functions transform as Γ_c and Γ_v representations of the group of $k = 0$. The possible overall exciton symmetries Γ_x for a given Γ_n are contained in the direct product $\Gamma_n \times \Gamma_v \times \Gamma_c$ (Landau and Lifschitz, 1958). The transition to Γ_x from the ground state (which has symmetry Γ_1) is allowed if $\Gamma_x \times \Gamma_d$ contains Γ_1 where Γ_d is a representation that the dipole operator belongs to.

From the evaluation of the strength of the direct allowed transitions the oscillator strength per molecule of the sharp lines was evaluated by Elliott (1957). For the simple case of $k_o = 0$ extrema with spherical masses, the absorption lines occur at

$$h\nu = E_G - G/n^2 \qquad \text{(A.20)}$$

where G is given by eq. (A.17).

It also results from this analysis that the absorption coefficient for the true continium taken as $h\nu - E_G \equiv \Delta E > 0$ has a proportionality

$$\alpha \sim E^{1/2} \tag{A.21}$$

under the condition that ΔE tends to infinity. (α is the absorption coefficient.)

This result finds application in analysis of experimental absorption spectra and in the absorption edge region this relationship is used as confirmation of the occurrence of direct transitions.

The indirect band-to-band absorption process (Bardeen et al., 1956) requires the annihilation or creation of phonons in order to conserve the electronic quasi-momentum Elliott (1957) has discussed the indirect absorption process which leads to creation of excitons with $K \neq 0$, and is similar to the band to band case except that the exciton nature of the states involved is taken into account. Direct and indirect band-to-band absorption are illustrated in Fig. A.4. In the indirect case when initially the conduction band is empty and the valence band filled, absorption of photon and phonon leads to the final state consisting of a hole with $k_h \cong 0$ and an electron with $k_e \approx k_B$. Absorption can be described in terms of one-particle states and the electron-hole interaction neglected. The more complete

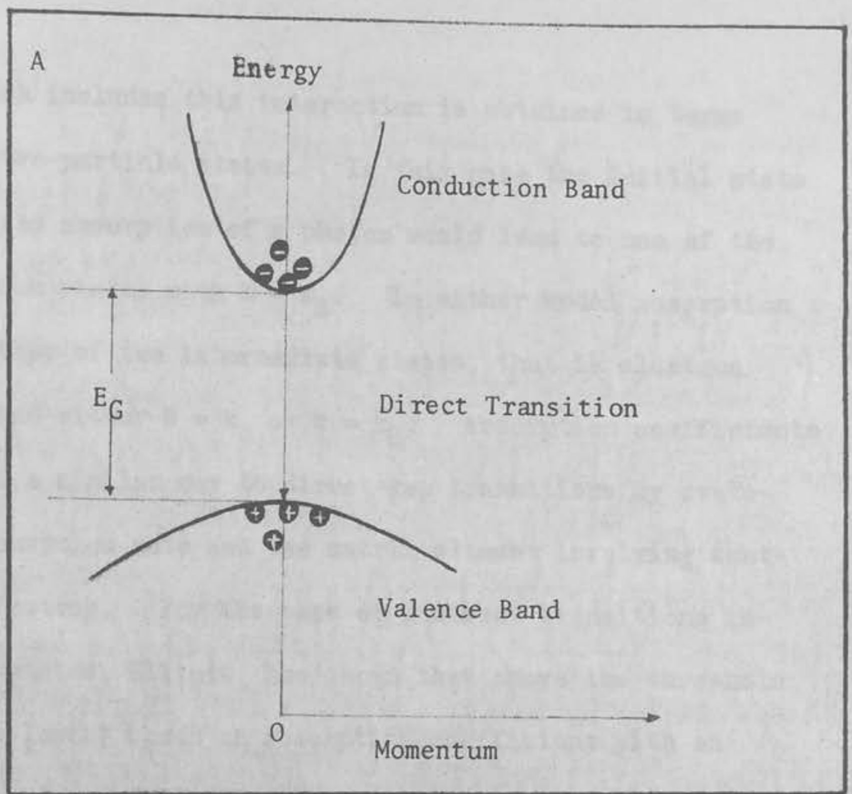

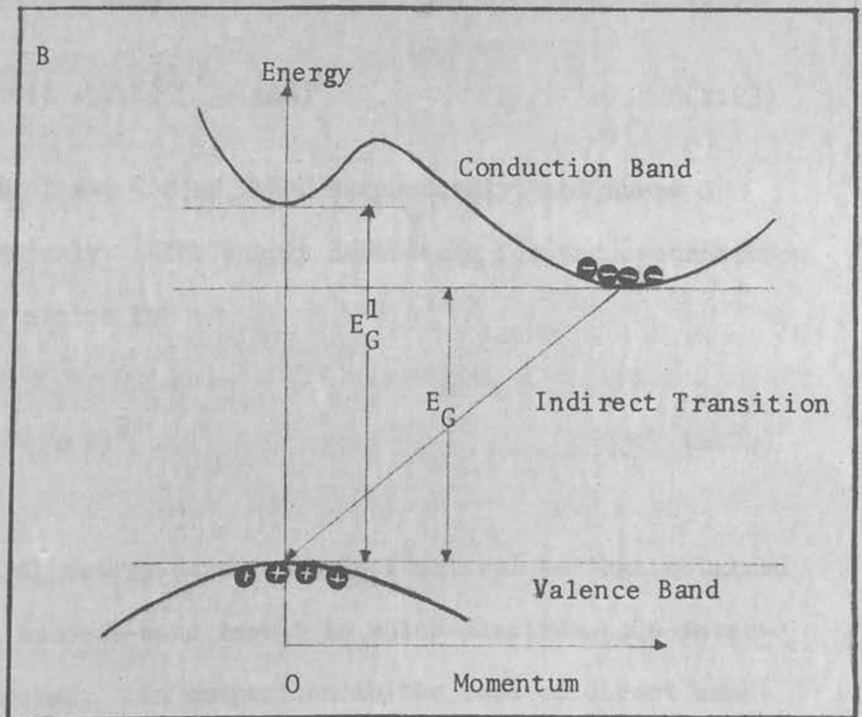

FIGURE A.4 Energy versus momentum for a direct gap (A) and indirect gap (B) semiconductor.

description which includes this interaction is obtained in terms of exciton, or two-particle states. In this case the initial state would be $K = 0$ and absorption of a photon would lead to one of the bound or continuum states with $K = k_B$. In either model absorption proceeds via either of two intermediate states, that is electron hole states around either $k = k_o$ or $k = k_B$. Absorption coefficients can be evaluated a similar way to direct-gap transitions by evaluation of the transition rate and the matrix element involving scattering of the electron. For the case of indirect transitions involving exciton states, Elliott has shown that above the threshold energies for the lowest bands an absorption coefficient with an approximate energy dependence given by

$$\alpha \sim (G + \Delta E)^{3/2} \tag{A.22}$$

$$\text{or} \quad \alpha \sim (G + \Delta E)^{3/2} - (\Delta E)^{3/2} \tag{A.23}$$

for $\Delta E = (h \;\; -E_G \pm h\omega) < 0$ or $\Delta E > 0$ respectively, and where G is as given previously. The energy dependence for the contribution of the continium states is

$$\alpha \sim (\Delta E)^2 \tag{A.24}$$

when $\Delta E \gg G$. This energy dependence is identical to that obtained for the indirect band-to-band result in which electron-hole interactions are neglected. In comparison to the case of direct band-to-band transitions there are here several relationships which can

be obeyed in the absorption edge region. As for the direct-transition case the relationships (A.22) - (A.24) are used in identifying the occurrence of indirect transitions in the edge region of absorption spectra.

It must be stressed that in the above treatments the band extrema are assumed nondegenerate.

The absorption spectrum of ZnTe has not been thoroughly investigated to date, and little experimentally derived data exists on ground state exciton energies, binding energies and relevant parameters such as reduced masses. At 4°K the exciton ground state energy has been evaluated at 2.831 eV with a binding energy of 0.010-013 eV (Aten et al., 1962). The band gap energy at this temperature is therefore approximately 2.391 eV. These results are associated with the upper or Γ_8 valence band (A series) (Appendices 1 and 2). At 77°K this exciton energy was evaluated by Cardona and Greenaway (1963) as 2.37 eV and the band gap associated with the Γ_7 (C series) split-off valence band 3.26 eV. (The valence band in the zincblende crystal has k = 0 valence band states of symmetry Γ_8 and Γ_7. These bands are labeled A and C; in conjunction with the conduction band each valence band gives rise to a series of exciton states).

REFERENCES

Albers, W., 1967, Physics and Chemistry of II-VI Compounds (J. Wiley and Sons, N.Y.).

Albers, W., and A. C. Aten, 1965, Philips Res. Repts. 20, 556.

A.S.T.M., 1966. Proposal prepared by the Committee on Materials for Microelectronic Devices and Microelectronics.

Aten, A. C., C. Z. Van Doorn and A. T. Vink, 1962, in: Proc. Intern. Conf. on Physics of Semiconductors, Exeter 1962. (Institute of Physics and The Physical Society).

Aven, M., 1965, Appl. Phys. Letters 7, 146.

Aven, M. and W. Garwacki, 1963, J. Electrochem. Soc. 110, 401.

Aven, M., and B. Segall, 1963, Phys. Rev. 130, 81.

Aven, M., and H. H. Woodbury, 1962, Appl. Phys. Letters 1, 53.

Baraff, G. A., 1962, Phys. Rev. 128, 2507.

Bardeen, J., F. J. Blatt, and L. H. Hall, 1965, in: Proc. of the Photoconductivity Conference, Atlantic City, 1954 (J. Wiley and Sons, N.Y.).

Benoit a la Guillaume, C., and J. S. Blakemore, 1962, Semiconductor Statistics (Pergamon Press, New York).

Bohm, D., 1951, Quantum Theory (Prentice-Hall, N.J.).

Boltaks, B. I., O. A. Matveev and V. P. Savinov, 1955, Zn. Tekhn. Fiz. 25, 2097.

Brooks, H., 1955, Advan. Electronics Electron Phys. 7, 156.

Bube, R. H., and E. L. Lind, 1957, Phys. Rev. 105, 1711.

Cardona, M., and D. C. Greenaway, 1963, ibid. 131, 98.

Cardona, M., and G. Harbeke, 1965, in: Proc. 7th Intern. Conf. on Physics of Semiconductors, Paris, 1964 (Dunod, Paris).

Carides, J., and A. G. Fischer, 1964, Solid State Comm. 2, 217.

Christyakov, I. D., and E. Krucheanu, 1961. Rev. Phys. 6, 211.

Cohen, M. H., and M. H. Bergstrasser, 1966, Phys. Rev. 141, 2.

Cohen, M. H., and V. Heine, 1961, ibid. 122, 1821.

Crowder, B. L., and W. N. Hammer, 1966, ibid. 150, 2, 541.

Cuthbert, J. D., and D. G. Thomas, 1967, ibid. 154, 763.

Dekker, A. J., 1957, Solid State Physics (Prentice-Hall, N.J.).

De Meis, W.M., and A. G. Fischer, 1967, Mat. Res. Bull. 2, 465.

Destriau, G., 1936, J. Chem. Phys. 33, 587.

Devlin, S. S., J. M. Jost and L. R. Shiozawa, 1960, Research on High Temperature Semiconductor Materials, Contract No. AF 33(616)3923, U.S. Air Force Aeronautical Research Labotatories.

Devlin, S. S., 1967, in: Physics and Chemistry of II-VI Compounds (J. Wiley and Sons, N.Y.).

Dietz, R. E., D. G. Thomas and J. J. Hopfield, 1962, Phys. Rev. Letters 9, 391

Dillon, Jr. J. A., 1962, J. Appl. Phys. 33, 669.

Dresselhaus, G., 1955, Phys. Rev. 100, 580.

Dresselhaus, G., 1956, J. Phys. Chem. Solids 1, 14.

Dresselhaus, G., 1957, Phys. Rev. 106, 76.

Dumke, W. P., 1957, ibid. 108, 1419.

Dumke, W. P., 1964, Bull. Am. Phys. Soc. 9, 217.

Eastman, P. C., 1966, private communication.

Eastman, P. C., R. R. Haering and P. A. Barnes, 1964, Solid St. Electron. 7, 879.

Ehrenreich, H., and A. W. Overhauser, 1956, Phys. Rev. 104, 331.

Eland, A. J., 1960-61, Philips Tech. Rev. 22, 266.

Eland, A. J., 1962-63, ibid. 24, 61.

Elliott, R. J., 1957, Phys. Rev. 108, 384.

Fischer, A. G., 1961, Investigation of Carrier Injection Electroluminescence. Report No.1, Contract No. AF 19(604) 8018, U.S. Air Force Cambridge Research Laboratories.

Fischer, A. G., 1964, in: Proceedings of the Symposium on Radiative Recombination, Paris, 1964 (Dunod, Paris).

Fischer, A. G., 1966, in: Luminescence of Organic Solids (Academic Press, N.Y.).

Fischer, A. G., and H. I. Moss, 1963, J. Appl. Phys. 34, 2112.

Gershenzon, M., F. A. Trumbore, R. M. Mikulyak and M. Kowalchik, 1965, J. Appl. Phys. 365, 1528.

Goldfinger, P., and M. Jeunehomme, 1963, Trans. Farad. Soc. 59, 2851.

Greene, L. C., D. C. Reynolds, S. J. Czyak and W. M. Baker, 1958, J. Chem. Phys. 29, 1375.

Halsted, R. E., 1967, in: Physics and Chemistry of II-VI Compounds (J. Wiley and Sons, N.Y.).

Halsted, R. E., and M. Aven, 1961, Am. Phys. Soc. 6, 312.

Halsted, R. E., M. R. Lorenz and B. Segall, 1961, J. Phys. Chem. Solids 22, 109.

Hauser, J. R., 1966, J. Appl. Phys. 37, 507.

Henisch, H. K., 1962, Electroluminescence (Pergamon Press, London).

Hopfield, J. J., 1960, J. Phys. Chem. Solids 15, 97.

Hopfield, J. J., D. G. Thomas, and R. T. Lynch, 1966, Phys. Rev. Letters 17, 312.

Hinotani, K., and H. Sugigami, 1965, Jap. J. Appl. Phys. 4, 731.

Ivey, H. F., 1963, Electroluminescence and Related Effects, 1962 (Academic Press, N.Y.).

Jaklevic, R. C., D. K. Donald, J. Lambe and W. C. Vassel, 1963, Appl. Phys. Letters 2, 7.

Kane, E. O., 1961, J. Appl. Phys. 32, 83.

Kennedy, D.I., and M. J. Russ, 1967a, Solid St. Electron. 10, 125.

Kennedy, D. I., and M. J. Russ, 1967b, J. Appl. Phys. 38, in press.

Kennedy, D. I., and M. J. Russ, 1967c, Solid St. Electron. to be published.

Kohn, W., 1957, Solid State Phys. 5, 258.

Komatsu, E., K. Hinotani, Y. Higuchi and Y. Hosami, 1964, Jap. J. Appl. Phys. 3, 733.

Kot, M. V., L. M. Panasyik, A. V. Simashkevich and A. E. Tsurkan, 1965, Soviet Phys.-Solid State 7, 999.

Kroger, P. A., 1965, J. Phys. Chem. 69, 3367.

Lampert, M. A., 1956, Phys. Rev. 103, 1648.

Lampert, M. A., 1962, ibid. 125, 126.

Landau, L., and E. M. Lifschitz, 1958. Quantum Mechanics (Pergamon Press, London).

Larach, S., R. E. Schrader and C. F. Stocker, 1957, Phys. Rev. 108, 587.

Loh, E. and R. Newman, 1961. J. Phys. Chem. Solids 21, 324.

Lossev, O. W., 1923, Telegrafia i Telephonia 18, 61.

Lynch, R. T., D. G. Thomas and R. E. Dietz, 1963, J. Appl. Phys. 34, 706.

Mandel, G., 1964, Phys. Rev. 134, A 1073.

Marple, D. T. F., 1966, Phys. Rev. 150, 728.

McMahon, H. O., 1950, J. Opt. Soc. Am. 40, 376.

McKay, K. G., 1954, Phys. Rev. 98, 877.

Moll, J. L., 1964, Physics of Semiconductors. (McGraw-Hill) - Ch.XI.

Morehead, F. F., 1965, in: Physics and Chemistry of II-VI Compounds (J. Wiley and Sons, N.Y.).

Morehead, F. F. and G. Mandel, 1964, Phys. Letters 10, 5.

Morehead, F., and G. Mandel, 1965, Phys. Rev. 137, A924.

Morgan, T. N., 1965, ibid. 139, A294.

Miksic, M. G., G. Mandel, F. F. Morehead, A. A. Onton, and E. S. Schlig, 1964, Phys. Letters 11, 202.

Nicoll, F. H., 1966, Appl. Phys. Letters 9, 13.

Parmenter, R. H., 1955, Phys. Rev. 100, 573.

Pashinkin, A. S., and L. M. Kovla, 1962, Soviet Phys.-Cryst. 7, 501.

Pauling, L., (1960) The Nature of the Chemical Bond, 3rd Ed. (Cornell University Press, N.Y.).

Piper, W. W., and S. J. Polich, 1961, J. Appl. Phys. 32, 1278.

Redfield, D., 1965, Phys. Rev. 140, A2056.

Reynolds, D. C., and S. J. Czyzak, 1950, ibid. 79, 543.

Reynolds, D. C., C. W. Litten and T. C. Collins, 1965, Phys. Stat. Solidi 9, 645.

Roberts, S., and D. T. F. Marple, 1967, reported by B. Segall and D. T. F. Marple in: Physics and Chemistry of II-VI Compounds, 1966 (J. Wiley and Sons, N.Y.).

Rose, A., 1964, J. Appl. Phys. 35, 3664.

Roth, W. L., 1967, in: Physics and Chemistry of II-VI Compounds (J. Wiley and Sons, N.Y.).

Rubinstein, M., 1966, J. Electrochem. Soc. 113, 623.

Russ, M. J., 1962, Ph.D. thesis, University of Birmingham.

Sagar, A. and W. Lehmann, 1965, Phys. Rev. 140, A923.

Segall, B., 1966, ibid. 50, 734.

Segall, B., 1967, in: Physics and Chemistry of II-VI Compounds (J. Wiley and Sons, N.Y.).

Segall, B., and D. T. F. Marple, 1967, ibid.

Shiozawa, L. R., J. M. Jost, S. S. Devlin, and D. R. M. Browdy, 1963-64. Research on II-VI Compound Semiconductors, Eighth, Ninth and Tenth Quarterly Repts., Contract No. AF33 (657)-7397 U.S. Air Force Aeronautical Research Laboratories.

Stern, F., 1963, Solid State Phys. 15, 300.

Takahashi, R., M. Oshima, and A. Kobayashi, 1966, Jap. J. Appl. Phys. 5, 39.

Teitler, S., and R. S. Wallis, 1960, J. Phys. Chem. Solids 16, 71.

Thiabault, N. W., 1944, Am. Mineralogist 29, 249.

Thomas, D. G., J. J. Hopfield and M. Power, 1960, Phys. Rev. 119, 570.

Thomas, D. G., and E. A. Sadowski, 1964, J. Phys. Chem. Solids 25, 477.

Title, R. S., G. Mandel and F. F. Morehead, 1964, Phys. Rev. 136, A300.

Tubota, H., 1963, Jap. J. Appl. Phys. 2, 259.

Tubota, H., H. Suzuki and K. Hirakawa, 1960, J. Phys. Soc. Japan 15, 1701.

Tubota, H., H. Suzuki and K. Hirakawa, 1961, ibid. 16, 1038.

Urbach, F., 1953, Phys. Rev. 92, 1324.

Van der Pauw, L. J., 1958, Philips Res. Repts. 13, 1.

Wagner, P., and M. R. Lorentz, 1966, I.B.M. Research Paper R.C. 1607.

Wannier, G., 1937, Phys. Rev. 52, 191.

Warekois, E. P., M. C. Lavine, A. N. Mariano and H. C. Gatos, 1962, J. Appl. Phys. 33, 6901.

Watanabe, N. 1966, J. Phys. Soc. Jap. 21, 713.

Watanabe, N., and S. Usui, 1966, Jap. J. Appl. Phys. 5, 569.

Watanabe, N., S. Usui and Y. Kanai, 1964, ibid. 3, 427.

Weiser, M., M. Drougard and R. Fern, 1967, J. Phys. Chem. Solids 29, 171.

Wolff, P. A., 1954, Phys. Rev. 95, 1415.

Yamanaka, T., and T. Shiraishi, Jap. J. Appl. Phys. 4, 826, 1965.

Ziman, J. M., 1960, Electrons and Phonons (Oxford University Press, London).

PUBLICATIONS

1. Alsford, R. W., R. E. Hayes and D. I. Kennedy, "Influence of Charge Effects on the Electrical Conductivity of Thin Metal Films", 1966, Electron. Letters 2, 327.

2. Kennedy, D. I., and M. J. Russ, "Room Temperature Electro-Luminescence in Semi-insulating Zinc Telluride", 1967, Solid-St. Electron. 10, 125.

3. Kennedy, D. I., R. E. Hayes and R. W. Alsford, "The Influence of Charge Effects on the Growth and Electrical Resistivity of Thin Metal Films", 1967, J. Appl. Phys. 38, 1986.

4. Russ, M. J., and D. I. Kennedy, "The Effect of Double Insulating Layers on the Electroluminescence of Evaporated ZnS:Mn Films", 1967, J. Electrochem. Soc. 114, 1066.

5. Kennedy, D. I., and M. J. Russ, "New Electroluminescent Spectrum in Zinc Telluride Resulting from Oxygen Incorporation", 1967, J. Appl. Phys. 38, 4378.

6. Kennedy, D. I., and M. J. Russ, "Electroluminescence in Polycrystalline ZnTe", Solid-St. Electron. to be published.

INFLUENCE OF CHARGE EFFECTS ON THE ELECTRICAL CONDUCTIVITY OF THIN METAL FILMS

The letter describes investigations made into the electrical resistance of evaporated films of lead, tin, indium and gold, less than 600 mÅ thick. It was found that lower-resistance films could be obtained if arrangements were made to reduce the accumulated charge appearing on the substrate.

Interest has recently been revived[1,2] in a phenomenon first described by us in 1963.[3] Our detailed results remain unpublished, but, since they complement those recently reported,[4] they are given briefly here. We were concerned with evaporating thin superconducting lead films onto 0·005 in-thick mica and glass substrates. By utilising an applied field, we were able to grow very thin conducting lead films, which were found to be superconducting. The field applied across the slide from edge contacts was 15 V/cm, and this was used to monitor the film resistance. Various contact materials such as gold, indium and Minalpha* were used, but they did not affect the results. The areas of the films varied between 0·5 and 1·5 cm^2, evaporated at a pressure of $\nless 10^{-5}$ torr.

Further experiments showed that other evaporated metal films, such as indium, gold and particularly tin, showed the same resistance effect. A plot taken during an evaporation of the resistance of a tin film is given in Fig. 1, the intermediate

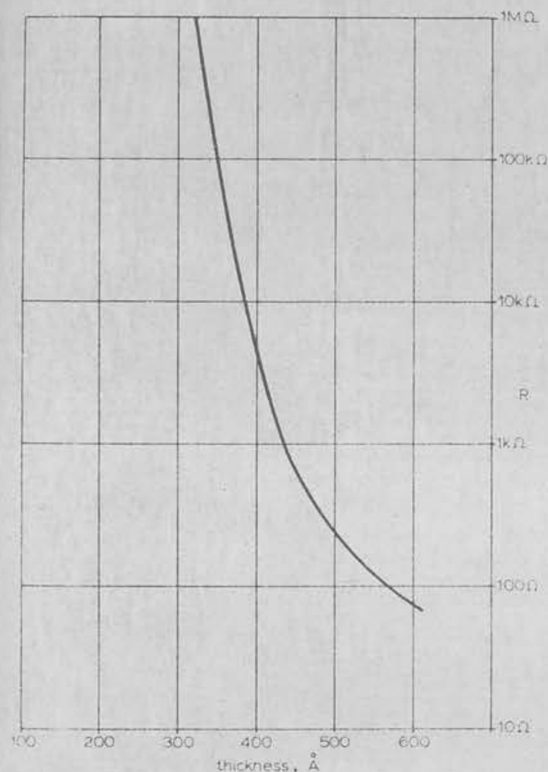

Fig. 1

thicknesses being deduced by the use of an accurate rate-meter.[5] The monitored films were found to be thinner than the isolated films. For thicknesses of less than 600 Å, all the metals tested had infinite resistance on an isolated substrate. It was then found that the lower-resistivity films could be obtained if the contacts were earthed to the evaporator.

It was suspected that this resistance variation was due to a charge collecting on the surface of the substrate. A probe placed above a heated empty evaporation source registered a negative charge. With lead being evaporated, the charge became positive. A cylindrical screen was therefore placed around the source, and the metal was evaporated through it. The low-resistance value was then obtained for isolated substrates, provided that the screen was earthed or maintained at a positive or negative potential.

Finally, a very thin (20 Å) just conducting layer of gold was evaporated onto a monitored slide, and the slide was then isolated. It was found that, for a further evaporation of lead, the resistance was the same as that of a monitored film.

R. W. ALSFORD
R. E. HAYES

The Plessey Co. Ltd.
Roke Manor, Romsey, Hants, England.

D. I. KENNEDY

Bowmar Canada Ltd.
Ottawa, Ont., Canada

4th August 1966

References

1 PASHLEY, D. W.: 'Structure of thin films', *Advances in Phys.*, 1965, **14**, p. 361
2 CHOPRA, K. L.: 'Growth of thin metal films under applied electric field', *Appl. Phys. Letters*, 1965, **7**, p. 140
3 CARTER, G.: Conference on sorption properties of evaporated metal films, Liverpool, April 1963, *Brit. J. Appl. Phys.*, 1963, **14**, p. 615
4 CHOPRA, K. L.: 'Influence of electric field on the growth of thin metal films', *J. Appl. Phys.*, 1966, **37**, p. 2249
5 HAYES, R. E., and ROBERTS, A. R. V.: 'A control system for the evaporation of silicon monoxide insulating films', *J. Sci. Instrum.*, 1962, **39**, p. 428

Reprinted from *Electronics Letters*, Vol. 2, No. 9, September 1966

Solid-State Electronics Pergamon Press 1967. Vol. 10, pp. 125–127. Printed in Great Britain

ROOM TEMPERATURE ELECTROLUMINESCENCE IN SEMI-INSULATING ZINC TELLURIDE

D. I. KENNEDY and M. J. RUSS

Bowmar Canada Ltd., Ottawa, Ontario, Canada

(*Received* 11 *July* 1966; *in revised form* 26 *August* 1966)

Abstract—Electroluminescence observed at 293°K in undoped semi-insulating zinc telluride, resistivity 2.5×10^4 Ω-cm. Emission intensities of 5 ft-L obtained at current densities of 0.2 A/cm². The mechanism of emission is discussed in terms of a bulk process.

Résumé—Observation de l'electroluminescence dans tellurid de zinc semi-conductif, non dopé à 293°K, restivité $2,5 \times 10^4$ Ω-cm. L'intensité d'emission de 5 ft-L obtenue à l'intensité d'un courant de 0,2 A/cm². Discussion du mechanism en terms d'une masse mechanism.

Zusammenfassung—Beobachtung von Elektrolumineszenz bei 293°K aus undotiertem halb leitendem Zinctellurid, Wiederstandswert $2{\cdot}5 \times 10^4$ Ω-cm. Emission intensitaten von 5 ft-L erhalten bei Stromdichten von 0·2 A/cm². Vorgang der Emission wird im Rahmen der Volumenmechanik besprochen.

THE SEARCH for an efficient electroluminescent emitter has led to investigations of the wide band-gap II–VI compounds. For application to display devices the characteristics of room temperature electroluminescence in these materials is of particular interest.

We report the observation of room temperature emission from undoped, semi-insulating ZnTe of sufficient intensity to allow consideration of the material for application in low level electroluminescent displays.

There have previously been several reports of electroluminescence observed in ZnTe single crystals containing various dopants[1–5] and also in nominally undoped single crystals.[6,7] The resistivities of these materials were typically in the range 1–50 Ω-cm. Efficient emission has been obtained from low resistivity ZnTe devices at 77°K.[4]

In the present work single crystals were prepared from high purity ZnTe by a modified horizontal Bridgman method. The resulting crystals had a room-temperature resistivity of 2.5×10^4 Ω-cm. Assuming a mobility of 100 cm²/V-sec[8] a carrier concentration of 10^{12}/cm³ is indicated.

Two types of composite device were fabricated. For the first type a layer of electroless Au was deposited on the top face of a 0.5 mm thick crystal and sections 1.0 mm square were cut from the wafer. The bottom face of the crystal was attached to a transistor header using 100 percent In solder. Connection to the top face was made using an Au wire and the same solder. For the second type a 10 mg piece of In was placed on the top face and the wafer was heated in vacuum until the In flowed and wet the surface. This process was carried out to allow diffusion of the In layer into the bulk ZnTe. The crystal was then sectioned and mounted in an identical manner to the first type. The properties of the samples used in these experiments were not found to be strongly dependent on surface treatment and similar results were obtained when contacts were made on cleaved, ground or etched surfaces.

Both forms of device exhibited some rectification in the I–V characteristics, higher current levels being obtained with the top contact positive with respect to the crystal. The electrical characteristics showed a marked temperature dependence.

Emission was obtained for both directions of current flow, generally in the form of isolated

spots located in the region of the header contact when a positive potential was applied to the top contact and in the region of the top contact when the polarity was reversed. The room temperature emission was orange in color. A DK2A spectrophotometer was used to measure the emission spectrum. At 293°K this emission peaked at 5750 Å and the spectrum width at half maximum intensity was 700 Å. This is indicative of radiative recombinations having near band-gap energy.

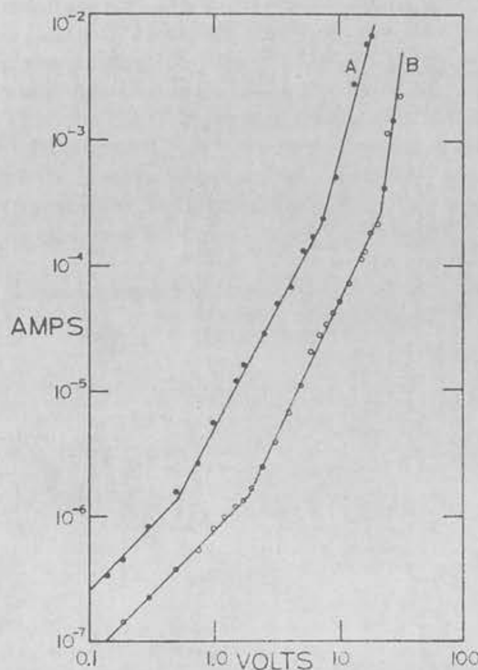

FIG. 1. I–V characteristic at 293°K for In (diffused)–ZnTe–In structure. *A*—forward direction, *B*—reverse direction.

Brightness, as measured by a Photo Research Spot Meter, was normally greater for the forward direction of current flow and light outputs of the order of 5 ft-L at current densities of 0.2 A/cm^2 were commonly observed. This corresponds to an external quantum efficiency of 10^{-4}. The light output increased proportionally with increasing current. At liquid nitrogen temperatures the emission spectrum shifted to shorter wavelengths.

Typical room temperature I–V characteristics are shown in Fig. 1. Three separate regions can be distinguished, the first and second corresponding to ohmic and square law behavior respectively. In the third region the current rises at a higher power of the applied voltage. For both directions of current flow the onset of emission coincided with the start of this region.

A variety of mechanisms have been postulated to explain the observations of electroluminescence in ZnTe. Although there have been reports of emission under reverse bias (e.g. EASTMAN *et al.*[1], in which emission is explained by a tunnel injection mechanism across a metal–semiconductor interface), the majority of reports describe forward bias emission. Of these, two have included observations of a discontinuity in the forward I–V characteristic. CROWDER *et al.*[4] obtained a breakdown effect in a forward biased metal–insulator–*p*-type ZnTe structure at 77°K. The mechanism postulated was considered to be the impact ionization, by avalanche breakdown, of electrons in the insulating region with subsequent injection and recombination of these carriers in the *p*-type ZnTe. HINOTANI and SUGIGAMI[9] have investigated the electrical properties of a metal–semi-insulator–semiconductor structure under forward bias at 77°K. The I–V characteristics were similar in some respects to those described here, but the onset of emission coincided with a square law region. These authors interpreted their results in terms of LAMPERT's theory of one-carrier space-charge-limited current[10] and electron injection into the semi-insulating layer.

Because the basic form of the I–V curves in the present experiments does not depend critically upon the ZnTe surface treatment or the type of contacts and because emission is observed at the commencement of the steep region of the I–V characteristic for both directions of current flow, we consider that the emission may be the result of a bulk process. This could consist of a collision excitation process followed by recombination via traps or shallow impurity levels. The fact that the voltage at which the steep region of the I–V characteristic commences is lower for the case of electroless Au or diffused In contacts than for the case of simple In contacts suggests that the contact barrier is higher for the latter contacts and that a greater local field is necessary at the contacts to provide the carrier supply required for the process which leads to emission.

Although the LAMPERT and ROSE theory of double injection in insulators[11] could provide an alternative mechanism for the electroluminescence in the semi-insulating ZnTe used in this work, no negative resistance effects were observed in the electrical measurements. On the basis of the double injection theory radiative recombinations could take place between electrons and holes injected into a trap filled solid.

The present measurements indicate emission of predominantly band-gap energy but the possibility exists that the spectrum of the recombination radiation may extend to shorter wavelengths, and is internally absorbed. Existence of such emission corresponding to greater than band-gap energy would tend to favor an avalanche type process. This possibility is presently being investigated.

In summary, we have demonstrated the feasibility of obtaining band-gap emission at room temperature in high-resistivity ZnTe; possible mechanisms have been briefly considered.

Acknowledgments—This work was carried out as part of a research program jointly sponsored by Bowmar Canada Limited and the Canadian Directorate of Industrial Research. The authors wish to thank W. A. WEBB for his assistance in preparing samples and carrying out some of the measurements.

REFERENCES

1. P. C. EASTMAN, R. R. HAERING and P. A. BARNES, *Solid-St. Electron.* **7,** 879 (1964).
2. M. G. MIKSIC, G. MANDEL, F. F. MOREHEAD, A. A. ONTON, and E. S. SCHILIG, *Phys. Letters* **11,** 202 (1964).
3. M. V. KOT, L. M. PANASYUK, A. V. SIMASHKEVICH and A. E. TSURKAN, *Soviet Phys.—Solid-St.* **7,** 999 (1965).
4. B. L. CROWDER, F. F. MOREHEAD and P. R. WAGNER, *Appl. Phys. Lett.* **8,** 148 (1966).
5. N. WATANABE, *Jap. J. appl. Phys.* **5,** 12 (1966).
6. N. WATANABE, S. USUI and Y. KANAI, *Jap. J. appl. Phys.* **3,** 427 (1964).
7. E. KOMATSU, K. HINOTANI, Y. HIGUCHI and Y. HOSOMI, *Jap. J. appl. Phys.* **3,** 733 (1964).
8. M. AVEN and B. SEGALL, *Phys. Rev.* **130,** 81 (1963).
9. K. HINOTANI and M. SUGIGAMI, *Jap. J. appl. Phys.* **4,** 731 (1965).
10. M. A. LAMPERT, *Phys. Rev.* **103,** 1648 (1956).
11. M. A. LAMPERT and A. ROSE, *Phys. Rev.* **121,** 26 (1961).

Reprinted from JOURNAL OF APPLIED PHYSICS, Vol. 38, No. 4, 1986–1987, 15 March 1967
Copyright 1967 by the American Institute of Physics
Printed in U. S. A.

The Influence of Charge Effects on the Growth and Electrical Resistivity of Thin Metal Films

D. I. KENNEDY*
Bowmar Canada Limited, Ottawa, Ontario, Canada
AND
R. E. HAYES AND R. W. ALSFORD
The Plessey Company Limited, Roke Manor, Romsey, Hampshire, England
(Received 18 August 1966; in final form 31 October 1966)

IN investigations of the growth and structure of thin metal films there has been considerable interest in the mechanisms by which the depositing material forms discrete three-dimensional nuclei, the subsequent growth of these nuclei to form isolated island structures, and, at critical stage, the sudden coalescence of these islands to produce a coherent electrically continuous film. The mechanisms involved in these early stages of film growth are not well understood. The various stages in the growth process can be significantly influenced by the deposition conditions, the nature and temperature of the substrate, and variations in other external parameters.

This communication reports on the influence of electrostatic charge effects on the growth and electrical resistivity of thin metal films. Similar effects have been observed by Hayes *et al.*[1,2] and Chopra[3,4] has reported the influence of moderate electric fields on the growth of gold, silver, and copper films. Related effects have been reported by Koedam[5] who observed that for silver and copper films greater homogeneity resulted from bombardment of the substrate with positive ions during the deposition process, and Stirland[6] who reported higher initial island densities for gold films deposited on a substrate undergoing electron bombardment. Hill[7] has investigated the effects of both positive and negative charge induced on a substrate during the deposition of gold films and found the nucleation density to be higher for the case of induced positive charge.

In our experiments on the low-melting-point metals, lead, tin and indium, we have investigated the effect of low electric fields applied in the plane of the substrate on the growth and electrical resistivity of the films and have correlated our results with the influence of residual charge carried by the incident vapor stream.

Using high-purity materials, thin films of lead, tin, and indium were evaporated at pressures of 10^{-6} mm Hg from a resistively heated molybdenum strip. The films were deposited onto glass substrates which had been ultrasonically cleaned and alcohol-vapor degreased.

The substrate, of dimensions 1.6×1.6 cm, was supported in an insulated holder which was isolated electrically from the vacuum system. This holder incorporated a mask which allowed the evaporation of two parallel isolated strips 0.6 cm$\times1.3$ cm on each substrate. It was found necessary to use this form of substrate holder to obviate variations in film thickness obtained if separate substrates were positioned in the system. Copper–manganese contact strips were pre-evaporated at the end of each strip. Spring clips were used to hold the substrate in position and to maintain contact between the copper–manganese areas and metal electrodes isolated from the supporting frame. The holder was fabricated in copper and thin Teflon sheet was used as the insulating material. This system provided a 'test' and 'control' film, either or both of which could be isolated, earthed or subjected to an applied electric field.

An electric field of 10 V/cm used in a resistance monitoring circuit was applied to one section of the substrate and the other section was isolated. In the initial experiments, lead films were evaporated to a monitored resistance of 10^4 $\Omega/\square$ at a deposition rate of 5–10 Å/sec. The substrate was removed from the vacuum system and the isolated strip was found to be electrically discontinuous. The thicknesses of the two films as measured by multiple interferometry techniques were in agreement. If films were evapo-

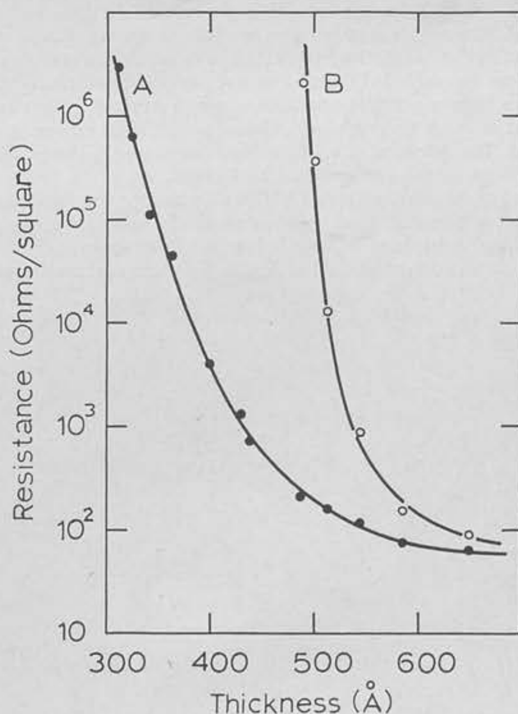

FIG. 1. The dependence of electrical resistance on film thickness for tin films evaporated on glass substrates: A. Electric field of 10 V/cm. B. No electric field.

rated to monitored resistance values of less than $10^4\ \Omega/\square$, the unmonitored strip became conducting although the resistance still differed by a large factor from the monitored strip. When the evaporation was continued until the monitored film resistance was in the region of $200\ \Omega/\square$, the resistance of the unmonitored film tended to the same value. Results of a similar nature were obtained for tin and indium films. Figure 1 shows the results obtained for tin films for the variation of unmonitored and monitored film resistance with increasing thickness.

It was found that with the field applied to one strip and the other earthed or connected to a floating ground, the variation of resistivity of both strips with increasing thickness was identical. If both strips were left isolated during evaporation, the variation of resistivity of both strips was again identical but followed the higher-resistance curve.

Changes in evaporation rate and residual pressure did not significantly influence the effect. However, the actual configuration of the substrate holder and the materials used in its construction, i.e., the capacity of the holder, had a marked effect on the relationship between the unmonitored and monitored film resistance values at any given thickness.

In order to elucidate the contribution of possible charge carriers in the vapor stream to this effect, a conical metal shield was placed above the evaporation source. If this shield was isolated, the same marked variation between monitored and unmonitored film was obtained. However, if the shield was connected to a positive or negative potential the effect was eliminated, the resistance of the monitored and unmonitored films again varying in an identical manner.

In place of the substrate, a small-area probe connected to a sensitive dc amplifier was placed in the vapor stream. Under normal evaporation conditions used for the low-melting-point metals investigation, no thermionic emission was detected from the molybdenum boat. However, with an evaporating metal charge in the boat, a positive charge was detected having an associated probe current of 5×10^{-9}A. This indicated that approximately one in 10^3 atoms incident on the substrate carried a unit positive charge. With the isolated shield in position this charge was unaltered. If a negative or positive potential in excess of 50 V was applied to the shield, the probe charge was reduced to zero. It can therefore be concluded that the rate of growth of electrically continuous films in which the positive charge is retained in the vapor stream is much different from those in which the charge is removed. The detection of a definite positive charge in the incident vapor stream was also reported by Chopra.

The results obtained indicate that films having 'low' resistance values compared to films evaporated to the same thickness on isolated substrates can be prepared in the following ways:

(a) Application of an electric field in the plane of the substrate.

(b) Earthing the substrate.

(c) Removal of the positive charge from the incident vapor stream.

The common factor here would appear to be the redistribution, via an extraction process, of the positive charge transported by the evaporating metal.

From the results of his investigations, Chopra considered that the influence of the applied electric field accelerated the effects of attractive electrostatic image charges residing on metal islands formed in the early stages of evaporation and resulted in the coalescence of these islands at an earlier stage in the growth of the film than would be the case in the absence of the field. For our experiments involving an applied electric field, the same charge redistribution mechanism could be operative. However, in terms of the results obtained, no significant variation was detected between this technique and the others outlined above. It could, therefore, be postulated that in the case of an isolated substrate the positive charge carried by the incident vapor stream is distributed over the initial nucleating metal islands forming mutually repulsive aggregates. By altering the substrate/holder configuration, earthing, or connecting a monitoring potential, this charge is reduced or removed and the resulting change in the equilibrium charge distribution allows the formation of an electrically continuous structure at an earlier stage in the growth of the film.

In summary, we have demonstrated that for a given film thickness higher resistivity or nonconducting films are obtained for evaporation onto an electrically isolated substrate, whereas lower-resistivity films result from the application of an electric field, earthing the substrate, or by removal of residual electrostatic charge from the incident vapor stream. These results can be explained by a redistribution mechanism in which the extraction of electrostatic charge inherent on the initial nucleating metal islands restricts the growth of mutually repulsive aggregates and promotes the more rapid coalescence of these islands to form an electrically continuous film.

The authors would like to thank the Plessey Company, Limited, for permission to publish this note.

* Formerly with the Plessey Company Limited, Roke Manor, Romsey, Hampshire, England.

[1] R. E. Hayes, R. W. Alsford, and D. I. Kennedy, Institute of Physics Conference, Liverpool, April 1963. Reported by D. W. Pashley, Advan. Phys. **14**, 361 (1965).

[2] R. E. Hayes, R. W. Alsford, and D. I. Kennedy, Electron. Letters **2**, 326 (1966).

[3] K. L. Chopra, Appl. Phys. Letters **7**, 140 (1965).

[4] K. L. Chopra, J. Appl. Phys. **37**, 2249 (1966).

[5] M. Koedam, Philips Res. Rept. **16**, 266 (1961).

[6] D. J. Stirland, Appl. Phys. Letters **8**, 328 (1966)

[7] R. M. Hill, Nature **210**, 512 (1966).

The Effects of Double Insulating Layers on the Electroluminescence of Evaporated ZnS:Mn Films

M. J. Russ and D. I. Kennedy

Reprinted from JOURNAL OF THE ELECTROCHEMICAL SOCIETY
Vol. 114, No. 10, October, 1967
Printed in U. S. A.
Copyright 1967

The Effects of Double Insulating Layers on the Electroluminescence of Evaporated ZnS:Mn Films

M. J. Russ and D. I. Kennedy

Bowmar Canada Limited, Ottawa, Ontario, Canada

ABSTRACT

The performance of ZnS: Mn electroluminescent layers deposited between double SiO insulating films is described. The dependence of emission properties on SiO and ZnS film thickness and Mn content are outlined. The relatively bright (700 ft-L) and efficient (1 lpw) emission is interpreted in terms of excursions from equilibrium trap occupation under high field conditions.

A considerable number of investigations of EL (electroluminescence) in thin ZnS films have been carried out using direct contact between the ZnS films and the conducting electrodes. In some investigations a single thin insulating layer has been used between the films and one of the electrodes. In most of the cases the results have shown marked asymmetry with respect to changes in polarity of the applied voltage. This situation has frequently led to difficulties in interpretation of the results. The present experiments were designed to eliminate some of the complexity by using thin insulating layers on both sides of the ZnS films.

In the past there have been a number of reports (1-11) on a-c EL in ZnS thin films. These reports have covered a variety of preparation techniques. Halsted and Koller (1) prepared EL (electroluminescent) ZnS: Mn films by the vapor reaction technique of Studer and Cusano (12), whereas Thornton (2) used the diffusion method of Feldman and O'Hara (13) to prepare ZnS: Mn: Cl and ZnS: Cu: Cl films. Vlasenko and Popkov (4) prepared ZnS: Mn films by separate evaporation and subsequent high-temperature diffusion of the constituents. Using a technique of coevaporation on a heated substrate proposed by Koller and Coghill (14), Antcliffe (15) has prepared EL ZnS: Mn films. Apart from variations in methods of producing the phosphor layer, various types of composite device have been investigated. Several authors (4, 6) have utilized an insulating layer between the phosphor film and the metal electrode. Harper (6) has reported that improved efficiencies and over-all brightness levels can be obtained by the use of an SiO_2 film of thickness between 7 and 160Å in this position.

The technique of coevaporation of ZnS and Mn on a heated substrate was adopted for the present experiments because of the simple, one-stage process.

Film Preparation

High-purity ZnS in either single crystal or compressed polycrystalline form was used as source material and, in the majority of experiments, Mn powder was added to the ZnS crystals in a range of concentrations from 0.04 to 6.0 w/o. To maintain uniform conditions in successive depositions the accurately weighed charges were evaporated to completion.

It was found that in order to obtain high-brightness EL the deposition conditions were critical. Substrate temperatures had to be maintained in the range 250°-300°C. Above 300°C significant crystallization of the ZnS film occurred and this resulted in the formation of an opaque white layer. For substrates maintained at temperatures between 20° and 250°C, only low-level emission was obtained. The critical deposition rate was found to be 1000 Å/min at a pressure of 10^{-5} Torr. The source temperature required to maintain this deposition rate at a distance of 7 in. from the substrate was 1230°C as determined by an optical pyrometer. The use of a lower evaporation rate did not permit sublimation of the added Mn, and a higher rate led to poor incorporation of the Mn in the film. This latter condition resulted in the deposition of a film having a black metallic coloration.

When the critical deposition conditions were met it was possible to obtain emission from panels with a range of ZnS film thicknesses and Mn concentrations. In order to obtain panels with a usable brightness, however, it was necessary to control the latter parameters also.

Prior to deposition of the ZnS film a layer of SiO was evaporated onto the unheated tin-oxide coated glass substrate. SiO thicknesses which were varied from 600 to 5000Å were used. Subsequent to the deposition of the phosphor film a second SiO layer was evaporated and finally metal electrodes were deposited. The properties of devices made with this structure were found to be independent of the metal electrode used (Al, Au, and In were each investigated). The results are based on an evaluation of at least 36 devices for each experiment.

Results

The emission resulting from a-c excitation of the ZnS:Mn films was located in the same region of the spectrum as reported by previous authors. Using a DK-2A spectrophotometer it was found that the peak occurred at 5780Å and the half-width was 450Å.

On first application of voltage to these devices it was found that the emission would grow steadily to a uniform brightness over the active area. This behavior contrasted strongly with previous experiments carried out in this laboratory and elsewhere on structures with no insulating layers or a single such layer. In the latter cases it was found that a "forming" process, in which the phosphor was subjected to a critical near-breakdown electric field, was required to produce over-all luminescence. This "forming" process was attended initially by high currents without the presence of EL, and the emission appeared gradually as the currents fell to lower values. These processes have been discussed by Goldberg and Nickerson (16) and Cusano (17). The use of single insulating layers reduces the severity of the break-in process, and the double layers described in this report virtually eliminate the effect.

Effects of SiO *layers.*—Using the deposition conditions described above a 1000Å film of SiO was evaporated on tin-oxide coated glass followed by deposition of a 1.5μ ZnS:Mn film (Mn concentration in source of 0.6 w/o). This was followed by deposition of SiO stripes which increased in thickness in steps over the range from 220 to 5000Å. Metal electrodes of area 6×10^{-2} cm^2 were then evaporated to complete the devices.

Figure 1 shows the results obtained on a-c excitation of these films at a frequency of 13 kHz in terms of the dependence on surface brightness on the rms electric field applied across the ZnS film. (This latter parameter was estimated from the total applied voltage using measured results for the dependence of the dielectric constants of ZnS and SiO on film thickness at the frequencies used.) The brightness was measured using a Spectra-Spot brightness meter. All results show a marked dependence of brightness on SiO thickness. As the SiO thicknesses were gradually increased it was found that the observed emission for a given field across the ZnS layers passed through maxima and minima. Although the emission process may be influenced by SiO thickness to some extent, the oscillatory nature of the characteristics pointed strongly to the existence of optical interference effects in the composite structure.

To maximize the observed emission in the above structure it was necessary to use particular values of SiO layer thickness. Utilization of data similar to that shown in Fig. 1 for dependence of brightness on SiO thickness at fixed values of ZnS field showed that the maximum brightness is obtained for an SiO thickness of 650Å. This differs from the theoretical value of 730Å calculated from reported refractive indices for the various layers; the difference probably

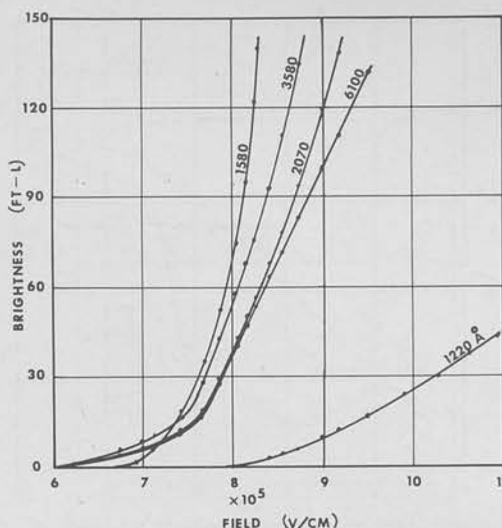

Fig. 1. Dependence of brightness on ZnS field at 13 kHz for various SiO layers. 1000Å SiO films were used between the ZnS and SnO_2 and thicknesses of 220-5100Å of SiO were used between the ZnS and Al.

results from the complex dependence of refractive index on film composition and thickness in the materials used. By varying the thickness of the SiO layer between the tin-oxide electrode and the ZnS film while maintaining the second SiO layer constant, it was possible to establish an optimum thickness value of 1300Å for the internal SiO layer. This value is in agreement with theory assuming $n_{SiO} < n_{SnO_2}$. A further increase in observed emission would be anticipated if the SiO or tin-oxide layers were replaced with materials with more ideally matched refractive indices.

It is interesting to note that the field strengths applied to the ZnS layers in our devices under routine operating conditions appear to be equal to or slightly higher than values normally used in this type of experiment and also than the reported dielectric breakdown strength for ZnS (4, 18). The calculated field strength values were obtained from separate measurements on SiO and ZnS layers of equivalent thicknesses and may not correspond exactly to the values which occur in composite structure. Nevertheless, the possibility exists that the double SiO layers eliminate one form of breakdown which occurs when direct metal/ZnS contact exists. The highest-efficiency EL in this work was observed when devices were operated in this field regime.

The dependence of brightness on frequency in the range from 1-20 kHz, showed, for all values of SiO thicknesses, a saturation effect above 8 kHz. As the frequency was increased above 13 kHz the average brightness at a given applied field decreased. Although this decrease may be associated with impedance effects in the various layers or with internal heating there is some evidence that it could be caused by failure of the excitation and recombination processes to reach completion within individual half cycles of the applied field.

Effect of manganese concentration.—There is little information in the literature on the dependence of ZnS film emission properties on Mn concentration. The majority of published work has been carried out on single values of Mn content in a range between 0.1 and 1 w/o. Vlasenko and Popkov (4) carried out experiments with several Mn concentrations and reported an optimum value of 0.6 w/o. In the present work a range of samples were prepared from sources containing from 0.04 to 6.0% Mn. In all cases the ZnS film thickness was maintained at 1.5μ, and a symmetrical structure with double SiO layers of 700Å thickness was used.

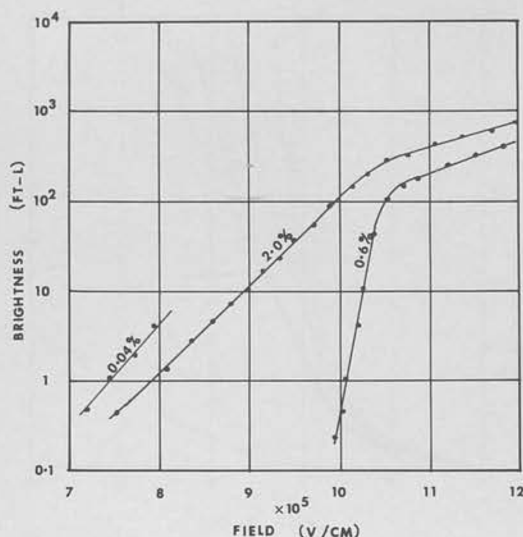

Fig. 2. Dependence of brightness on ZnS field at 13 kHz for various Mn concentrations. A ZnS thickness of 1.5μ was used in conjunction with double 700Å SiO layers.

Figure 2 shows the dependence of integrated brightness on the applied field at 13 kHz for three Mn concentrations. A considerable improvement in brightness levels was obtained as the Mn concentration increased. The maximum brightness for a phosphor containing 2 w/o Mn was in excess of 700 ft-L compared with 5 ft-L for a 0.044 w/o phosphor. If the Mn concentration was increased to 6%, the maximum brightness was reduced to 10 ft-L, and the panels were found to burn out at low applied voltages; this would appear to be due to the reduction in the resistivity of the phosphor with high Mn content. At 6 w/o Mn the films had a metallic black rather than yellow coloration. In the concentration range from 0.04 to 2.0 w/o the maximum brightness and discrimination ratio increased with increasing Mn content. Although 2% Mn was the maximum level of incorporation which led to repeatably good results using the described procedures it is felt that higher concentrations could be achieved using more sophisticated source materials and deposition procedures. In this case it should be possible to obtain even brighter emission from the devices. The present results are in agreement with Kodzhespirov *et al.* (8) who reported that emission intensities of ZnS:Mn devices increased with increasing Mn content. The maximum concentration used by these authors was 4.0 w/o and the ratio of emission intensity in the high-concentration devices to those with 0.04 w/o Mn was reported to be 10^3:1.

The dependence of the El output on frequency exhibited little variation as the Mn concentration was altered.

Effect of ZnS *thickness*.—There is little information in the literature on the effects of variation of phosphor film thickness on device performance. The results from the present work are shown in Fig. 3. In these experiments the concentration of Mn was maintained at 0.6 w/o, and the film was again sandwiched between 700Å SiO layers. The maximum obtainable brightness increased with ZnS thickness to 1.3μ, but did not increase appreciably thereafter. The discrimination ratio attained a maximum value for films in the region of 1.3μ in thickness. The figure also demonstrates that the field strength required to develop a given emission intensity falls towards a lower limit as the ZnS film thickness is increased. Vlasenko and Popkov (4) observed that emission intensity increased with increasing film thickness and the field strength at which emission was first discernible to the eye decreased with increasing thickness. The latter authors interpreted the results to be evidence

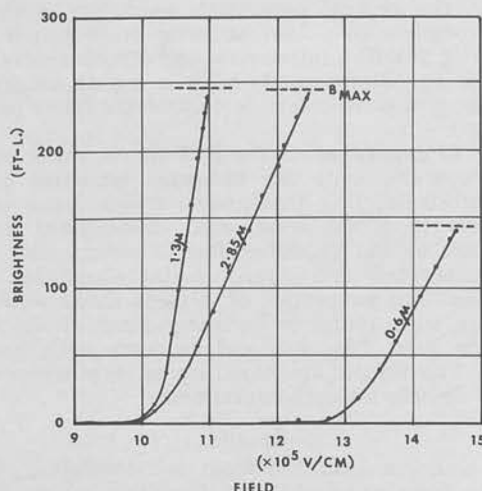

Fig. 3. Dependence of brightness on ZnS field at 13 kHz for various ZnS film thicknesses. A Mn concentration of 0.6 w/o was used and double 700Å SiO layers were employed.

of recombination throughout the bulk of the phosphor.

The dependence of electroluminescent output on frequency was found to saturate for all thicknesses of ZnS layers but, as the ZnS thickness was increased beyond 1.3μ, saturation occurred at successively lower frequencies.

In measurements of I-V curves on a number of panels over a brightness range from 1 to 700 ft-L it was found that the current increased linearly with voltage. As the SiO thickness was decreased or as the Mn content was decreased a given change in applied voltage would produce a greater change in current.

The relationship between brightness and rms applied voltage was measured for a number of films and was found to consist of two exponential regions. The curves, which are illustrated in Fig. 4 for several ZnS thicknesses, obey the following relation

$$B = B_1 \left(\exp \frac{V}{V_1} - 1 \right) + B_2 \left(\exp \frac{V}{V_2} - 1 \right)$$

where B is the surface brightness, V is the rms applied voltage, and B_1, B_2, V_1, and V_2 are constants. Kolomeitsev *et al.* (9) also found their results to obey this expression.

Efficiency-voltage characteristic.—Figure 5 shows the efficiency-voltage curves for several typical de-

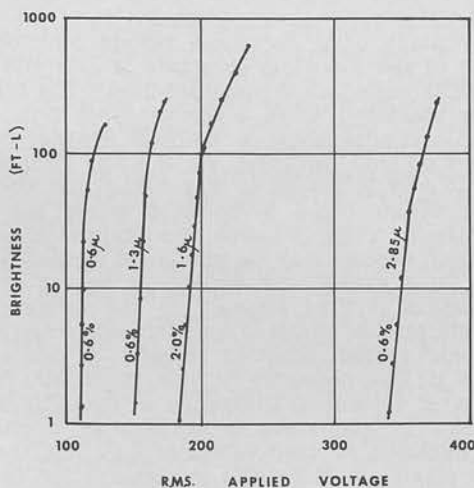

Fig. 4. Dependence on brightness on rms applied voltage for various ZnS film thicknesses and Mn concentrations using 700Å SiO layers.

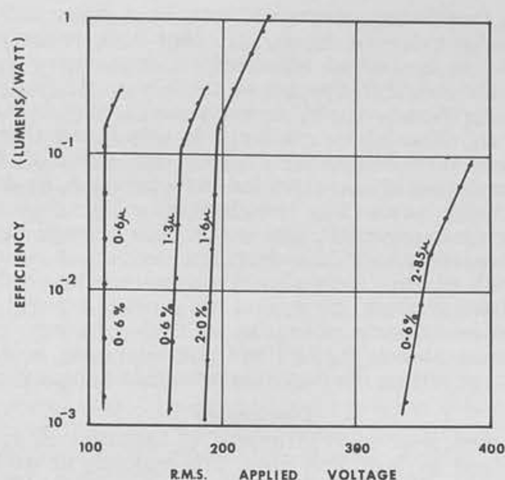

Fig. 5. Efficiency vs. rms applied voltage for various ZnS film thicknesses and Mn concentrations using 700Å SiO layers.

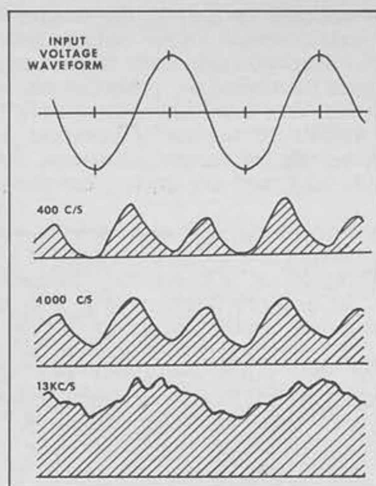

Fig. 6. Tracings of the emission waveforms obtained under sinusoidal excitation at several frequencies from a typical 2% Mn 1.6μ ZnS film.

vices. Once again double SiO layers were used and an excitation frequency of 13 kHz was employed. Emission efficiencies in the range from 0.1 to 1.0 lpw were regularly obtained; the higher efficiency results usually occurred when ZnS with 2 w/o Mn was evaporated, and the devices had the optimum SiO thicknesses for maximum emission.

The reduction in rate of increase of efficiency with applied voltage shown in Fig. 5 was also reported by Kodzhespirov and Kostylev (8). The dependence of efficiency on SiO thickness attained a maximum for values similar to those described in the section dealing with optical effects in these layers. Therefore, the improvement in efficiency can also be associated with these effects. The improvements in efficiency reported by Harper (6) for SiO_2 layers were associated with tunneling and accumulation effects in these layers; for these thin films (7-160Å) significant optical enhancement would not be anticipated.

In comparing the performance of thin-film and powder El phosphors it is significant that the efficiency of films increases with applied voltage whereas the efficiency of powder phosphors reaches a peak at approximately one-half of the desirable operating brightness and falls off with further increase of voltage. Although powder cells have exhibited maximum efficiencies of 14 lpw at low brightness, a value of 3 lpw is a more typical efficiency under normal operating conditions. The efficiency of thin-film panels of the type described here operating under similar conditions compares favorably with this value.

Emission characteristics under sinusoidal and pulsed excitation.—The shapes of the emission output waveforms were detected by a type 7625 photomultiplier and displayed on a Hewlett-Packard 175A dual-trace oscilloscope. Tracings of photographs of the waveforms obtained under sinusoidal excitation are shown in Fig. 6; the wavetrains progress from left to right of the diagrams. It was noted at low frequencies that there were two emission pulses per cycle of applied voltage and that the maximum emission lagged the maximum voltage for both polarities by 0.6 to 0.8 msec. At 400 Hz the two pulses were distinct but at 4 kHz the emission from a particular pulse did not decay to zero before onset of the succeeding pulse. At 13 kHz the emission pulses appeared only as a slight structure superimposed on a continuous level of emission.

It was found in a number of devices that, although similar time and frequency dependence of the emission peaks occurred, their amplitudes were not always equal. In these cases where the emission pulses were not equal in amplitude it was found that the light output corresponding to positive voltage applied to the tin oxide electrode could exceed the reverse case by up to 50%. Because of the similarity of behavior of the two peaks in all other aspects and because of the independence of results on the nature of the electrodes it is felt that the asymmetry results from nonuniform excitation or emission properties through the ZnS layer or at its interfaces with SiO. The nature of the device fabrication unfortunately introduces asymmetry in two respects. First, the distribution of Mn through the depth of the ZnS film may be nonuniform due to rapid depletion of Mn at the start of evaporation or deposit of an excess at the completion [in previous work (14) the Mn:Zn ratio has been shown to vary from 0.003 to 0.007 to 0.011 in subsequent 1-min deposition intervals]. A second factor arises from the sequential film deposition procedures which involve substrate heating during the ZnS evaporation. This process inevitably introduces inequalities in the properties of the initial and final SiO layers.

Figure 7 shows the response of a panel to symmetrical pulse excitation. Again two pulses per cycle were observed, and the maximum light emission lagged the voltage switching time by about 0.6 msec. Similar results were obtained for the cases where the tin-oxide electrode was pulsed positive and negative with respect to the metal electrode; the only slight distinction occurred in cases where the two emission

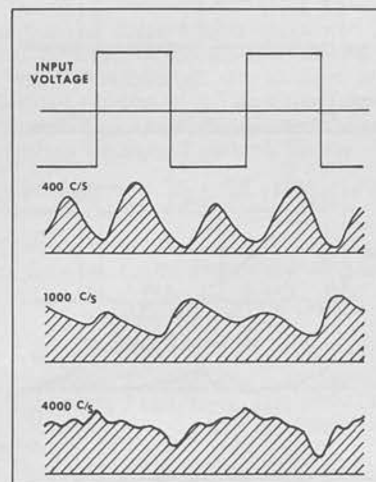

Fig. 7. Tracings of the emission waveforms obtained under symmetrical pulse excitation at several frequencies.

pulses were unequal in amplitude. In the latter case the larger pulse would occur when the tin-oxide layer was switched positive with respect to the metal electrode regardless of the potential at which the metal electrode was held (0 volts or full negative potential). At 400 Hz the two pulses per cycle were distinct but, as higher frequencies were applied, the light emission did not decay to zero between field reversals.

An interesting result was obtained by varying the mark: space ratio of the pulse waveform at a repetition rate in the region of 400 Hz, *i.e.*, below saturation frequencies. At a 50:50 duty cycle it was found that two approximately equal pulses per cycle were obtained, but as the ratio was moved to 85:15 the amplitude of one pulse decreased and the second pulse increased. At 85:15 only a single pulse occurred each cycle and this was approximately twice the size of its counterpart in the 50:50 duty cycle case. The single pulse was found to reach a peak approximately 0.6 msec after the termination of the 85% part of the cycle.

A series of experiments were performed in which the metal electrode was held at ground potential and the tin oxide was pulsed to full positive potential for 15% of each cycle. These experiments were repeated for the same pulse durations but with application of negative pulses to the tin oxide. Both sets of experiments were repeated using longer pulse durations so that the pulse occupied 85% of the cycle times. In all cases the results were similar, and the samples behaved as if the condition in which 85% of the time was spent was the equilibrium state and emission took place only after the applied voltage switched to the 15% state. Figure 8 illustrates two of these cases. It can be seen that the decay to zero emission following each light pulse takes several milliseconds.

Ageing.—One major disadvantage of thin-film El panels is their extremely rapid ageing characteristic. Apart from exceptional cases, thin films prepared by the above techniques show a reduction to half initial brightness within tens of operating hours. This figure is similar to values obtained by other authors. Ageing was accelerated by elevating the ambient temperature. It was noted, however, that the lifetime parameter showed distinct variations from one batch of devices to another prepared at a different time but in ostensibly the same manner, whereas from one device to another within any one particular batch there was consistency in ageing characteristics. There is evidence to suggest that this property is related to controlled and uniform manganese incorporation and that the use of more sophisticated material preparation and evaporation procedures may yield significant improvements. It was found that the lifetime of panels capable of several hundred foot-Lamberts could be extended by operation at lower brightness levels. The initial decay of brightness is not truly exponential, and a fast decay occurs during the application of the first few cycles of voltage. Because of this it is almost impossible to establish the true starting time for the decay process and therefore to state the true half-life. In our work we have taken the initial brightness as a value measured within the first minute of field application.

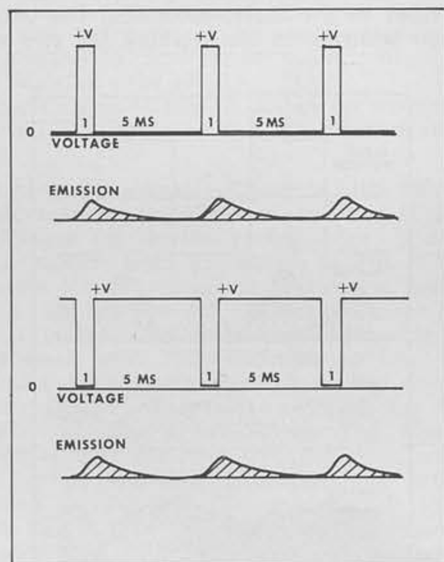

Fig. 8. Dependence of emission waveform on the applied pulse duty cycle.

Discussion

A great deal of controversy is apparent in recent published work on ZnS films. The majority of workers suggest that the best structure for obtaining efficient emission has a blocking layer at the positive metal electrode while others report that blocking contacts at the cathode are advisable [these points are reviewed in ref. (19)]. In the present work using relatively thick double insulating layers the emission was found in almost every case to be similar for both applied polarities regardless of the nature of the metal electrodes. This result implies that the metal/insulator interface properties are of secondary importance and that the carriers required for the recombination process originate either in the ZnS film itself or in the ZnS/SiO interface barriers, for example, in an accumulation layer of the type described by Harper (6).

The most favored mechanisms for explaining electroluminescence in Zns films include injection effects from adjacent layers (16, 20) or internal p-n junctions (5), and electronic impact ionization (6, 21). It is almost certain that light emission can and does result from these and other processes depending on the film preparation and contact properties. In the case of the present devices where average fields of 10^6 V/cm exist in the films under the optimum operating conditions one would anticipate a high-field mechanism to be operative. Impact excitation is likely to occur at these fields. The source of carriers for the emission process may be thermally generated electrons, but it is also possible that field effects lead to depopulation of traps in the various parts of the devices and that these could represent a significant contribution (23, 25). It should be noted that an average field of 8×10^5 V/cm was normally required for the efficient emission process in our layers and that the light output increased typically from 1 to 600 ft-L with a minor increase of field to 1.2×10^6 V/cm. Although inefficient emission was detected at lower fields its characteristics were different; the bright emission process appeared to have a definite field threshold. (Since there was evidence of space-charge effects in the devices it was possible that nonuniform field distribution occurred within the layers and that considerably higher than the average local fields may have been present.)

The emission from the films was similar to emission from a variety of ZnS: Mn devices and is believed to result from excitation of Mn centers by collision or resonance transfer. It is unlikely that direct field excitation of the Mn center itself occurred because of the high calculated field strength required for this process (22).

The emission waveform was considerably simpler than described results from ZnS films with other activator systems. The secondary peaks often described in work with other films were not observed in the present experiments. After a single step increment in voltage the emission was found to grow to a peak after 0.6 to 0.8 msec and then to decay over a considerably longer time interval. This behavior together with the observations under various applied waveforms could be explained in the following manner.

It is a well-established fact that ZnS films, interfaces, and oxide insulators possess a number of trapping levels with time constants ranging from microseconds to hours. The degree of occupation of these levels in structures such as the present panels is a complex function of applied voltage, ambient temperature, illumination, and past history. On changing the applied voltage a series of events occurs which leads to a new distribution of the carrier population throughout the devices. At first the free carriers and easily excited carriers flood toward their new positions and, more gradually, the deeper levels adjust in population according to a complex time dependence. Some of the adjustment occurs at a rate determined by thermal detrapping, but additional field-enhanced detrapping at fields as low as 5×10^3 V/cm could also occur (23). The internal field in each part of the structure cannot instantaneously acquire a new equilibrium value when the applied voltage is increased, but rather it will rise to a new value according to a time dependence determined by the level repopulation processes. Based on these premises it is tempting to conclude that it is this gradual field growth after a change in applied voltage which leads to the 0.6 msec delay before peak emission occurs. In other words the required field for the collision process does not appear across the total volume of the main emitting regions until 0.6 msec after application of the required voltage (the 0.6 msec time being a particular property of the present panels under these applied conditions).

As equilibrium is approached the flow of carriers diminishes and this leads to a gradual reduction in the number of excitations and recombinations. This is likely to be the explanation for the observed decay in emitted brightness after the peak value at 0.6 msec. A small residual light emission after equilibrium is established caused by thermally generated carriers entering the high-field regions might also be expected.

The above picture provides a simple and self-consistent explanation of the observed emission waveforms. Under sinusoidal or symmetrical pulse excitation there are equal excursions about each side of an average condition. This creates two major disturbances of equilibrium per cycle and could be expected to lead to two emission pulses per cycle. If the symmetry of the pulse excitation is altered to an 85:15 duty cycle, the equilibrium will be biased predominantly to the 85% condition. This being the case only one major excursion from equilibrium per cycle occurs. The excursion will be larger in magnitude than in the 50:50 duty cycle, and the result would be the observed single emission pulse of larger amplitude following the onset of the 15% parts of the waveform. This situation would occur regardless of the actual voltage experienced by the panel during the 85% part of the cycle.

The frequency dependence of the results is also explained. At high frequencies the 0.6 msec required by the present devices to reach full emission is not available. Instead the emission only grows to part of the maximum value. As the frequency is raised, however, the number of partial emissions per second is increased. These two effects counterbalance until, above 15 kHz the emission per pulse is so weak that the increased repetition rate no longer compensates and the output falls off. At low frequencies the growth of emission to a peak after 0.6 msec followed by a decay may be completed before the end of the applied voltage pulse. The total emission would in this case be simply determined by the pulse repetition rate. This linear emission fall off with reduced frequency was in fact observed.

With no applied field the distribution of occupied traps takes on its field-free form. Under sinusoidal or pulse excitation, parts of the ZnS films and adjacent layers become depopulated during a fraction of each voltage cycle and the population of deeper levels slowly adjusts to a value determined by the average occupation of the shallow levels. This operational equilibrium is different from the field-free case, and the transition from one situation to the other is believed to be responsible for the gradual build-up of emission during the first few cycles of voltage which is frequently described in the literature (26-28).

Conclusion

The experiments that have been reported have shown that the use of insulating layers on both sides of a ZnS:Mn film can lead to bright and relatively efficient electroluminescence (700 ft-L at 1 lpw). It is considered that the emission results from an impact excitation process which occurs when the various energy states in the device are disturbed from equilibrium under high-field conditions. It is also believed that the present efficient emission occurs in a regime of electric field in which the ZnS layer would normally experience breakdown if placed in direct contact with a metal electrode.

The proposed mechanism for the EL provides a consistent and straightforward explanation of the present observations, and it can also be shown to provide a simple alternative explanation of several other experiments which are described in the literature. The mechanism is amenable to experimental verification although the procedures are complex because of the small range of applied voltage during which the panels pass from 1 to 700 ft-L emission. A study of the time-dependence of the repopulation effects and their relation to ambient temperature, field, and illumination will clarify the situation.

The critical nature of the film deposition parameters required to produce efficient devices can be attributed to two factors. First, the required electrical properties of the ZnS layer are strongly dependent on the degree of crystallinity and the structural properties of the film. Second, the incorporation of high concentrations of Mn without serious disruption of the film must be achieved.

The brightness, efficiency, and ageing characteristics of the ZnS devices all appear to be related to the successful incorporation of Mn without film disruption. The present films improved in these characteristics as the Mn content in the source material was increased from 0.04 to 2.0 w/o. There is every reason to believe that further improvements will be possible when more sophisticated deposition techniques are used.

Acknowledgment

The authors would like to thank Mr. W. Carkner for his assistance in the fabrication of the ZnS devices and the Bowmar Instrument Corporation for permission to publish information contained in the First and Second Annual Research Reports on DIR Grant E54. The work was carried out as part of a research program jointly supported by Bowmar Canada Limited and the Defence Industrial Research Program operated by the Canadian Defence Research Board.

Manuscript received May 15, 1967; revised manuscript received June 12, 1967.

Any discussion of this paper will appear in a Discussion Section to be published in the June 1968 JOURNAL.

REFERENCES

1. R. E. Halsted and L. R. Koller, *Phys. Rev.*, **93**, 349 (1954).
2. W. A. Thornton, *J. Appl. Phys*, **30**, 123 (1959)
3. W. A. Thornton, *Phys. Rev.*, **116**, 893 (1959).
4. N. A. Vlasenko and Iu. A. Popkov, *Optics & Spectros*, **8**, 39 (1960).
5. W. A. Thornton, *This Journal*, **108**, 636 (1961).
6. W. J. Harper, *ibid.*, **109**, 103 (1962).
7. V. L. Bakumenko, G. S. Kojina, and V. N. Favorin, *Optics & Spectros*, **15**, 262 (1963).

8. F. F. Kodzhespirov and S. A. Kostylev, *Optics & Spectros*, **12**, 144 (1964).
9. F.I. Kolomoitsev, F. F. Kodzhespirov, and S. A. Kostylev, *ibid.*, **12**, 497 (1964).
10. A. G. Gol'dman, G. A. Zholkevich, and N. P. Lazar, *Soviet Phys., Doklady*, **10**, 1148 (1966).
11. V. A. Vlasenko and S. A. Zyn'o, *Zn. Priklad. Spectrosk (USSR)*, **5**, 67 (1966).
12. R. J. Studer and D. A. Cusano, *J. Opt. Soc. Amer.*, **42**, 878 (1952).
13. C. Feldman and M. O'Hara, *ibid.*, **47**, 300 (1957).
14. L. R. Koller and H. D. Coghill, *This Journal*, **107**, 973 (1960).
15. G. A. Antcliffe, *Brit. J. Appl. Phys.*, **16**, 1467 (1965).
16. P. Goldberg and J. W. Nickerson, *J. Appl. Phys.*, **34**, 1601 (1963).
17. D. A. Cusano, Doctoral Dissertation, Rensselaer Polytech. Inst. (Jan. 1959).
18. K. L. Chopra, *J. Appl. Phys.*, **36**, 655 (1965).
19. P. Goldberg in "Luminescence of Inorganic Solids," P. Goldberg, Editor, p. 408, Academic Press, New York (1966).
20. R. C. Jaklevic, D. K. Donald, J. Lambe, and W. C. Vassell, *Appl. Phys. Letters*, **2**, 7, (1961).
21. D. A. Cusano in "Luminescence of Organic and Inorganic Materials," H. P. Kallman and G. M. Spruch, Editors, p. 494, John Wiley & Sons, Inc. New York (1962).
22. W. W. Piper and F. E. Williams in "Solid State Physics," Volume VI, p. 96, Academic Press, New York (1958).
23. K. W. Boër and U. Kümmel, *Ann. Phys.*, **16**, 181 (1955).
24. G. F. Alfrey and J. B. Taylor, *Proc. Phys. Soc.*, **68B**, 775 (1955).
25. M. J. Russ, Ph.D. Thesis, University of Birmingham (1962).
26. S. Kawashima, *This Journal*, **113**, 1083 (1966).
27. H. F. Ivey in "Electroluminescence and Related Effects," p. 65, Academic Press, New York (1963).
28. H. K. Henisch in "Electroluminescence," MacMillan, New York (1962).

JOURNAL OF APPLIED PHYSICS VOLUME 38, NUMBER 11 OCTOBER 1967

New Electroluminescent Spectrum in ZnTe resulting from Oxygen Incorporation

D. I. KENNEDY AND M. J. RUSS
Bowmar Canada Limited, Ottawa, Ontario, Canada

(Received 31 May 1967)

Electroluminescence was observed in ZnTe devices fabricated from crystals in which oxygen was incorporated. Main emission peaks were located at 6960 Å at 293°K and 6580 Å at 77°K, and external quantum efficiencies of 10^{-3}–10^{-4} were obtained at room temperature. The emission from these devices is considered to result from recombinations taking place at oxygen centers which appear to be located approximately 0.4 eV from the band edge. Improvements in the emission properties of these devices over similar diodes fabricated from undoped material are described.

In a report on absorption and fluorescence in ZnTe crystals, Dietz *et al.*[1] described optical transitions associated with a center located 0.4 eV below the bandgap energy. In similar investigations on crystals grown from a melt containing ZnO, Hopfield *et al.*[2] later suggested that these transitions were due to oxygen substituting isoelectronically for Te.

This article describes the hitherto unreported electroluminescent properties of ZnTe devices fabricated from crystals containing deep impurity levels which are believed to be associated with oxygen incorporation.

In the crystal-growth procedure, a charge, prepared from high-purity Zn and Te and containing excess Zn, was placed in a quartz ampoule. The ampoule was then placed in a furnace maintained at 1200°C. A short capillary tube extended from the ampoule into a second temperature zone maintained at 900°C. From within this temperature zone a tube of larger diameter connected the capillary tube to an externally located reservoir containing inert gas plus 5% oxygen. Typical growth runs extended over a period of 24 h and resulted in the production of a boule of ZnTe and also an additional small quantity of white crystals; these latter crystals were found by analysis to be ZnO. ZnTe crystals of approximate size 10×6×6 mm were extracted from the boule. These crystals exhibited a red coloration when viewed in transmission. A spark mass spectrographic analysis of the crystals showed oxygen to be present in a concentration in excess of 10^{18}/cc. Electrical transport measurements showed the material to be *p*-type, with a room-temperature resistivity of 8 Ω·cm and carrier concentration of 2×10^{16}/cc.

Figure 1 illustrates the room-temperature absorption coefficient of a typical crystal. A DK2-A spectrophotometer was used for the measurement of the absorption spectra. For comparison the absorption coefficient of a nominally undoped crystal grown by a similar technique but in an oxygen-free atmosphere is also shown. Both crystals were of similar thickness (0.1 mm) and chemically polished prior to measurement. For the oxygen-doped material the absorption coefficient exhibits a complex dependence on photon energy. In this broadened absorption spectrum there are two regions where the absorption shows a pronounced increase with increasing photon energy. One is located at 1.76 eV and the other in the same region of the spectrum as the absorption edge of the undoped material. (The direct bandgap energy for undoped ZnTe was determined to be 2.21 eV).

Devices were fabricated from the ZnTe crystals using

[1] R. E. Dietz, D. G. Thomas, and J. J. Hopfield, Phys. Rev. Letters **8**, 391 (1962).
[2] J. J. Hopfield, D. G. Thomas, and R. T. Lynch, Phys. Rev. Letters **17**, 312 (1966).

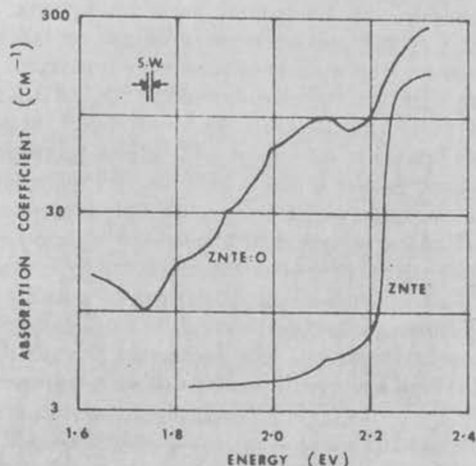

FIG. 1. Absorption spectra of ZnTe:O and nominally undoped crystal at 293°K.

a technique described previously[3] involving diffused-In and In/Ag-soldered contacts. The area and thickness of the devices were 1 mm^2 and 0.5 mm, respectively.

The emission spectrum of a typical device is shown in Fig. 2. In these measurements a 250-mm monochromator was used in conjunction with a photomultiplier having an S-20 response. The curves shown were corrected for the response of the photomultiplier. At 293°K the main emission peak was located at 6960 Å with a spectrum half-width of 680 Å. A secondary peak which had relative intensity 1/50th of the main peak was located at a wavelength of 5750 Å, i.e., just above the absorption edge of the undoped material. For devices fabricated from oxygen-free crystals, no emission was detected in the red region of the spectrum. In this case the emission spectrum consisted of a single peak located at 5750 Å. At 293°K, no emission was detected at wavelengths below 5500 Å. The difference between the energy corresponding to the emission peak and the experimentally determined value of the bandgap at room temperature indicates that recombinations may involve a center located 0.43 eV from the valence or conduction band edge.

At 77°K the main peak shifted to shorter wavelengths and was located at 6580 Å, the half-width being reduced to 420 Å. The shift in this peak between the two temperatures is in agreement with the reported temperature dependence of the bandgap energy.[4] In this case a secondary peak was detected at 5400 Å; the ratio of the intensity of this peak to that of the main peak was found to be 1:100. No emission was detected at wavelengths below 5230 Å. As in the room-temperature spectrum the emission charsceteristic for oxygen-free crystals consisted of a single peak; in this case the peak was located at 5400 Å. The displacement of the main emission peak from the reported value of the bandgap energy at 77° K[4] indicates that recombinations may involve a center located 0.48 eV from the valence or conduction-band edge. It is possible that at both 293° and 77°K the spectrum of the emitted radiation extends to shorter wavelengths than the values corresponding to the bandgap energies at these temperatures, but that the emission is internally absorbed. At both 293° and 77°K no shifts of the emission peaks were observed for devices operating over a wide range of current levels.

In Fig. 3 the current–voltage characteristics of typical devices at room temperature and 77°K are shown. The room-temperature characteristics for both directions of current flow through the device were Ohmic at low-current levels with transitions to higher-power-law relationships taking place as the voltage was increased. The conductivity of the devices was considerably reduced as the temperature was lowered. The difference in the degree of rectification at the two contacts was evidenced by displacement of the V–I characteristics. The onset of emission was normally associated with the commencement of the steep portion of the V–I characteristic. At room temperature the lowest voltage level at which emission was detectable was found to be approximately 4.5 V. Little variation was noted between the V–I characteristics of doped and undoped crystals.

Although electroluminescence was observed in these devices for both directions of current flow, the most intense emission was obtained for the higher-current direction. This was obtained when the diffused In contact was maintained at a negative potential with respect to the bulk of the crystal. For this polarity emission was observed throughout the bulk of the crystal. For the opposite polarity the emission was restricted to a series of isolated spots located in the region of the negative contact. Apart from the emission spectrum, the main distinction between the characteristics of the electroluminescence observed in doped and undoped ZnTe was the observation, in the former,

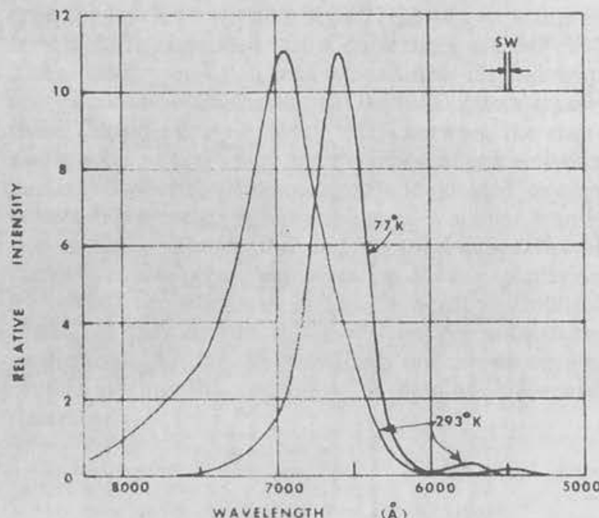

FIG. 2. Emission spectra of ZnTe:O at 293° and 77°K.

[3] D. I. Kennedy and M. J. Russ, Solid State Electron. 10, 125 (1967).

[4] M. Cardona and D. L. Greenaway, Phys. Rev. 131, 98 (1963).

of general emission throughout the volume of the crystal for one direction of current flow.

Brightness–current relationships were measured using an RCA 7265 photomultiplier at low brightness levels and a Photo Research spectra spot meter at higher brightness levels. The results for a typical device are shown in Fig. 4. This exhibits two regions, one approximating to a square law with a transition to a linear relationship occurring at high current levels. Due to the absence of an associated reduction in the slope of the 293°K V-I characteristic at similar current levels it is considered that at this temperature the reduced emission efficiency is associated with an increased probability of nonradiative transitions. Brightness levels of 25 ft·L were commonly obtained.

Measurements of external quantum efficiency were made using an array of solar cells of calibrated efficiency. It was found that the efficiency of devices made from a doped material was a factor of 10–100 times greater than that of devices fabricated by an identical technique but from nominally undoped material. Room temperature efficiencies of the order of 10^{-4}–10^{-3} were obtained. At liquid nitrogen temperatures efficiencies were a factor of ten higher. These results indicate that thermal quenching of the emission is not pronounced for this form of the material.

The electrical characteristics of these devices and the observation of emission in the bulk of the material allows consideration of an excitation mechanism in which minority carriers are created as a result of impact ionization in a localized high-field region in the vicinity of the cathodic contact with subsequent injection into the bulk of the crystal. A similar "avalanche injection" mechanism has been advanced by Crowder *et al.*[5] to explain electroluminescence observed in a ZnTe M–i–p device. From the results of the present experiments it is considered that, due to variations in the blocking nature of the two contacts, the injection processes are not identical for both polarities.

Preliminary results obtained from electrical transport measurements show no evidence of electrically active deep centers. The improved efficiency and pronounced emission peak observed in oxygen-doped devices is attributed to the role of oxygen as a recombination center, electroluminescence resulting from recombination of minority carriers bound to these centers with free carriers or with carriers originating from shallow acceptor levels (Aven and Segall[6] reported an acceptor level in ZnTe associated with a Zn vacancy at 0.048 eV). The secondary-emission peak located near the bandgap energy could be associated with residual direct transitions. Considerable similarity exists between the emission spectra reported here and the reported pair emission in GaP[7] involving Zn acceptors and ionized oxygen donors. There exists the possibility of a similar transition in ZnTe. The optical and electrical properties of the devices also permit consideration of the explanation for optical transitions in ZnTe advanced by Hopfield *et al.*[2] On the basis of this model oxygen substitutes isoelectronically for Te providing uncharged oxygen centers having the capability of binding holes and electrons.

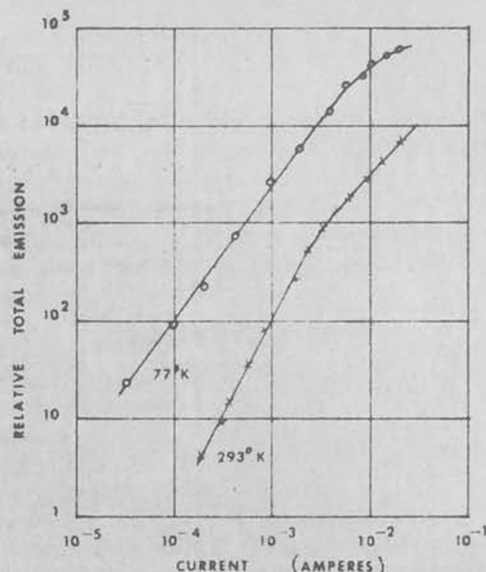

FIG. 4. Brightness–current characteristics of ZnTe:O devices at 293° and 77°K.

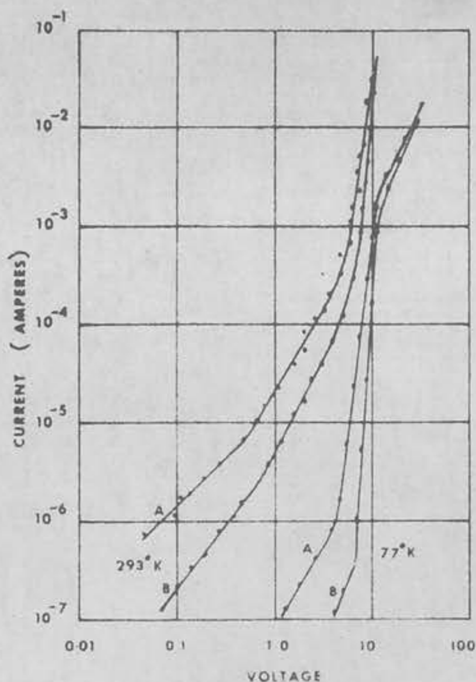

FIG. 3. Current–voltage characteristics of ZnTe:O at 293° and 77°K. (A) In-diffused contact negative; (B) In-diffused contact positive.

[5] B. L. Crowder, F. Morehead, and P. Wagner, Appl. Phys. Letters **8**, 148 (1966).

[6] M. Aven and B. Segall, Phys. Rev. **130**, 81 (1963).

[7] M. Gershenzon, F. A. Trumbore, R. M. Mikulyak, and M. Kowalchik, J. Appl. Phys. 365, 1528 (1965).

Oxygen in ZnTe was described in the latter work as an isoelectronic acceptor possessing the characteristics of an electron trap. The low-temperature optical transitions reported by these authors involved a trap located at 0.4 eV below the bandgap energy and show a degree of correlation with the positions of the emission peaks reported here. Further investigations are being carried out into the low-temperature absorption, fluorescent and photoluminescent properties of these crystals to allow elucidation of the nature of the optical transitions.

In summary, we have reported the electroluminescence of ZnTe crystals associated with oxygen centers. It is possible that these centers are incorporated in the lattice in the form of uncharged impurity centers substituting isoelectronically for Te. The source of carriers for the electroluminescence is believed to be "avalanche injection" of minority carriers created by impact ionization in a localized high-field region. The efficiency of devices fabricated from this material is a considerable improvement over that of undoped ZnTe. There exists the possibility that the fabrication of devices from this material utilizing improved blocking contacts, insulating barrier layers, or alloyed heterojunctions may result in the attainment of efficient room-temperature emission.

ACKNOWLEDGMENTS

The authors thank W. A. Webb for his assistance in fabricating devices and would like to express their appreciation to R. K. Willardson of the Bell & Howell Research Center for arranging a spark mass spectrographic analysis of ZnTe crystals.

This work was carried out as part of a research program jointly sponsored by Bowmar Canada Limited and the Defence Industrial Research Program operated by the Canadian Defence Research Board.

ELECTROLUMINESCENCE IN POLYCRYSTALLINE ZnTe

D. I. Kennedy and M.J. Russ

ABSTRACT - The properties of electroluminescent devices fabricated from polycrystalline ZnTe are described. Broad emission bands are observed at room temperature under direct current excitation and 77°K under alternating field excitation. The emission is associated with impact ionisation in localised high-field regions. Emission efficiencies at room temperature are in the range 10^{-5} to 10^{-7} photons/electron.

RÉSUMÉ - Les propriétés des appareils electroluminescenses fabriqués de polycristalline ZnTe sont décrits. De larges bandes d'émission sont observées sous la température intérieure sur l'excitation du courant direct et 77°K sur l'excitation du champ alternatif. L'émission est associé avec la collision d'ion localisées dans la region des haut champs. L'éfficacités d'émission à température intérieure est dans la catégarie de 10^{-5} a 10^{-7} photons/electron.

ZUSAMMENFASSUNG - Die Eigenschaften von Elektrolumineszenz Bauteile fabriziert von Polykristalline ZnTe sind beschrieben. Breite strahlungsbander sind festgestellt in Raumtemperatur mit Gleichstrom anregung und mit 77°K unter Wechselstrom anregung. Die Ausstrahlung ist zusammenhängend mit dem Aufschlag der Schwellstrome in örtlichen Hochfeld Regionen. Die beste Leistung der Ausstrahlung Raumtemperatur wird in der Spanne von 10^{-5} zu 10^{-7} photons/electron ereichet.

ELECTROLUMINESCENCE IN POLYCRYSTALLINE ZnTe

D. I. Kennedy and M. J. Russ

Previous investigations of electroluminescence in single crystal ZnTe[1-3] have indicated that the emission may result from high field processes in the vicinity of the contacts. Since long range order and high quality bulk material may not be essential for these processes to be operative and since single crystal ZnTe is difficult to produce it was of some importance to determine whether emission could be obtained from devices fabricated from polycrystalline material.

The material was prepared by sealing a quantity of high-purity Zn and Te in amounts deviating from stoichiometry by +1 wt% Te in an evacuated quartz ampoule, and annealing the reacted mixture for 15 hours at 1080°C. The resulting ZnTe, excluding the remaining excess elemental Te, was placed in a quartz tube and inserted in a furnace maintained at 950°C. The tube extended from the furnace into the room temperature ambient and was connected to a running vacuum. Over a period of two hours the ZnTe vaporized from the 950°C zone and recondensed in an intermediate temperature zone at about 700°C. The condensate was in the form of a polycrystalline boule of grain size in the 2×10^{-3} to 5×10^{-2} cm. Simple measurements on the material indicated that the effective resistivity was 4×10^{5} ohm-cm. and thus that the material was semi-insulating.

Devices were fabricated from $1mm^2$ chips of material which were sawn from the boule. The chips were reduced to a thickness of 0.1 to 0.5 mm. by grinding with alumina and were subsequently etched in a CP-4 solution to remove the surface layers. Three techniques were used to make contact to the chips; first, simple In contacts were made to the top and bottom surfaces, second the top surface was coated with electroless Au and, third, the top surface was subjected to an In vacuum-alloying process. In all cases the bottom contacts of pure In were attached to conventional transistor headers. Since the brightest emission was obtained from the first technique using pure In on both sides of the chip, this contacting process was adopted for the subsequent investigations.

The current-voltage characteristics of a typical device at 300°K and 77°K are shown in Figure 1. The linear, square-law, and higher power-law dependencies in the room temperature characteristic are similar to those observed in single crystal material. Also the onset of emission usually coincided with the commencement of a steep portion of the I-V characteristic and occurred at voltage levels of approximately 6 volts. As the temperature was lowered pronounced reductions were observed in the conductivity of the

material as shown in the 77°K I-V characteristic. The displacement of the d.c. I-V curve to lower currents with cooling was accompanied by a reduction in emission intensity and it was not possible to detect emission from the devices at 77°K using an RCA 7625 photomultiplier. By excitation of the devices with alternating fields at 4kHz, however, the 77°K emission characteristics of the material were readily measurable - in this case the emission peaks were found to occur at maxima and minima in the applied voltage waveform.

At room temperature, emission was obtained from these devices for both directions of current flow. The emission appeared to originate from localised regions near the In contacts and was always associated with the positive contact. On polarity reversal the emission switched to the opposite contact. The variation in the blocking nature of the two contacts was reflected in higher current levels being obtained for one polarity; concomitantly the emission intensity, for a given applied voltage, was normally higher for this current direction (the latter situation occurred for both d.c. and a.c. excitation).

At 77°K the ZnTe exhibited marked photoconductivity, and in the dark the current was further reduced by a factor of 100. The

reduction of current was further reduced by a factor of 100. The reduction of current on the extinction of the illumination was exponential with time, a period of approximately 15 minutes being required for the current to achieve a final stabilized value. Exposure of the device to light of greater than band-gap energy resulted in an immediate increase in current to the original level. At room temperature or under a.c. excitation no significant photoconductivity could be detected.

The emission spectra were investigated using a 250mm. monochromator in conjunction with a photomultiplier having an S-20 cathode response. Typical results obtained from d.c. excitation at 300°K and a.c. excitation at 77°K are shown in Figure 2 - these results are corrected for the photomultiplier response. The room temperature emission spectrum shows a broad emission band centered at 6800Å with a half-width of 1900Å. The reduction of emission at wavelengths below 6550Å was correlated with the distributed absorption edge of the polycrystalline material. A similar broad emission spectrum is frequently observed in measurements on single crystal ZnTe devices and is commonly associated with an impact-ionisation excitation process - in these cases the attenuation of the peak at higher energies is altered because of the sharper absorption edge. At 77°K the emission consisted of a major peak

at 7550Å, a secondary peak at 5900Å and a minor peak at 6550Å.

At room temperature the emission intensity of these devices as a function of current was measured under both d.c. and pulsed excitation and a linear relationship was obtained. This was true for both types of excitation and for both directions of current flow. Using pulse excitation of repetition rate 50 cps and a duty cycle of 1:1000 the measurements were extended to current densities in the range of $30A/cm^2$. The emission rise-time (from 10% to 90% of full emission) was found to be 2.5 μsecs.

While caution must be exercised in interpreting results from the polycrystalline material used in this investigation, some general observations are valid. First, there is a strong similarity between the I-V characteristics and the room temperature emission properties of the polycrystalline and single crystal devices. The broad emission spectrum is suggestive of impact-ionization processes. The localization of emission to the contact regions also suggests that high-fields in the vicinity may lead to the impact-excitation. The similarity of I-V characteristics between single crystal and polycrystalline material suggests that the conduction processes are "contact-dominated".

Although the room-temperature results on both types of material are similar, the emission from polycrystalline devices diminishes at

low temperatures. The extinction of emission at 77°K is attributed to the reduction of bulk conductivity of the polycrystalline material to a point where the conduction processes become limited by bulk effects (such as the impedance of grain boundaries, for example.) Under a.c. excitation it is not necessary for carriers to traverse the bulk of the material and charge transport within the surface and barrier layers can lead to a.c. current flow and, presumably, to concomitant excitation and emission processes.

The complex distributed emission spectrum obtained at 77°K is still in keeping with an impact ionization mechanism. The shape and position of the peak at 7550Å indicates the presence of a deep recombination center of unknown origin and the peak at 5900Å appears to result from recombination of hole-electron pairs of near band-gap energy. An emission peak at 6580Å was previously reported[3] to occur in the 77°K spectrum of devices fabricated from ZnTe single crystals incorporating oxygen centres. The possibility exists that the minor peak observed here at 6550Å is attributable to this same center. Because of the abundance of energy states anticipated at grain boundaries in polycrystalline material a more detailed speculation would be of no value.

As anticipated these investigations revealed that electroluminescence observed in this form of ZnTe was inferior to that obtained in monocrystalline material. One of the disadvantages stems from the high resistivity of the material and the high voltage levels required to induce electroluminescence. The room temperature external quantum efficiency estimated from the observed emission intensities was of the order of 10^{-6} to 10^{-7} photons/electron.

ACKNOWLEDGEMENTS

This work was carried out as part of a research program jointly supported by Bowmar Canada Limited and the Defence Industrial Research Program operated by the Canadian Defence Research Board.

REFERENCES

1. B. L. Crowder, F. F. Morehead and P. R. Wagner. Appl.Phys.Lett. 8, 148 (1966).

2. D. I. Kennedy and M. J. Russ. Solid-St. Electron. 10, 127 (1967).

3. D. I. Kennedy and M. J. Russ Jnl.Appl.Phys. in press.

FIGURE 1 Current-Voltage Characteristics of a Polycrystalline ZnTe Device at 300°K and 77°K.
A - top contact negative
B - top contact positive.

FIGURE 2 Emission Spectrum of a Polycrystalline ZnTe Device at 300°K and 77°K.
Excitation - 300°K : d.c., 20V, 2mA.
77°K : 4 Kc/s, 175V, 2mA.

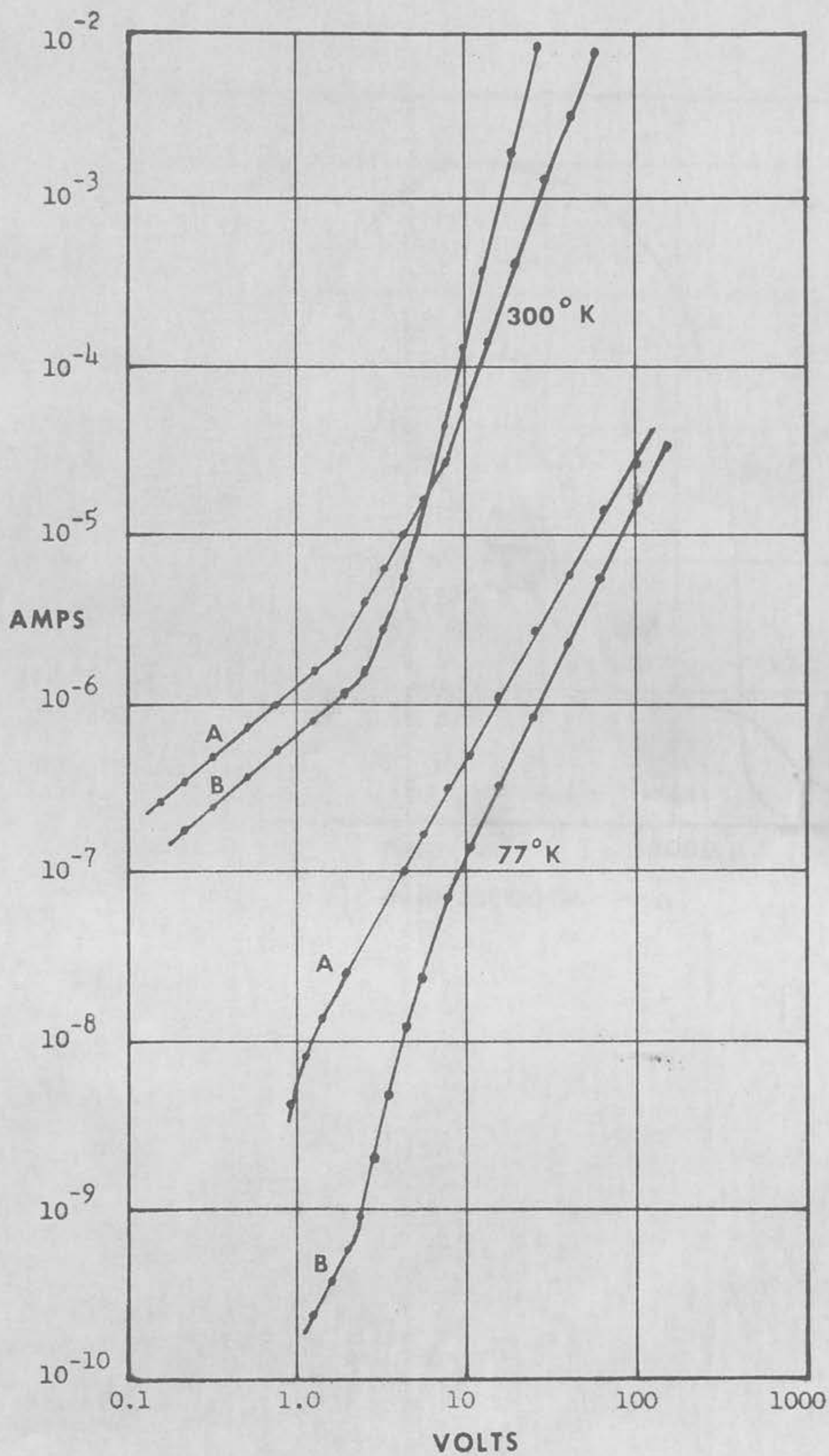

10^{-2}
10^{-3}
10^{-4}
10^{-5}
10^{-6}
10^{-7}
10^{-8}
10^{-9}
10^{-10}
AMPS
300° K
77° K
A
B
A
B
0.1
1.0
10
100
1000
VOLTS

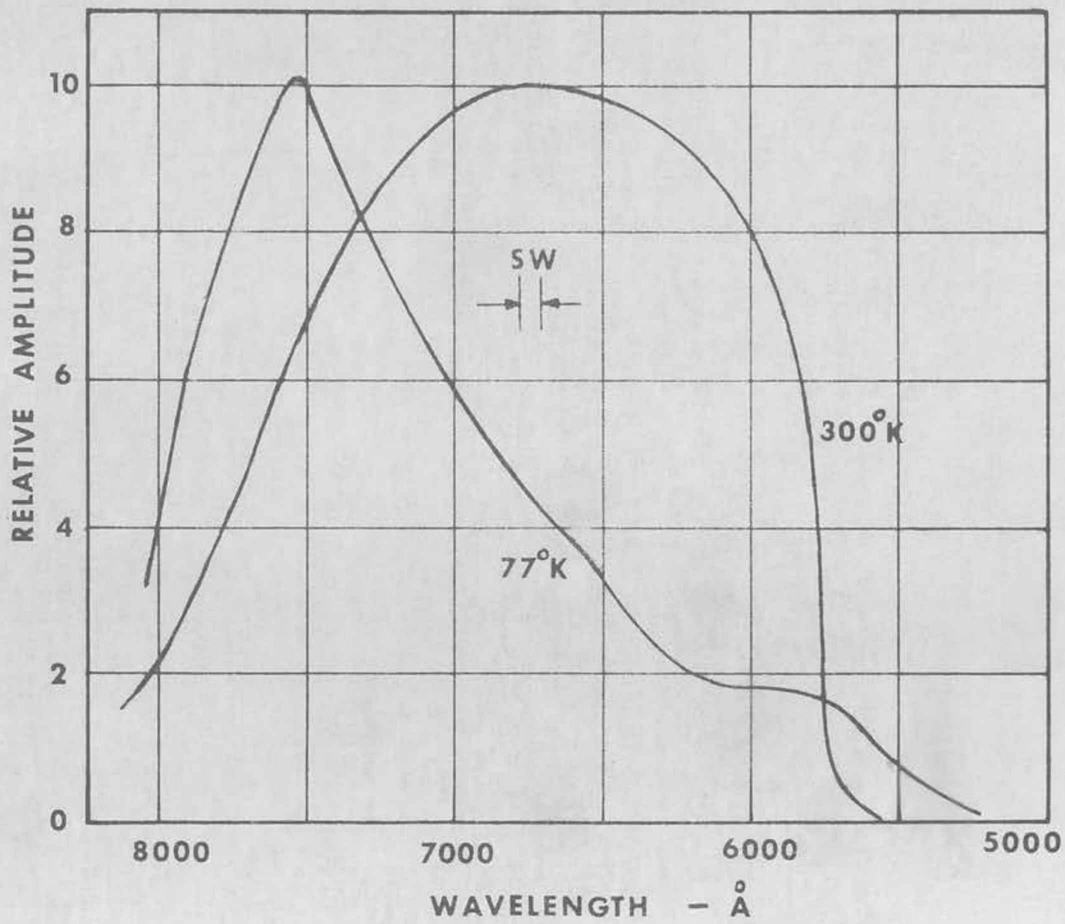
RELATIVE AMPLITUDE
10
8
6
4
2
0
SW
300°K
77°K
8000
7000
6000
5000
WAVELENGTH – Å